NASA TECHNICAL MEMORANDUM

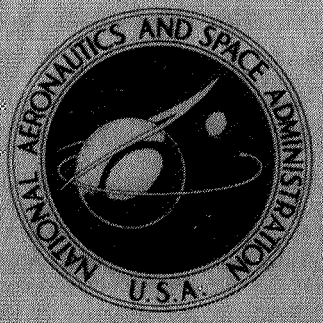

NASA TM X-3009

NASA TM X-3009

WIND-TUNNEL INVESTIGATION OF AN EXTERNALLY BLOWN FLAP STOL TRANSPORT MODEL INCLUDING AN INVESTIGATION OF WALL EFFECTS

by Garl L. Gentry, Jr.

Langley Research Center
Hampton, Va. 23665

NATIONAL AERONAUTICS AND SPACE ADMINISTRATION • WASHINGTON, D. C. • SEPTEMBER 1974

1. Report No.	2. Government Accession No.	3. Recipient's Catalog No.
NASA TM X-3009		

4. Title and Subtitle	5. Report Date
WIND-TUNNEL INVESTIGATION OF AN EXTERNALLY BLOWN FLAP STOL TRANSPORT MODEL INCLUDING AN INVESTIGATION OF WALL EFFECTS	September 1974
	6. Performing Organization Code
7. Author(s)	8. Performing Organization Report No.
Garl L. Gentry, Jr.	L-9435
	10. Work Unit No.
9. Performing Organization Name and Address	760-61-02-02
NASA Langley Research Center Hampton, Va. 23665	11. Contract or Grant No.
	13. Type of Report and Period Covered
12. Sponsoring Agency Name and Address	Technical Memorandum
National Aeronautics and Space Administration Washington, D.C. 20546	14. Sponsoring Agency Code

15. Supplementary Notes

16. Abstract

A wind-tunnel investigation was conducted in the Langley V/STOL tunnel and in a scaled version of the Ames 40- by 80-foot tunnel test section installed as a liner in the Langley V/STOL tunnel to determine the effect of test-section size on aerodynamic characteristics of the model. The model investigated was a swept-wing, jet-powered, externally blown flap (EBF) STOL transport configuration with a leading-edge slat and triple-slotted flaps. The model was an 0.1645-scale model of a 11.58-meter (38.0-ft) span model designed for tests in the 40- by 80-foot tunnel at the Ames Research Center. The data presented compare the aerodynamic characteristics of the model with and without the tunnel liner installed.

Data are presented as a function of thrust coefficient over an angle-of-attack range of 0^{o} to 25^{o}. A thrust-coefficient range up to approximately 4.0 was simulated, most of the tests being conducted at a free-stream dynamic pressure of 814 newtons/meter^2 (17 lb/ft^2). The data are presented with a minimum of analysis.

17. Key Words (Suggested by Author(s))	18. Distribution Statement
Wall effects STOL transport External blowing flap	Unclassified — Unlimited STAR Category 01

19. Security Classif. (of this report)	20. Security Classif. (of this page)	21. No. of Pages	22. Price*
Unclassified	Unclassified	172	$5.00

*For sale by the National Technical Information Service, Springfield, Virginia 22151

WIND-TUNNEL INVESTIGATION OF AN EXTERNALLY BLOWN FLAP STOL TRANSPORT MODEL INCLUDING AN INVESTIGATION OF WALL EFFECTS

By Garl L. Gentry, Jr.
Langley Research Center

SUMMARY

A wind-tunnel investigation was conducted in the Langley V/STOL tunnel and in a scaled version of the Ames 40- by 80-foot tunnel test section installed as a liner in the Langley V/STOL tunnel to determine the effect of test-section size on aerodynamic characteristics of the model. The model investigated was a swept-wing, jet-powered, externally blown flap (EBF) STOL transport configuration with a leading-edge slat and triple-slotted flaps. The model was an 0.1645-scale model of a 11.58-meter (38.0-ft) span model designed for tests in the 40- by 80-foot tunnel at the Ames Research Center. The data presented compare the aerodynamic characteristics of the model with and without the tunnel liner installed.

Data are presented as a function of thrust coefficient over an angle-of-attack range of 0^{o} to 25^{o}. A thrust-coefficient range up to approximately 4.0 was simulated, most of the tests being conducted at a free-stream dynamic pressure of 814 newtons/meter^2 (17 lb/ft^2). The data are presented with a minimum of analysis.

INTRODUCTION

Interest in the development of a jet-powered STOL transport has led to serious consideration of an externally blown flap (EBF) configuration as a means of producing the high lift required for STOL operation. (See refs. 1 to 7.) In this effort, a 11.58-meter (38.0-ft) span model was fabricated for tests in the Ames 40- by 80-foot tunnel. This model was originally conceived as a generalized EBF STOL transport airplane configuration powered by four TF-34 turbofan engines. The scale relationship was based on the relationship of the sizes of the TF-34 engines and the JT-15D engines simulated in the

present investigation. The EBF high-lift system for this configuration employed a full-span triple-slotted flap with a large-chord leading-edge slat.

In order to determine tunnel wall effects and Reynolds number effects for a 11.58-meter (38.0-ft) span model to be tested in the Ames 40- by 80-foot tunnel, a small-scale model of this configuration was tested in the Langley V/STOL tunnel with and without a tunnel liner installed to simulate the Ames tunnel test section. Comparisons between data from the 0.1645-scale model of this investigation (liner installed) and data from the 11.58-meter (38.0-ft) model in the Ames 40- by 80-foot tunnel will yield scale effects directly.

This investigation was also undertaken to provide small-scale data for a model of a jet STOL research airplane with four engines. Longitudinal and lateral-directional aerodynamic and control characteristics were investigated for various power conditions in the transition-speed range. These data are presented herein without analysis.

SYMBOLS

The measurements of this investigation are presented in the International System of Units (SI) and the U.S. Customary Units are shown in parentheses. Measurements were made in U.S. Customary Units. Details of the use of SI Units, together with physical constants and conversion factors, are presented in reference 8.

Longitudinal forces and moments are referred to the stability-axis system and lateral-directional forces and moments are referred to the body-axis system. (See fig. 1.) The origin of the axes is a point in the plane of symmetry corresponding to the longitudinal location of the 40-percent chord of the mean aerodynamic chord. The vertical location of the origin is 6.731 centimeters (2.650 in.) above the fuselage center line.

b wing span, meters (ft)

C_D drag coefficient, $\frac{\text{Drag}}{q_\infty S}$

C_L lift coefficient, $\frac{\text{Lift}}{q_\infty S}$

C_l rolling-moment coefficient, $\frac{M_X}{q_\infty Sb}$

C_{l_β} effective-dihedral parameter, $\frac{\Delta C_l}{\Delta \beta}$ $(\beta = \pm 5^o)$

C_m pitching-moment coefficient, $\frac{M_Y}{q_\infty S\bar{c}}$

C_n yawing-moment coefficient, $\frac{M_Z}{q_\infty Sb}$

C_{n_β} directional stability parameter, $\frac{\Delta C_n}{\Delta \beta}$ $(\beta = \pm 5^o)$

C_T total engine gross-thrust coefficient, $\frac{T}{q_\infty S}$

C_Y side-force coefficient, $\frac{F_Y}{q_\infty S}$

C_{Y_β} side-force parameter, $\frac{\Delta C_Y}{\Delta \beta}$ $(\beta = \pm 5^o)$

c local wing chord, meters (ft)

$\bar{c}$ wing mean aerodynamic chord, meters (ft)

c_f flap chord measured in percent wing chord, c

c_s local chord, horizontal stabilizer, meters (ft)

F_A axial force, newtons (lb)

F_D drag force, newtons (lb)

F_L lift force, newtons (lb)

F_N normal force, newtons (lb)

F_X force along X-axis, positive forward, newtons (lb)

F_Y	side force, positive to right, newtons (lb)
F_Z	force along Z-axis, positive downward, newtons (lb)
i_t	incidence of horizontal tail with respect to fuselage center line, deg
M_X	rolling moment, centimeter-newtons (in-lb)
M_Y	pitching moment, centimeter-newtons (in-lb)
M_Z	yawing moment, centimeter-newtons (in-lb)
q_∞	free-stream dynamic pressure, newtons/meter^2 (lb/ft^2)
S	wing area, meters^2 (ft^2)
T	gross thrust, newtons (lb)
X,Y,Z	body reference axes
X_S,Y_S,Z_S	stability reference axes
x	chordwise station measured from airfoil nose in percent chord
z_ℓ	lower surface distance perpendicular to chord in percent chord
z_u	upper surface distance perpendicular to chord in percent chord
α	angle of attack, deg
β	angle of sideslip, deg
δ_e	elevator deflection, deg
δ_f	flap deflection, deg

δ_j jet or thrust deflection angle, arc tan $\frac{F_N}{F_A}$, deg

δ_s wing leading-edge slat deflection with respect to wing chord, deg

MODEL AND APPARATUS

A three-view drawing and photographs of the model are presented in figures 2 and 3, respectively. The airfoil section of the wing at the root was NACA 63_2A214 and at the tip NACA 63_2A211. The ordinates for the wing are presented in table I. The ordinates near the trailing edge have been slightly modified to provide a finite trailing-edge thickness. The wing had an area of 0.499 meter^2 (5.374 ft^2), a mean aerodynamic chord of 0.278 meter (0.9125 ft), and an aspect ratio of 7.269. It was swept 25° at the quarter chord and had a span of 1.905 meters (6.254 ft).

The geometry of the three-segment leading-edge slat and the triple-slotted flaps is shown in figure 2(b), and the ordinates are presented in tables II and III, respectively. The outboard leading-edge slat segment had a St. Cyr 178 airfoil section, modified to have a thickness of 0.0065c at the trailing edge and a chord that was 25 percent of the local wing chord. Its span extended from the outboard engine pylon to the wing tip. In the deployed position, the slat gap was 0.015c. The chord of the other slat segments was 15 percent of the local wing chord. The inboard segment extended from the fuselage to the inboard engine and the middle segment extended between the inboard and outboard engines. With this slat configuration, there was a gap between the slats and the engine pylons and fuselage. For the extended leading-edge slat configuration in the deployed position, no gaps existed between the slats and either of the engine pylons or the fuselage.

The full-span flap had chords of 15-, 20-, and 22.5-percent local wing chord for the first, second, and third elements, respectively. The first flap element was geometrically similar to the leading-edge slat. The second flap element had a St. Cyr 178 airfoil section modified slightly to allow flap nesting in the undeflected configuration and to provide a finite trailing-edge thickness. The third flap element had a NACA 4412 section modified to a finite thickness at the trailing edge. All flap-slot gaps were 0.015 wing local chord.

The geometry of the horizontal tail is shown in figure 2(c) and its ordinates are presented in table IV. It had a NACA 64-012 airfoil section, an area of 0.18 meter^2 (1.94 ft^2), a mean aerodynamic chord of 0.221 meter (0.724 ft), and an aspect ratio of 3.995. It was swept 25° at the quarter chord and had a span of 0.847 meter (2.78 ft). The horizontal tail pivoted about the 55.5-percent root chord and had an incidence range from -5° to 15°. It had a 15-percent-chord inverted leading-edge slat which was deflected to -40° and a full-span elevator which was adjustable to three settings – 0°, -25°, and -50°.

The vertical tail had a leading-edge sweep of 40.6°, an aspect ratio of 1.328, a NACA 0012 airfoil section (see table IV for ordinates), a span of 0.493 meter (1.617 ft), an area of 0.183 meter^2 (1.968 ft^2), and a mean aerodynamic chord of 0.374 meter (1.228 ft).

Four air ejector engine simulators were used to simulate the JT-15D fan-jet engines which have a bypass ratio of approximately 3.2. The bypass ratio is defined as the ratio of total fan-exit mass flow to total gas generator exit mass flow. Each engine simulator was a two-part ejector with individual air-supply lines and control valves to provide the efflux of the fan and gas generator. Their center lines were parallel with wing reference chord and with the fuselage center line.

The liner for the V/STOL tunnel was fabricated to represent the test section of the Ames 40- by 80-foot tunnel in a proper scale relationship for a 1.905-meter (6.25-ft) span model. Figure 4 shows a comparison of test sections between the V/STOL tunnel and the Ames tunnel liner. The model was an 0.1645-scale version of an 11.58-meter (38-ft) span model to be tested at Ames. Tests in the Ames 40- by 80-foot tunnel are conducted with the model supported by vertical support struts instead of a sting support as in the present tests in the V/STOL tunnel. The strut configuration used in the Ames 40- by 80-foot tunnel tests was simulated in the present investigation (fig. 3(c)) in order to determine whether there were any appreciable strut interference effects on the model data.

TEST PROCEDURES AND CORRECTIONS

The model was tested for three basic airplane configurations – cruise, take-off, and landing. (See fig. 5.) The cruise configuration was defined as the model with 0° flaps, no wing leading-edge slats, no horizontal-tail leading-edge slats, and with the elevator set at

0^{o}. The take-off configuration was defined as the model with the three elements of the flap system set at 0^{o}, 20^{o}, and 40^{o}; wing leading-edge slat deployed at 50^{o}; horizontal-tail leading-edge slat deployed at -40^{o}; and elevator set at -25^{o}. The landing configuration was defined as the model with the three elements of the flap system set at 15^{o}, 35^{o}, and 55^{o}; wing leading-edge slat deployed at 50^{o}; horizontal-tail leading-edge slat deployed at -40^{o}; and elevator set at -25^{o}. The wing cross sections for these configuration are presented in figure 2(b).

Tests were conducted at a nominal free-stream dynamic pressure of 814 newtons/meter^2 (17 lb/ft^2) for a Reynolds number of 0.70×10^6 based on the wing mean aerodynamic chord of 27.81 centimeters (10.95 in.). A 0.25-centimeter-wide (0.1-in.) transition strip of No. 40 carborundum was located on the surfaces of the wing, nose of the fuselage, nacelles, and vertical and horizontal tails at a point 3.10 centimeters (1.22 in.) aft of the leading edge measured in a streamwise direction along the surface. The transition strips were used for all tests. Most of the tests were made over an angle-of-attack range of 0^{o} to 25^{o} and a total gross-thrust coefficient range up to about 4.0. The various thrust levels were obtained by setting the primary air-supply pressure at the model plenum in accordance with a previously determined relationship between model plenum and model thrust.

A test run consisted of a variation in either angle of attack or thrust with all other conditions fixed. At each test point during a given run, electrical signals from the six-component balance, pitch-angle sensor, pressure transducers, and fixed tunnel instrumentation were recorded. Attachment to the model of the air-supply lines for the engine simulators affects the sensitivity of the strain-gage balance used to measure the model forces and moments. Variations in air-line pressure also produce forces and moments on the balance. Calibrations were made to determine these nonaerodynamic effects on the balance measurements and both of these effects were found to be consistently repeatable; the data presented have been corrected for these effects. In addition, corrections to the data have been made to account for wind-tunnel wall effects by using the method described in reference 9.

PRESENTATION OF DATA

The data from this investigation are basically presented in four major groups. The first group includes the longitudinal aerodynamic characteristics over a range of

angle of attack and thrust coefficient with the model in the V/STOL tunnel with the liner installed to simulate the Ames 40- by 80-foot tunnel. The second group includes typical longitudinal aerodynamic data for the model in the Langley V/STOL tunnel without the liner. The third group includes some data from both the first two groups with and without wall corrections on both sets of data. The fourth group includes lateral-directional stability derivatives obtained with the model in the V/STOL tunnel without the liner installed for small sideslip angles over a range of angle of attack and thrust coefficient. All data in the first, second, and fourth groups have been corrected for wall effects.

Results of the investigation are presented in the following figures:

DISCUSSION OF RESULTS

The data in this report are presented without analysis. Some discussion of the longitudinal aerodynamic characteristics of this model, including results obtained from four other types of engine-simulator configurations, is presented in reference 7. Some discussion of effects of wall corrections to the data for the test in the V/STOL tunnel

with and without the liner is presented. In addition, the effects of dummy strut mounts on the longitudinal aerodynamic characteristics are presented.

The effect of wall corrections on the measured aerodynamic characteristics of the model in the V/STOL tunnel with the liner installed is shown in figures 46 to 48 for cruise, take-off, and landing model configurations. These data show a noticeable increase in angle of attack and a slight increase in the magnitude of force and moment coefficients with wall correction applied to a given data point. The effect of wall corrections on aerodynamic characteristics with the model in the V/STOL tunnel without the liner is shown in figures 49 to 51 for cruise, take-off, and landing model configurations. These data basically show only a small change in angle of attack with wall correction applied to a given data point.

The comparisons of the corrected data for the model with and without the tunnel liner installed are shown in figures 52 to 54. The two sets of data agree reasonably well for all model configurations. These data show that models of the size relationship of the model in the Ames 40- by 80-foot tunnel can be used to obtain reliable aerodynamic data for each STOL model when the wall effects are properly accounted for.

The effect of simulating the Ames tunnel support struts on represented configurations is shown in figure 19. These data indicate that there is little, if any, effect on aerodynamic characteristics of the configurations tested because of the change in the type of model support, except at high thrust coefficients on higher lift model configurations.

CONCLUDING REMARKS

A wind-tunnel investigation was conducted in the Langley V/STOL tunnel and in a liner installed in the tunnel that was a scaled version of the Ames 40- by 80-foot tunnel test section. The purpose of the investigation was to determine the effect of test-section size on the aerodynamic characteristics of the model which was a swept-wing, jet-powered, externally blown flap STOL transport configuration with a leading-edge slat and triple-slotted flaps. Data are presented without analysis for the aerodynamic characteristics of the model in the tunnel with and without the liner. Data are presented as a function of thrust coefficient over an angle-of-attack range of 0^{o} to 25^{o}.

Langley Research Center,
National Aeronautics and Space Administration,
Hampton, Va., April 4, 1974.

REFERENCES

1. Parlett, Lysle P.; Freeman, Delma C., Jr.; and Smith, Charles C., Jr.: Wind-Tunnel Investigation of a Jet Transport Airplane Configuration With High Thrust-Weight Ratio and an External-Flow Jet Flap. NASA TN D-6058, 1970.

2. Freeman, Delma C., Jr.; Parlett, Lysle P.; and Henderson, Robert L.: Wind-Tunnel Investigation of a Jet Transport Airplane Configuration With an External-Flow Jet Flap and Inboard Pod-Mounted Engines. NASA TN D-7004, 1970.

3. Vogler, Raymond D.: Wind-Tunnel Investigation of a Four-Engine Externally Blowing Jet-Flap STOL Airplane Model. NASA TN D-7034, 1970.

4. Anon.: STOL Technology. NASA SP-320, 1972.

5. Smith, Charles C., Jr.: Effect of Wing Aspect Ratio and Flap Span on Aerodynamic Characteristics of an Externally Blown Jet-Flap STOL Model. NASA TN D-7205, 1973.

6. Parlett, Lysle P.; Smith, Charles C., Jr.; and Megrail, James L.: Wind-Tunnel Investigation of Effects of Variations in Reynolds Number and Leading-Edge Treatment on the Aerodynamic Characteristics of an Externally Blown Jet-Flap Configuration. NASA TN D-7194, 1973.

7. Hoad, Danny R.: Longitudinal Aerodynamic Characteristics of an Externally Blown Flap Powered-Lift Model With Several Propulsive System Simulators. NASA TN D-7670, 1974.

8. Mechtly, E. A.: The International System of Units - Physical Constants and Conversion Factors (Second Revision). NASA SP-7012, 1973.

9. Heyson, Harry H.: Use of Superposition in Digital Computers To Obtain Wind-Tunnel Interference Factors for Arbitrary Configurations, With Particular Reference to V/STOL Models. NASA TR R-302, 1969.

TABLE I.- WING AIRFOIL ORDINATES

[Stations and ordinates given in percent of airfoil chord]

(a) Spanwise location, root; leading-edge radius, 0.531 cm (0.209 in.); c, 37.441 cm (14.741 in.)

x	z_u	z_ℓ
0	0	0
.55	1.356	-----
.88	----	-1.275
1.00	1.748	-1.358
3.00	2.957	-2.324
5.00	3.802	-2.962
8.00	4.774	-3.662
10.00	5.304	-4.032
12.50	5.873	-4.419
15.00	6.357	-4.741
20.00	7.127	-5.232
25.00	7.680	-5.558
30.00	8.087	-5.740
35.00	8.220	-5.772
40.00	8.217	-5.662
45.00	8.046	-5.422
50.00	7.730	-5.071
55.00	7.288	-4.633
60.00	6.738	-4.137
65.00	6.091	-3.643
70.00	5.363	-3.149
80.00	3.742	-2.161
85.00	2.839	-1.667
90.00	1.912	-1.173
95.00	.971	-.679
100.00	0	-.185

(b) Spanwise location, 24.384 cm (9.600 in.); leading-edge radius, 0.402 cm (0.158 in.); c, 31.690 cm (12.477 in.)

x	z_u	z_ℓ
0	0	0
.55	1.320	-----
.88	----	-1.241
1.00	1.703	-1.322
3.00	2.885	-2.259
5.00	3.712	-2.877
8.00	4.662	-3.555
10.00	5.181	-3.915
12.50	5.738	-4.287
15.00	6.212	-4.598
20.00	6.966	-5.073
25.00	7.508	-5.387
30.00	8.224	-5.562
35.00	8.039	-5.591
40.00	8.037	-5.482
45.00	7.871	-5.247
50.00	7.564	-4.905
55.00	7.133	-4.479
60.00	6.597	-3.999
65.00	5.965	-3.522
70.00	5.254	-3.045
75.00	4.483	-2.567
85.00	2.784	-1.611
90.00	1.875	-1.135
95.00	.952	-.658
100.00	0	-.180

(c) Spanwise location, 10.234 cm (4.029 in.); leading-edge radius, 0.475 cm (0.187 in.); c, 35.028 cm (13.790 in.)

x	z_u	z_ℓ
0	0	0
.55	1.342	-----
.88	----	-1.262
1.00	1.731	-1.344
3.00	2.930	-2.299
5.00	3.768	-2.930
8.00	4.732	-3.621
10.00	5.257	-3.988
12.50	5.822	-4.369
15.00	6.302	-4.687
20.00	7.066	-5.171
25.00	7.615	-5.493
30.00	8.017	-5.672
35.00	8.151	-5.703
40.00	8.149	-5.594
45.00	7.980	-5.356
50.00	7.667	-5.008
55.00	7.229	-4.574
60.00	6.684	-4.085
65.00	6.043	-3.597
70.00	5.322	-3.109
75.00	4.540	-2.622
80.00	3.714	-2.134
85.00	2.818	-1.646
90.00	1.898	-1.159
95.00	.964	-.671
100.00	0	-.183

(d) Spanwise location, 31.804 cm (12.521 in.); leading-edge radius, 0.367 cm (0.144 in.); c, 29.940 cm (11.788 in.)

x	z_u	z_ℓ
0	0	0
.55	1.307	-----
.88	----	-1.229
1.00	1.686	-1.308
3.00	2.858	-2.234
5.00	3.677	-2.845
8.00	4.620	-3.514
10.00	5.134	-3.870
12.50	5.687	-4.237
15.00	6.157	-4.544
20.00	6.905	-5.012
25.00	7.442	-5.322
30.00	8.137	-5.494
35.00	7.970	-5.522
40.00	7.969	-5.413
45.00	7.805	-5.181
55.00	7.075	-4.420
60.00	6.543	-3.947
65.00	5.918	-3.476
70.00	5.213	-3.005
75.00	4.449	-2.534
80.00	3.641	-2.063
85.00	2.763	-1.590
90.00	1.861	-1.121
95.00	.945	-.650
100.00	0	-.178

TABLE I.- WING AIRFOIL ORDINATES – Concluded

(e) Spanwise location, 40.005 cm (15.750 in.); leading-edge radius, 0.329 cm (0.130 in.); c, 28.006 cm (11.026 in.)

x	z_u	z_ℓ
0	0	0
.55	1.200	-----
.88	----	-1.213
1.00	1.665	-1.291
3.00	2.824	-2.203
5.00	3.634	-2.804
8.00	4.567	-3.463
10.00	5.076	-3.815
12.50	5.622	-4.174
15.00	6.087	-4.476
20.00	6.828	-4.936
25.00	7.361	-5.240
30.00	8.028	-5.409
35.00	7.883	-5.435
40.00	7.883	-5.328
45.00	7.722	-5.098
50.00	7.422	-4.763
55.00	7.001	-4.346
60.00	6.476	-3.881
65.00	5.858	-3.418
70.00	5.161	-2.955
75.00	4.406	-2.492
80.00	3.606	-2.029
85.00	2.736	-1.563
90.00	1.843	-1.102
95.00	.936	-.639
100.00	0	.-176

(f) Spanwise location, 71.887 cm (28.302 in.); leading-edge radius, 0.205 cm (0.081 in.); c, 21.986 cm (8.656 in.)

x	z_u	z_ℓ
0	0	0
.55	1.193	-----
.88	----	-1.122
1.00	1.544	-1.194
3.00	2.629	-2.027
5.00	3.390	-2.574
8.00	4.265	-3.173
10.00	4.743	-3.498
12.50	5.257	-3.818
15.00	5.695	-4.091
20.00	6.393	-4.505
25.00	6.895	-4.777
30.00	7.411	-4.926
35.00	7.393	-4.945
40.00	7.397	-4.841
45.00	7.250	-4.625
55.00	6.583	-3.929
60.00	6.095	-3.509
65.00	5.518	-3.091
70.00	4.868	-2.673
75.00	4.160	-2.254
80.00	3.409	-1.837
85.00	2.587	-1.412
90.00	1.743	-1.000
95.00	.884	-.582
100.00	0	-.163

(g) Spanwise location, 48.424 cm (19.065 in.); leading-edge radius, 0.293 cm (0.116 in.); c, 26.021 cm (10.244 in.);

x	z_u	z_ℓ
0	0	0
.55	1.269	-----
.88	----	-1.194
1.00	1.640	-1.271
3.00	2.783	-2.166
5.00	3.583	-2.756
8.00	4.504	-3.403
10.00	5.007	-3.749
12.50	5.546	-4.100
15.00	6.006	-4.396
20.00	6.737	-4.847
25.00	7.264	-5.144
30.00	7.900	-5.308
35.00	7.781	-5.333
40.00	7.782	-5.227
45.00	7.624	-4.999
50.00	7.328	-4.670
55.00	6.914	-4.260
60.00	6.397	-3.804
65.00	5.787	-3.350
70.00	5.100	-2.896
75.00	4.355	-2.443
80.00	3.565	-1.989
85.00	2.705	-1.532
90.00	1.822	-1.081
95.00	.925	-.627
100.00	0	-.174

(h) Spanwise location, 95.250 cm (37.500 in.); leading-edge radius, 0.131 cm (0.052 in.); c, 14.976 cm (5.896 in.)

x	z_u	z_ℓ
0	0	0
.55	1.060	-----
.88	----	-.998
1.00	1.379	-1.061
3.00	2.363	-1.785
5.00	3.055	-2.259
8.00	3.851	-2.776
10.00	4.288	-3.065
12.50	4.757	-3.329
15.00	5.157	-3.562
20.00	5.796	-3.915
25.00	6.258	-4.143
30.00	6.566	-4.265
35.00	6.721	-4.273
40.00	6.730	-4.174
45.00	6.604	-3.978
50.00	6.358	-3.699
60.00	5.572	-2.999
65.00	5.053	-2.643
70.00	4.465	-2.286
75.00	3.824	-1.929
80.00	3.138	-1.573
85.00	2.382	-1.204
90.00	1.605	-.859
95.00	.760	-.502
100.00	0	-.146

TABLE II.- LEADING-EDGE SLAT AIRFOIL ORDINATES

[Station and ordinates given in percent of airfoil chord]

(a) Inboard root; spanwise location, 10.234 cm (4.029 in.); $c_s = 15$

x	z_u	z_ℓ
0	0.914	0.914
1.25	4.454	-2.377
2.50	6.135	-3.372
5.00	8.417	-4.549
7.50	10.012	-5.235
10.00	11.208	-5.526
15.00	13.102	-5.712
20.00	14.398	-5.403
25.00	15.303	-4.503
30.00	16.003	-3.203
40.00	16.016	-.712
50.00	14.634	1.464
60.00	12.348	2.050
70.00	9.658	1.736
80.00	6.767	1.123
90.00	3.482	.309
95.00	1.786	-.289
100.00	.094	-.695

(b) Inboard tip; spanwise location, 40.005 cm (15.750 in.); $c_s = 15$

x	z_u	z_ℓ
0	0.851	0.851
1.25	4.275	-2.287
2.50	5.885	-3.265
5.00	8.095	-4.353
7.50	9.673	-4.985
10.00	10.850	-5.240
15.00	12.728	-5.373
20.00	14.005	-5.028
25.00	14.928	-4.128
30.00	15.628	-2.828
40.00	15.695	-.373
50.00	14.385	1.714
60.00	12.152	2.247
70.00	9.498	1.880
80.00	6.642	1.212
90.00	3.410	.345
95.00	1.732	-.246
100.00	.073	-.678

(c) Outboard root; spanwise location, 40.005 cm (15.750 in.); $c_s = 25$

x	z_u	z_ℓ
0	0.851	0.851
1.25	4.275	-2.287
2.50	5.885	-3.265
5.00	8.095	-4.353
7.50	9.673	-4.985
10.00	10.850	-5.240
15.00	12.728	-5.373
20.00	14.005	-5.028
25.00	14.928	-4.128
30.00	15.628	-2.828
40.00	15.695	-.373
50.00	14.385	1.714
60.00	12.152	2.247
70.00	9.498	1.880
80.00	6.642	1.212
90.00	3.410	.345
95.00	1.732	-.246
100.00	.073	-.678

(d) Outboard tip; spanwise location, 95.250 cm (37.500 in.); $c_s = 25$

x	z_u	z_ℓ
0	0.579	0.579
1.25	3.500	-1.900
2.50	4.800	-2.800
5.00	6.698	-3.500
7.50	8.200	-3.900
10.00	9.300	-4.000
15.00	11.100	-3.900
20.00	12.300	-3.400
25.00	13.301	-2.500
30.00	14.000	-1.200
40.00	14.300	1.100
50.00	13.301	2.800
60.00	11.300	3.100
70.00	8.800	2.500
80.00	6.100	1.600
90.00	3.100	.500
95.00	1.500	-.060
100.00	.020	-.600

TABLE III.- FLAP AIRFOIL ORDINATES

[Station and ordinates given in percent of airfoil chord]

(a) First flap element

Spanwise location, root; $c_f = .15$

x	z_u	z_ℓ
0	0.930	0.930
1.25	4.500	-2.400
2.50	6.200	-3.400
5.00	8.500	-4.600
7.50	10.100	-5.300
10.00	11.300	-5.600
15.00	13.200	-5.800
20.00	14.500	-5.500
25.00	15.400	-4.600
30.00	16.100	-3.300
40.00	16.100	-.800
50.00	14.700	1.400
60.00	12.400	2.000
70.00	9.700	1.700
80.00	6.800	1.100
90.00	3.500	.300
95.00	1.800	-.300
100.00	.100	-.700

Spanwise location, tip; $c_f = 15$

x	z_u	z_ℓ
0	0.580	0.580
1.25	3.500	-1.900
2.50	4.800	-2.800
5.00	6.700	-3.500
7.50	8.200	-3.900
10.00	9.300	-4.000
15.00	11.100	-3.900
20.00	12.300	-3.400
25.00	13.300	-2.500
30.00	14.000	-1.200
40.00	14.300	.000
50.00	13.300	2.800
60.00	11.300	3.100
70.00	8.800	2.500
80.00	6.100	1.600
90.00	3.100	.500
95.00	1.500	-.060
100.00	-.020	-.600

(b) Second flap element

Spanwise location, root; $c_f = 20$

x	z_u	z_ℓ
0	0.930	0.930
1.25	4.570	-2.380
2.50	6.200	-3.420
5.00	8.480	-4.680
7.50	10.230	-5.270
10.00	11.500	-5.450
15.00	13.270	-5.020
20.00	14.380	-3.850
25.00	15.200	-2.250
30.00	15.680	-.480
40.00	15.330	2.150
50.00	13.730	3.600
60.00	11.350	3.800
70.00	8.600	3.210
80.00	5.800	2.200
90.00	2.900	.830
95.00	1.480	.070
100.00	.070	-.730

Spanwise location, tip; $c_f = 20$

x	z_u	z_ℓ
0	0.580	0.580
1.25	3.450	-1.900
2.50	4.830	-2.730
5.00	6.643	-3.580
7.50	8.250	-3.920
10.00	9.470	-3.870
15.00	11.250	-3.180
20.00	12.470	-1.910
25.00	13.400	-.290
30.00	14.000	1.330
40.00	13.930	3.570
50.00	12.720	4.730
60.00	10.520	4.780
70.00	7.990	3.860
80.00	5.380	2.600
90.00	2.670	1.050
95.00	1.270	.200
100.00	.020	-6.620

(c) Third flap element

Spanwise location, root; $c_f = 22.5$

x	z_u	z_ℓ
0	0	0
.50	1.70	----
.88	----	-1.25
1.00	2.69	-1.38
2.00	3.53	-2.11
4.00	4.87	-2.79
6.00	5.88	-3.20
8.00	6.72	-3.45
10.00	7.43	-3.61
15.00	8.81	-3.75
20.00	9.77	-3.68
25.00	10.40	-3.50
30.00	10.76	-3.26
35.00	10.87	-3.02
40.00	10.77	-2.77
45.00	10.47	-2.53
50.00	10.08	-2.28
55.00	9.55	-2.01
60.00	8.91	-1.75
65.00	8.16	-1.49
70.00	7.32	-1.25
75.00	6.42	-1.02
80.00	5.33	-.82
85.00	4.22	-.65
90.00	2.95	-.45
95.00	1.60	-.29
100.00	.41	-.41

Spanwise location, tip; $c_f = 22.5$

x	z_u	z_ℓ
0	0	0
.50	1.26	----
.88	---	-1.00
1.00	2.05	-1.10
2.00	2.81	-1.63
4.00	3.94	-2.08
6.00	4.82	-2.31
8.00	5.56	-2.43
10.00	6.19	-2.49
15.00	7.43	-2.44
20.00	8.31	-2.26
25.00	8.91	-2.01
30.00	9.26	-1.76
35.00	9.38	-1.53
40.00	9.32	-1.32
45.00	9.09	-1.14
50.00	8.75	-.96
55.00	8.30	-.78
60.00	7.76	-.62
65.00	7.72	-.47
70.00	6.39	-.35
75.00	5.57	-.24
80.00	4.66	-.17
85.00	3.69	-.14
90.00	2.57	-.09
95.00	1.39	-.10
100.00	.33	-.33

TABLE IV.- EMPENNAGE AIRFOIL ORDINATES

[Station and ordinates given in percent of airfoil chord]

(a) Horizontal tail

x	z_u	z_ℓ
0	0	0
.50	.978	-.978
.75	1.179	-1.179
1.25	1.490	-1.490
2.50	2.035	-2.035
5.00	2.810	-2.810
7.50	3.394	-3.394
10.00	3.871	-3.871
15.00	4.620	-4.620
20.00	5.173	-5.173
25.00	5.576	-5.576
30.00	5.844	-5.844
35.00	5.978	-5.978
40.00	5.981	-5.981
45.00	5.798	-5.798
50.00	5.480	-5.480
55.00	5.056	-5.056
60.00	4.500	-4.500
62.00	3.982	-4.279
64.00	2.747	-4.057
65.00	1.928	-3.950
66.00	1.213	-3.836
68.00	.141	-3.613
70.00	-.674	-3.393
72.00	-1.277	-3.175
74.00	-1.680	-2.948
75.00	-1.842	-2.837
76.00	-1.979	-2.727
78.00	-2.141	-2.496
80.00	-2.190	-2.280

(b) Horizontal-tail leading-edge slat

x	z_u	z_ℓ
0	0.828	0.825
1.25	4.207	-2.254
2.50	5.790	-3.224
5.00	7.973	-4.278
7.50	9.544	-4.890
10.00	10.715	-5.132
15.00	12.585	-5.244
20.00	13.856	-4.885
25.00	14.785	-3.985
30.00	15.485	-2.685
40.00	15.573	-.244
50.00	14.290	1.810
60.00	12.078	2.322
70.00	9.436	1.934
80.00	6.595	1.246
90.00	3.383	.359
95.00	1.712	-.230
100.00	.065	-.671

(c) Elevator

x	z_u	z_ℓ
0	0	0
1.25	1.630	-2.800
2.50	2.230	-3.890
5.00	2.860	-5.400
7.50	2.780	-6.290
10.00	2.720	-7.510
15.00	2.570	-9.030
20.00	2.430	-10.060
25.00	2.280	-10.750
30.00	2.140	-11.140
40.00	1.860	-11.200
50.00	1.570	-9.710
60.00	1.280	-8.280
70.00	1.000	-6.290
80.00	.710	-4.290
90.00	.420	-2.280
95.00	.290	-1.230
100.00	.140	-.140

(d) Vertical tail

x	z_u	z_ℓ
0	0	0
1.25	1.894	-1.894
2.50	2.615	-2.615
5.00	3.555	-3.555
7.50	4.200	-4.200
10.00	4.683	-4.683
15.00	5.345	-5.345
20.00	5.737	-5.737
25.00	5.941	-5.941
30.00	6.002	-6.002
40.00	5.803	-5.803
50.00	5.294	-5.294
60.00	4.563	-4.563
70.00	3.664	-3.664
80.00	2.623	-2.623
90.00	1.448	-1.448
95.00	.807	-.807
100.00	.126	-.126

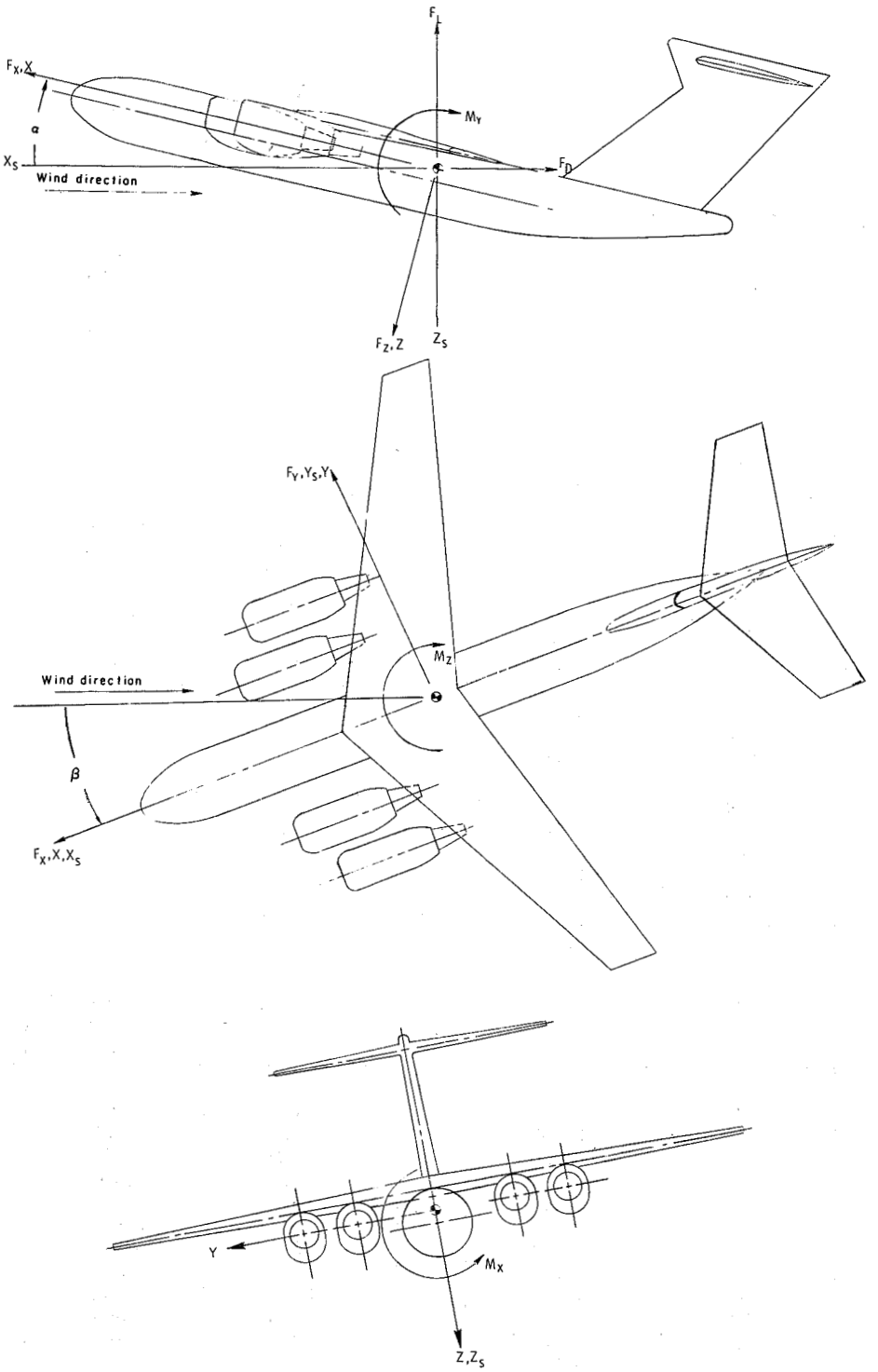

Figure 1.- System of axes; positive directions of forces, moments, and angles are indicated by arrows.

Wing:	
Airfoil section-root	NACA 63_2A214
Airfoil section-tip	NACA 63_2A211
Area, sq m (sq ft)	.499 (5.374)
Mean aerodynamic chord, m (ft)	.278 (.913)
Span, m (ft)	1.905(6.250)
Aspect ratio	7.269
Horizontal tail:	
Airfoil section	NACA 64-012
Area, sq m (sq ft)	.180 (1.940)
Mean aerodynamic chord, m (ft)	.221 (.724)
Span, m (ft)	.849 (2.784)
Aspect ratio	3.995
Vertical tail:	
Airfoil section	NACA 0012
Area, sq m (sq ft)	.183(1.968)
Mean aerodynamic chord, m (ft)	.374(1.228)
Span, m (ft)	493(1.617)
Aspect ratio	1.328

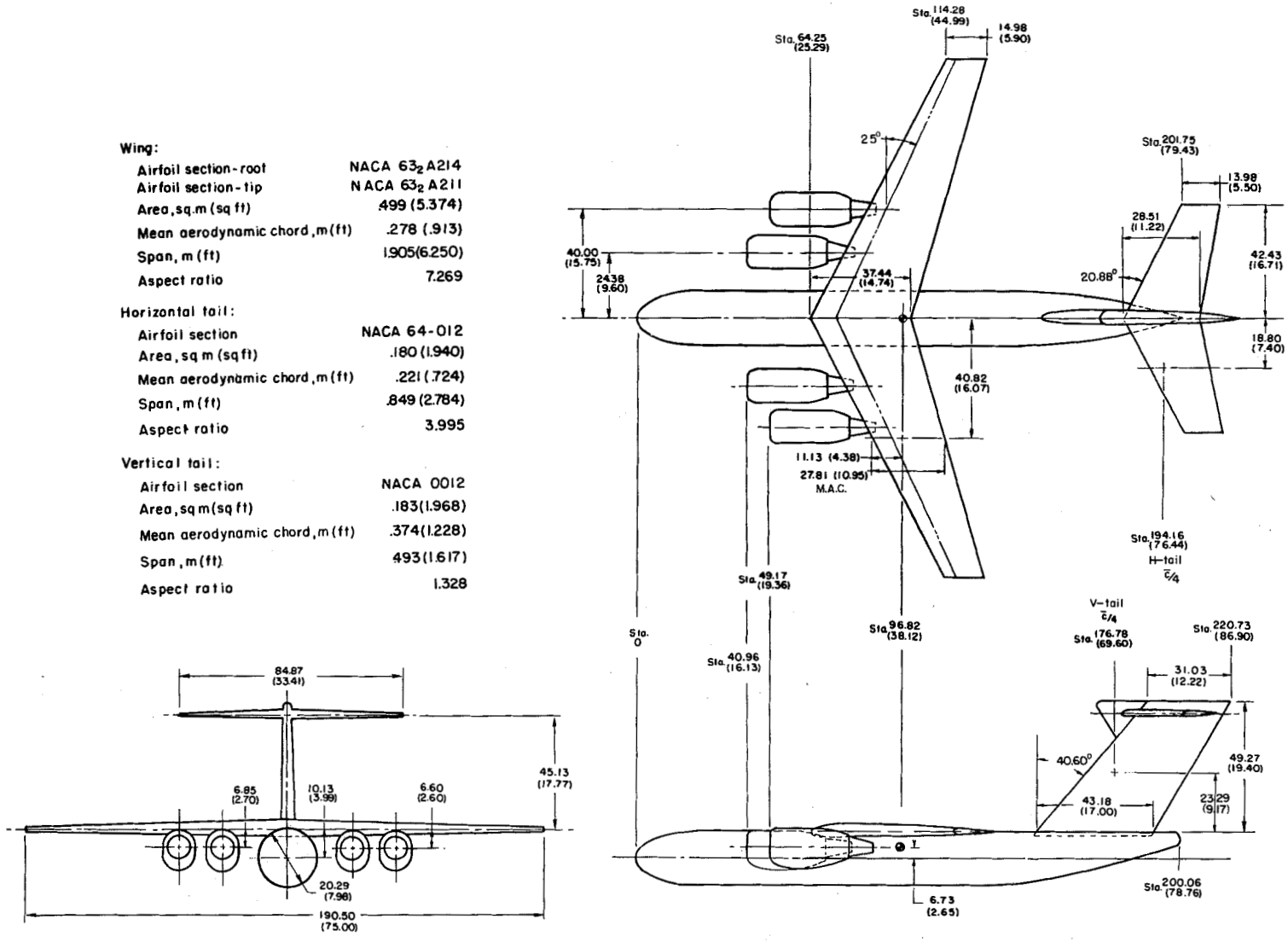

(a) Three-view drawing of complete model.

Figure 2.- Drawings of model used in investigation. All dimensions are in centimeters (inches) unless otherwise noted.

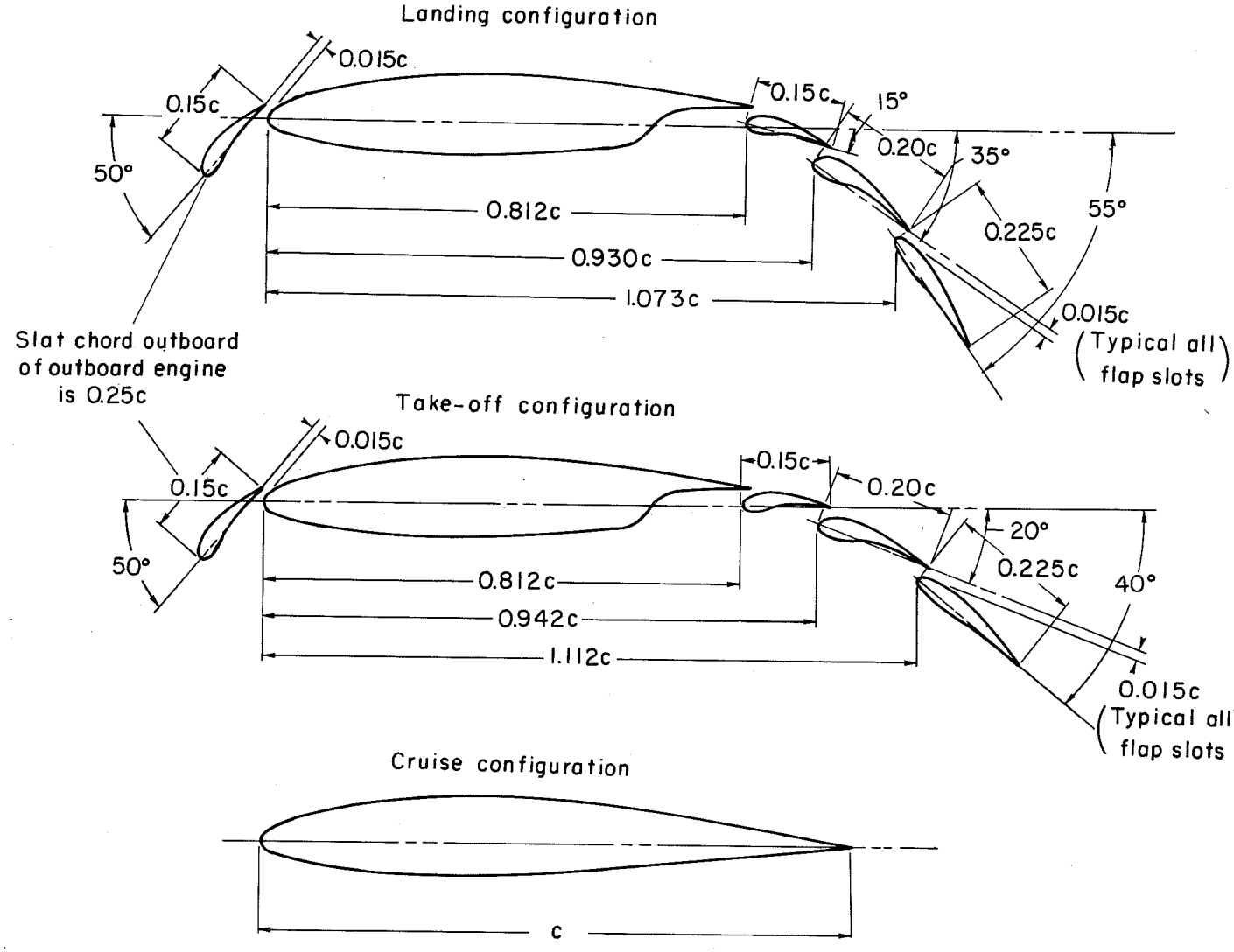

(b) Details of flap and slat assembly.

Figure 2.- Continued.

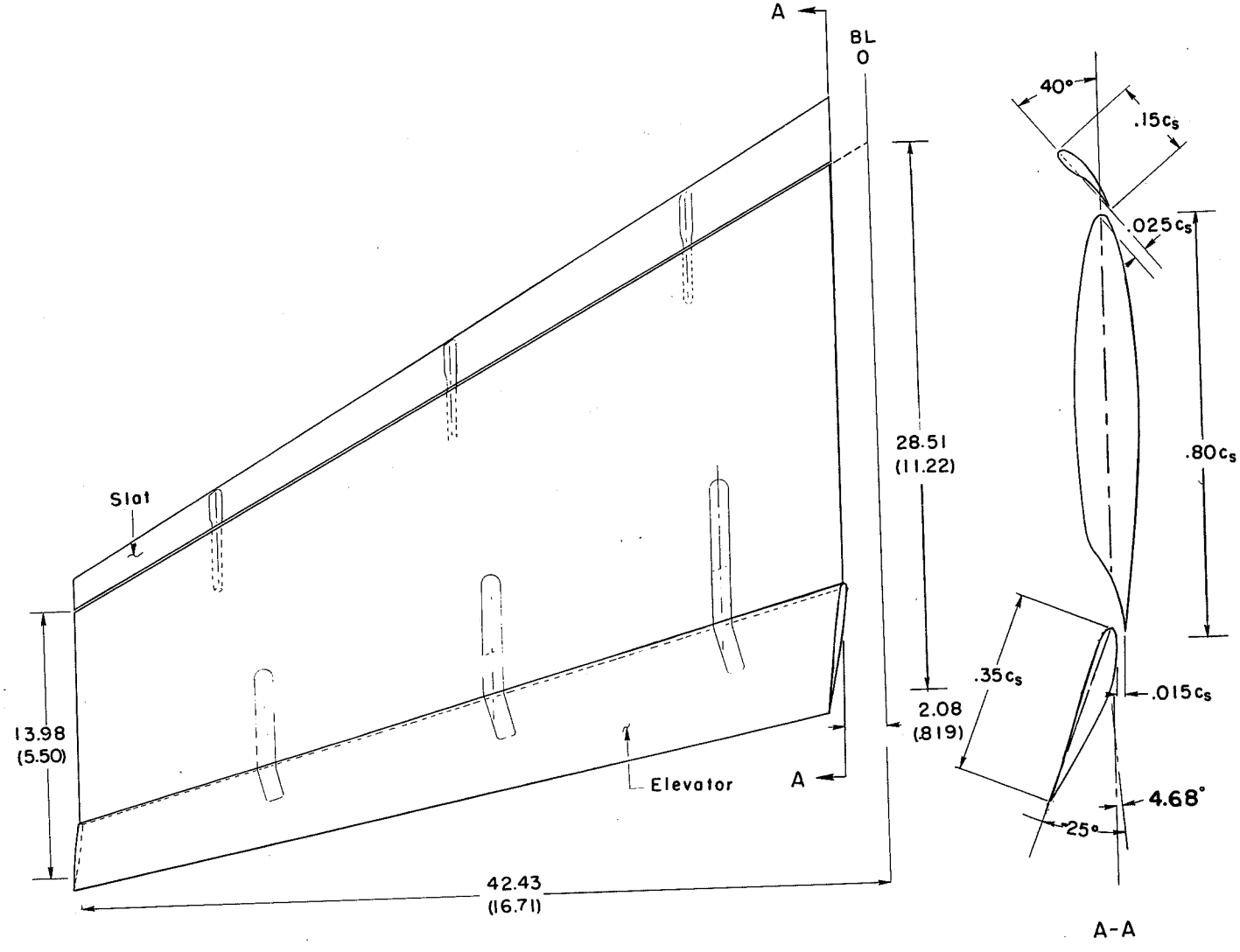

(c) Details of horizontal tail. (Elevator in middle setting.)

Figure 2.- Continued.

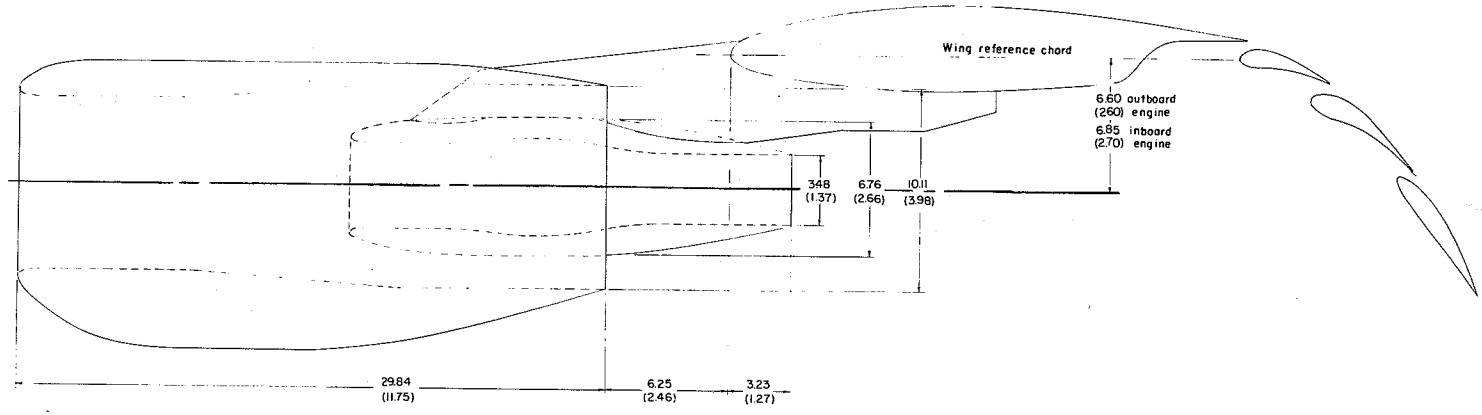

(d) Details of nacelle and engine pylon.

Figure 2.- Concluded.

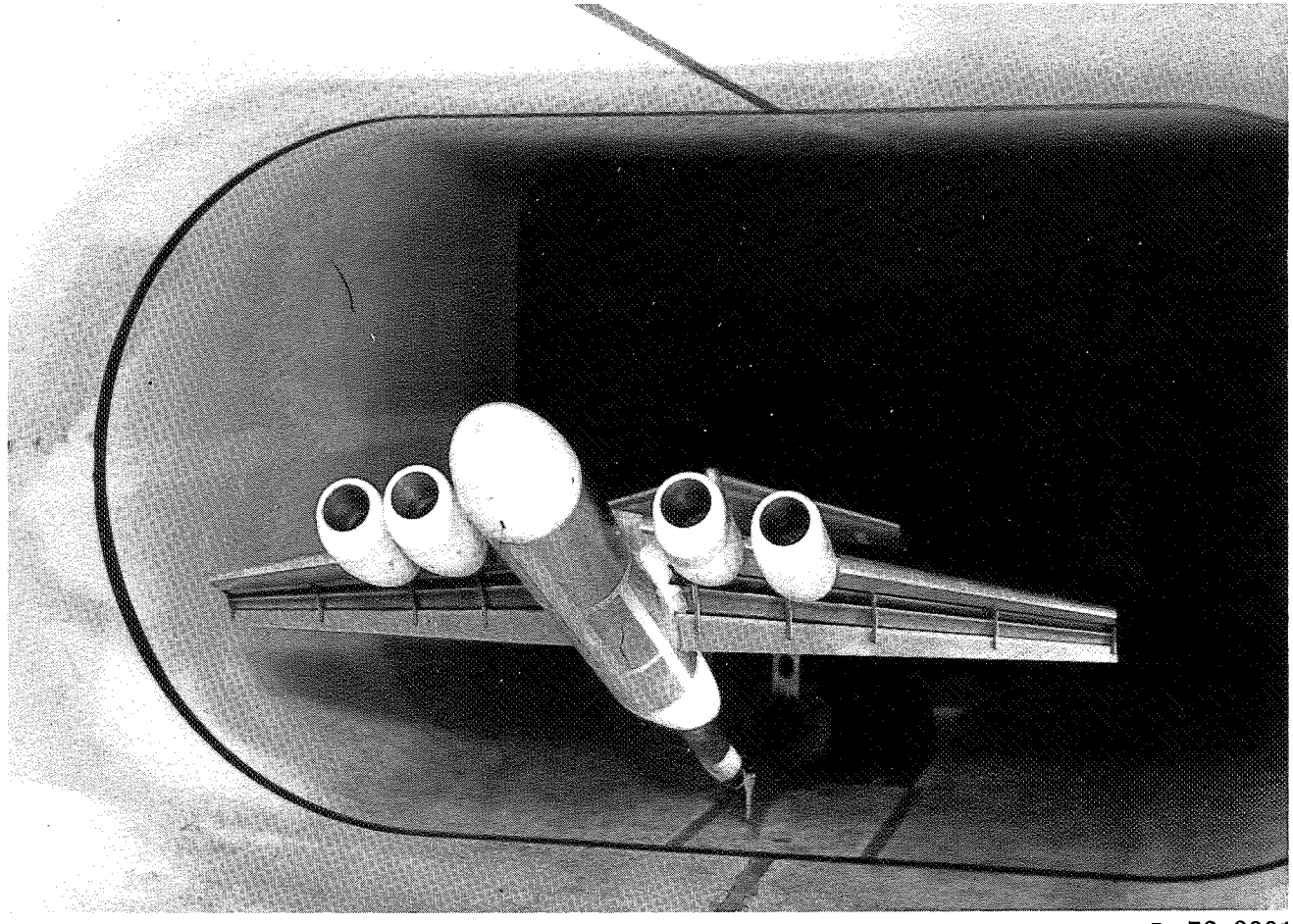

L-72-3001

(a) Three-quarter side view of landing configuration.

Figure 3.- Photographs of the model in the simulated Ames 40- by 80-foot tunnel test section installed in the Langley V/STOL tunnel. $\alpha = 25^{o}$.

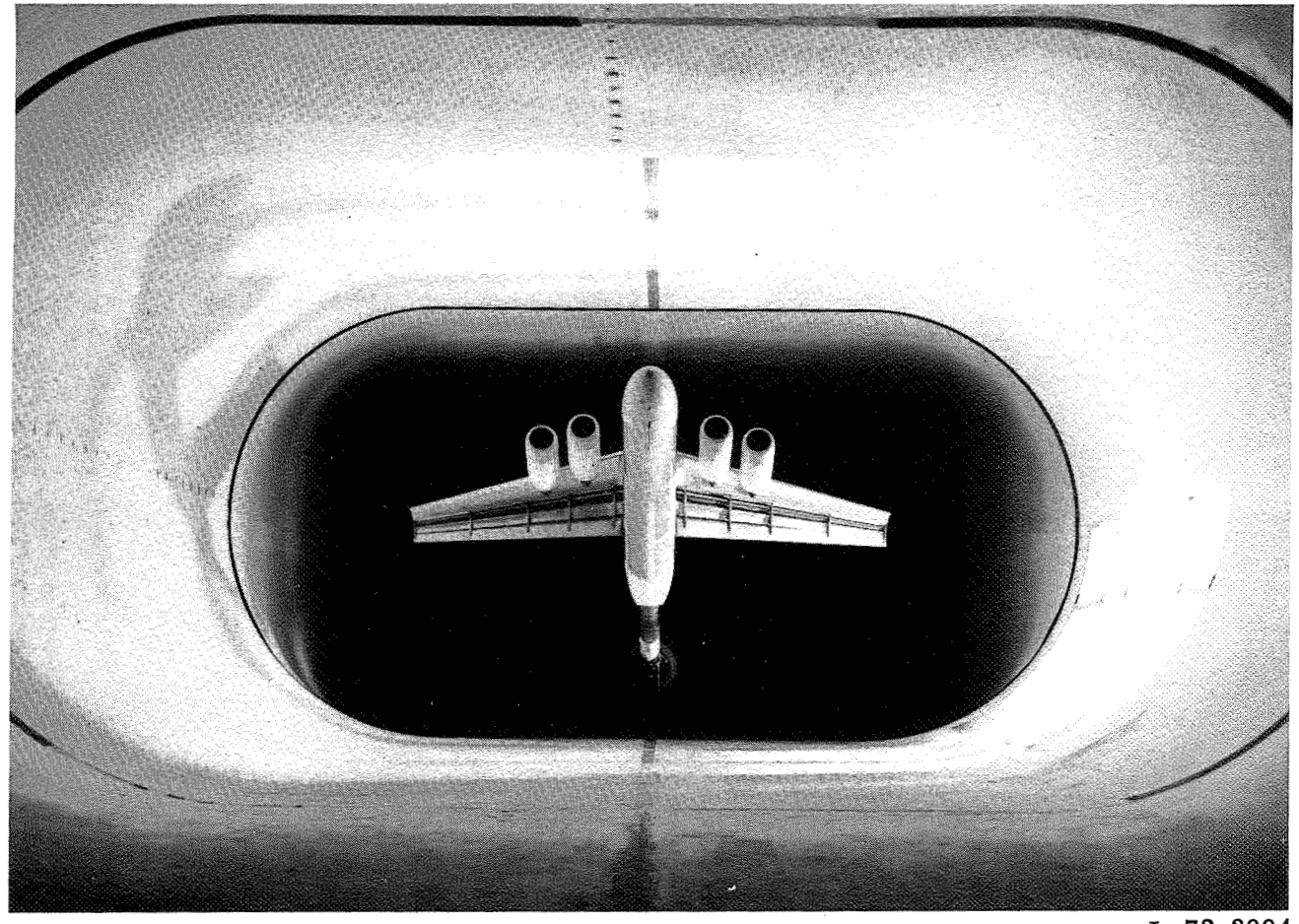

L-72-3004

(b) Front view of landing configuration in the liner simulating the Ames tunnel.

Figure 3.- Continued.

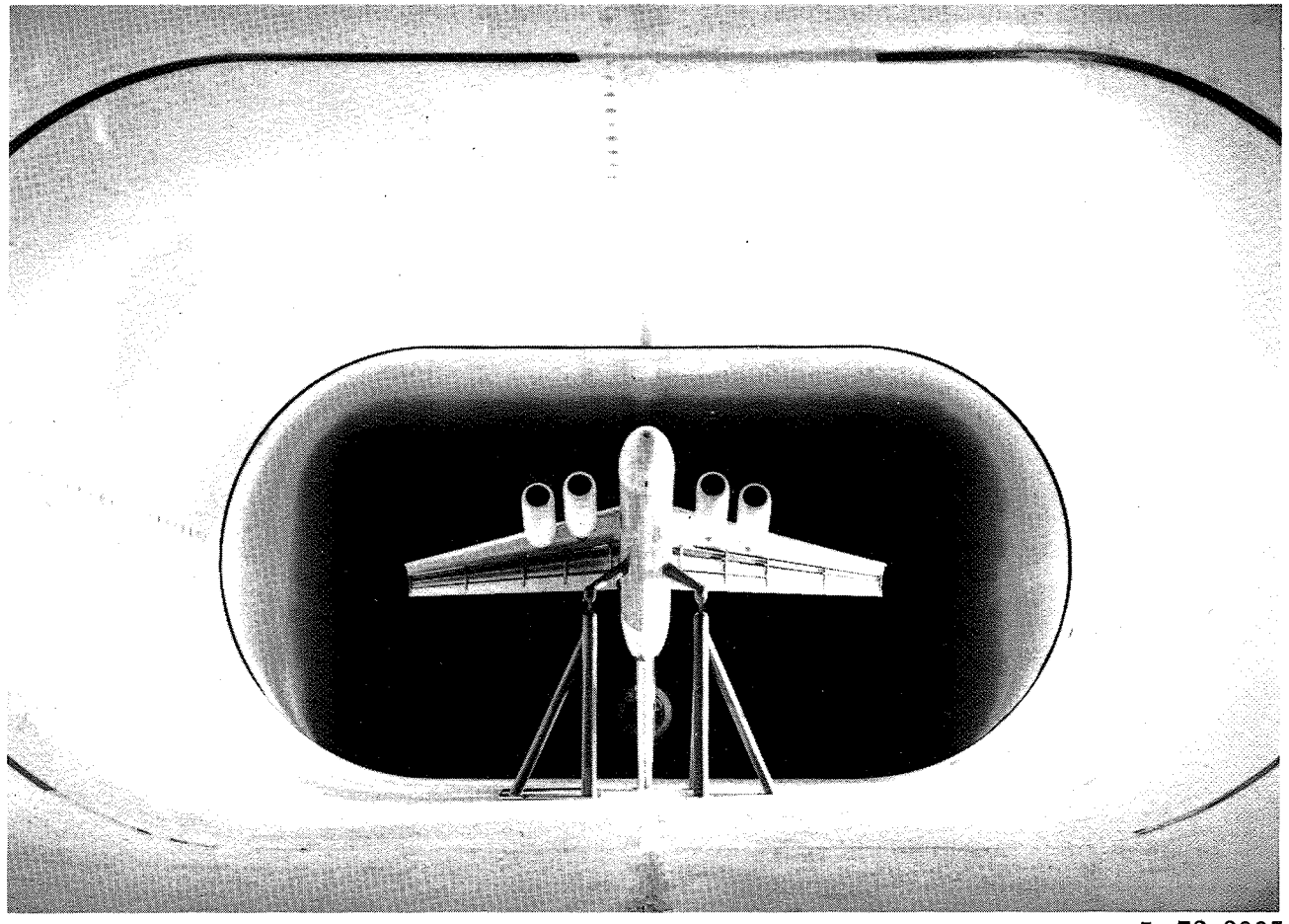

L-72-3005

(c) Front view of landing configuration in the liner with simulated mounting struts installed.

Figure 3.- Concluded.

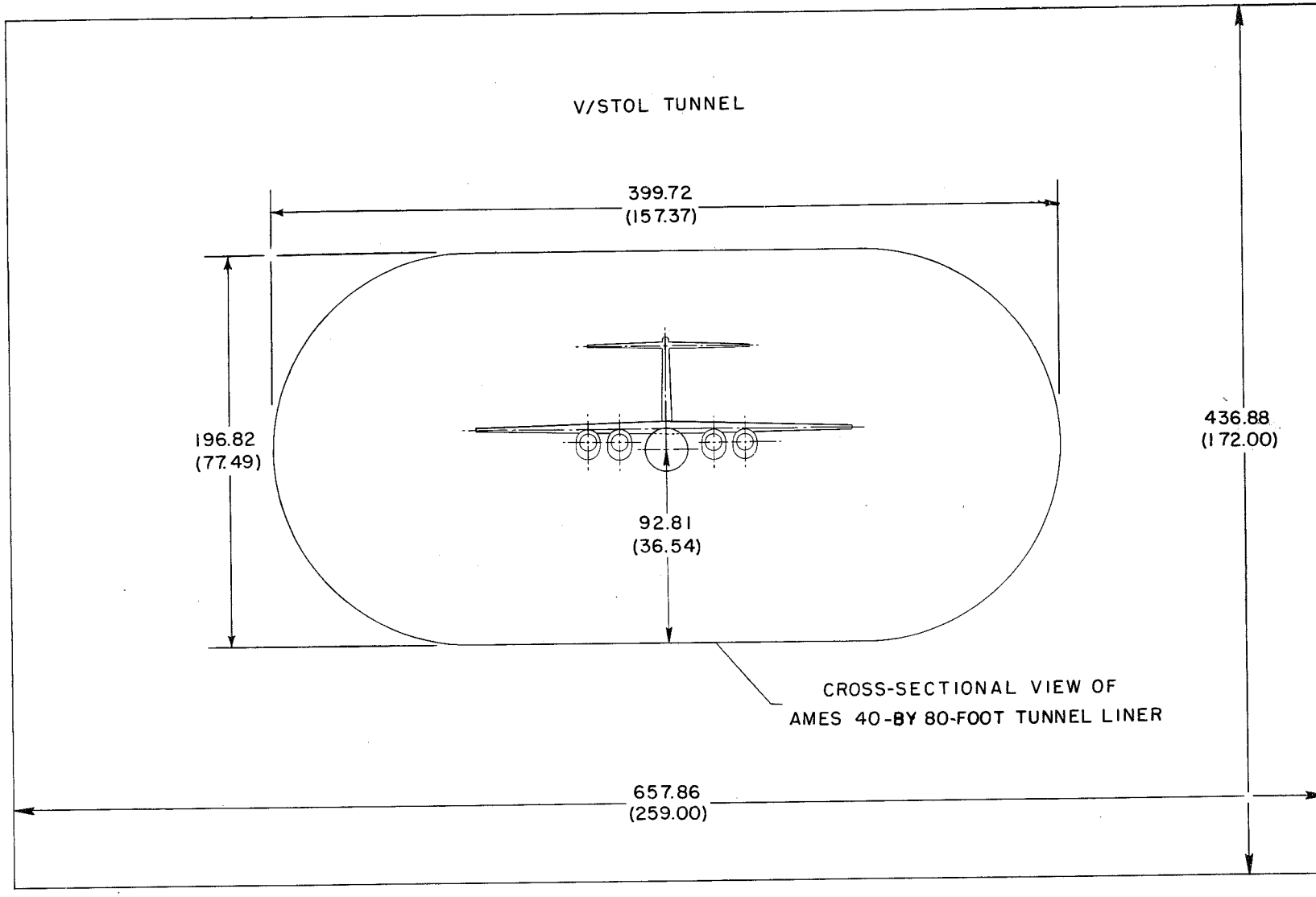

Figure 4.- Cross-sectional view of Ames 40- by 80-foot tunnel liner in the Langley V/STOL tunnel test section. All dimensions are in centimeters (inches).

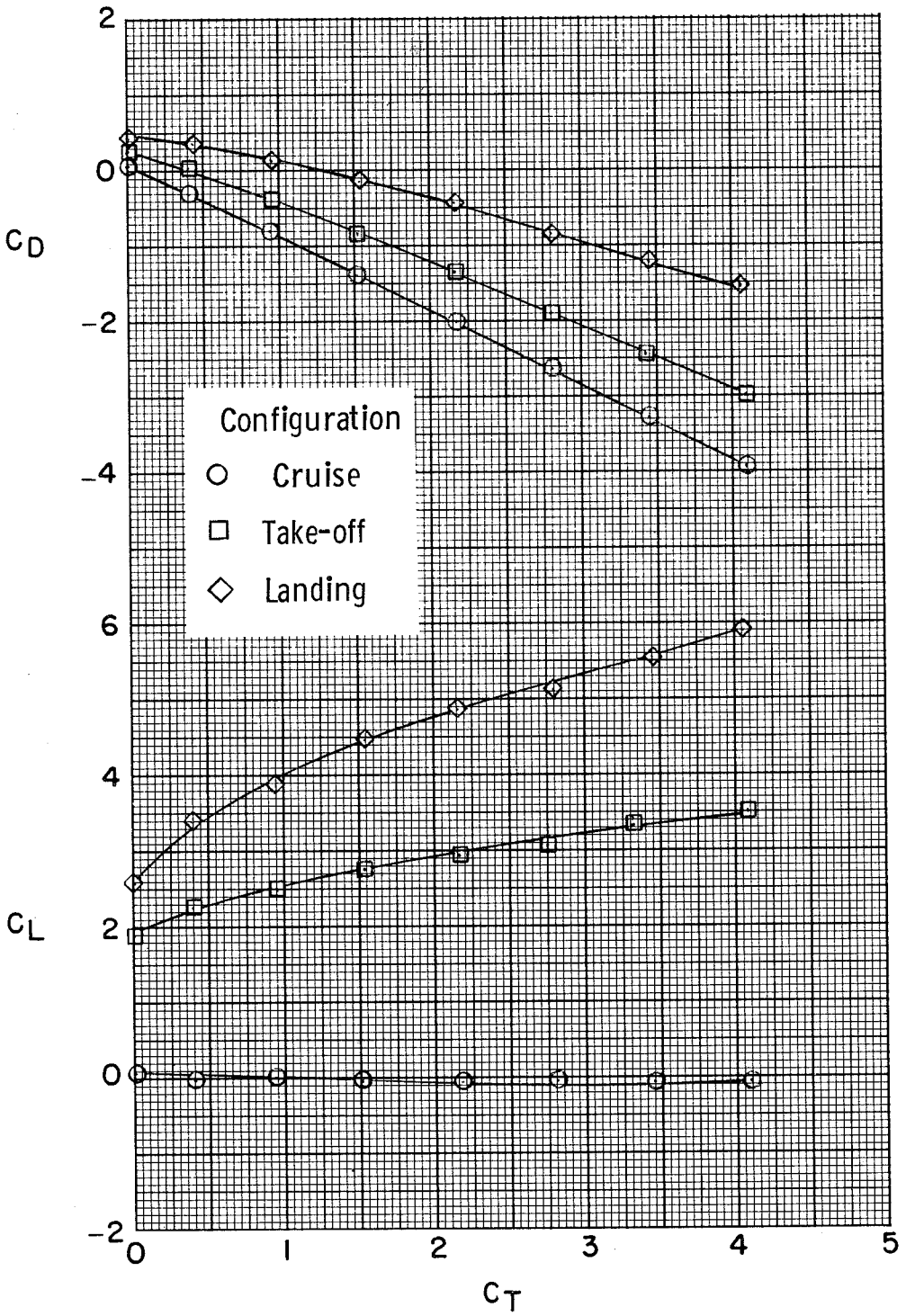

(a) Variation of longitudinal characteristics with thrust coefficients.

Figure 5.- Effect of flap deflections. $\alpha = 0^{o}$; tail off.

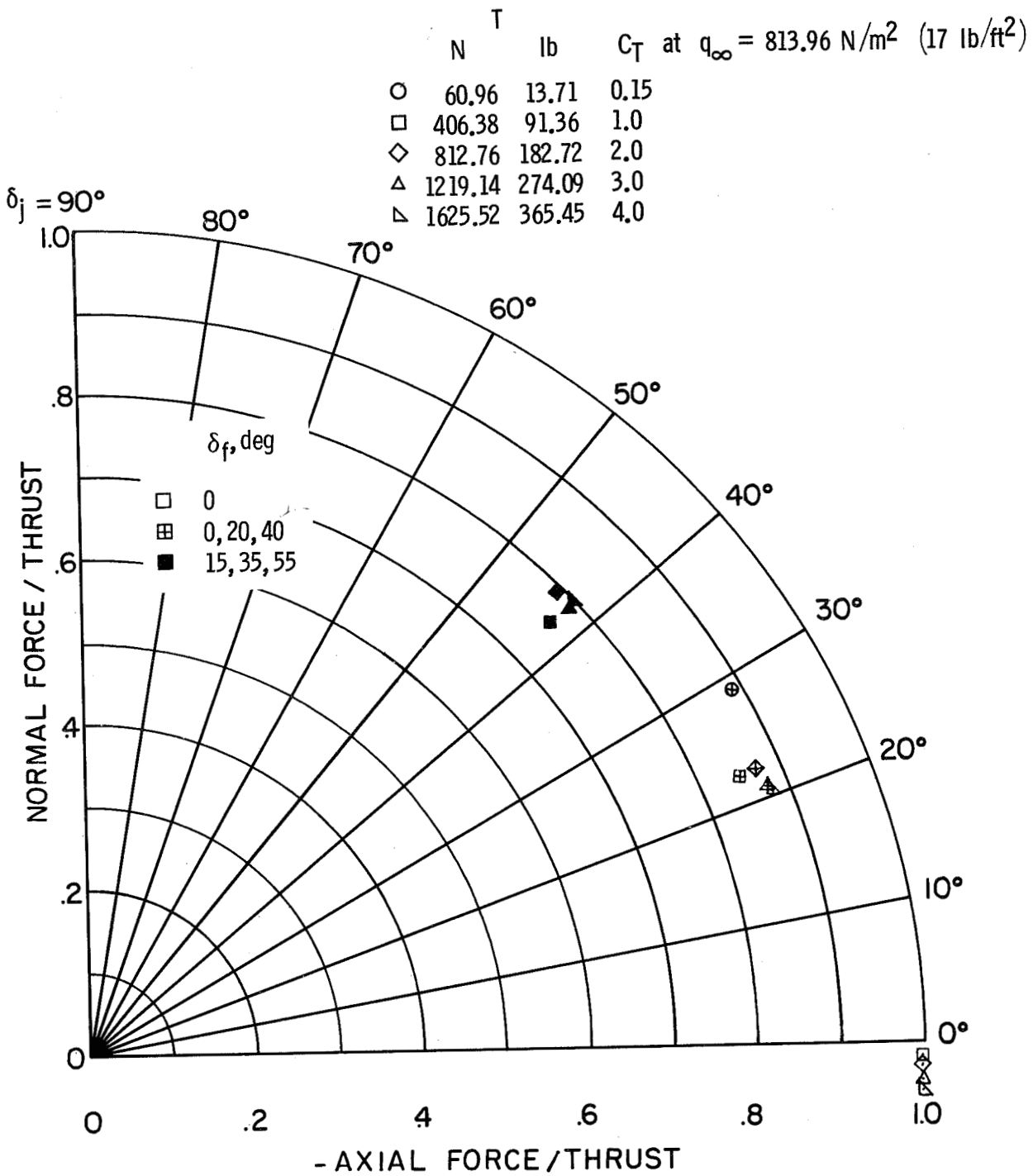

(b) Static turning characteristics.

Figure 5.- Concluded.

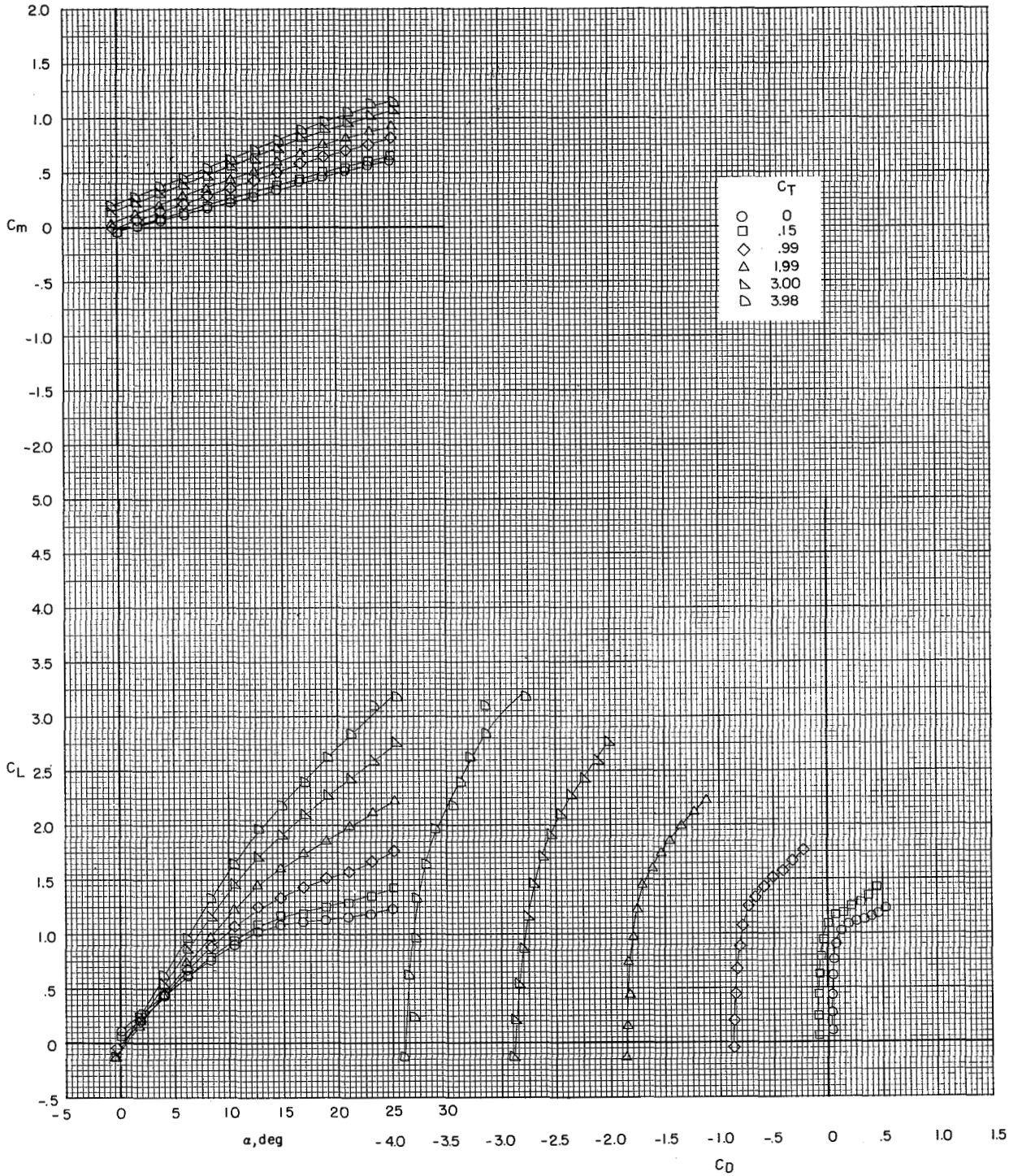

Figure 6.- Effect of thrust coefficient on longitudinal aerodynamic characteristics of the cruise configuration. Tail off. Model in the V/STOL tunnel with the tunnel liner installed.

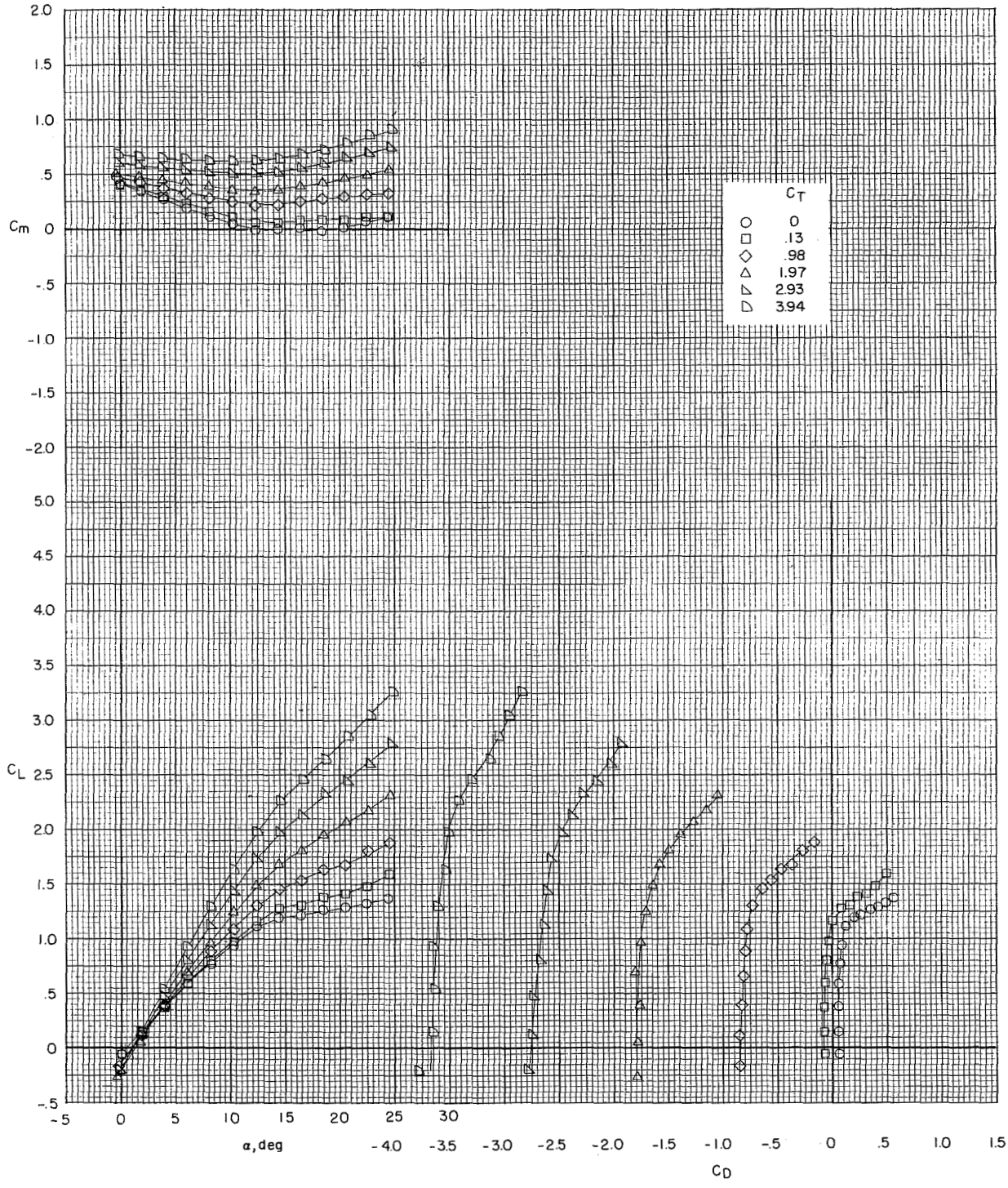

(a) $i_t = -5^o$.

Figure 7.- Effect of thrust coefficient on longitudinal aerodynamic characteristics of the cruise configuration. $\delta_e = 0^o$; model in the V/STOL tunnel with the tunnel liner installed.

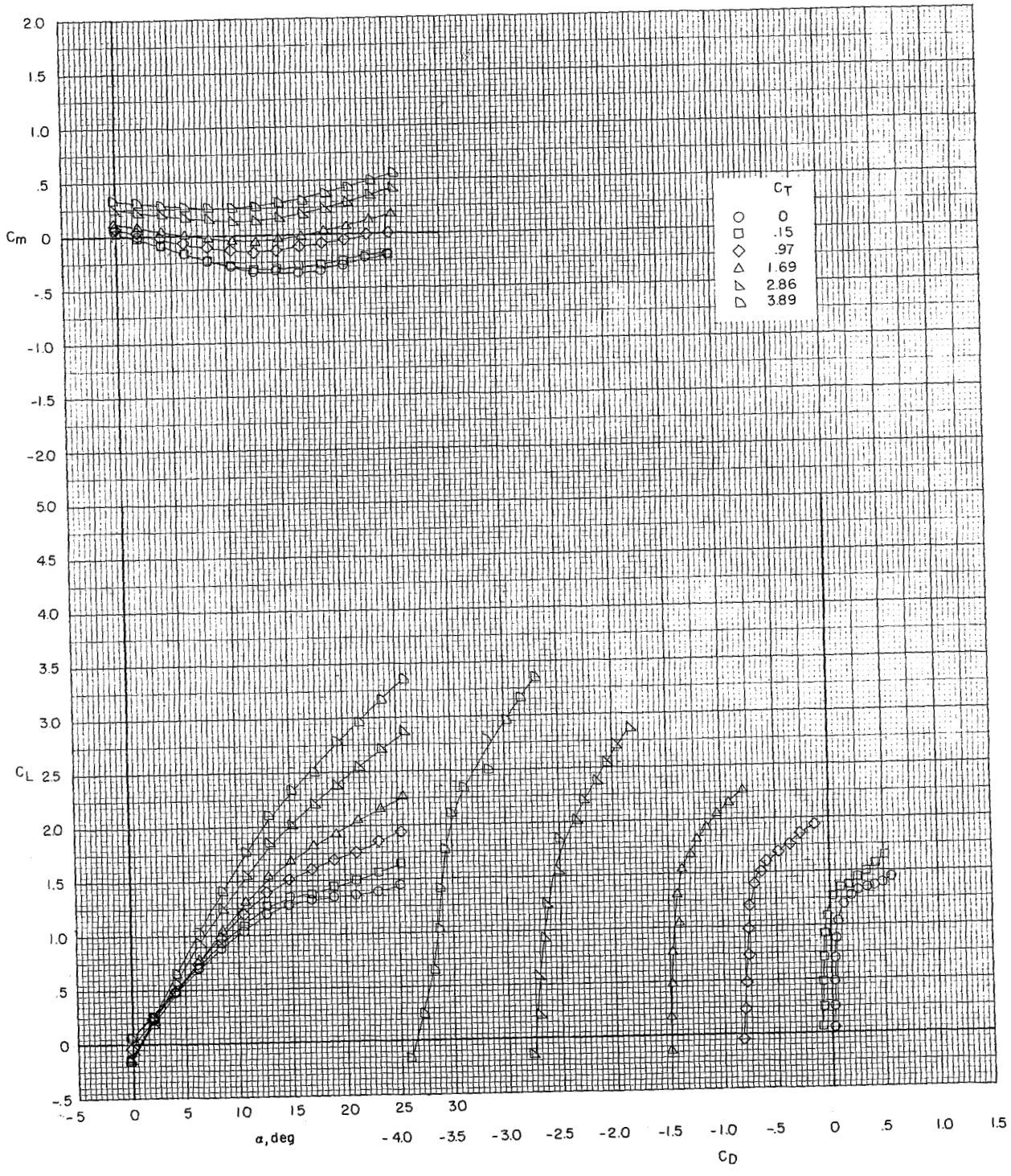

(b) $i_t = 0^o$.

Figure 7.- Continued.

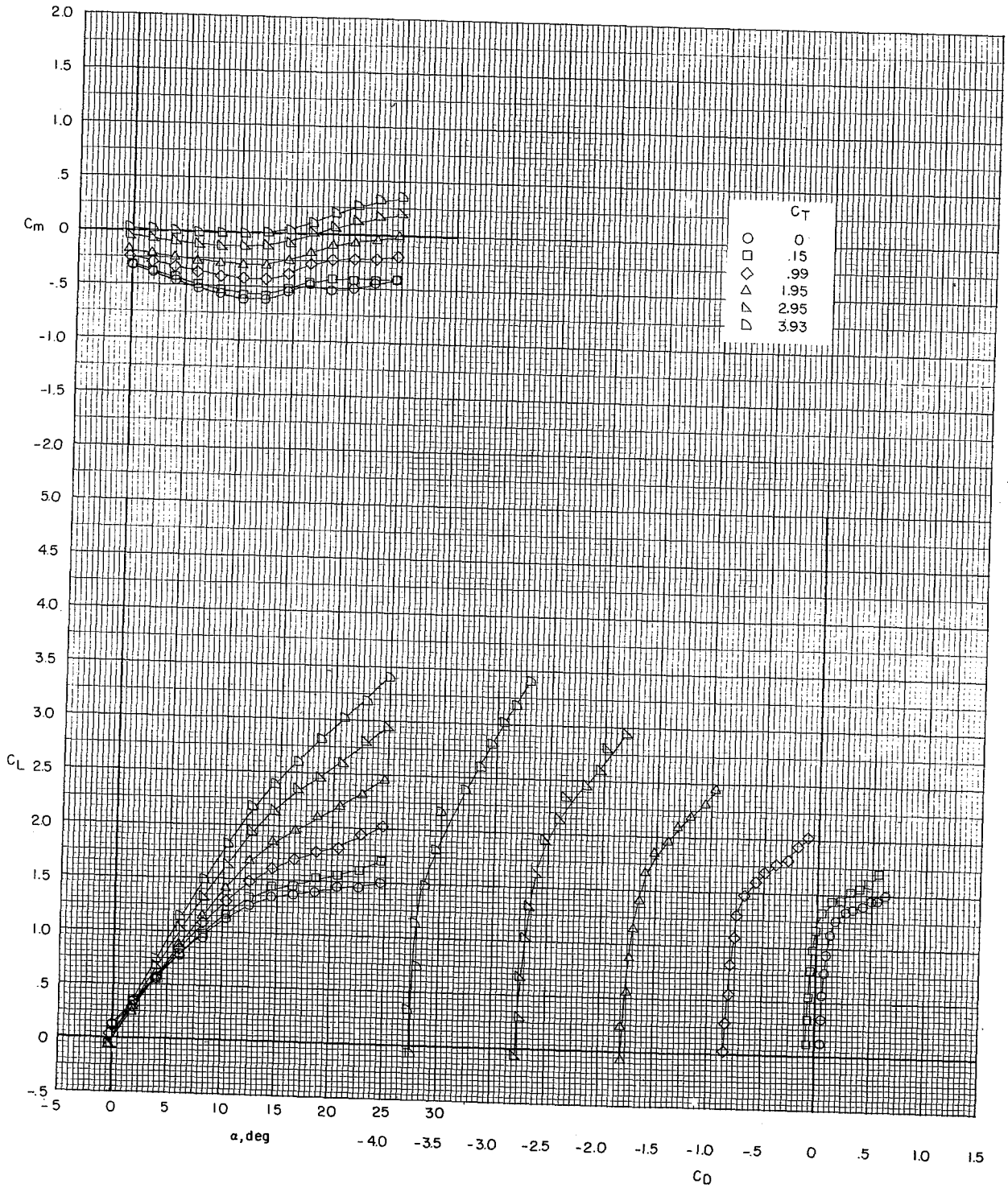

(c) $i_t = 5^o$.

Figure 7.- Concluded.

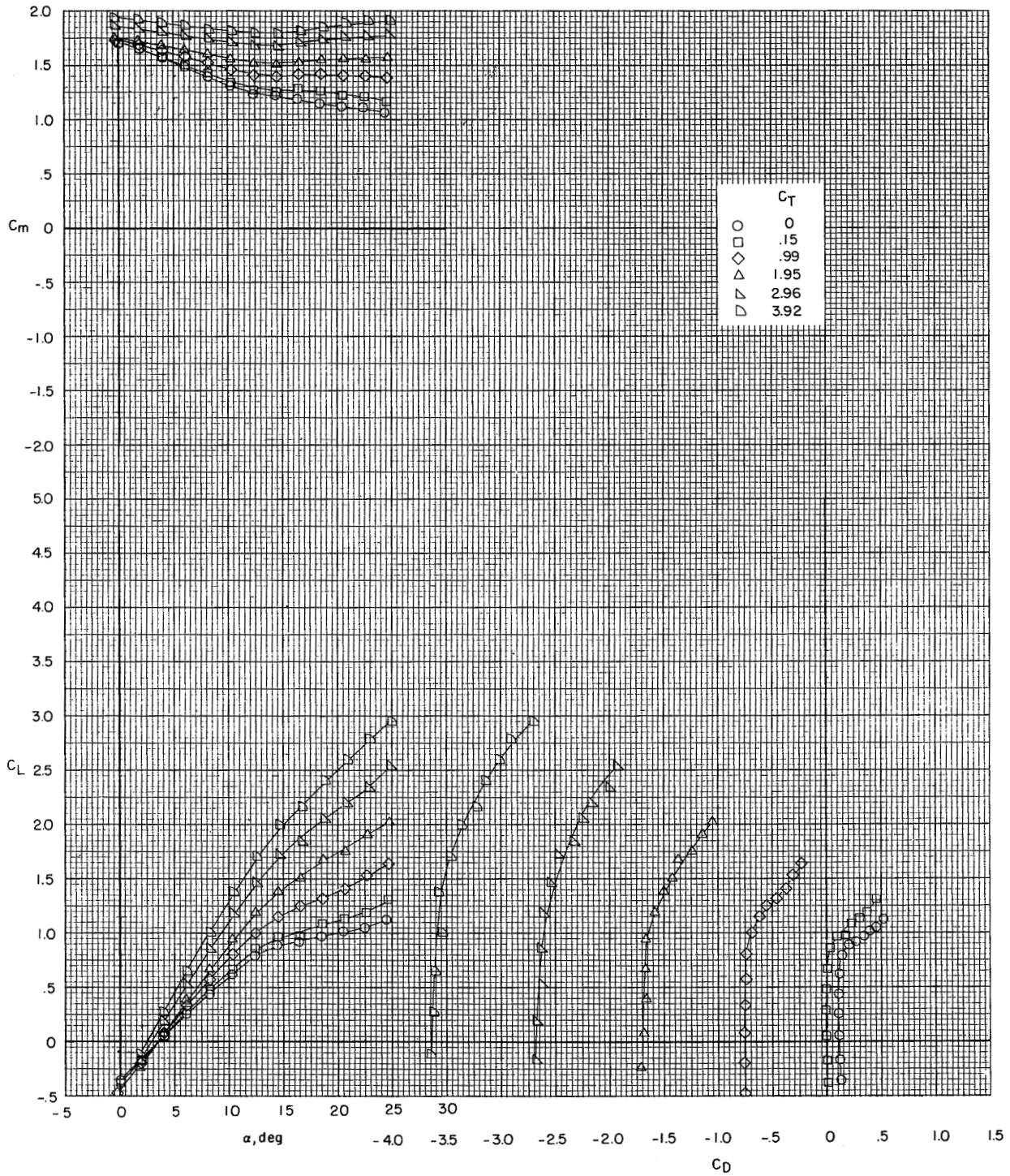

(a) $i_t = -5^o$.

Figure 8.- Effect of thrust coefficient on longitudinal aerodynamic characteristics of the cruise configuration. $\delta_e = -25^o$; model in the V/STOL tunnel with the tunnel liner installed.

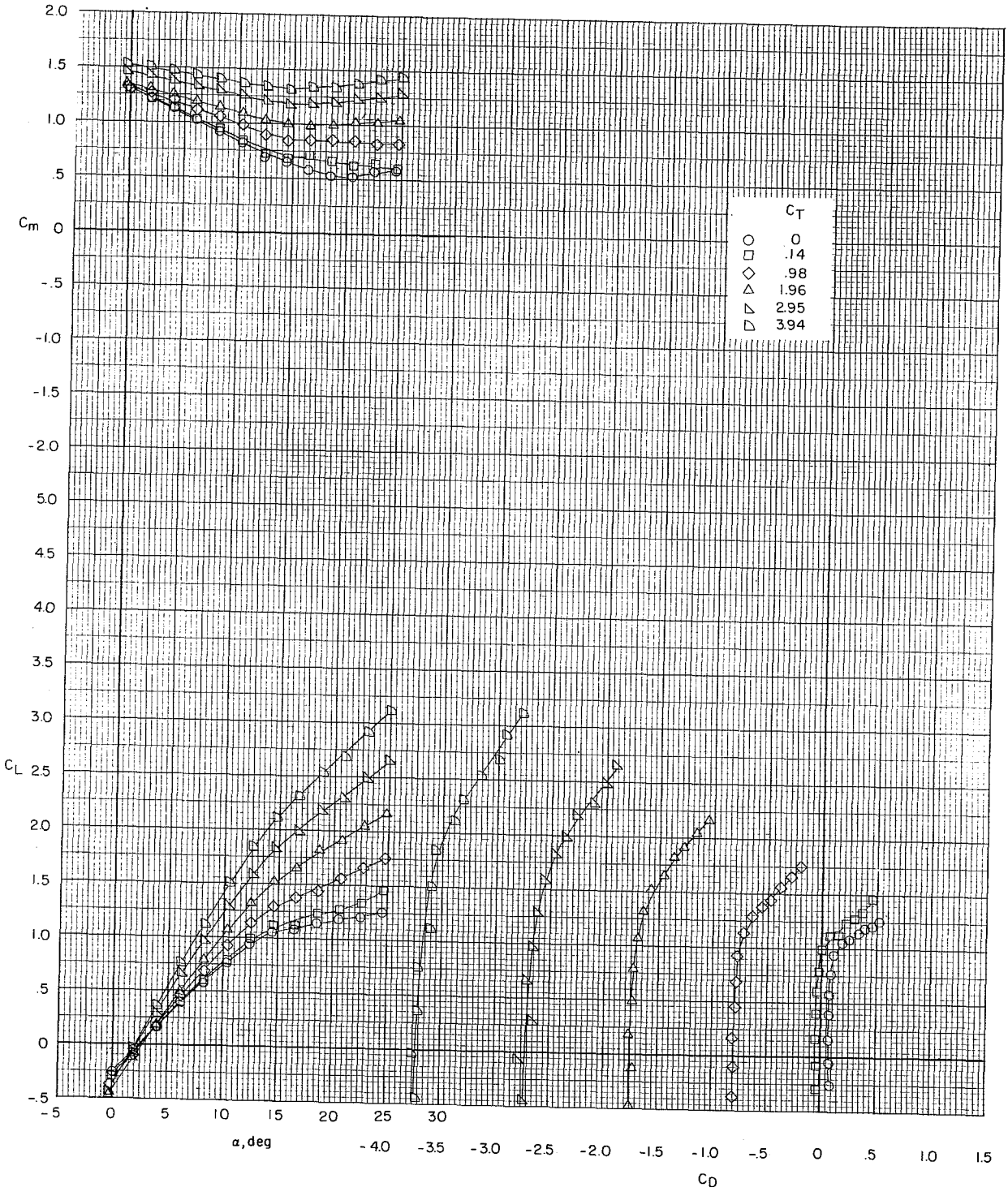

(b) $i_t = 0^o$.

Figure 8.- Continued.

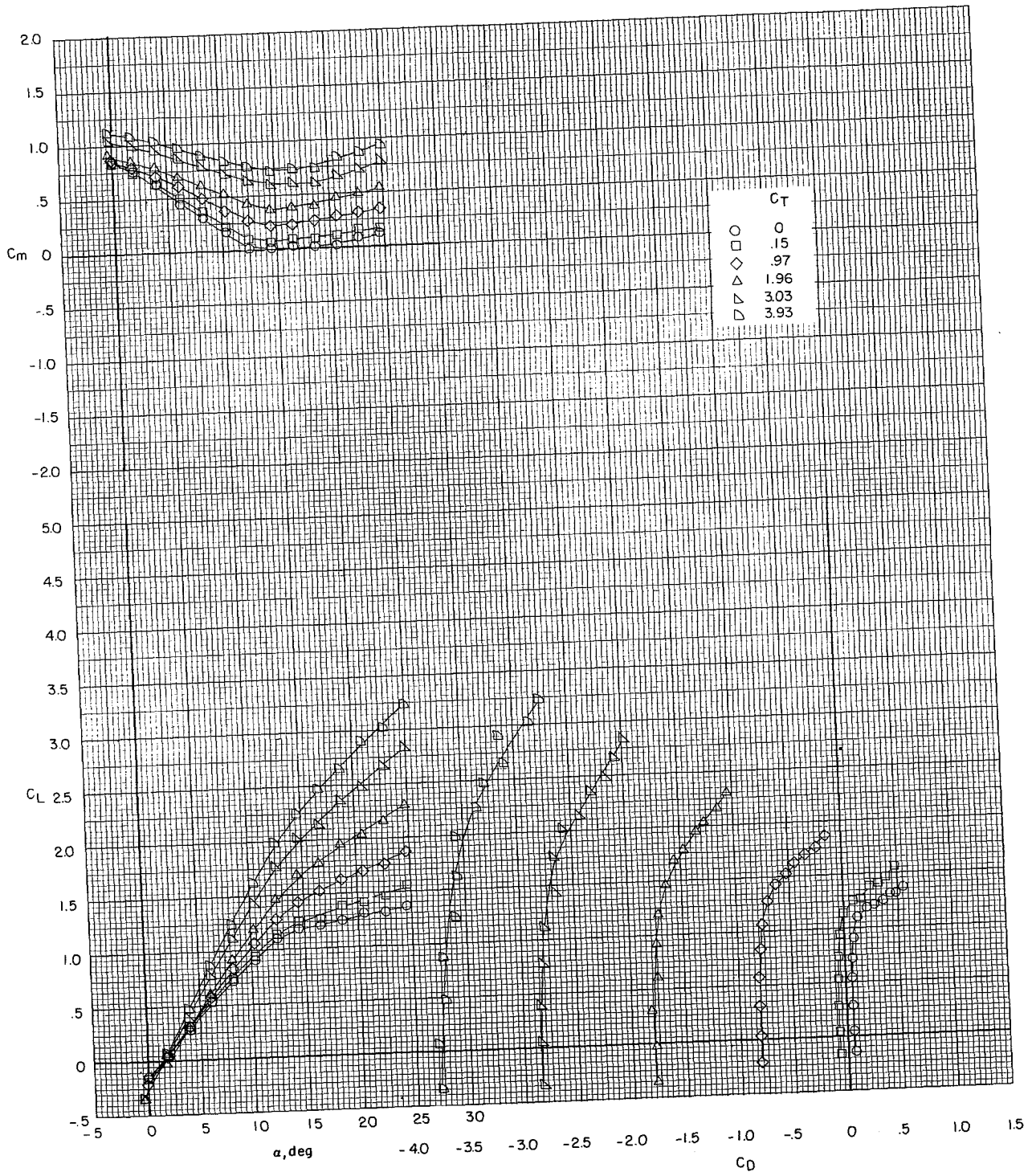

(c) $i_t = 5^o$.

Figure 8.- Concluded.

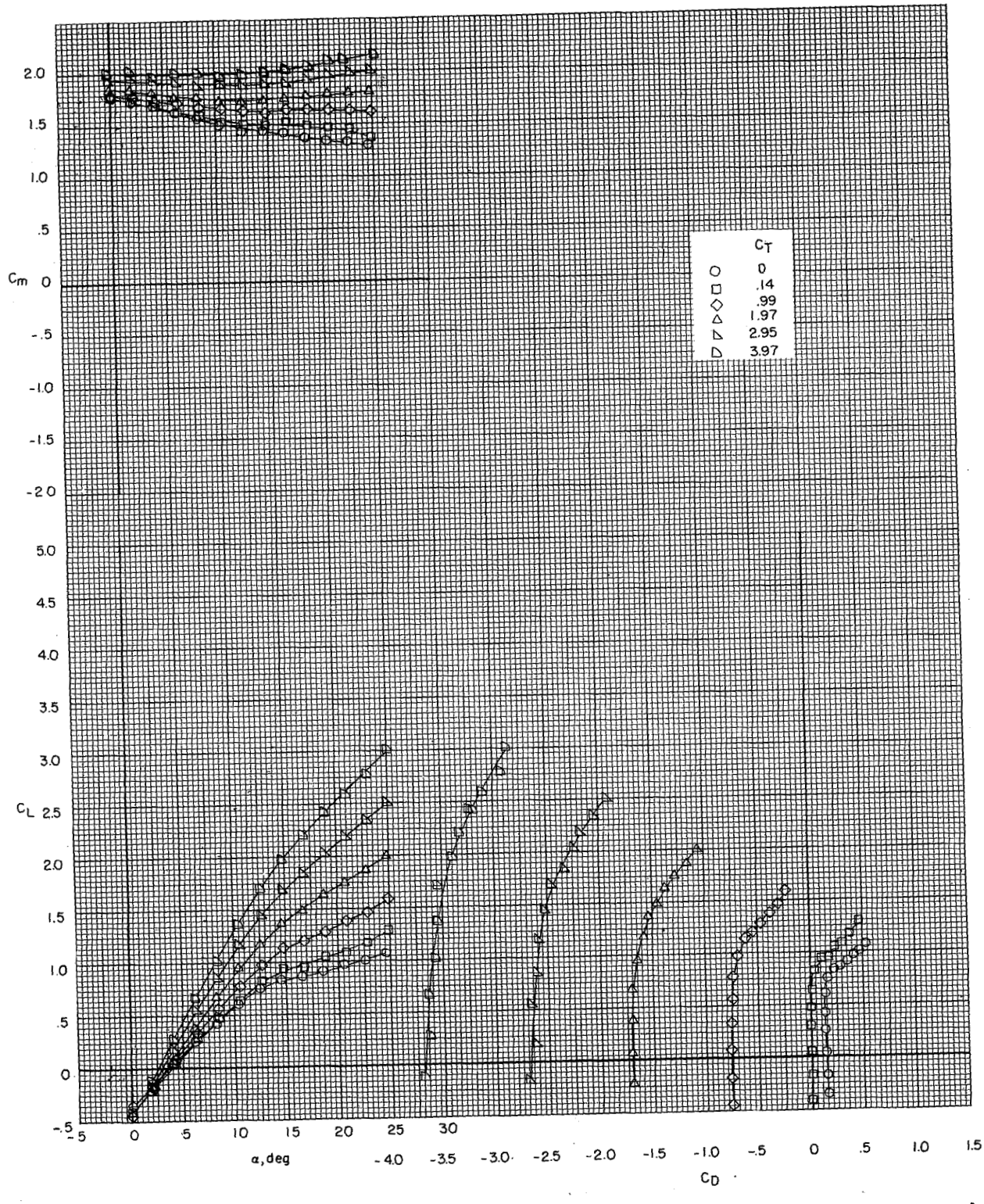

Figure 9.- Effect of thrust coefficient on longitudinal aerodynamic characteristics of the cruise configuration. $\delta_e = -50^o$; model in the V/STOL tunnel with the tunnel liner installed. $i_t = 0^o$.

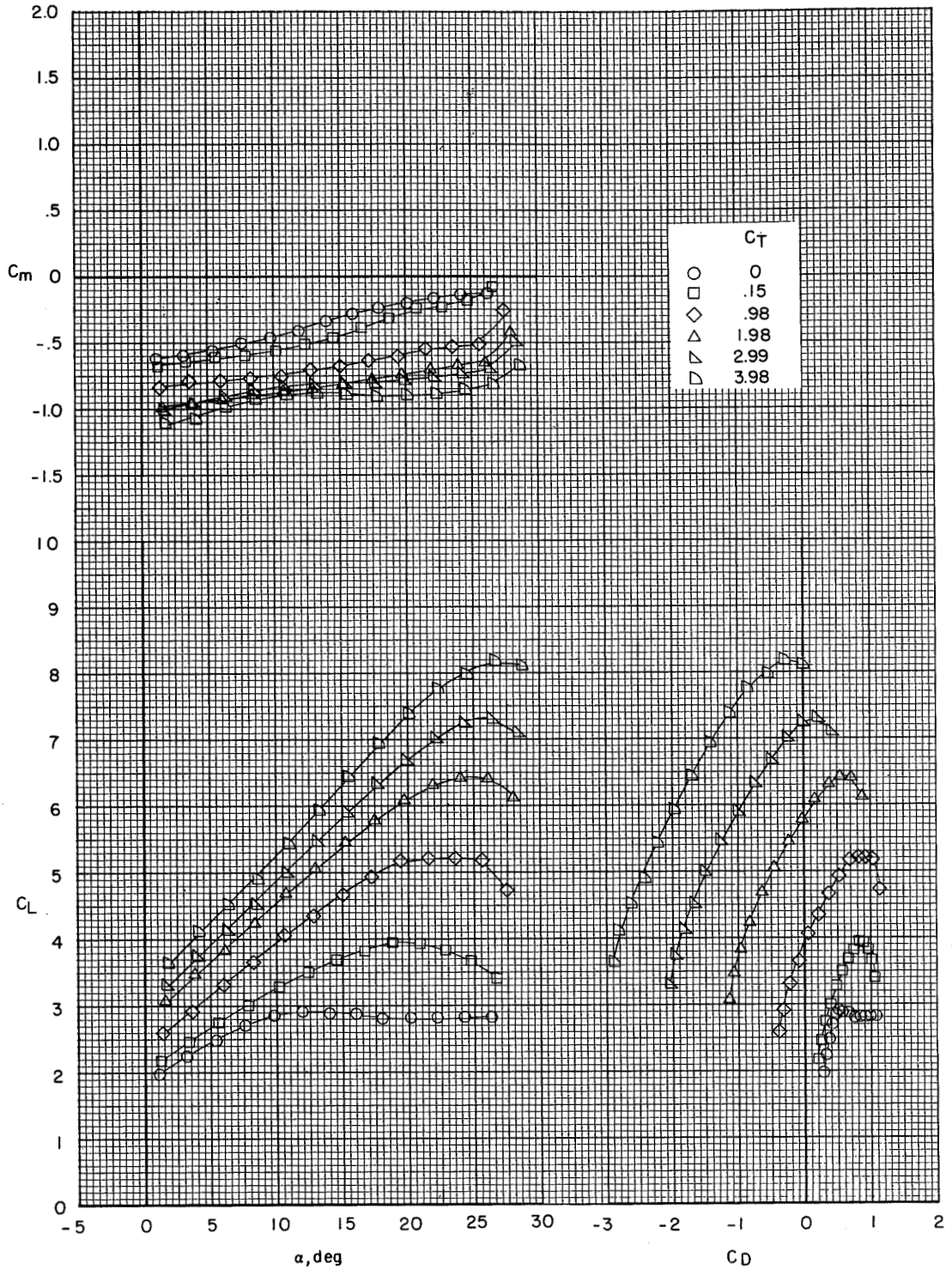

Figure 10.- Effect of thrust coefficient on longitudinal aerodynamic characteristics of the take-off configuration. Tail off. Model in the V/STOL tunnel with the tunnel liner installed.

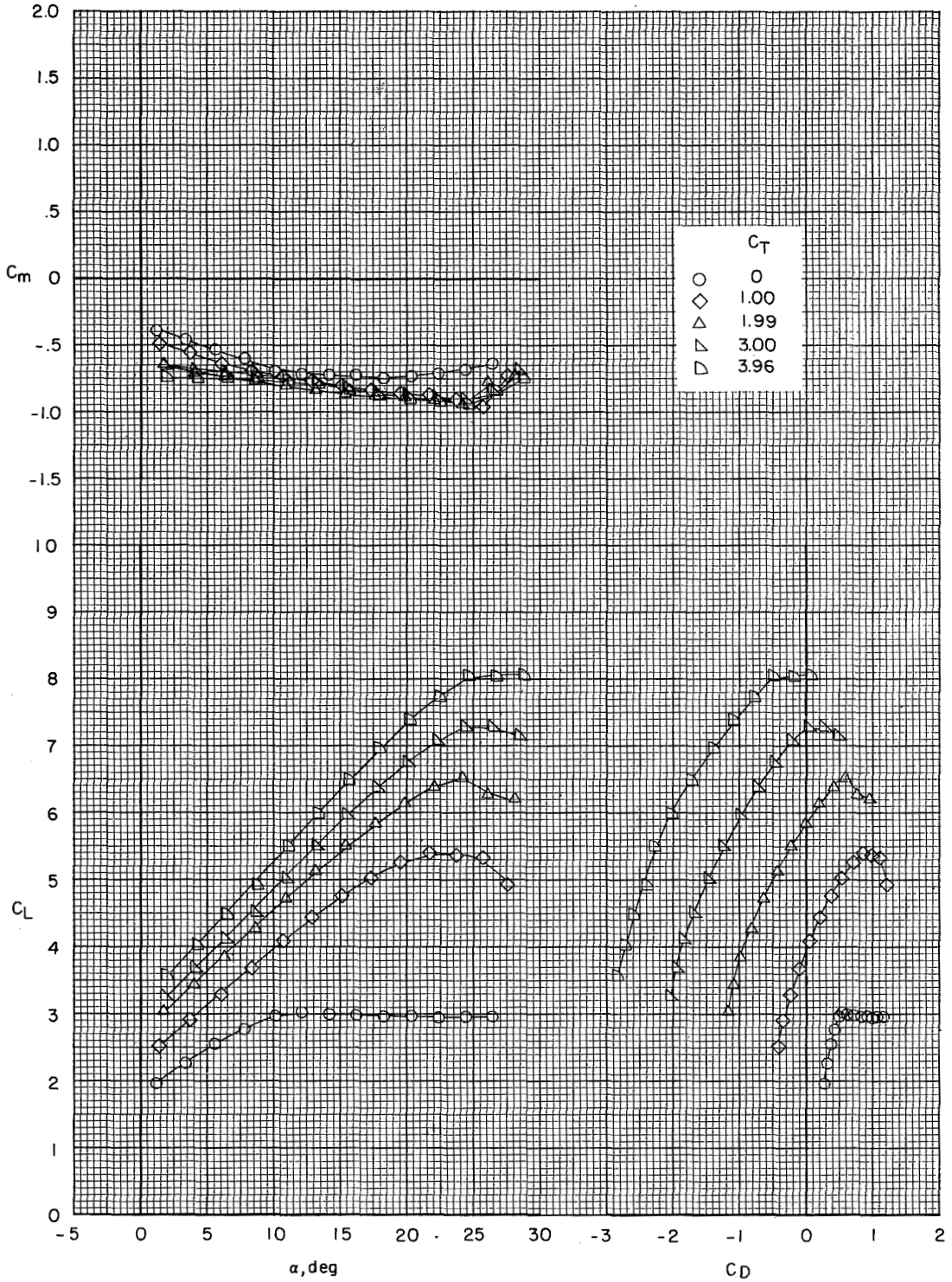

(a) $i_t = 0^o$.

Figure 11.- Effect of thrust coefficient on longitudinal aerodynamic characteristics of the take-off configuration. $\delta_e = 0^o$. Model in the V/STOL tunnel with the tunnel liner installed.

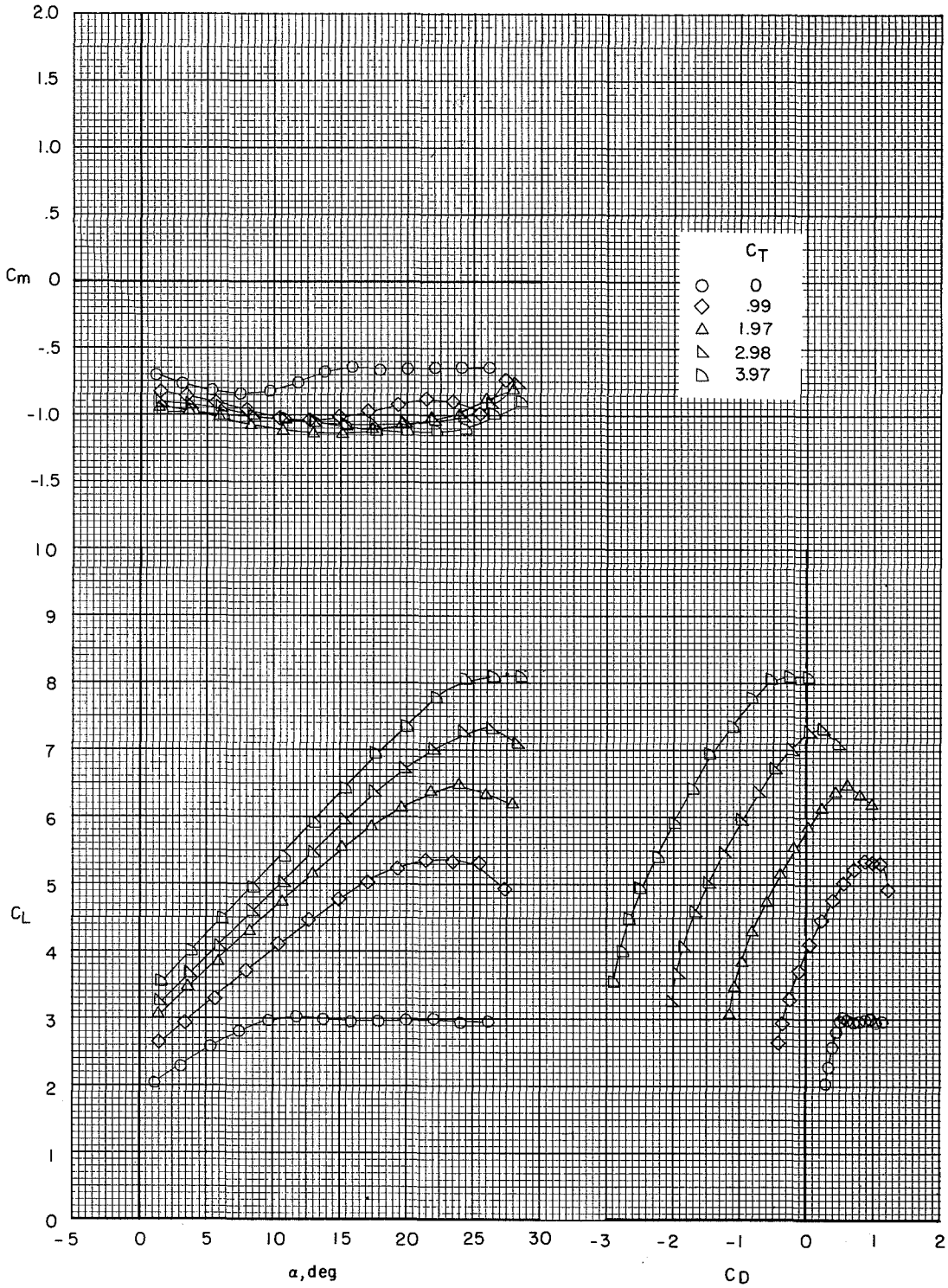

(b) $i_t = 5^o$.

Figure 11.- Continued.

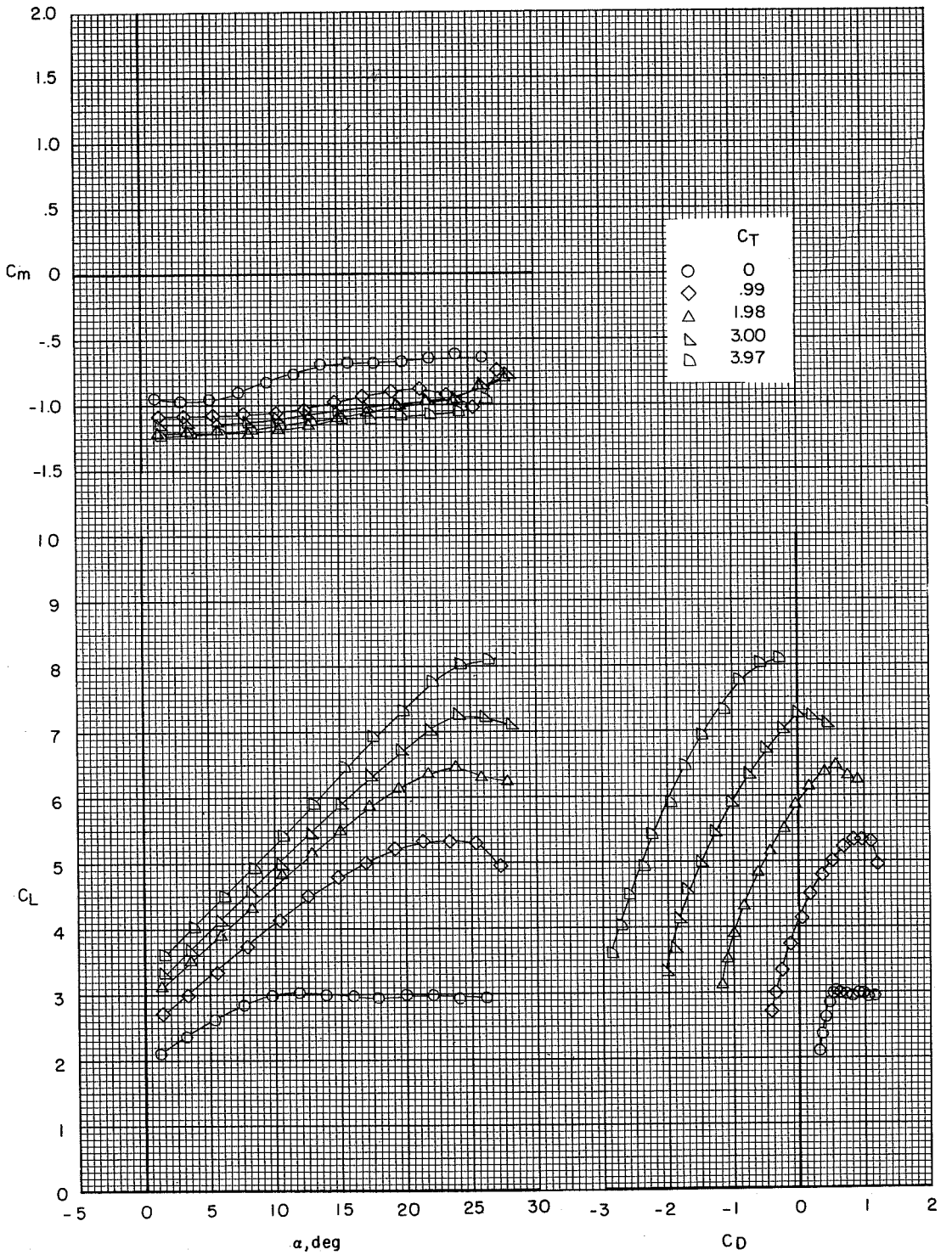

(c) $i_t = 10^o$.

Figure 11.- Concluded.

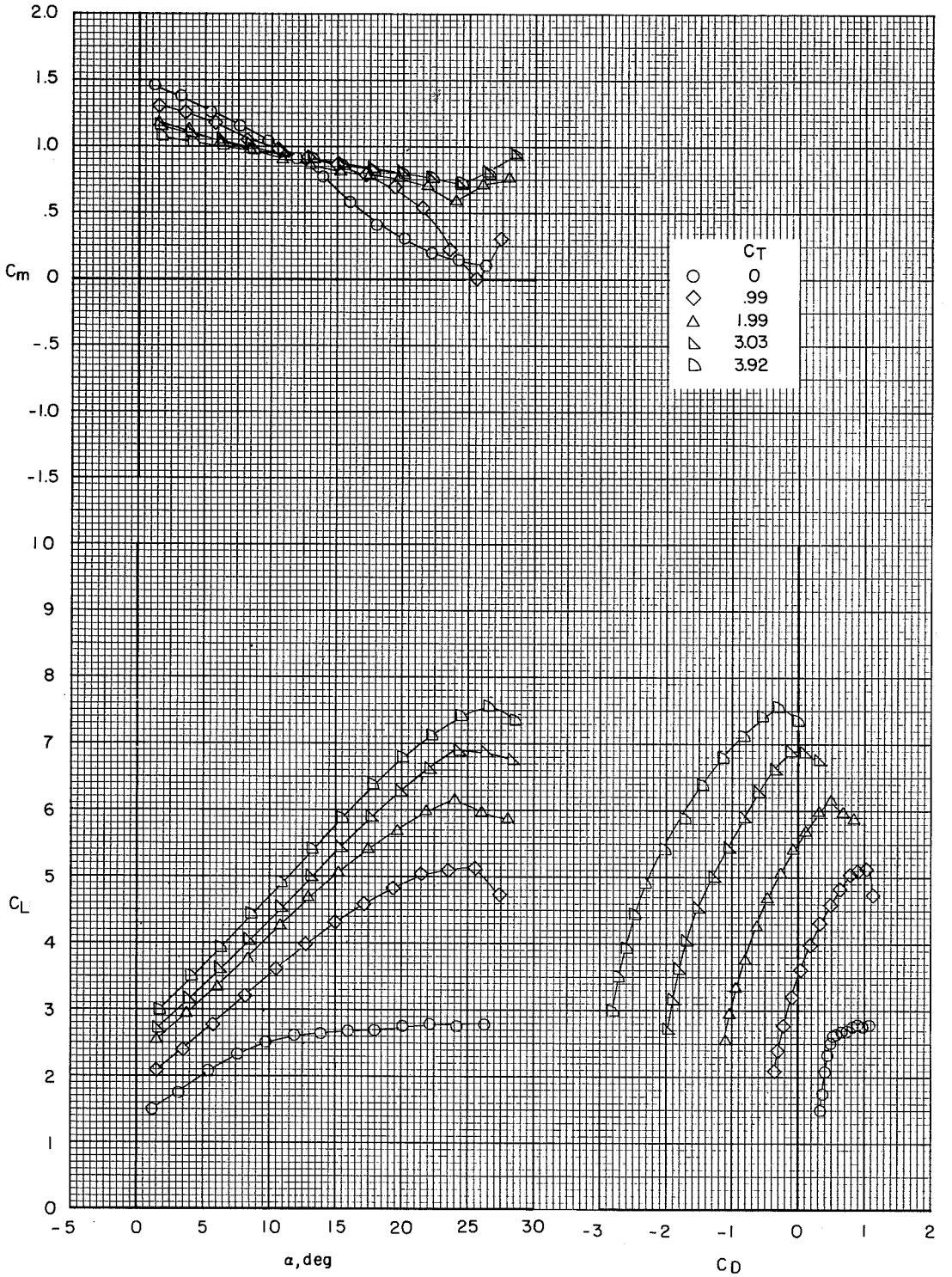

(a) $i_t = -5^o$.

Figure 12.- Effect of thrust coefficient on longitudinal aerodynamic characteristics of the take-off configuration. $\delta_e = -25^o$. Model in the V/STOL tunnel with the tunnel liner installed.

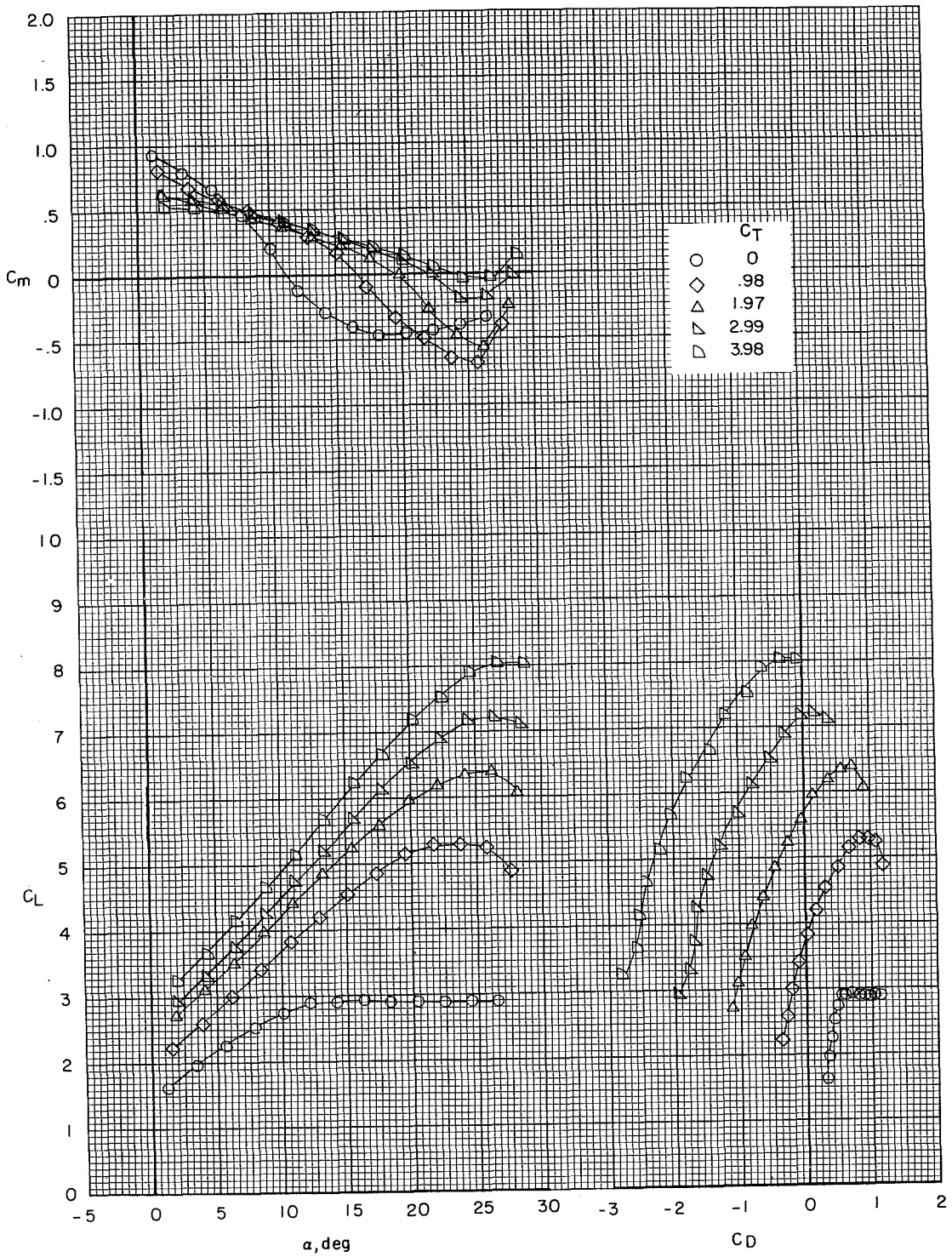

(b) $i_t = 0^o$.

Figure 12.- Continued.

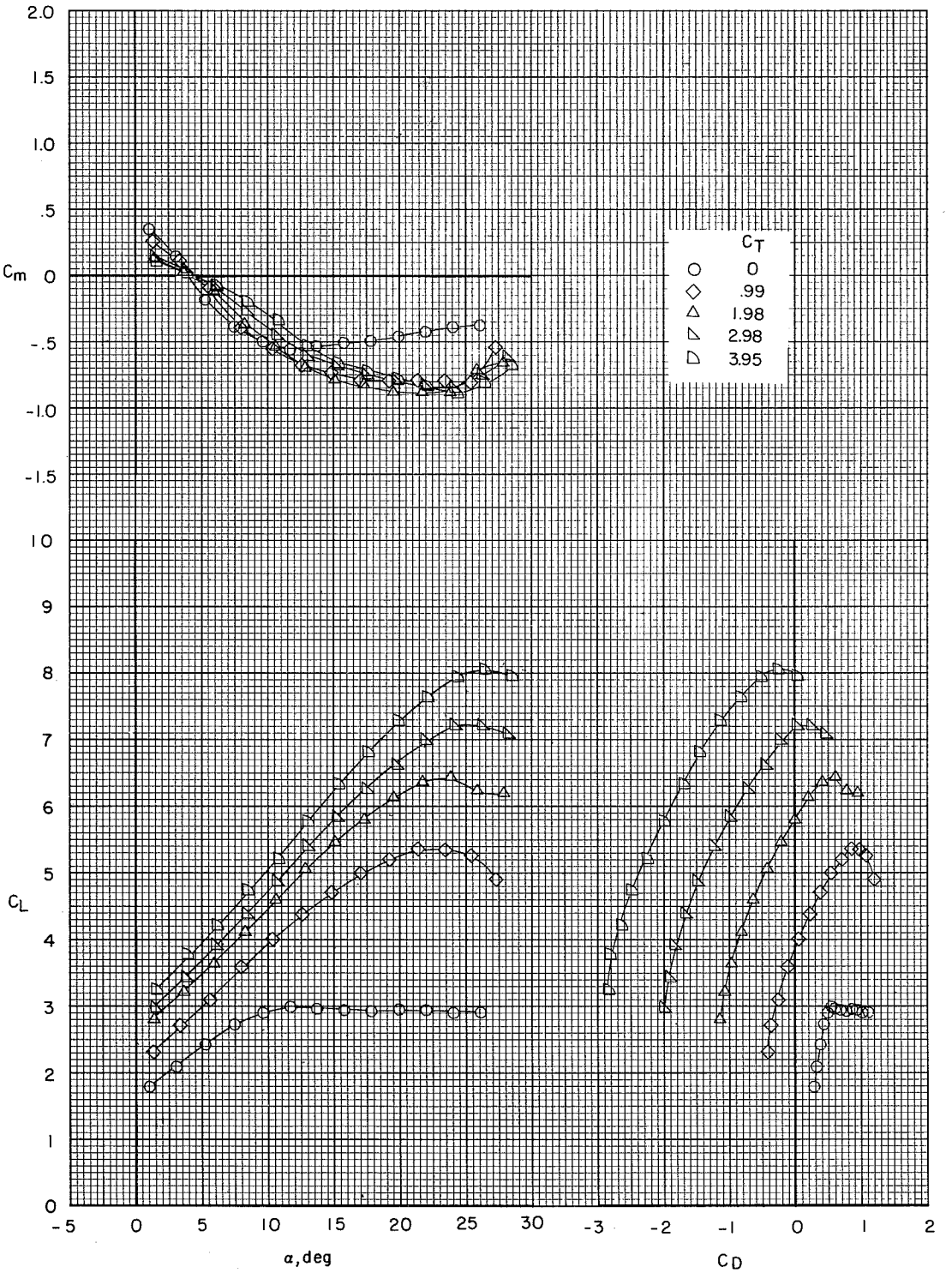

(c) $i_t = 5^o$.

Figure 12.- Continued.

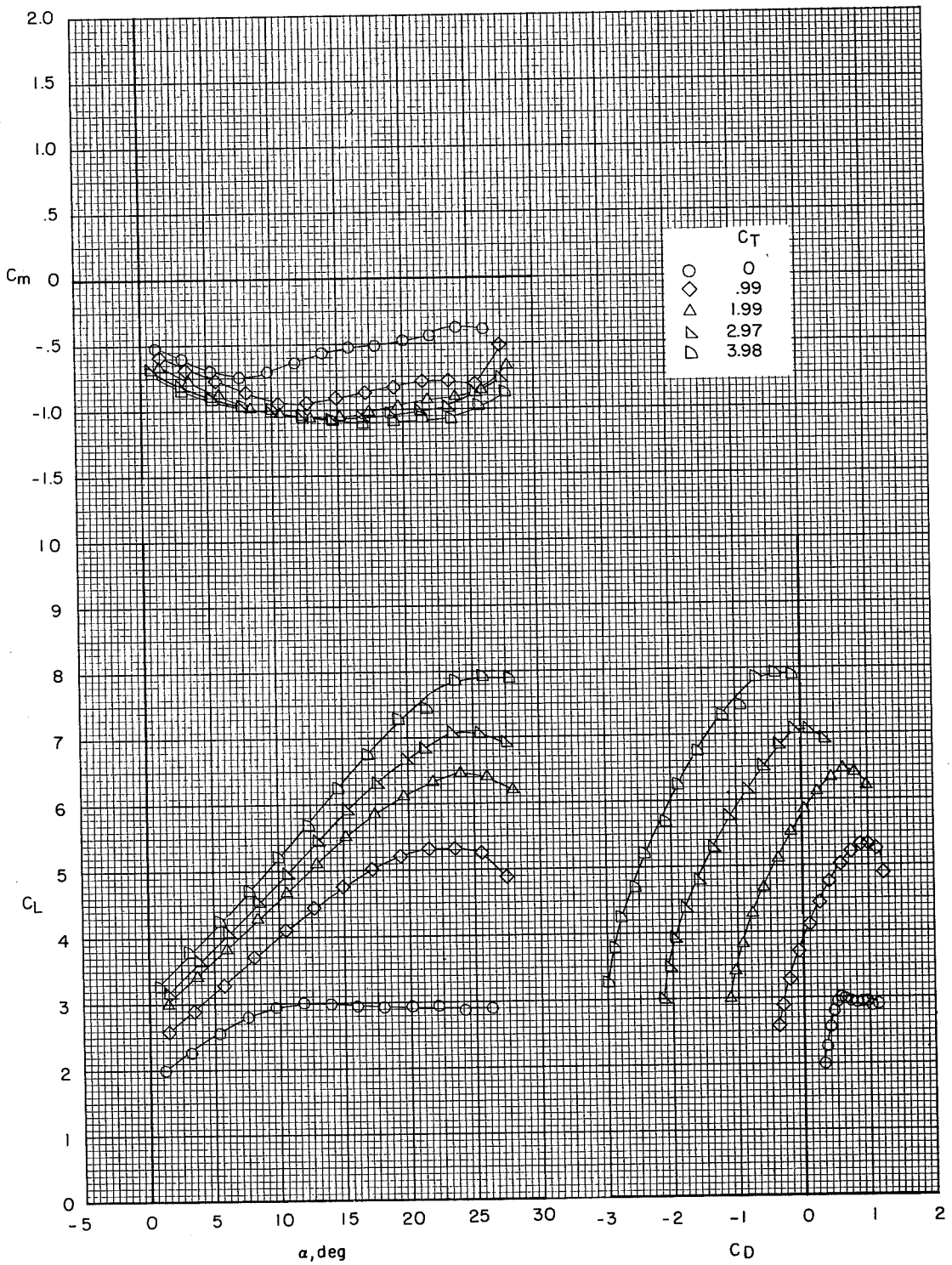

(d) $i_t = 10^o$.

Figure 12.- Concluded.

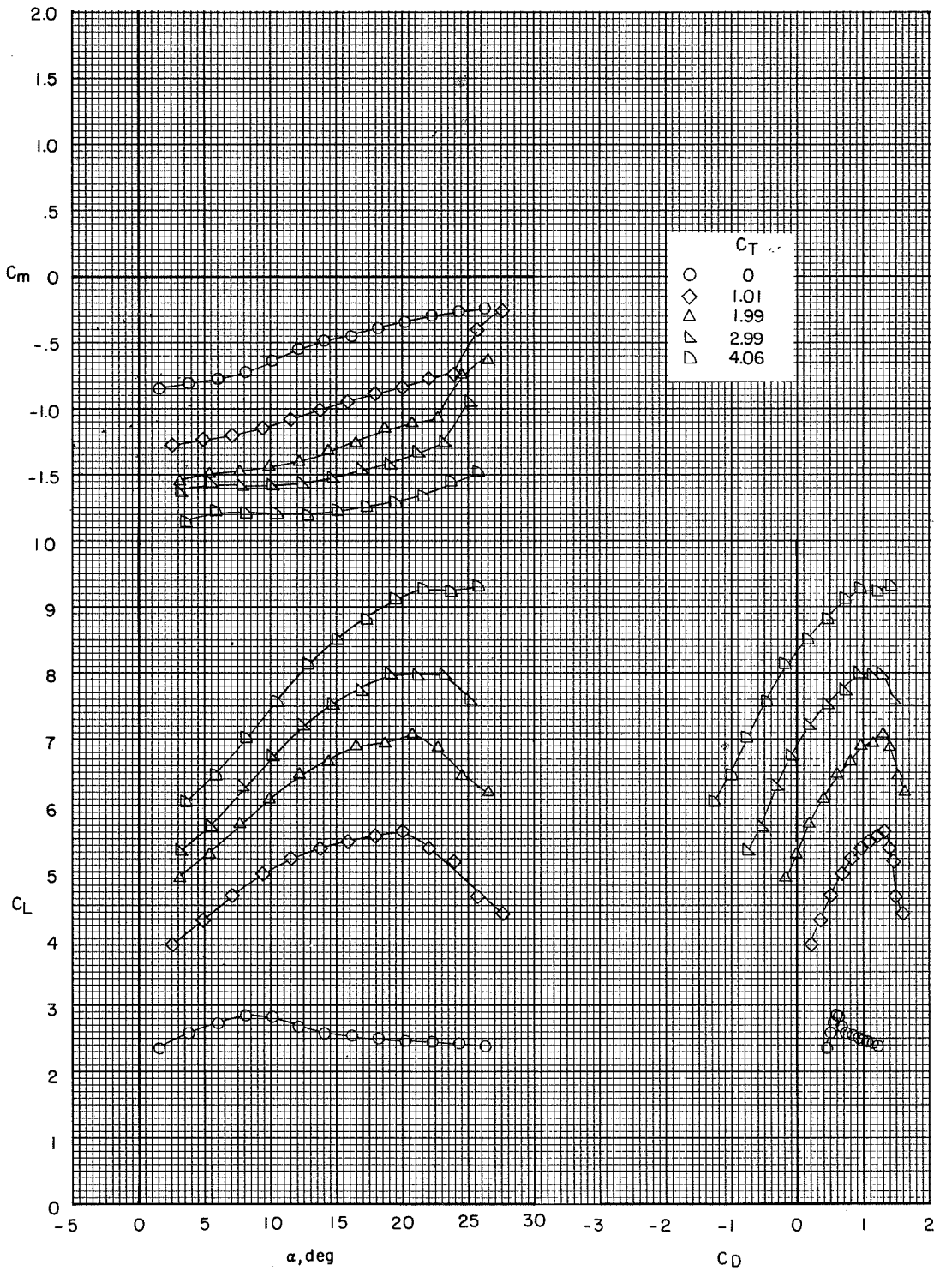

Figure 13.- Effect of thrust coefficient on longitudinal aerodynamic characteristics of the landing configuration. Tail off. Model in the V/STOL tunnel with the tunnel liner installed.

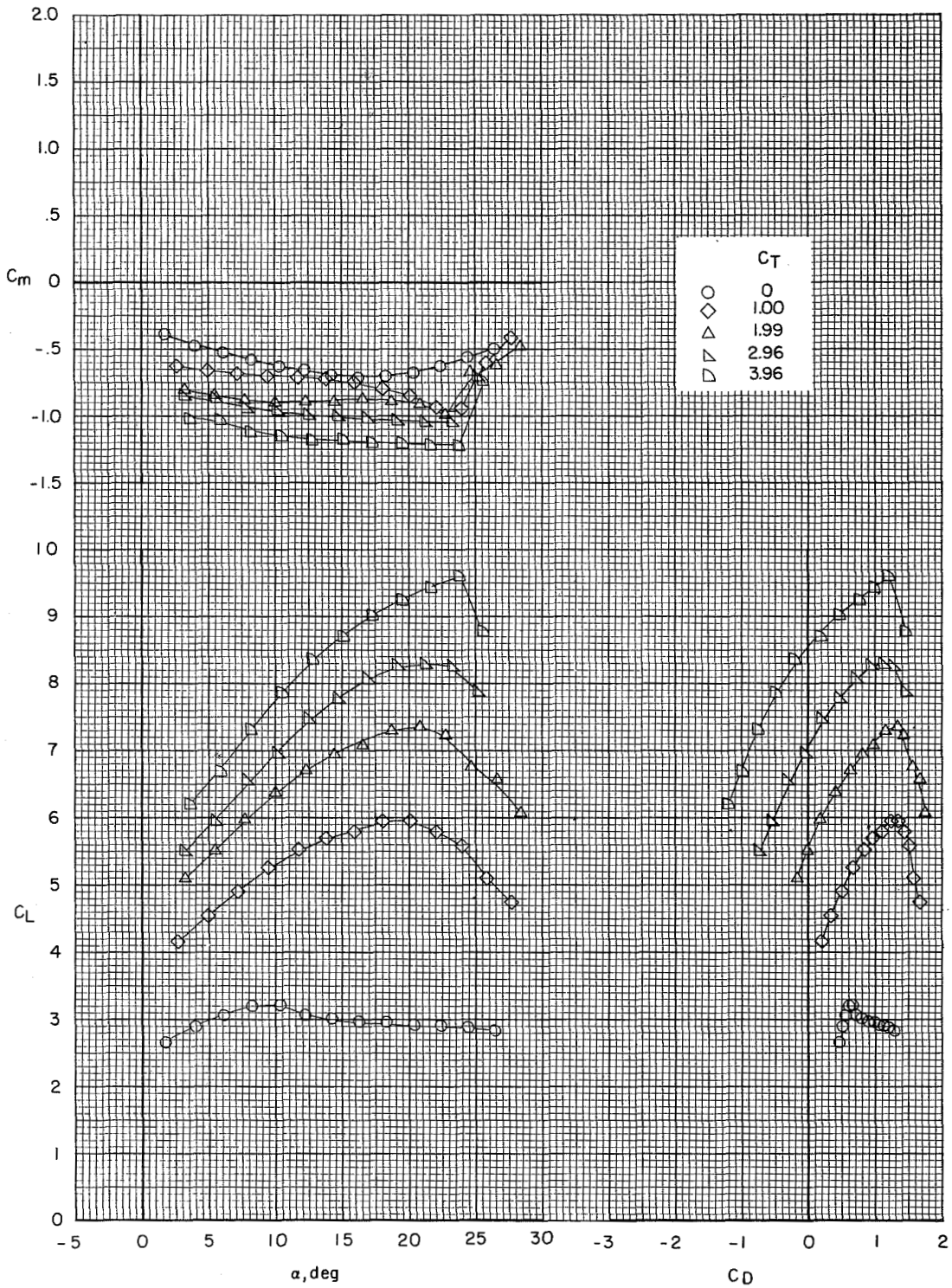

Figure 14.- Effect of thrust coefficient on longitudinal aerodynamic characteristics of the landing configuration. Model in the V/STOL tunnel with the tunnel liner installed. $\delta_e = 0^o$; $i_t = 0^o$.

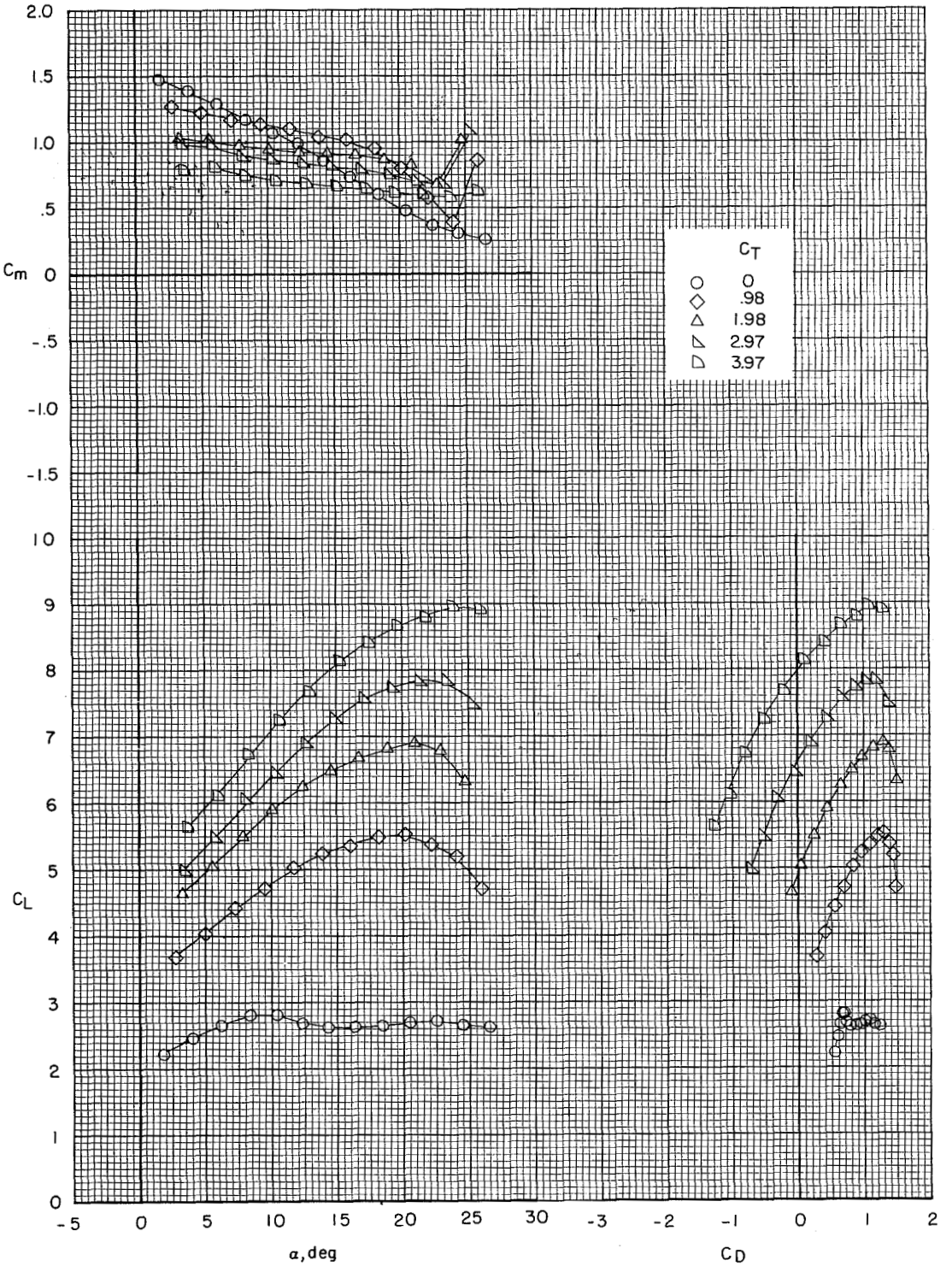

(a) $i_t = -5^o$.

Figure 15.- Effect of thrust coefficient on longitudinal aerodynamic characteristics of the landing configuration. $\delta_e = -25^o$. Model in the V/STOL tunnel with the tunnel liner installed.

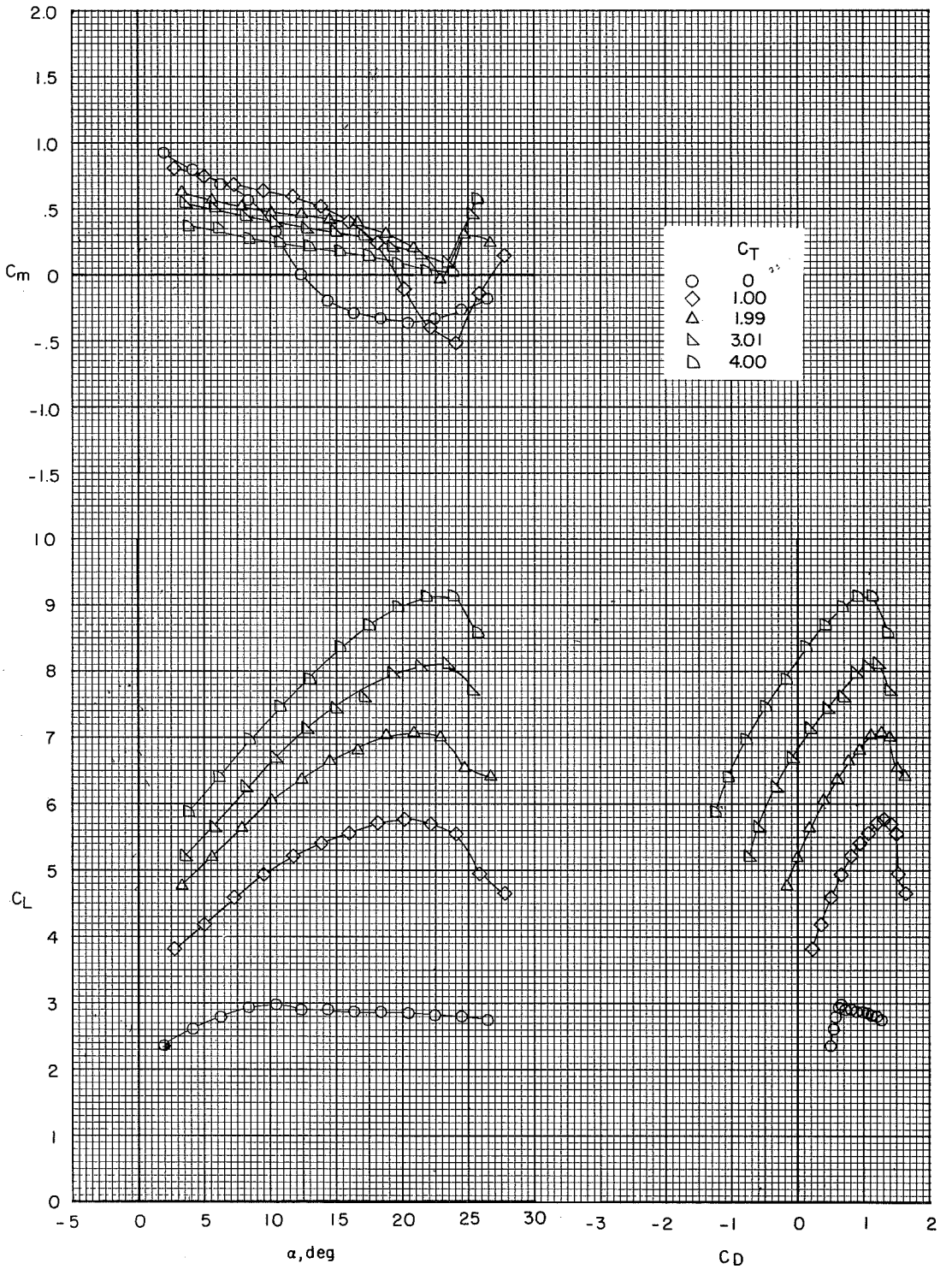

(b) $i_t = 0^o$.

Figure 15.- Continued.

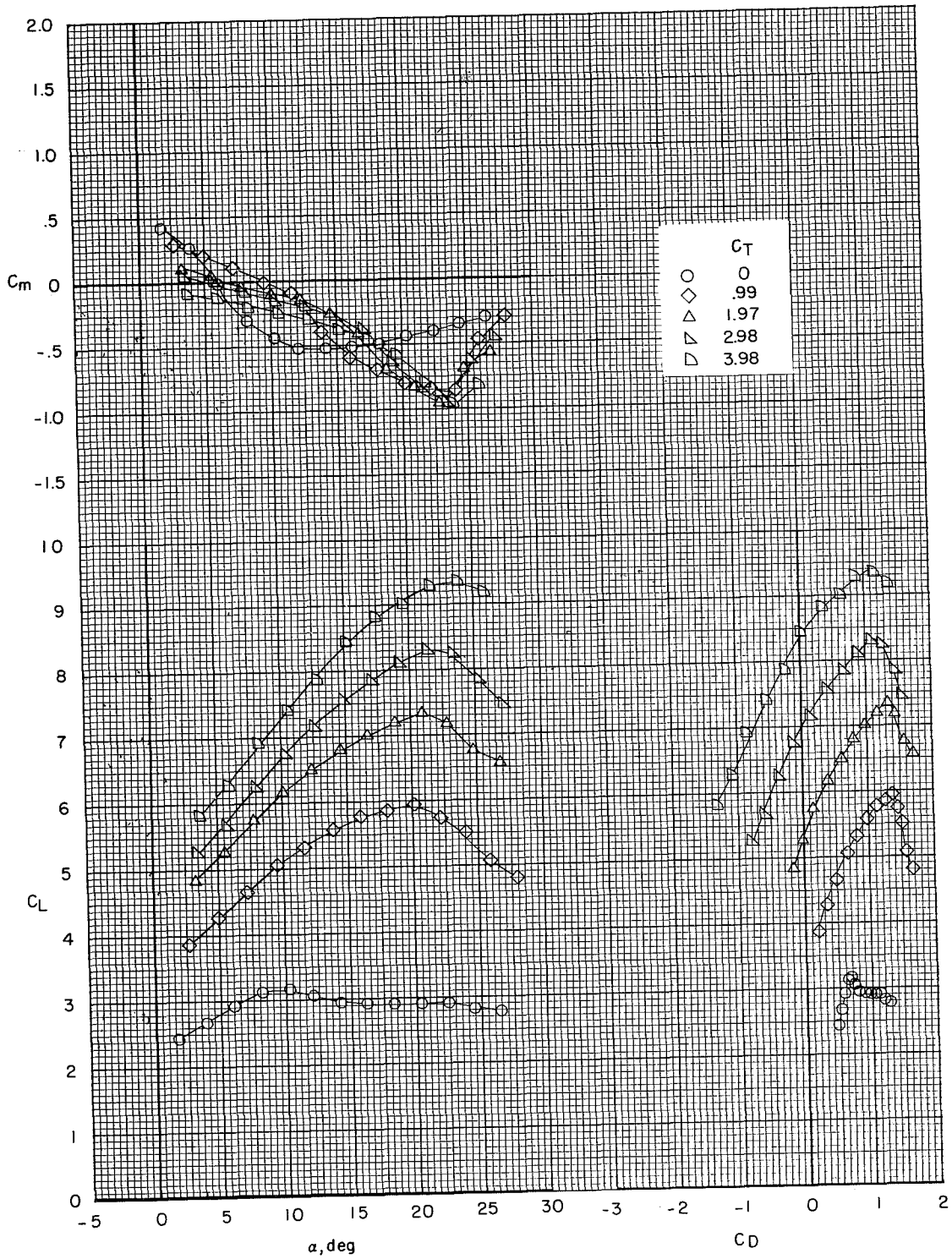

(c) $i_t = 5^o$.

Figure 15.- Continued.

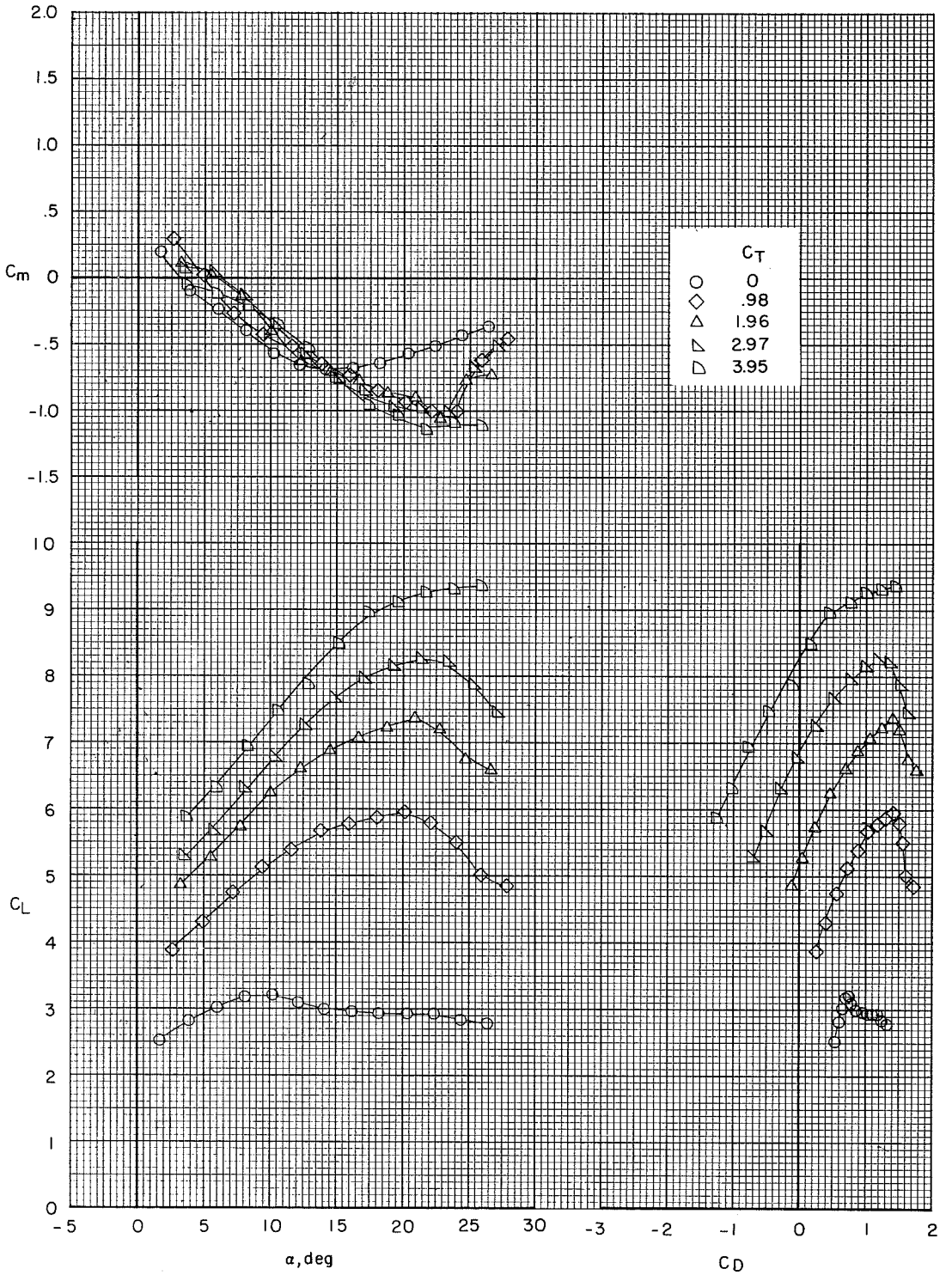

(d) $i_t = 10^o$.

Figure 15.- Concluded.

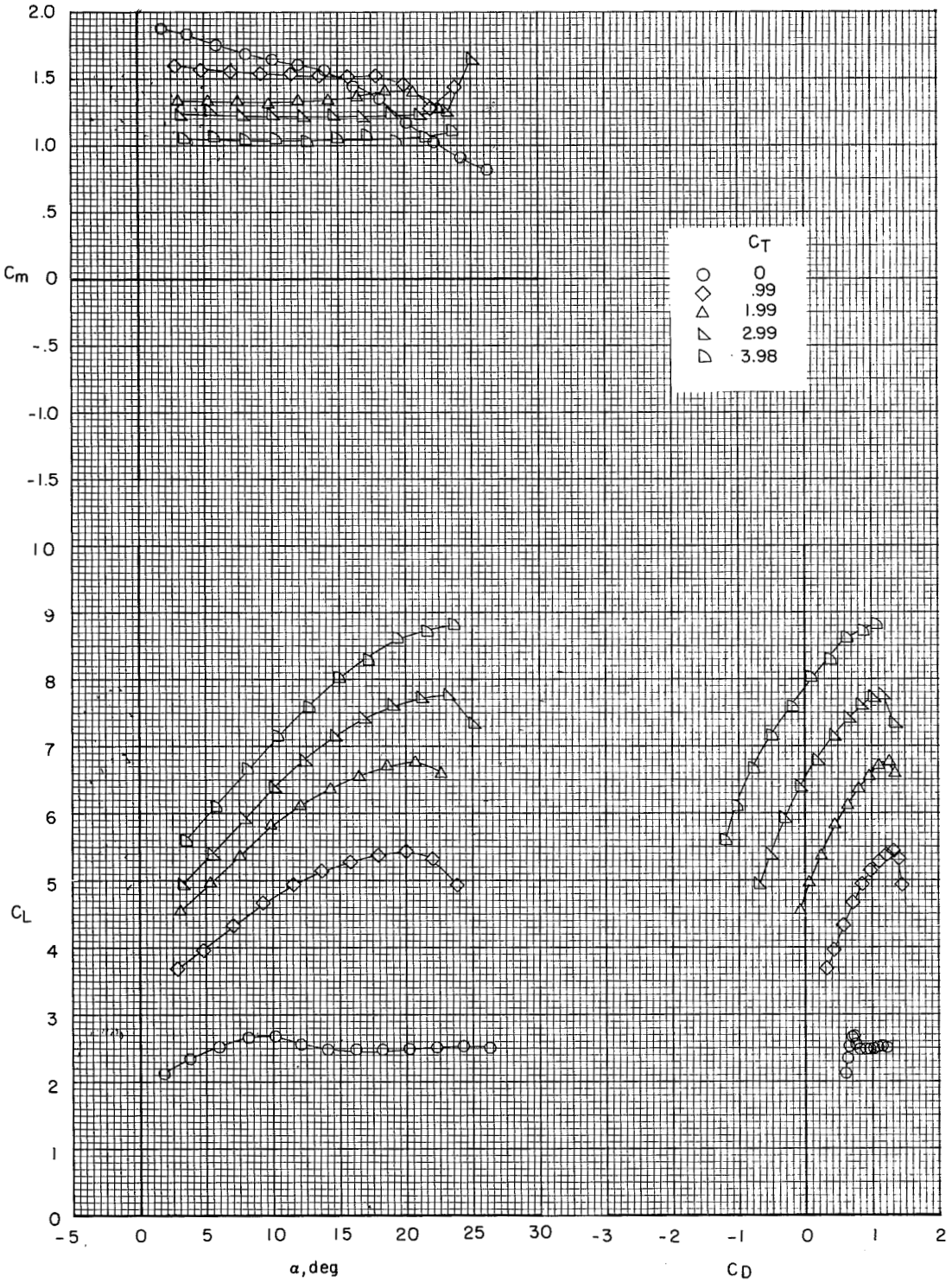

(a) $i_t = -5^o$.

Figure 16.- Effect of thrust coefficient on longitudinal aerodynamic characteristics of the landing configuration. $\delta_e = -50^o$. Model in the V/STOL tunnel with the tunnel liner installed.

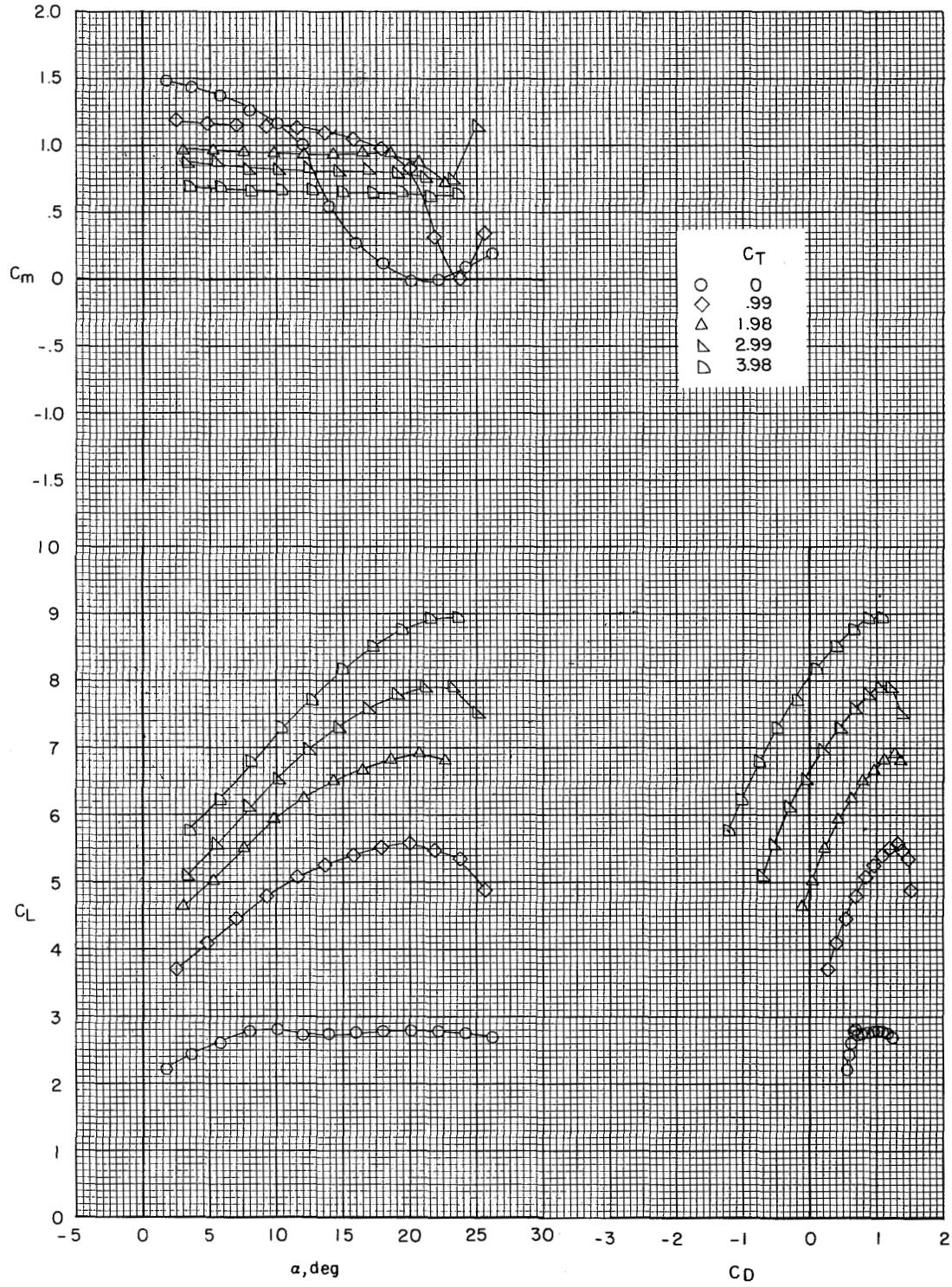

(b) $i_t = 0^o$.

Figure 16.- Continued.

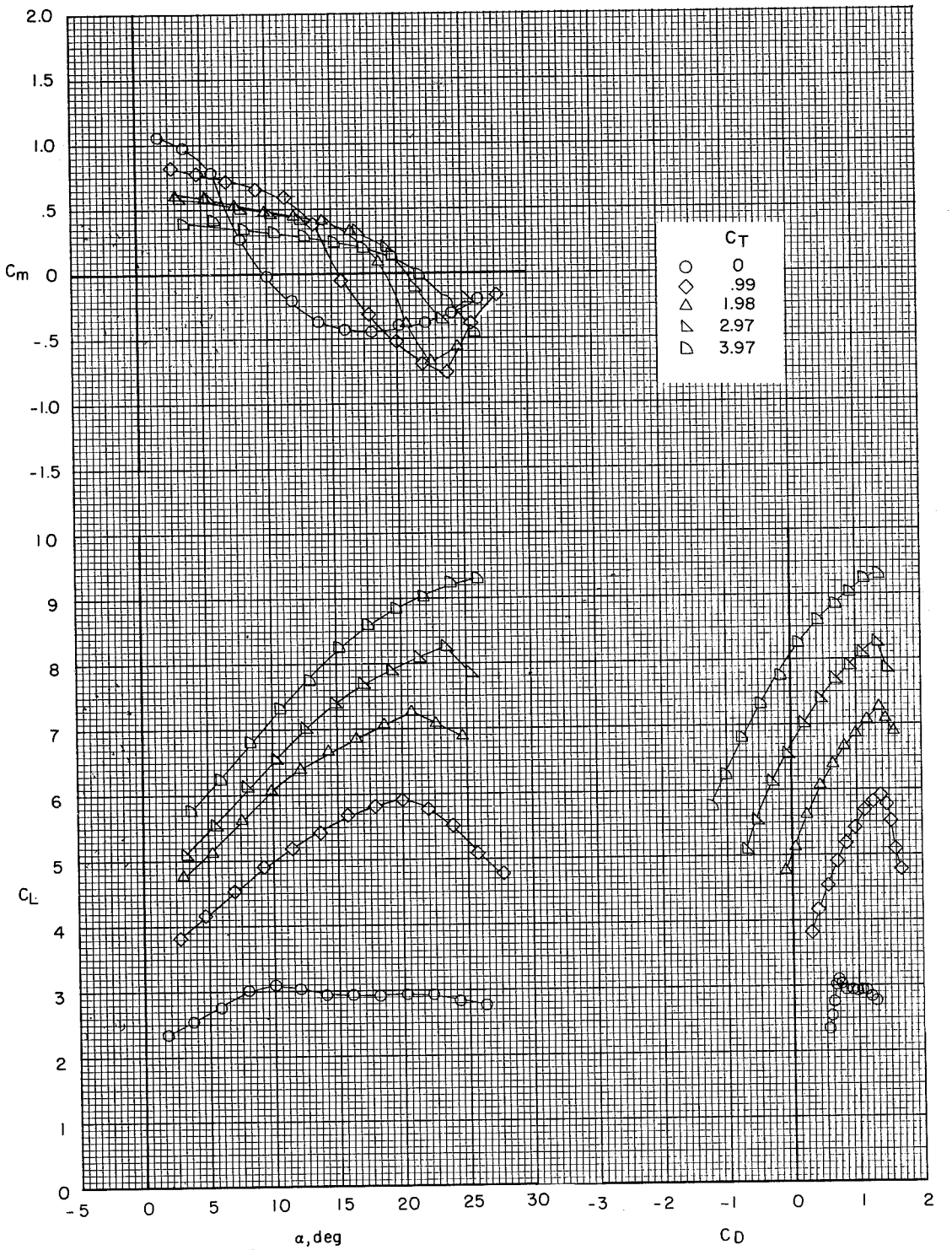

(c) $i_t = 5^o$.

Figure 16.- Continued.

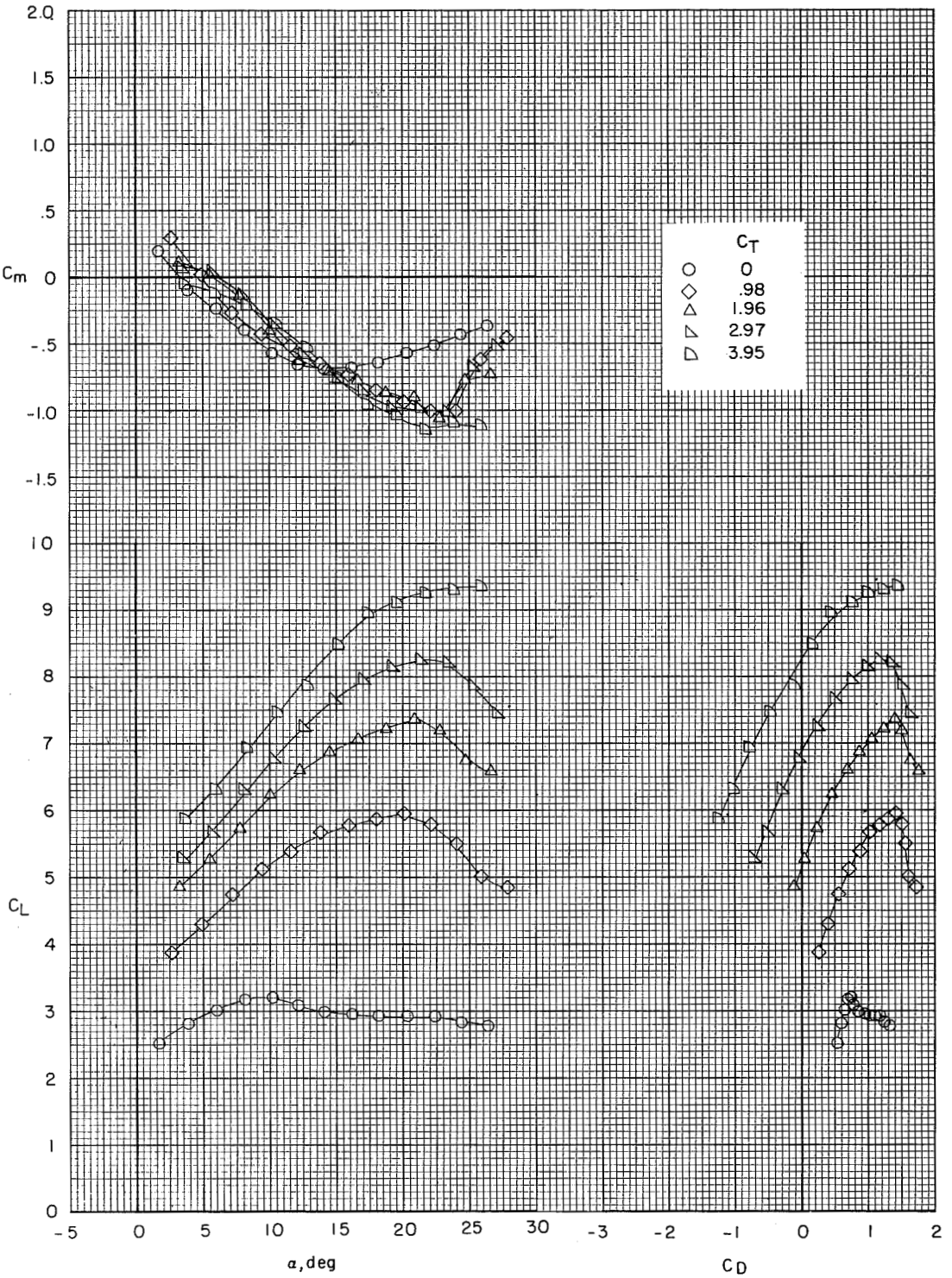

(d) $i_t = 10^o$.

Figure 16.- Concluded.

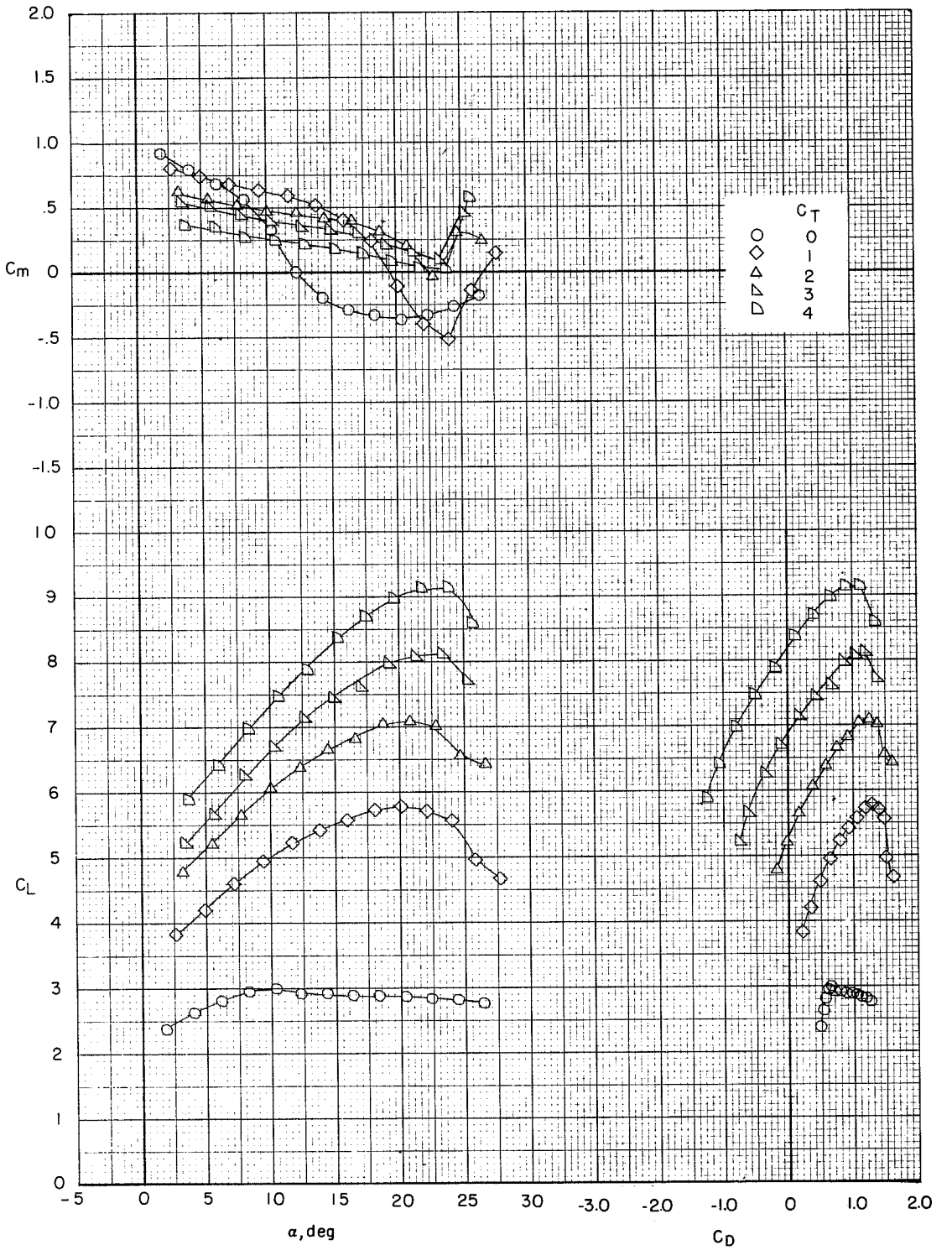

(a) All engines operating.

Figure 17.- Effect of thrust coefficient on aerodynamic characteristics of the landing configuration. $\delta_e = -25^o$; $i_t = 0^o$. Model in the V/STOL tunnel with the tunnel liner installed.

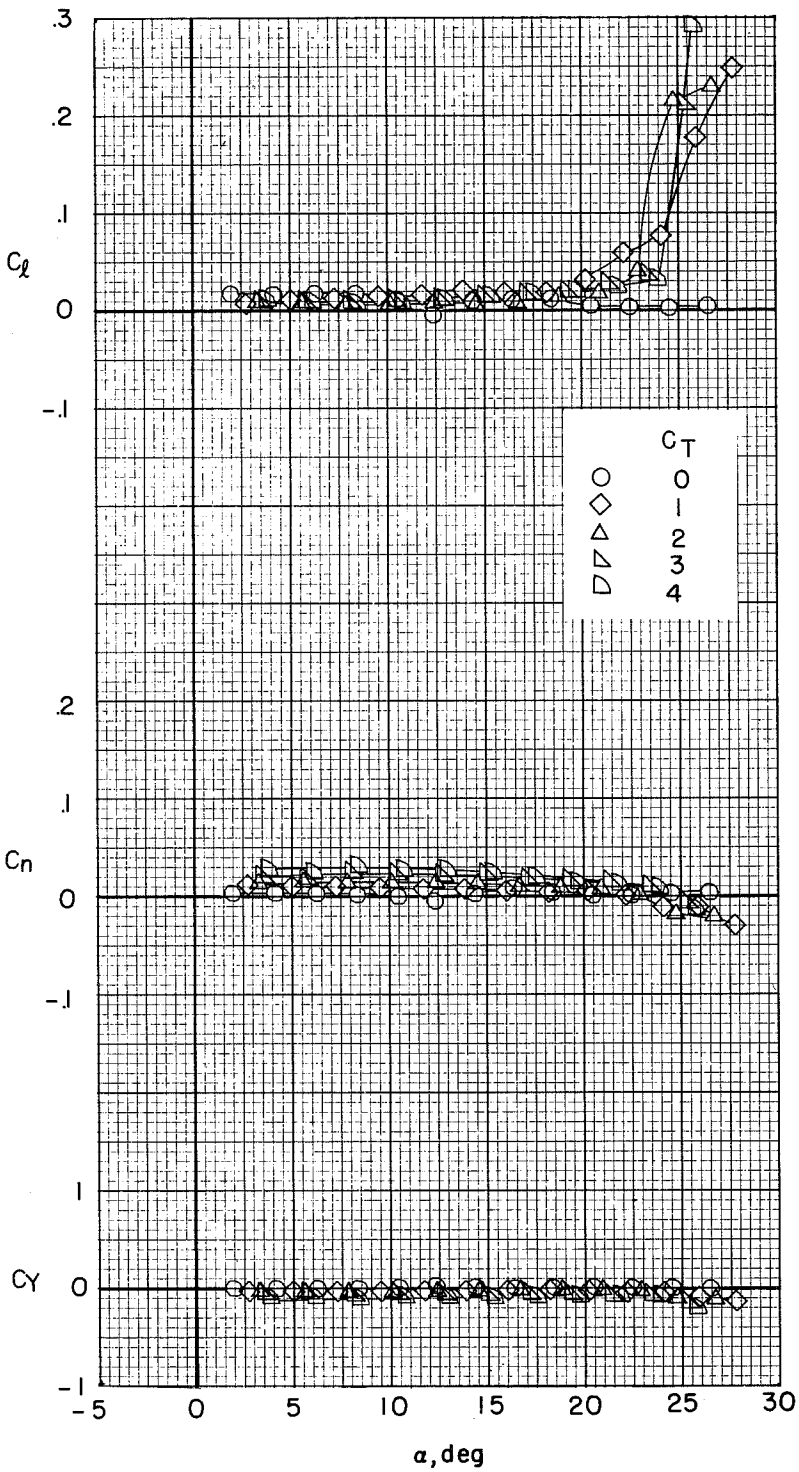

(a) Concluded.

Figure 17.- Continued.

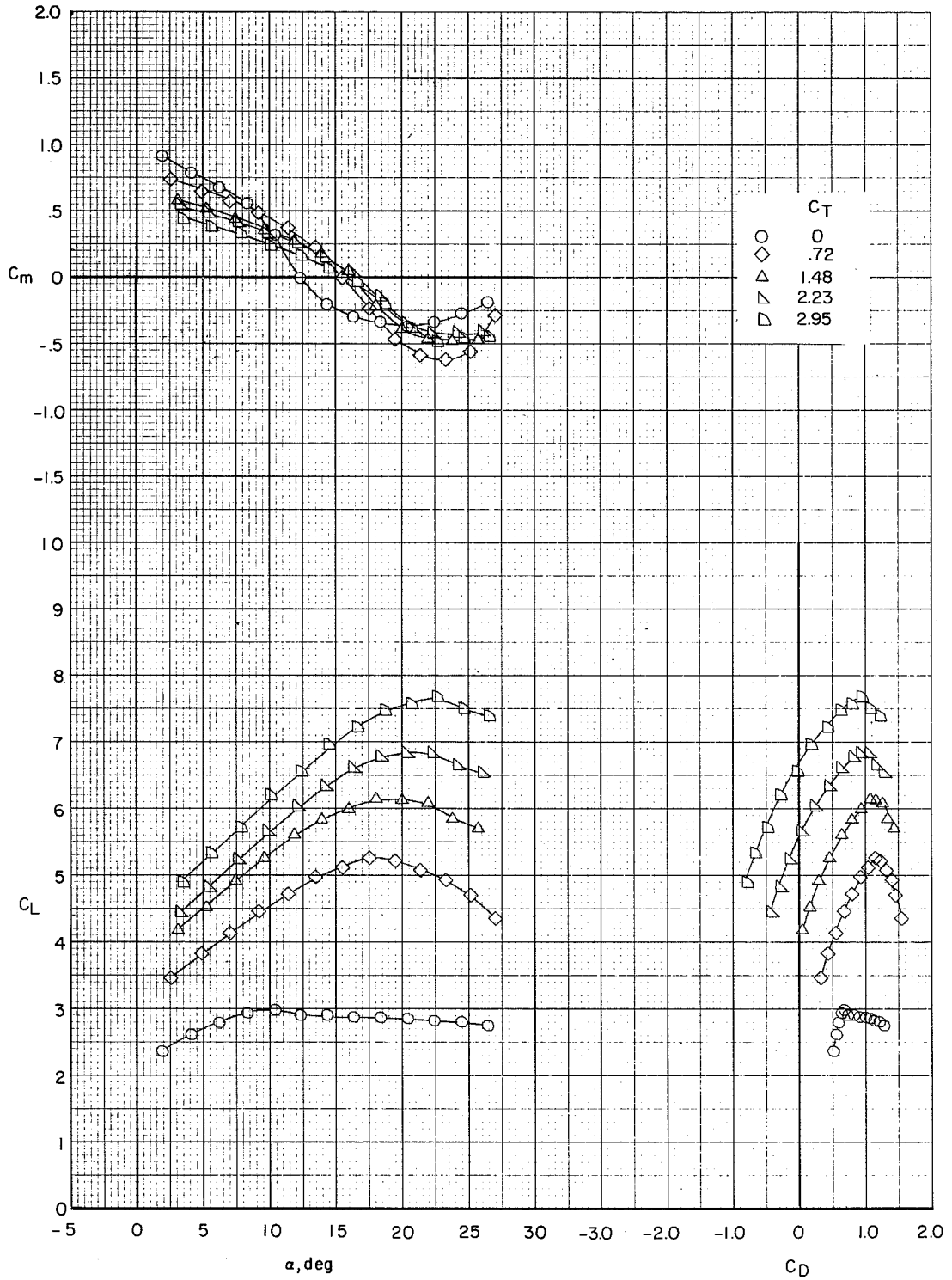

(b) Right inboard engine out.

Figure 17.- Continued.

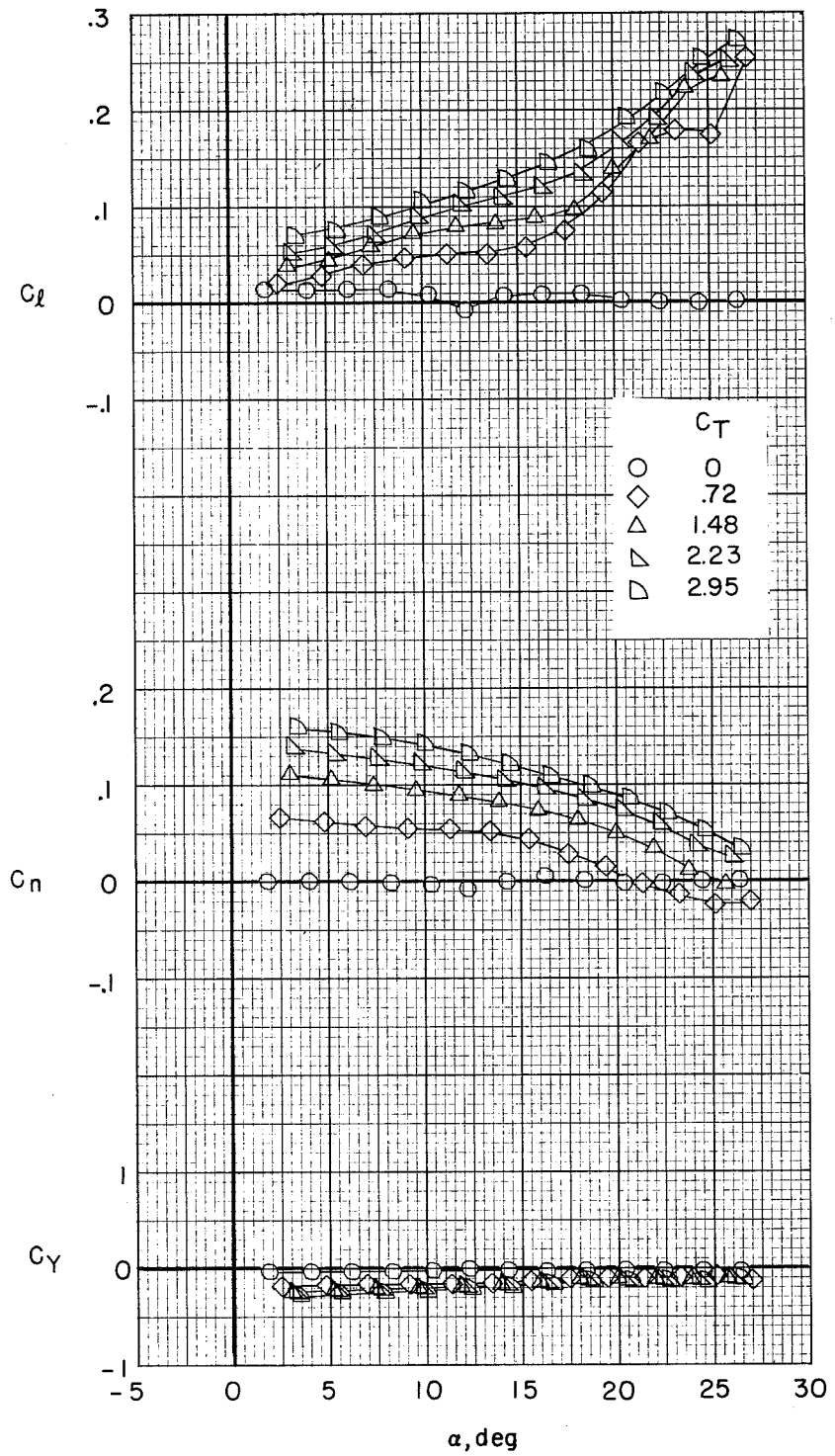

(b) Concluded.

Figure 17.- Continued.

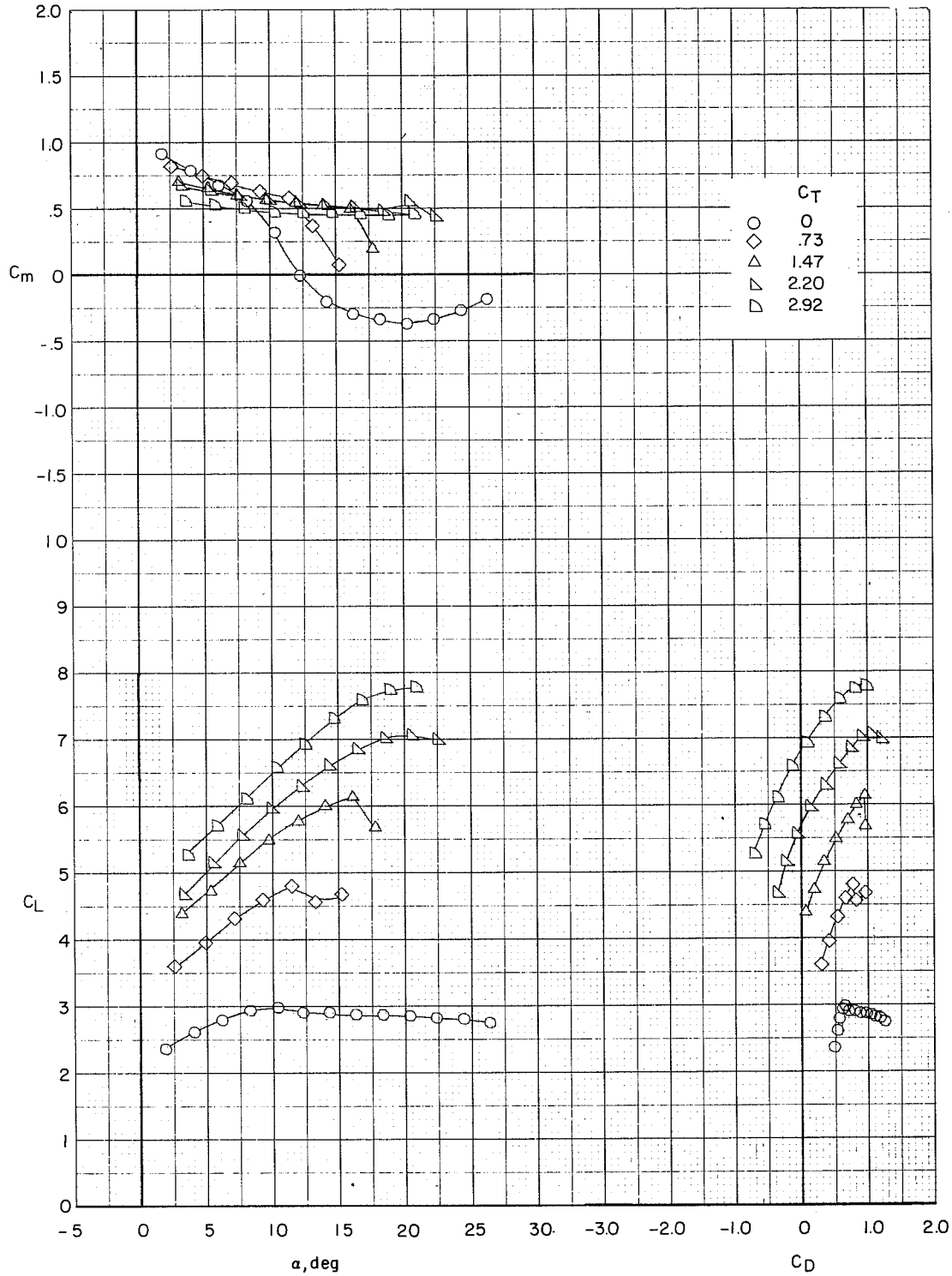

(c) Right outboard engine out.

Figure 17.- Continued.

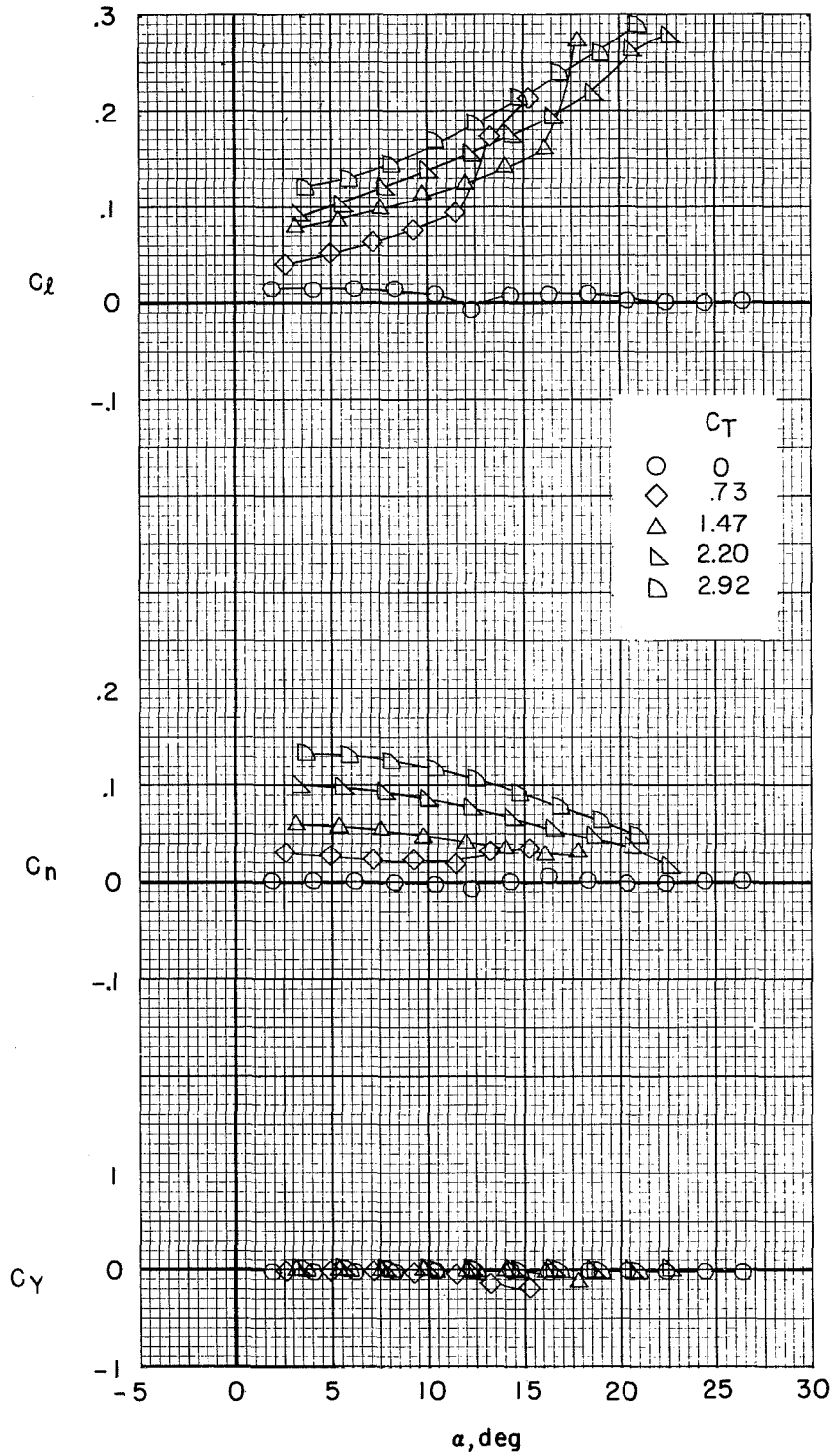

(c) Concluded.

Figure 17.- Concluded.

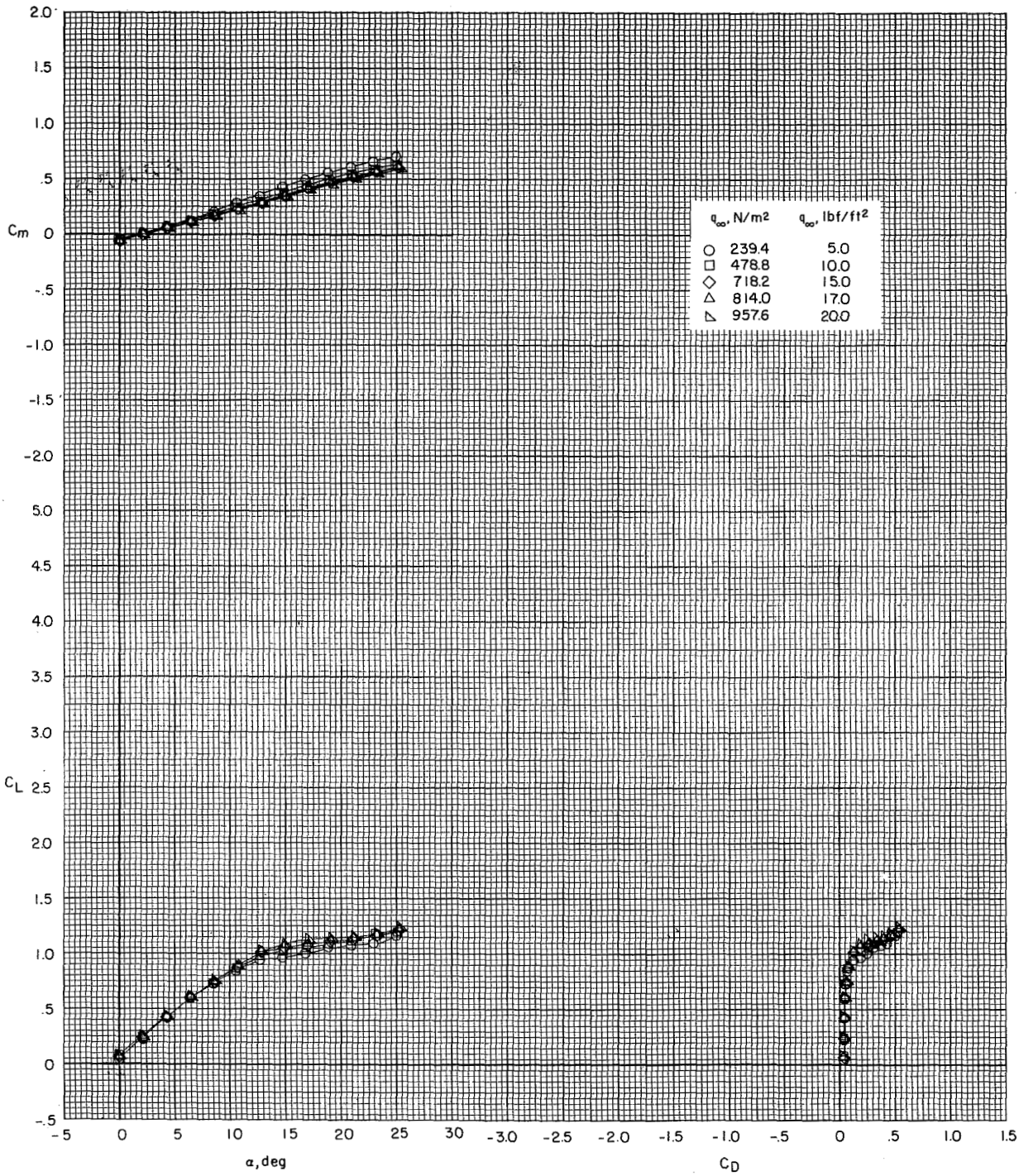

(a) $\delta_f = 0^o$.

Figure 18.- Effect of dynamic pressure on longitudinal aerodynamic characteristics. Model in the V/STOL tunnel with the tunnel liner installed. Tail off.

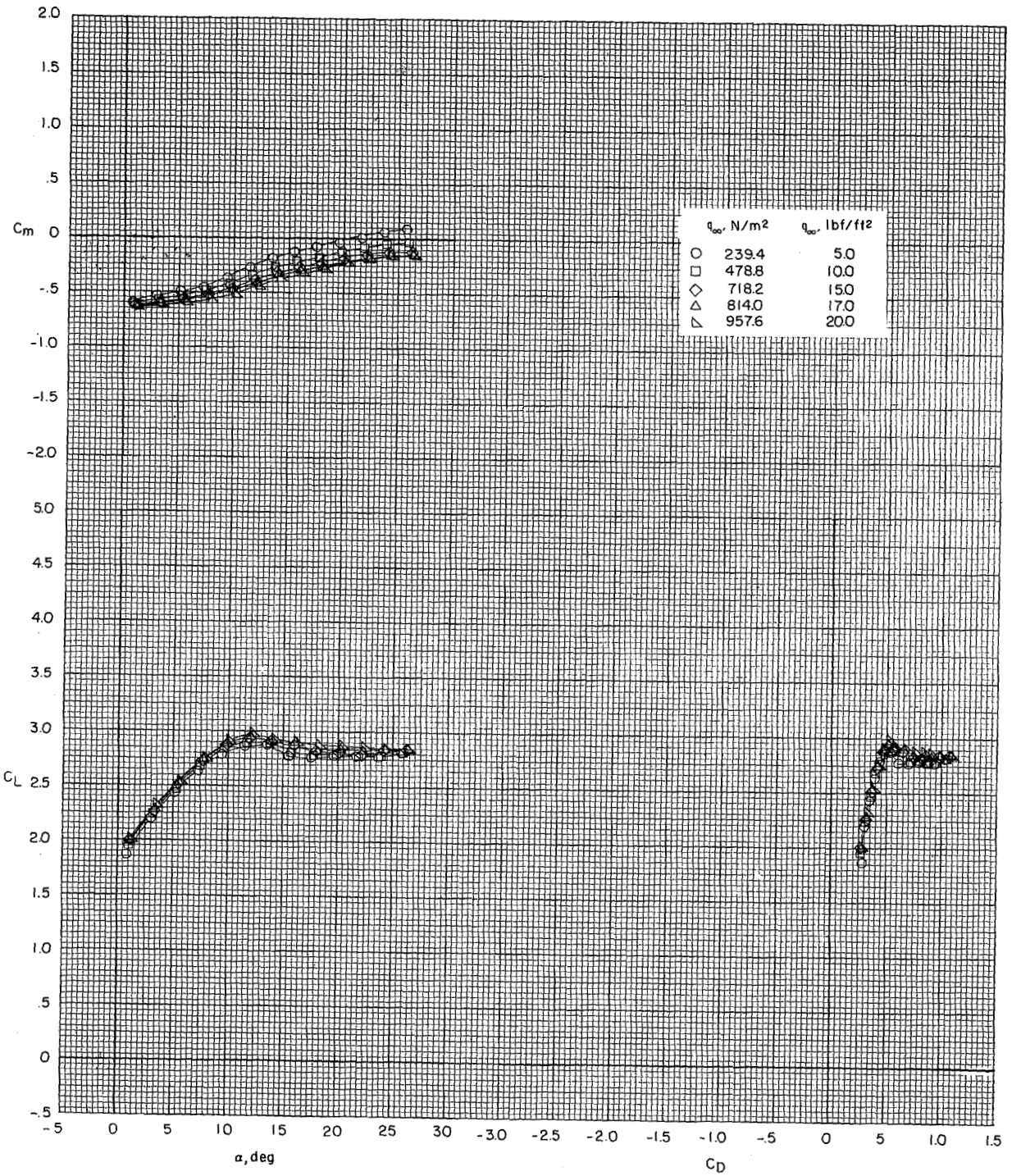

(b) $\delta_f = 40^o$.

Figure 18.- Continued.

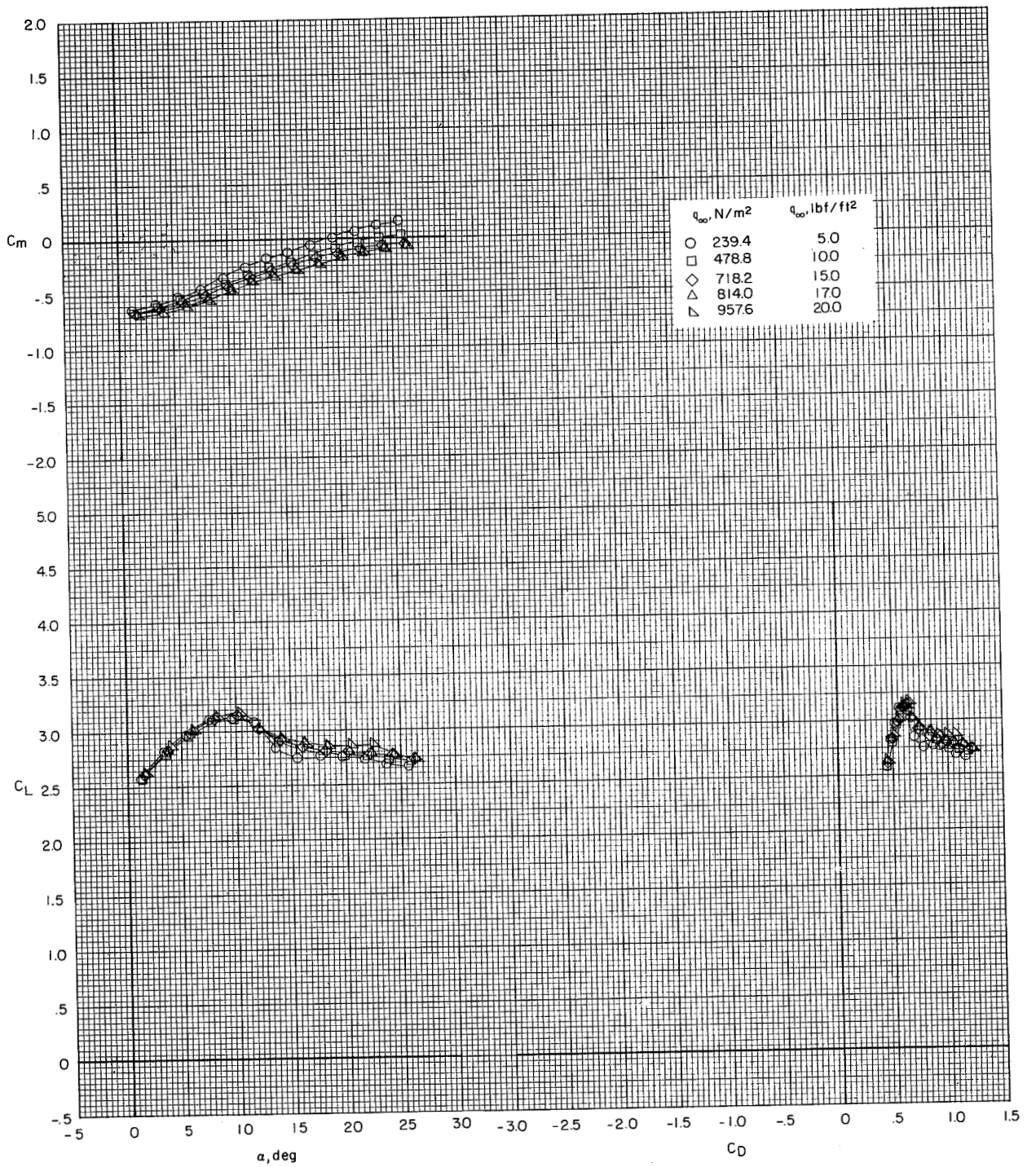

(c) $\delta_f = 55^o$.

Figure 18.- Concluded.

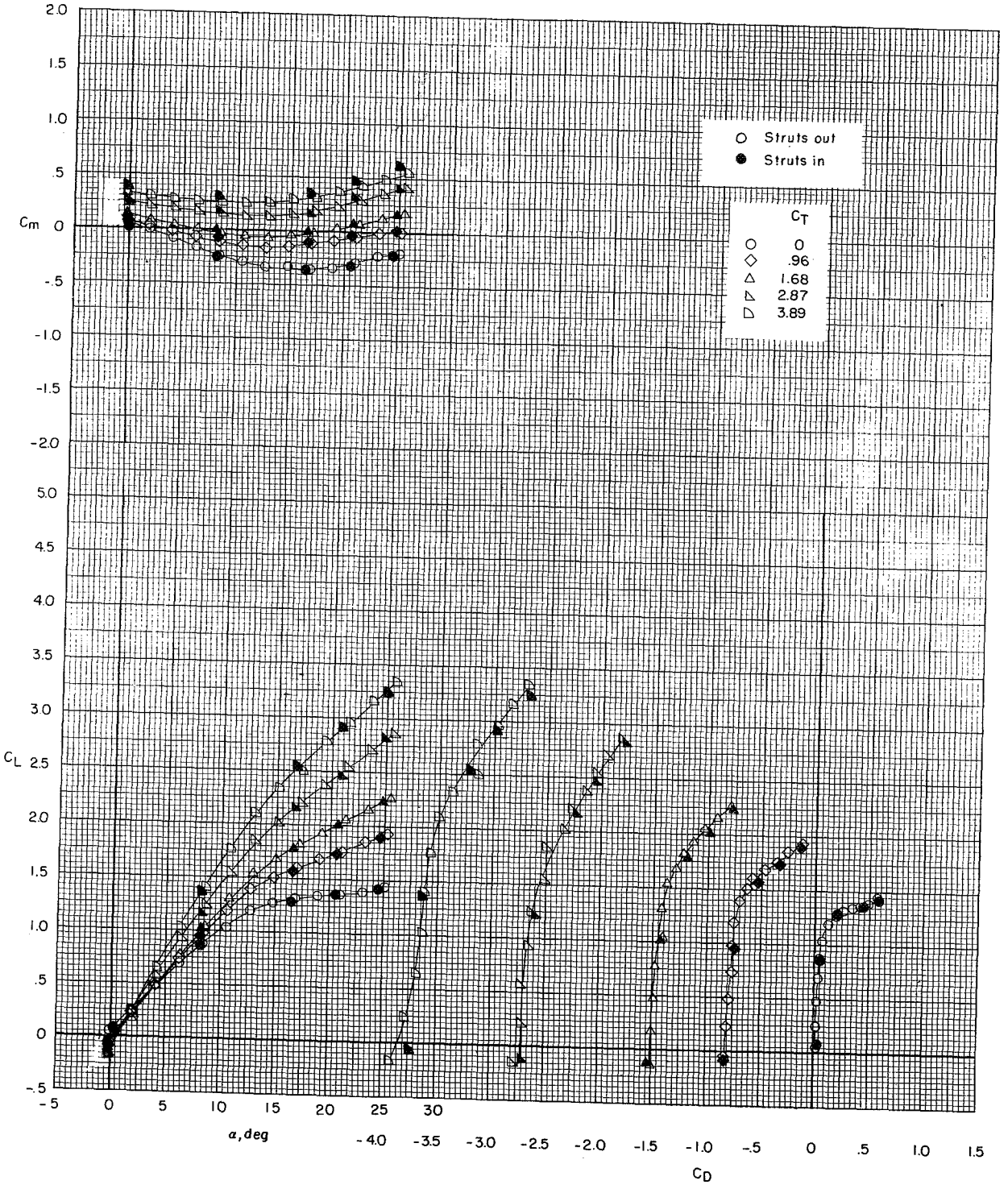

(a) $\delta_f = 0^o$; $i_t = 0^o$.

Figure 19.- Effect of struts on longitudinal aerodynamic characteristics. Model in the V/STOL tunnel with the tunnel liner installed.

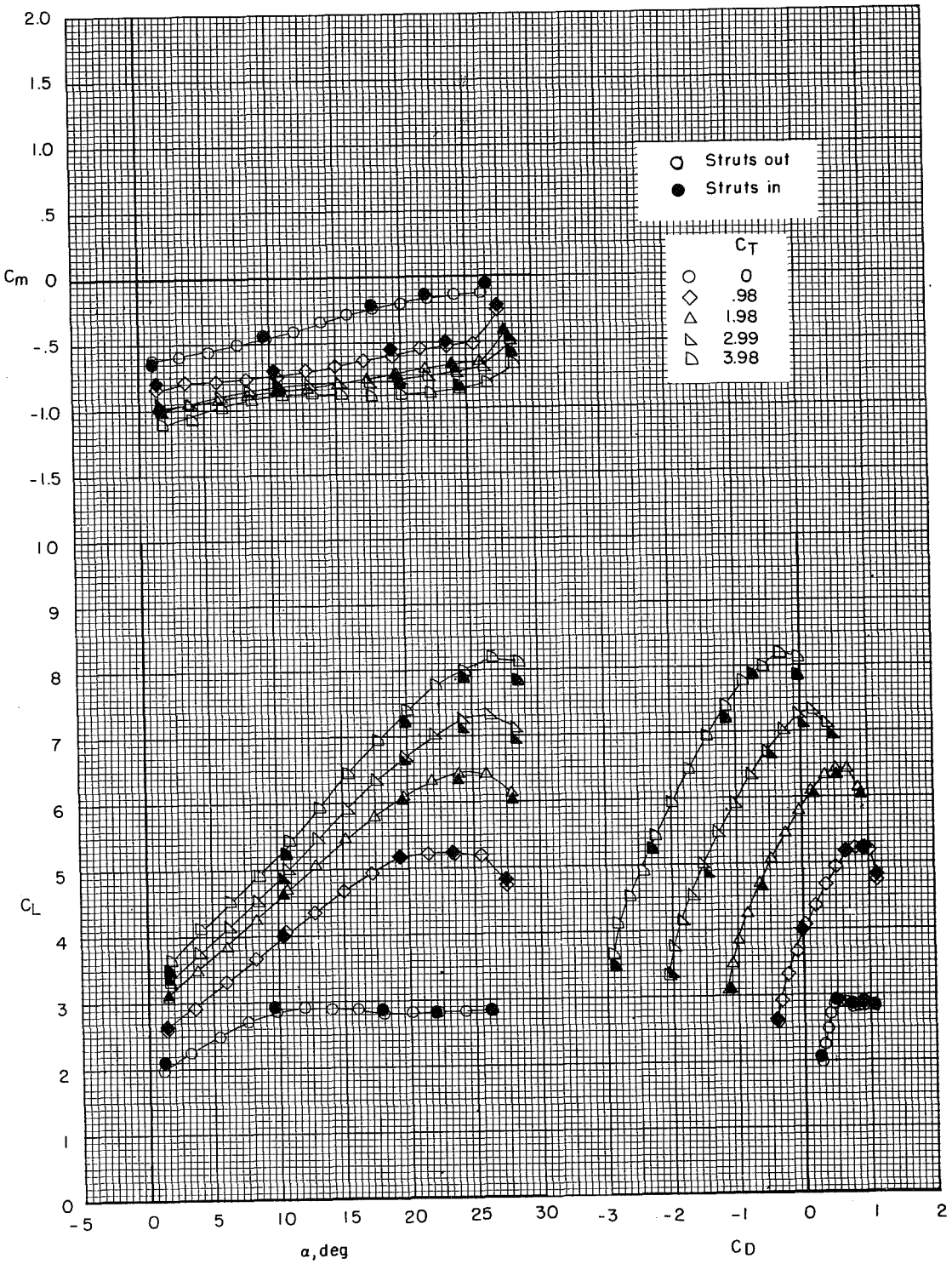

(b) $\delta_f = 40^o$; tail off.

Figure 19.- Continued.

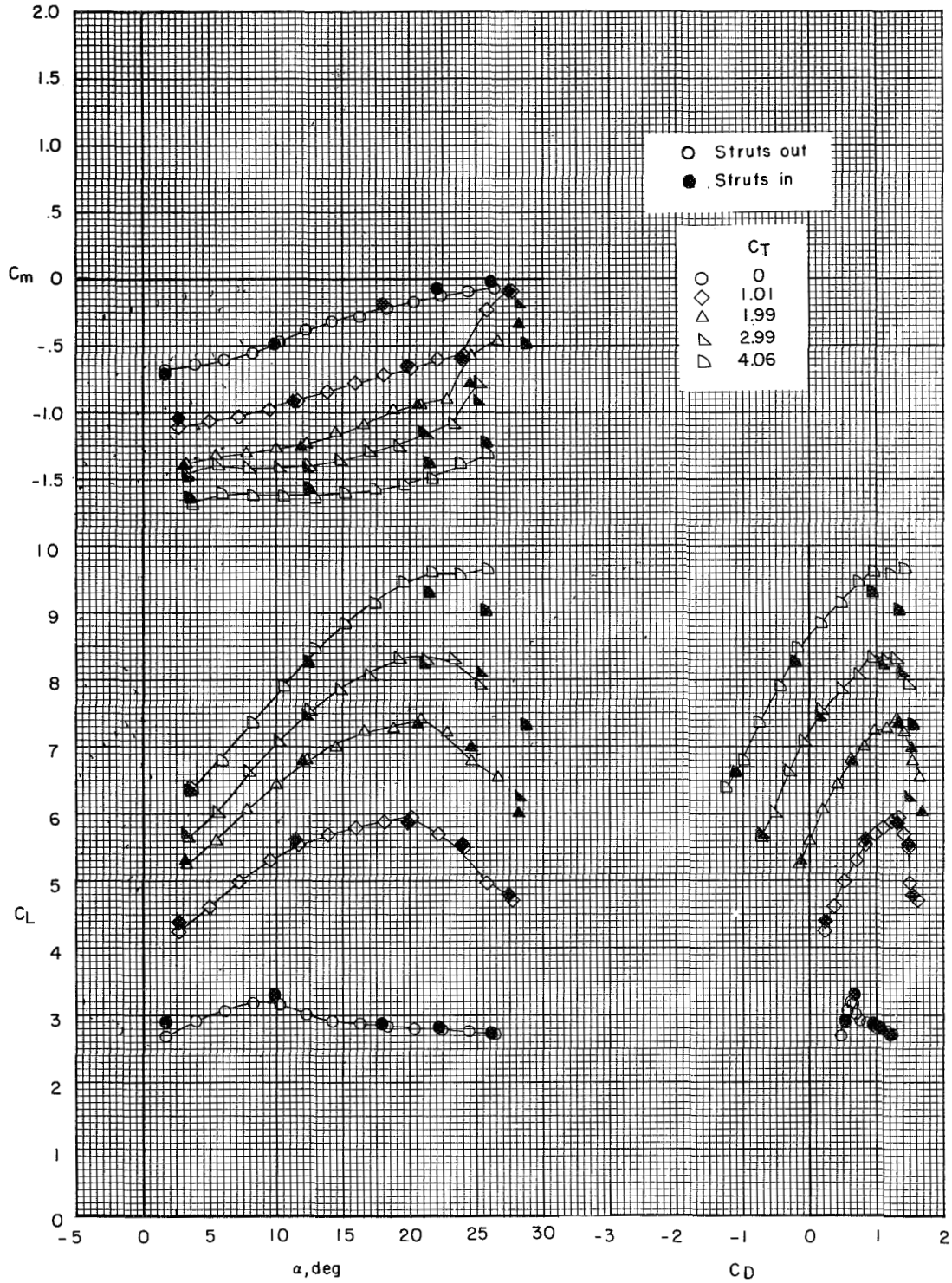

(c) $\delta_f = 55^o$; tail off.

Figure 19.- Concluded.

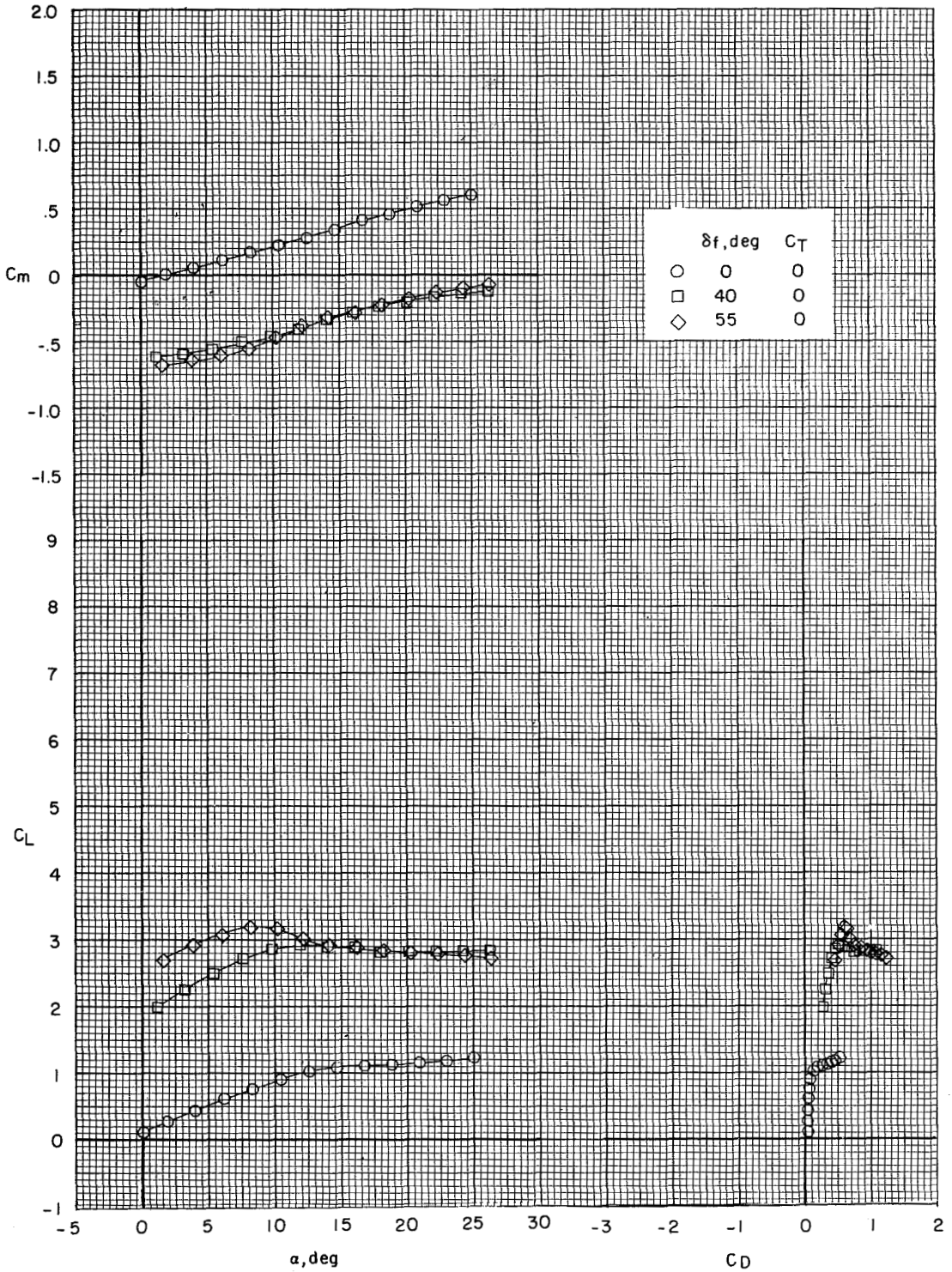

(a) $C_T = 0$.

Figure 20.- Effect of flaps on longitudinal aerodynamic characteristics. Model in the V/STOL tunnel with the tunnel liner installed. Tail off.

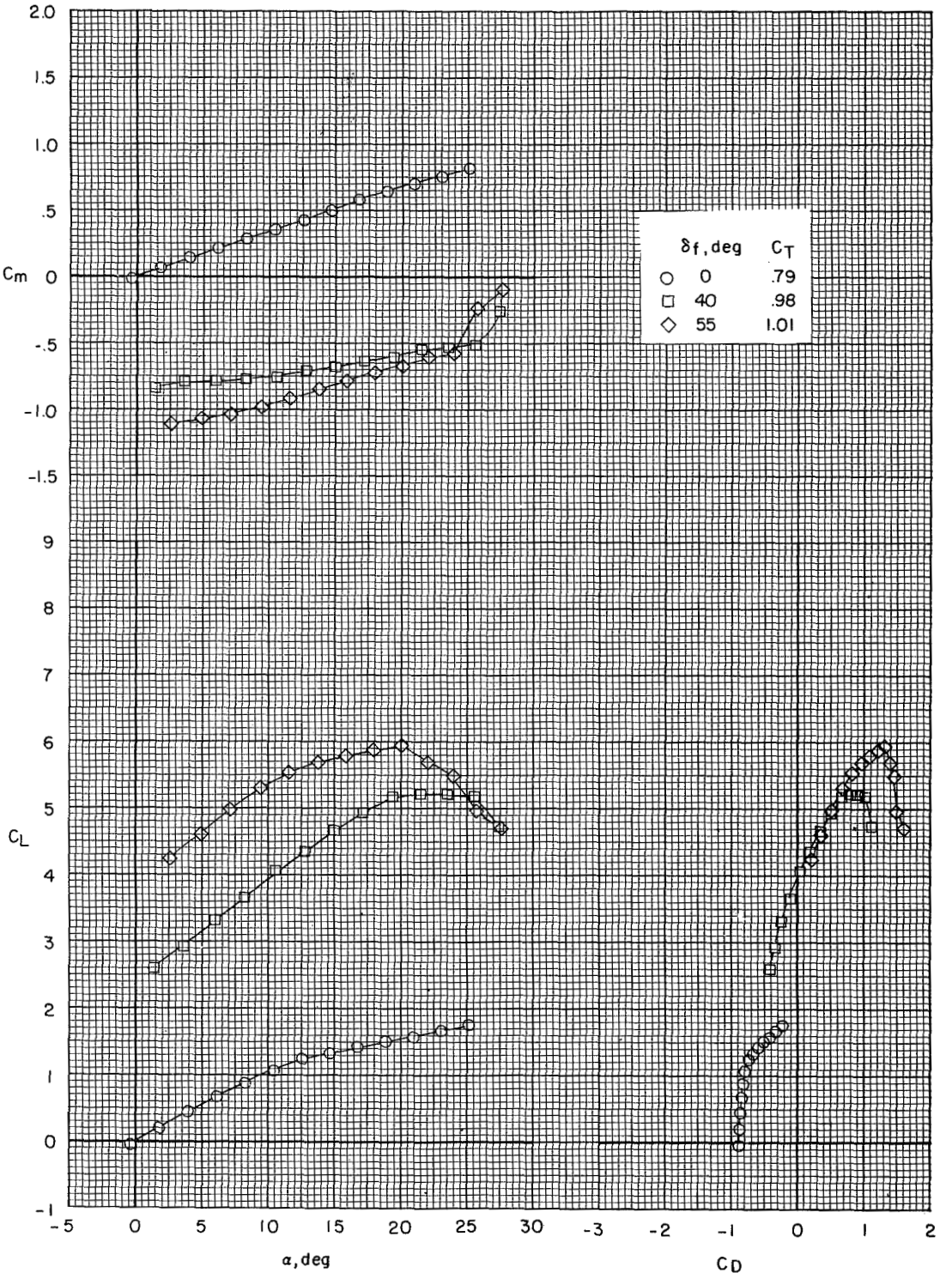

(b) $C_T \approx 1$.

Figure 20.- Continued.

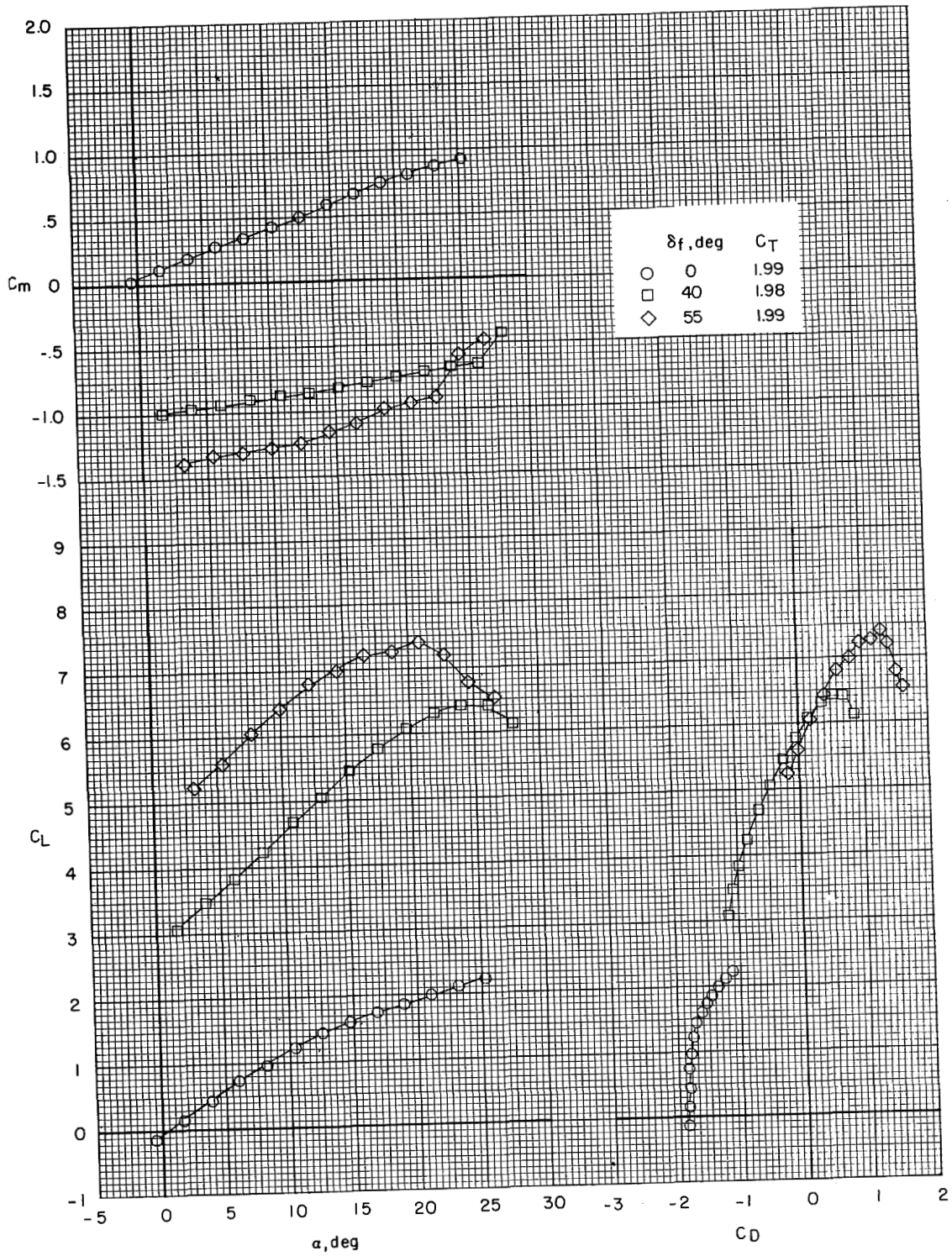

(c) $C_T \approx 2$.

Figure 20.- Continued.

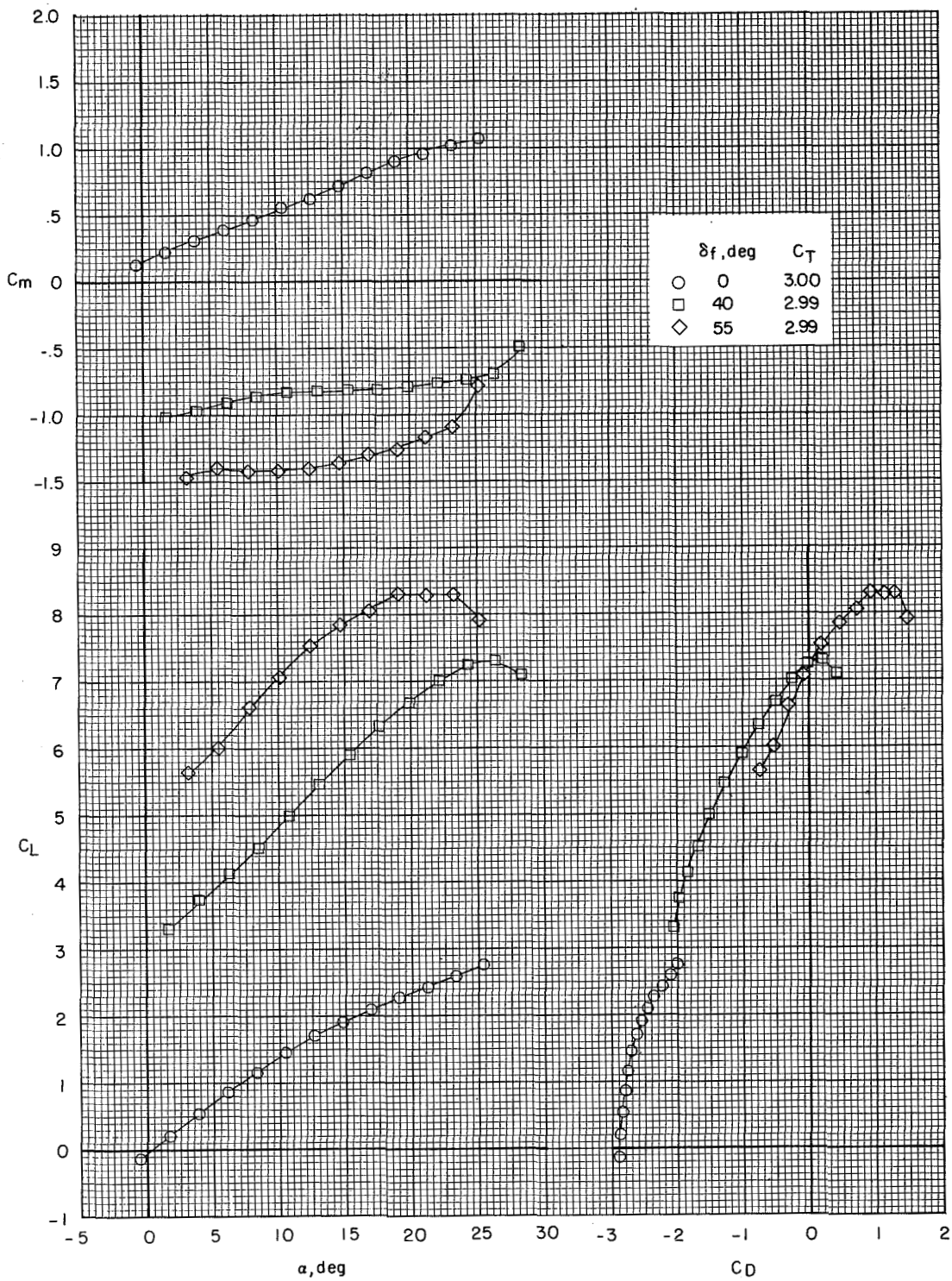

(d) $C_T \approx 3$.

Figure 20.- Continued.

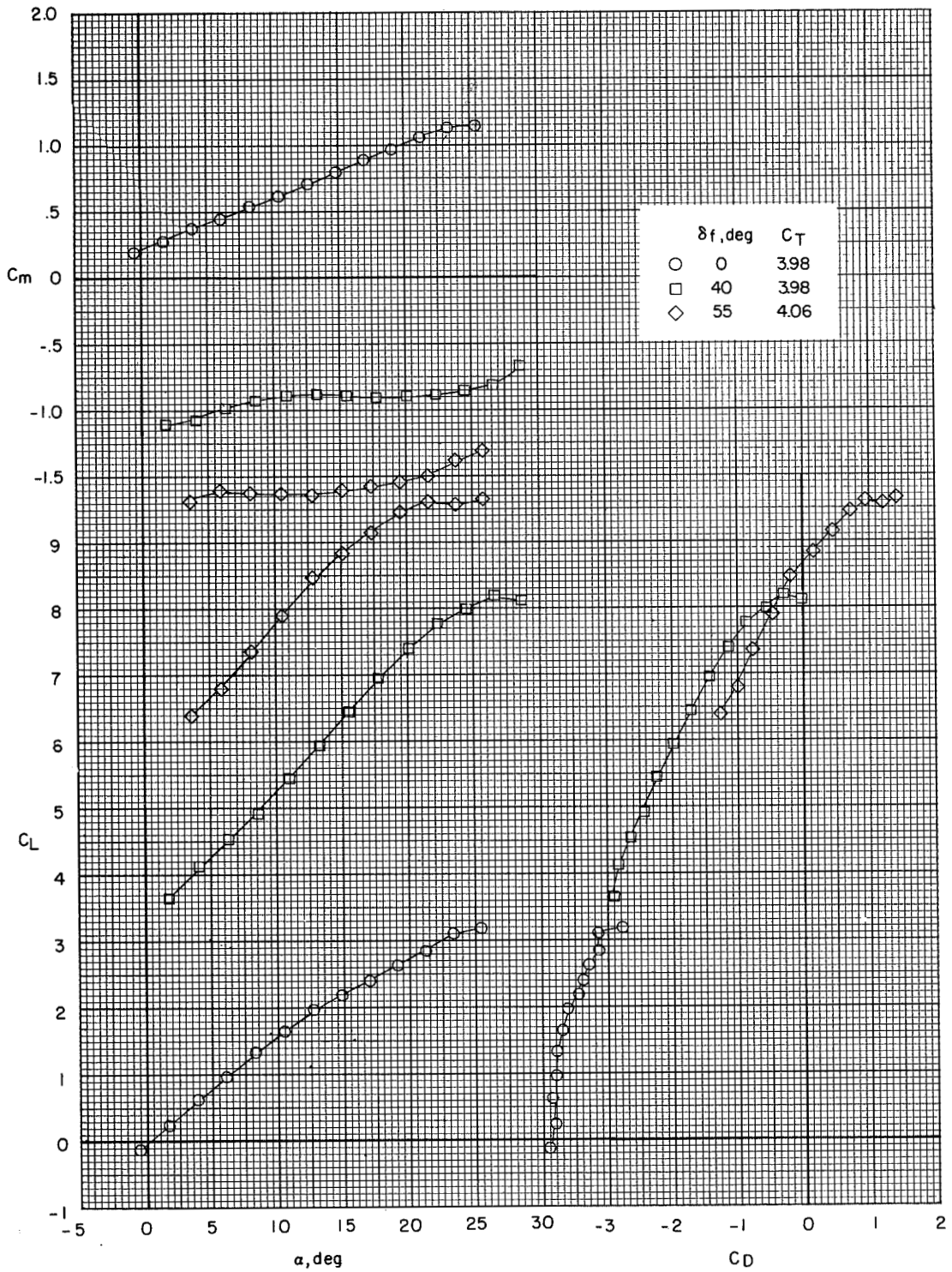

(e) $C_T \approx 4$.

Figure 20.- Concluded.

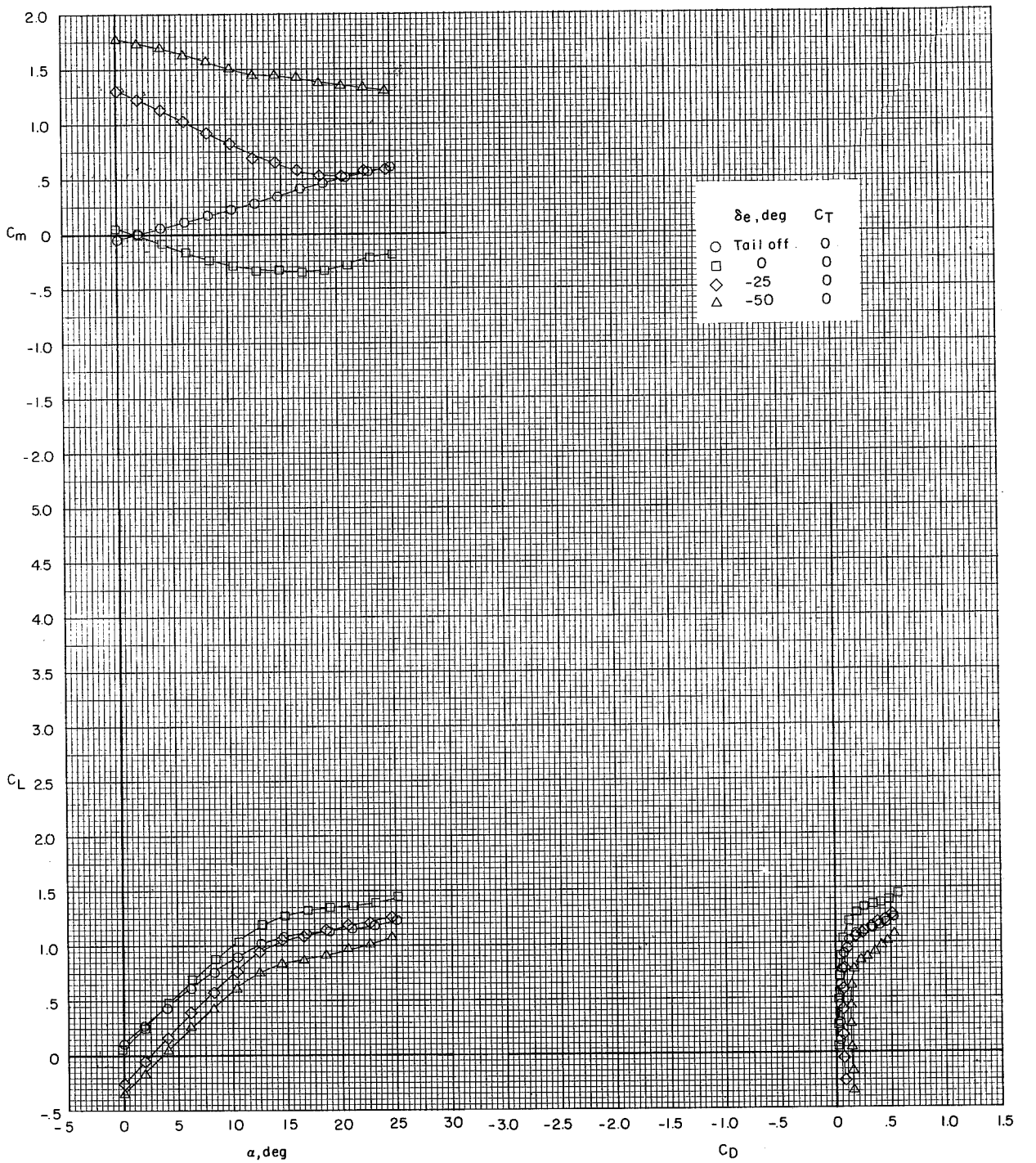

(a) $C_T = 0$.

Figure 21.- Effect of elevator deflection on longitudinal aerodynamic characteristics of the cruise configuration. Model in the V/STOL tunnel with the tunnel liner installed. $i_t = 0^o$.

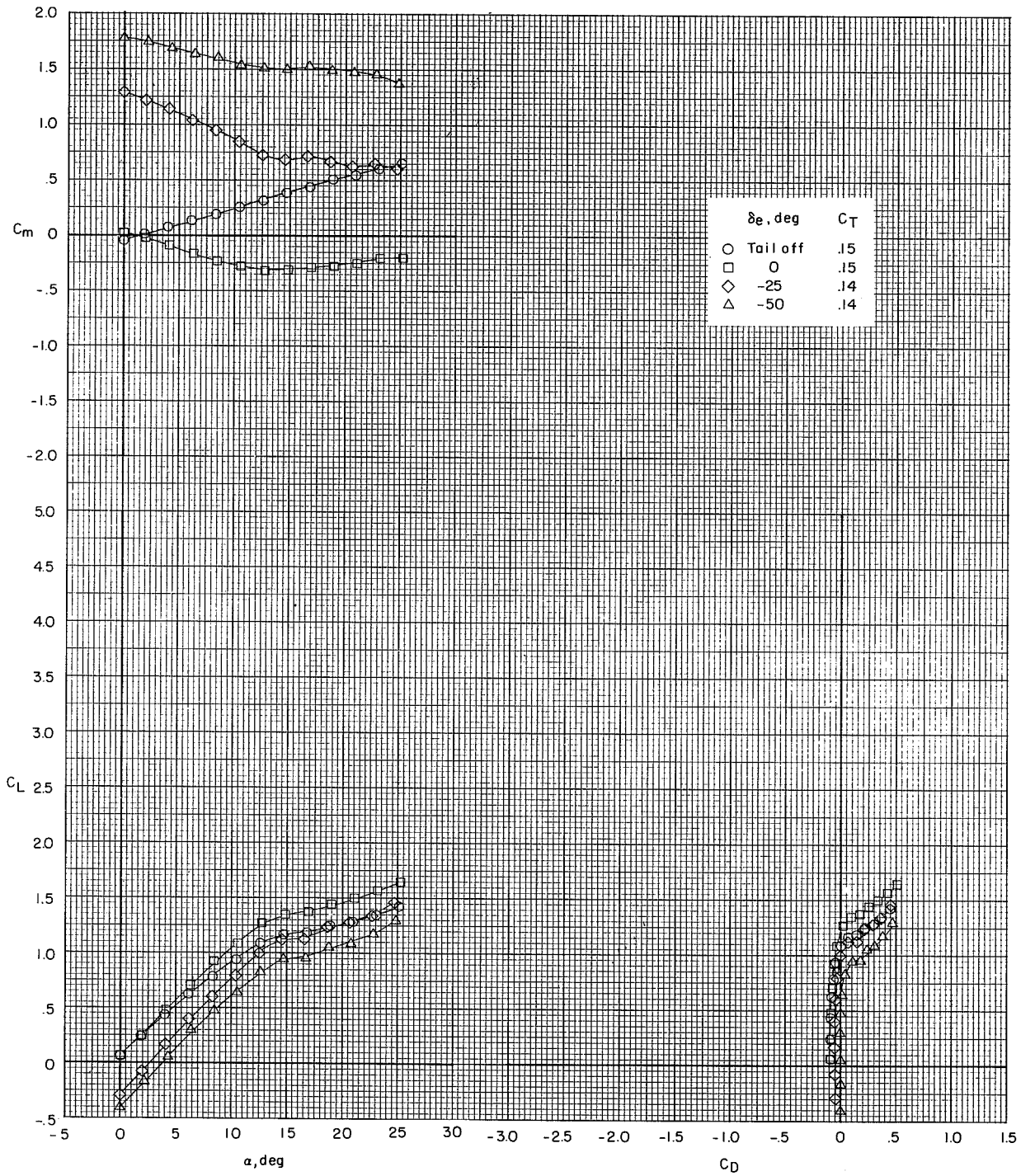

(b) $C_T \approx 0.15$.

Figure 21.- Continued.

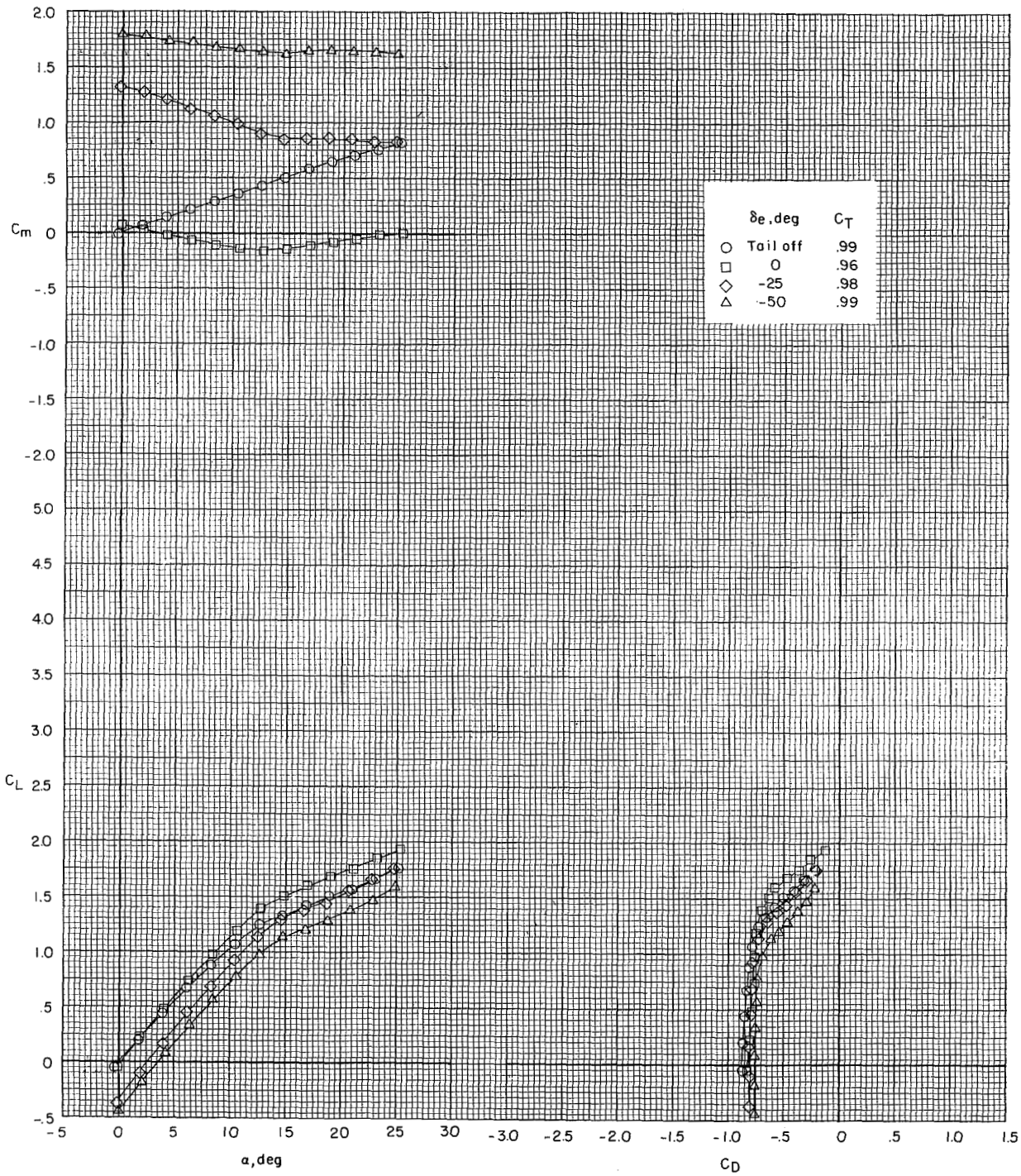

(c) $C_T \approx 1$.

Figure 21.- Continued.

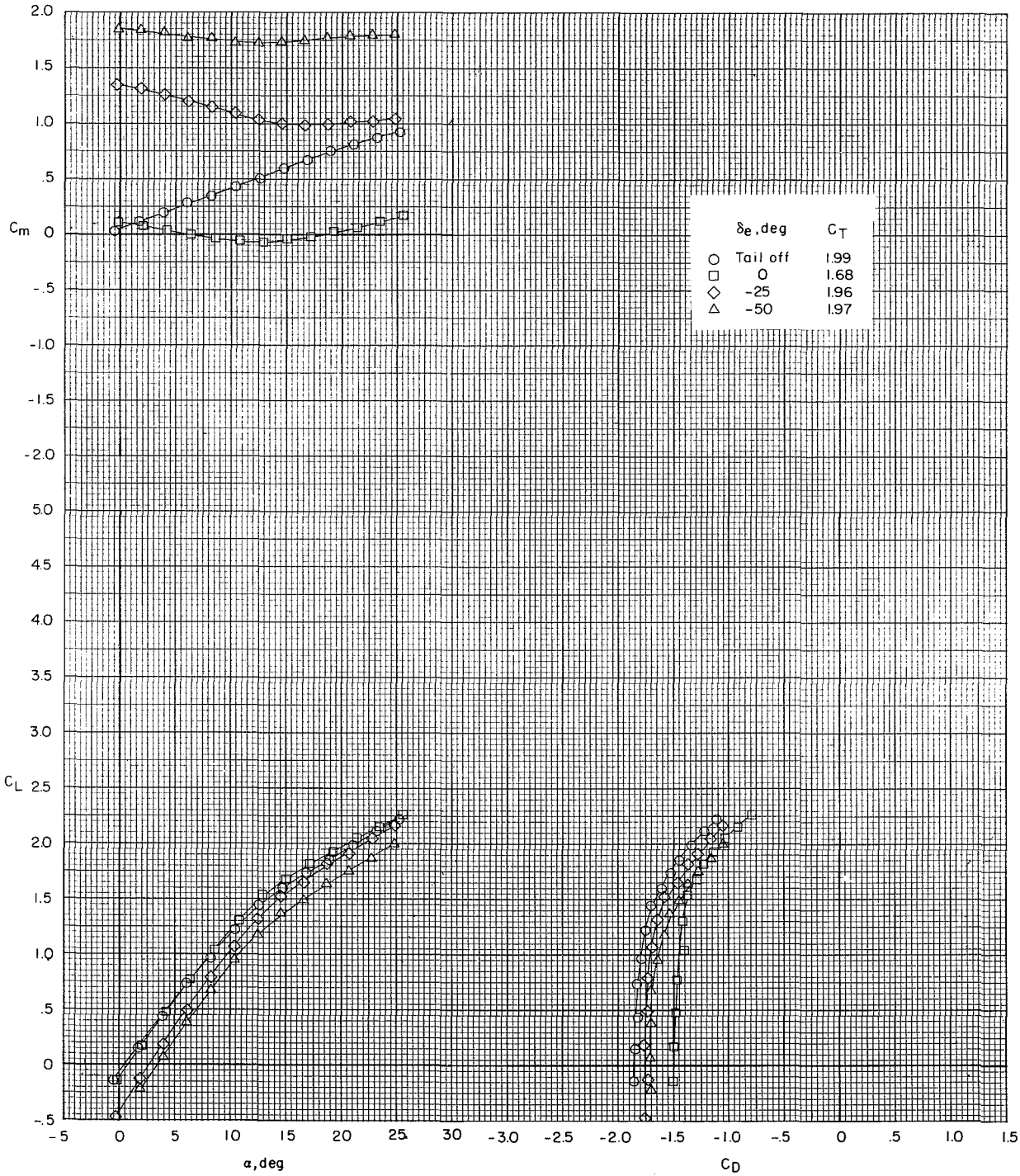

(d) $C_T \approx 2$.

Figure 21.- Continued.

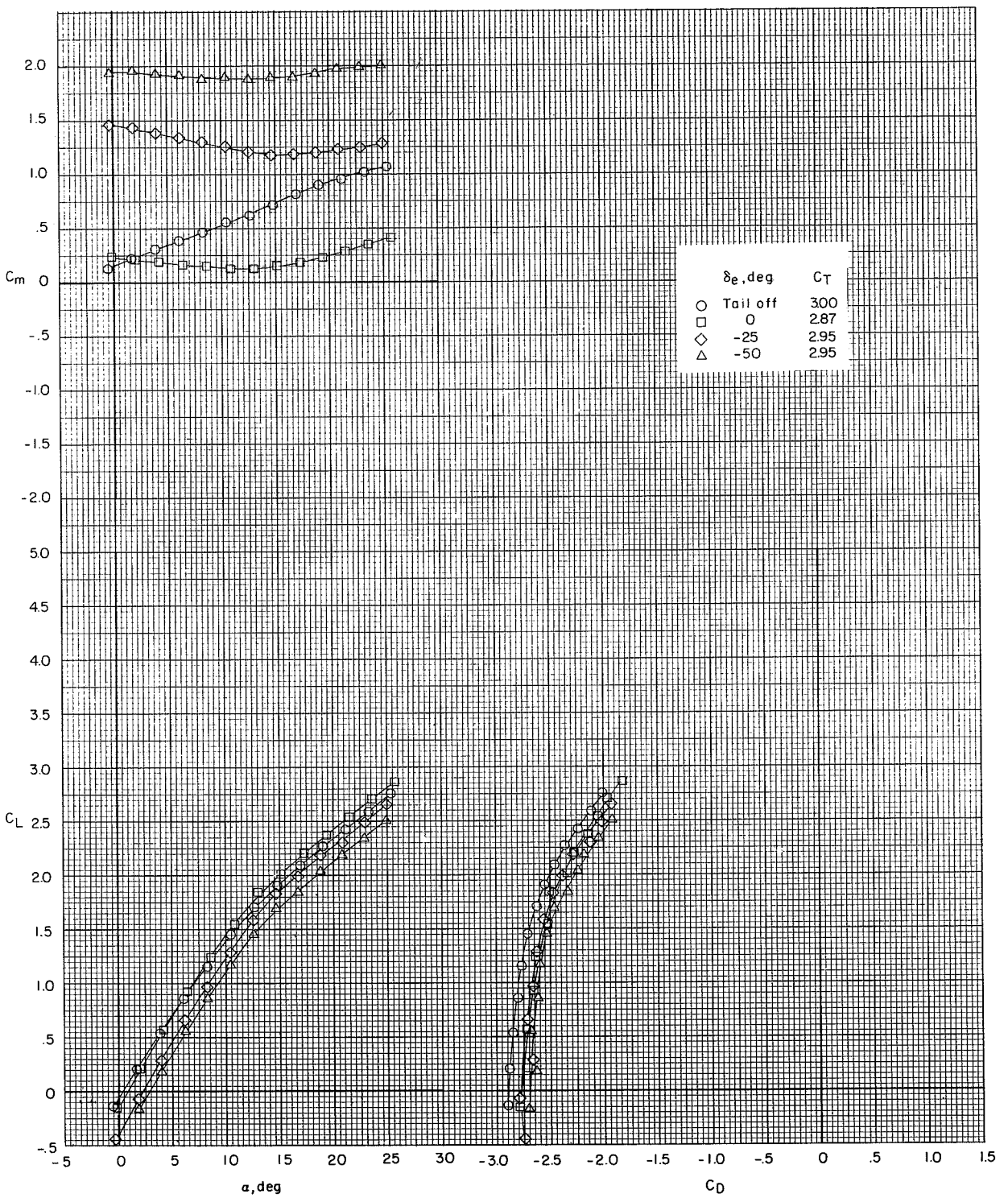

(e) $C_T \approx 3$.

Figure 21.- Continued.

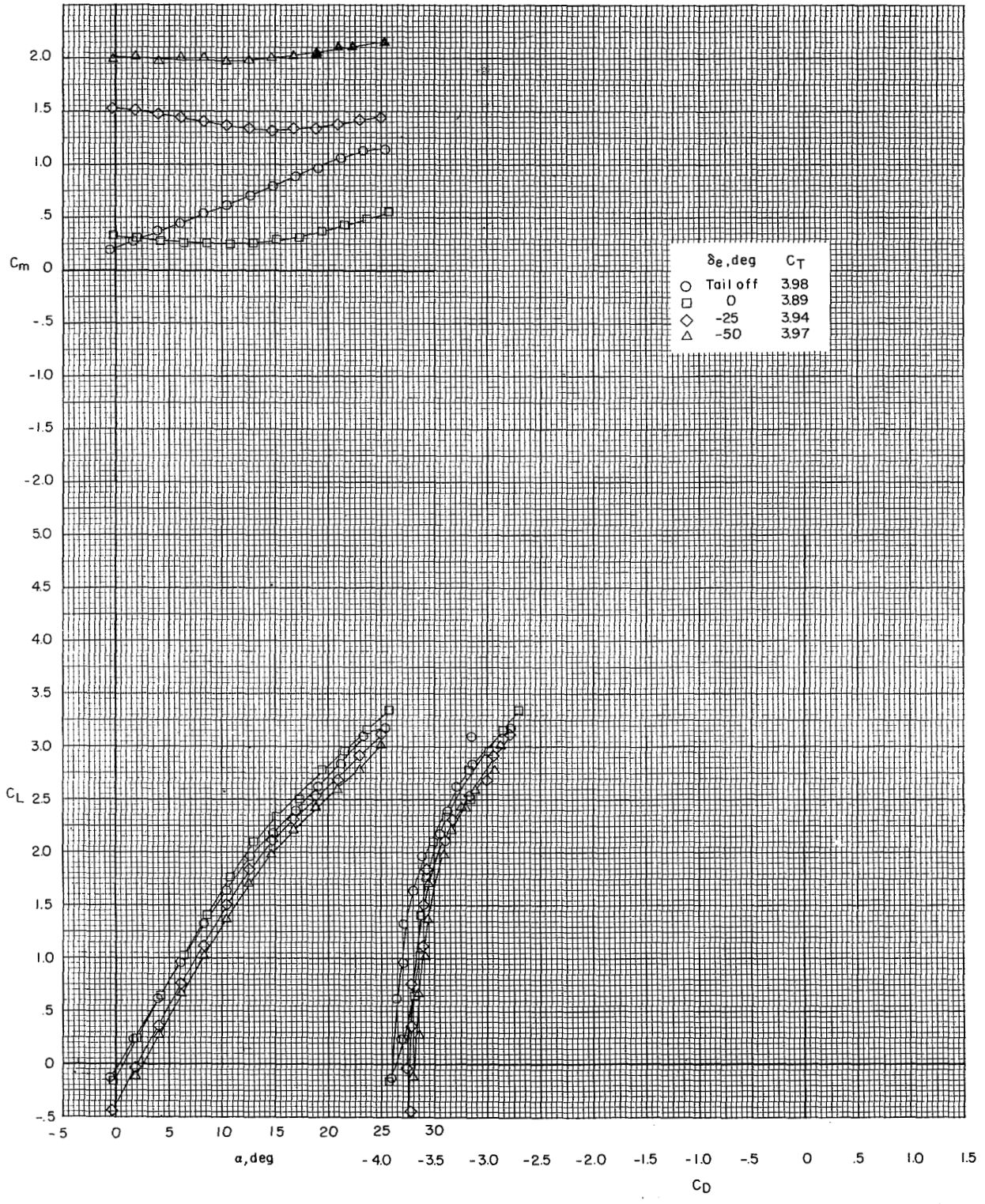

(f) $C_T \approx 4$.

Figure 21.- Concluded.

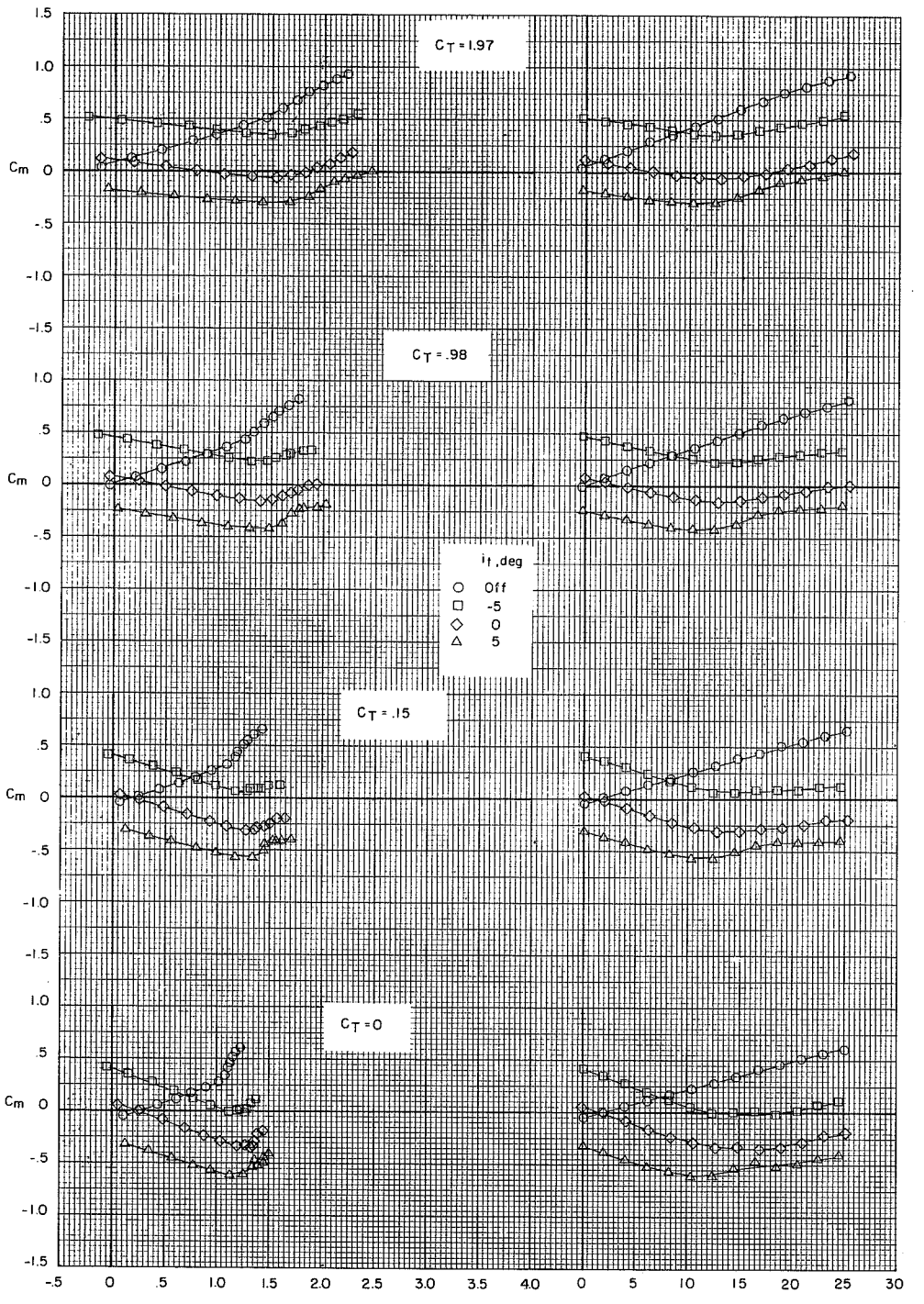

(a) $\delta_e = 0^o$.

Figure 22.- Effect of tail incidence on longitudinal aerodynamic characteristics of the cruise configuration. Model in the V/STOL tunnel with the tunnel liner installed.

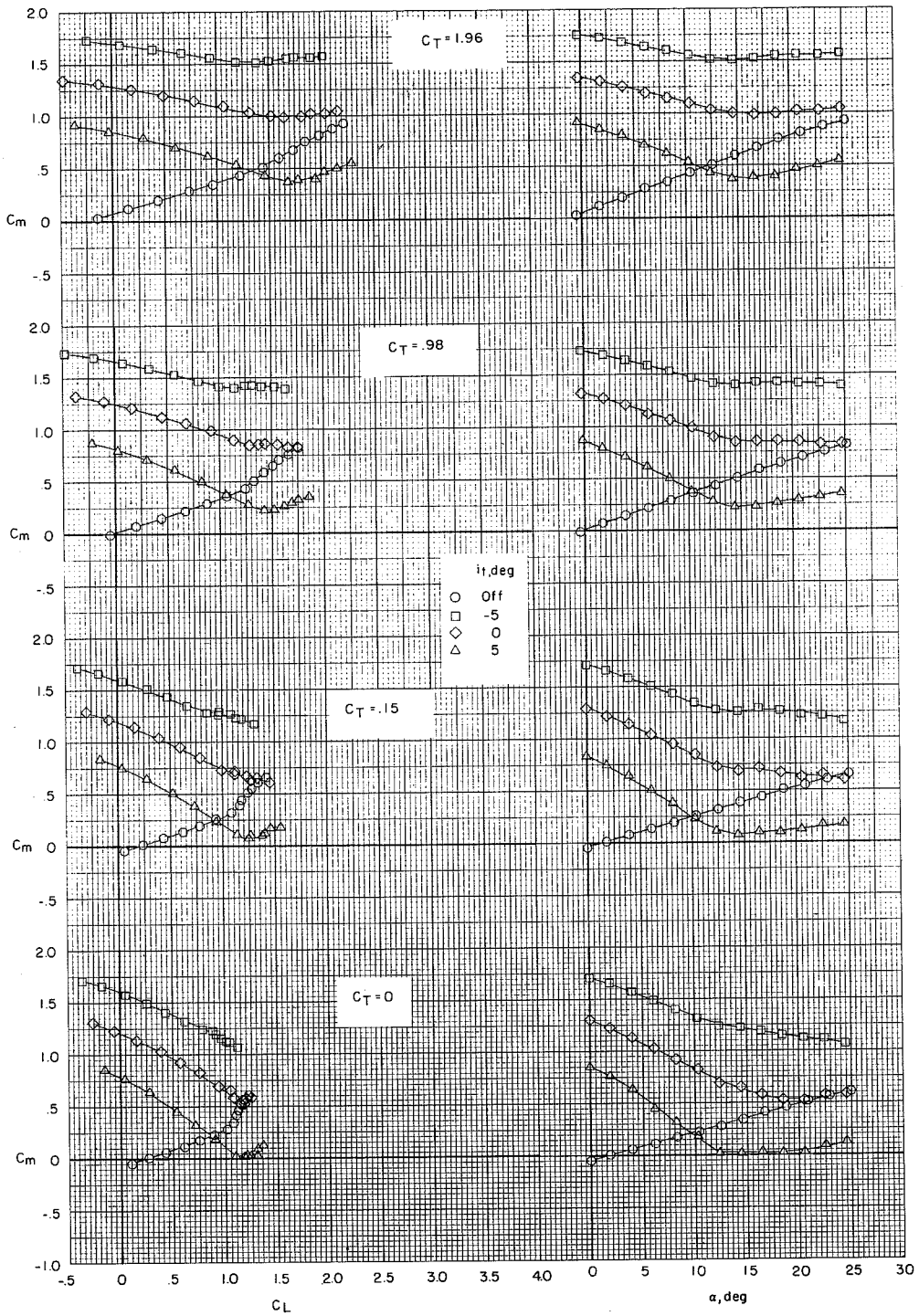

(b) $\delta_e = -25^o$.

Figure 22.- Concluded.

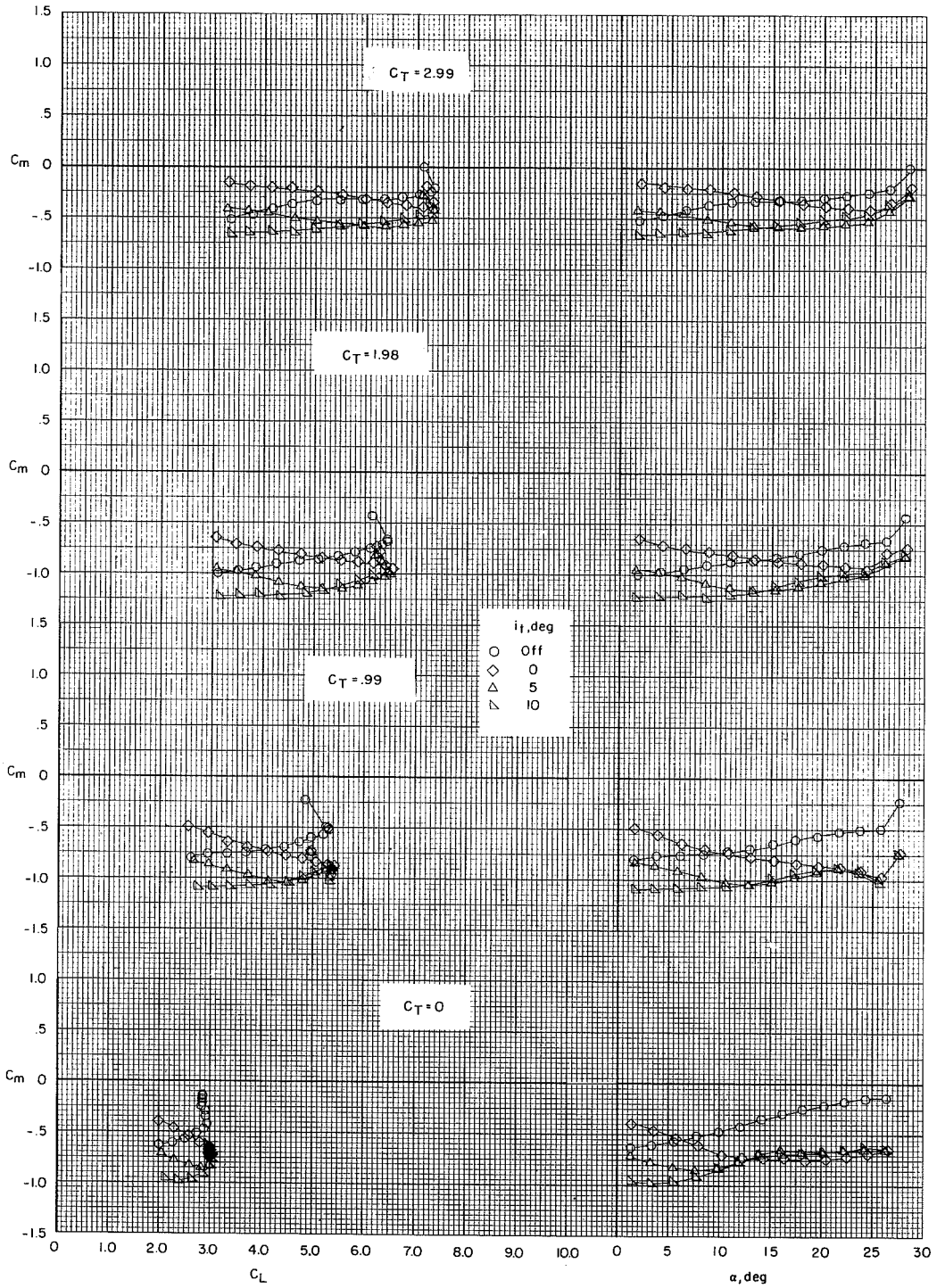

(a) $\delta_e = 0^o$.

Figure 23.- Effect of tail incidence on longitudinal aerodynamic characteristics of the take-off configuration. Model in the V/STOL tunnel with the tunnel liner installed.

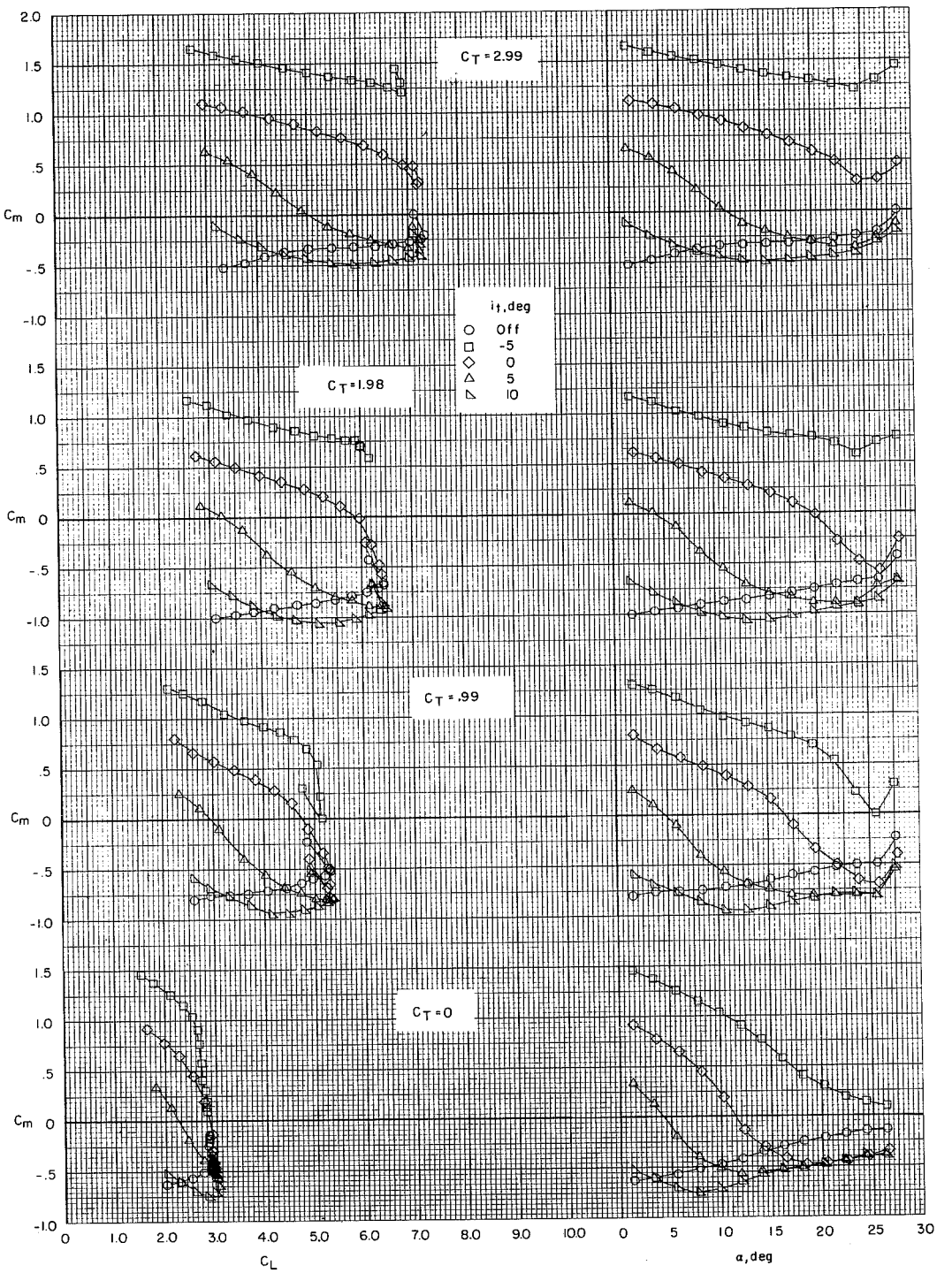

(b) $\delta_e = -25^o$.

Figure 23.- Concluded.

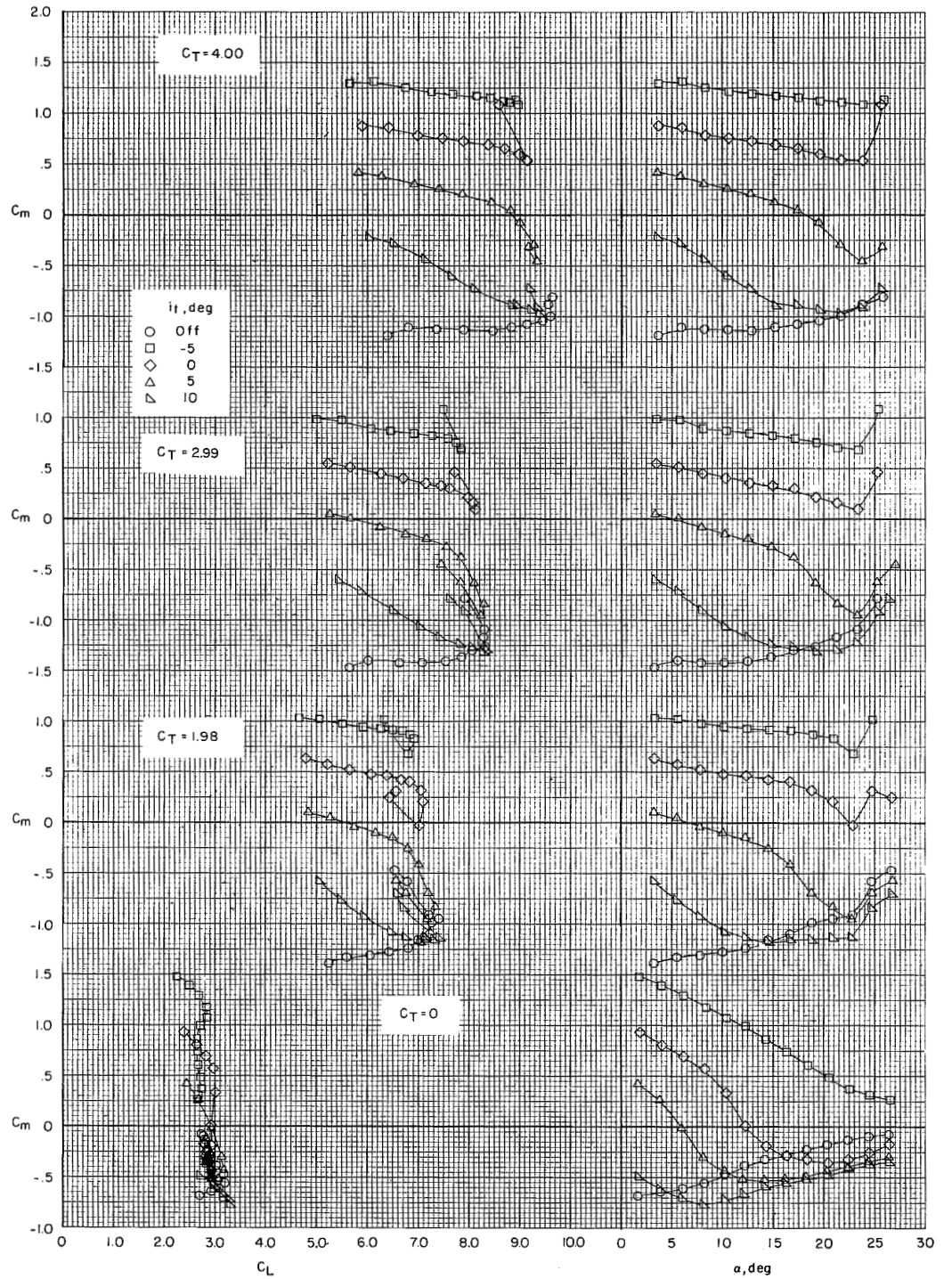

(a) $\delta_e = -25^o$.

Figure 24.- Effect of tail incidence on longitudinal aerodynamic characteristics of the landing configuration. Model in the V/STOL tunnel with the tunnel liner installed.

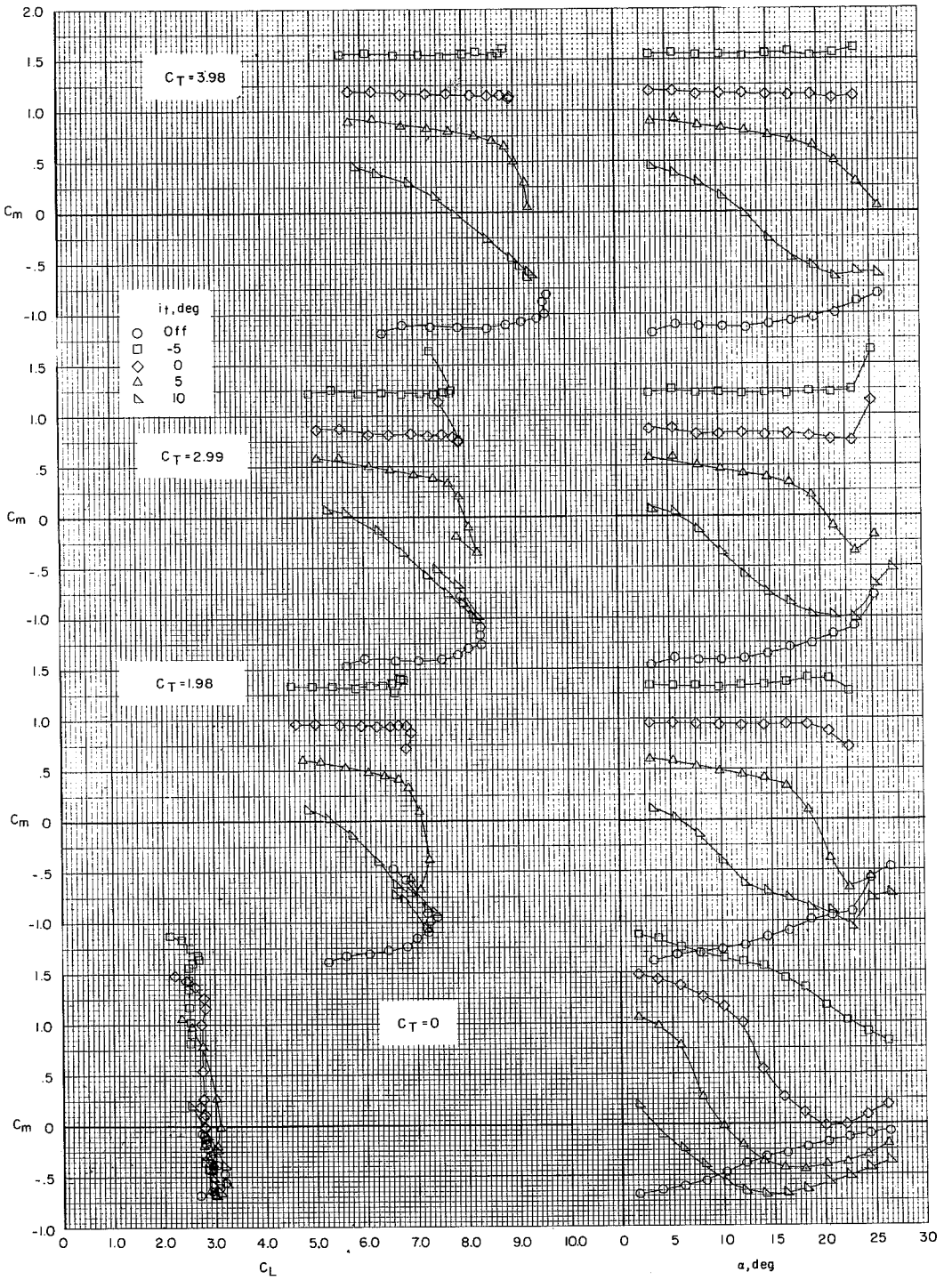

(b) $\delta_e = -50^o$.

Figure 24.- Concluded.

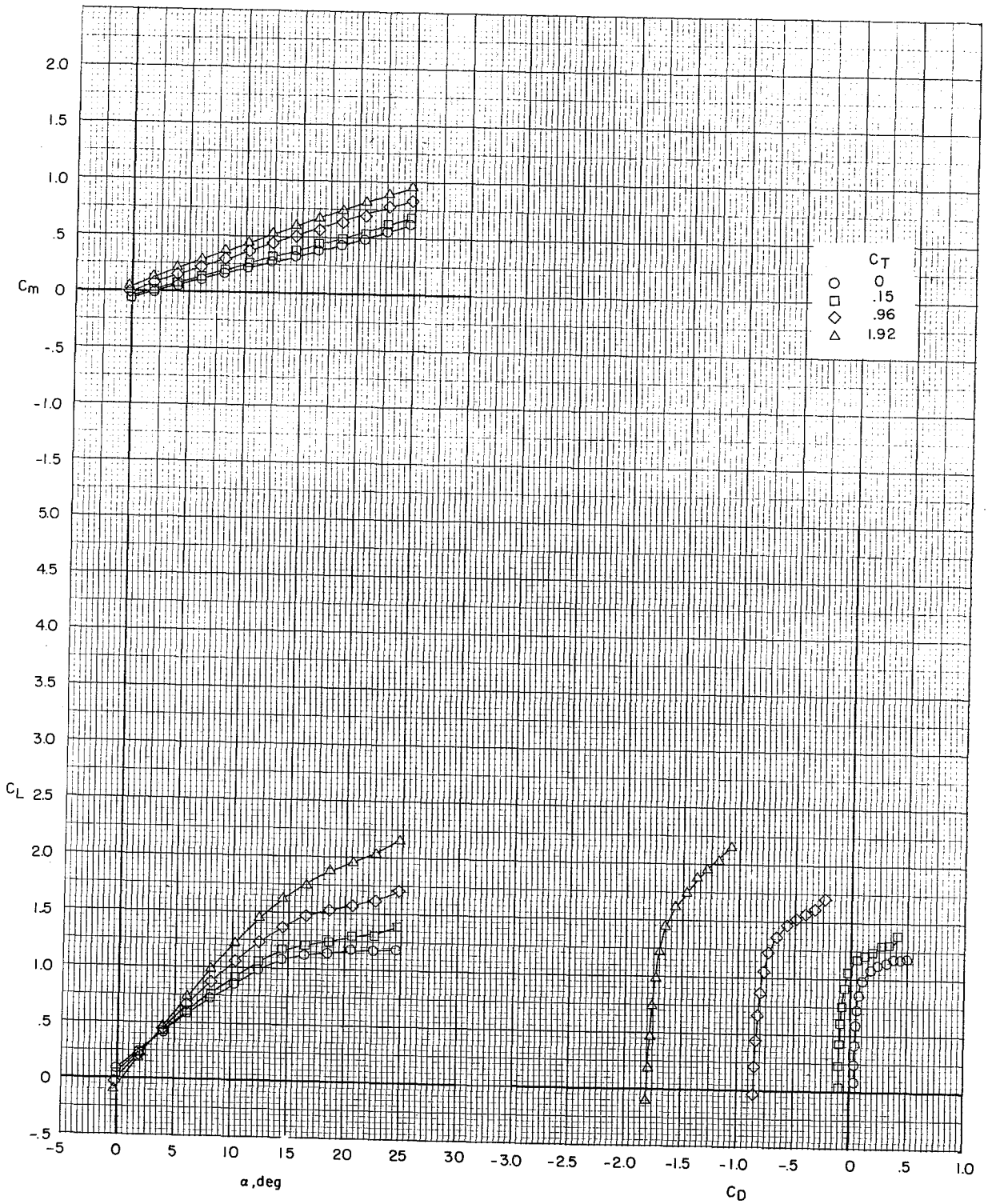

Figure 25.- Effect of thrust coefficient on longitudinal aerodynamic characteristics of the cruise configuration. Tail off. Model in the V/STOL tunnel without the tunnel liner installed.

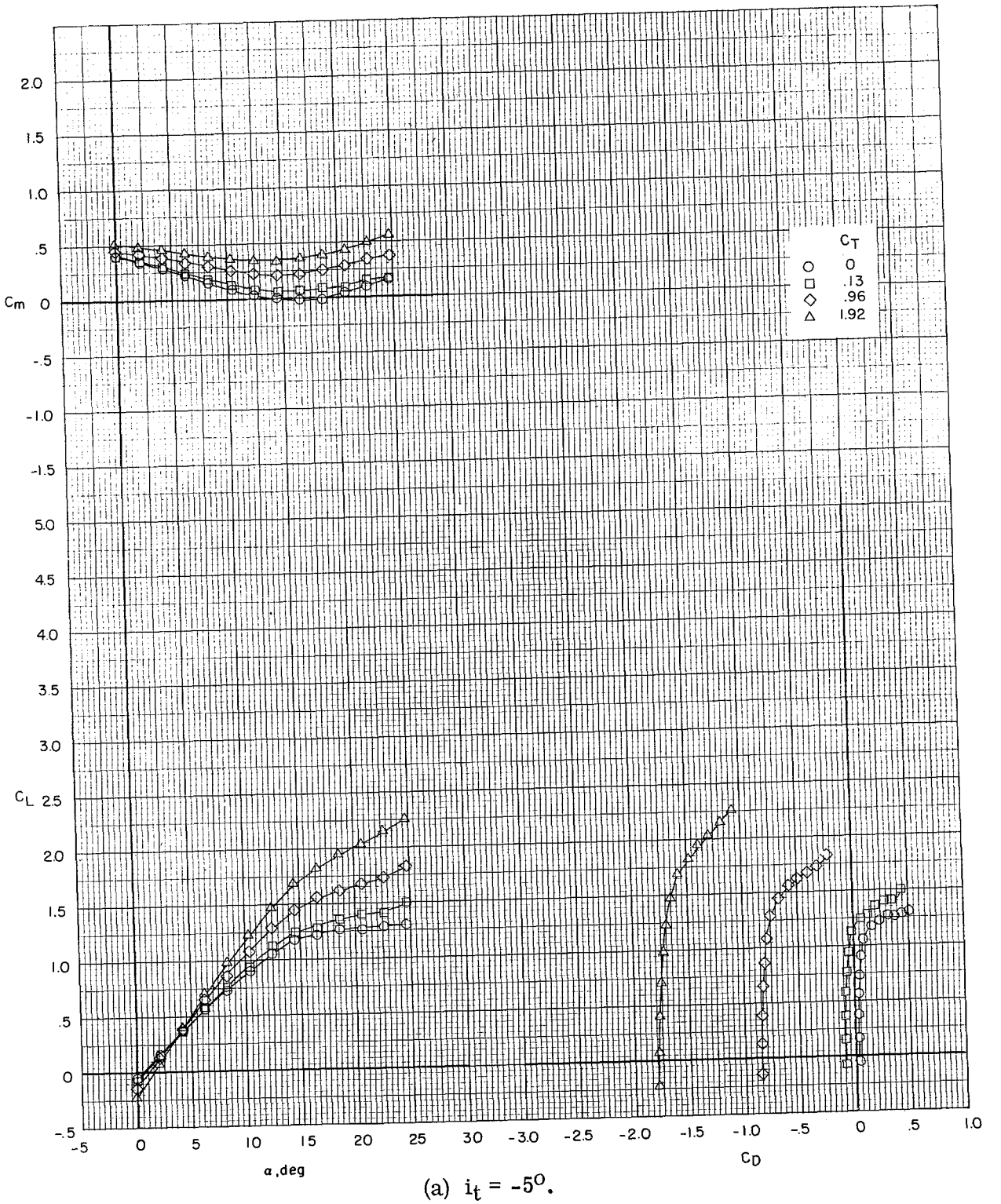

(a) $i_t = -5^o$.

Figure 26.- Effect of thrust coefficient on longitudinal aerodynamic characteristics of the cruise configuration. $\delta_e = 0^o$. Model in the V/STOL tunnel without the tunnel liner installed.

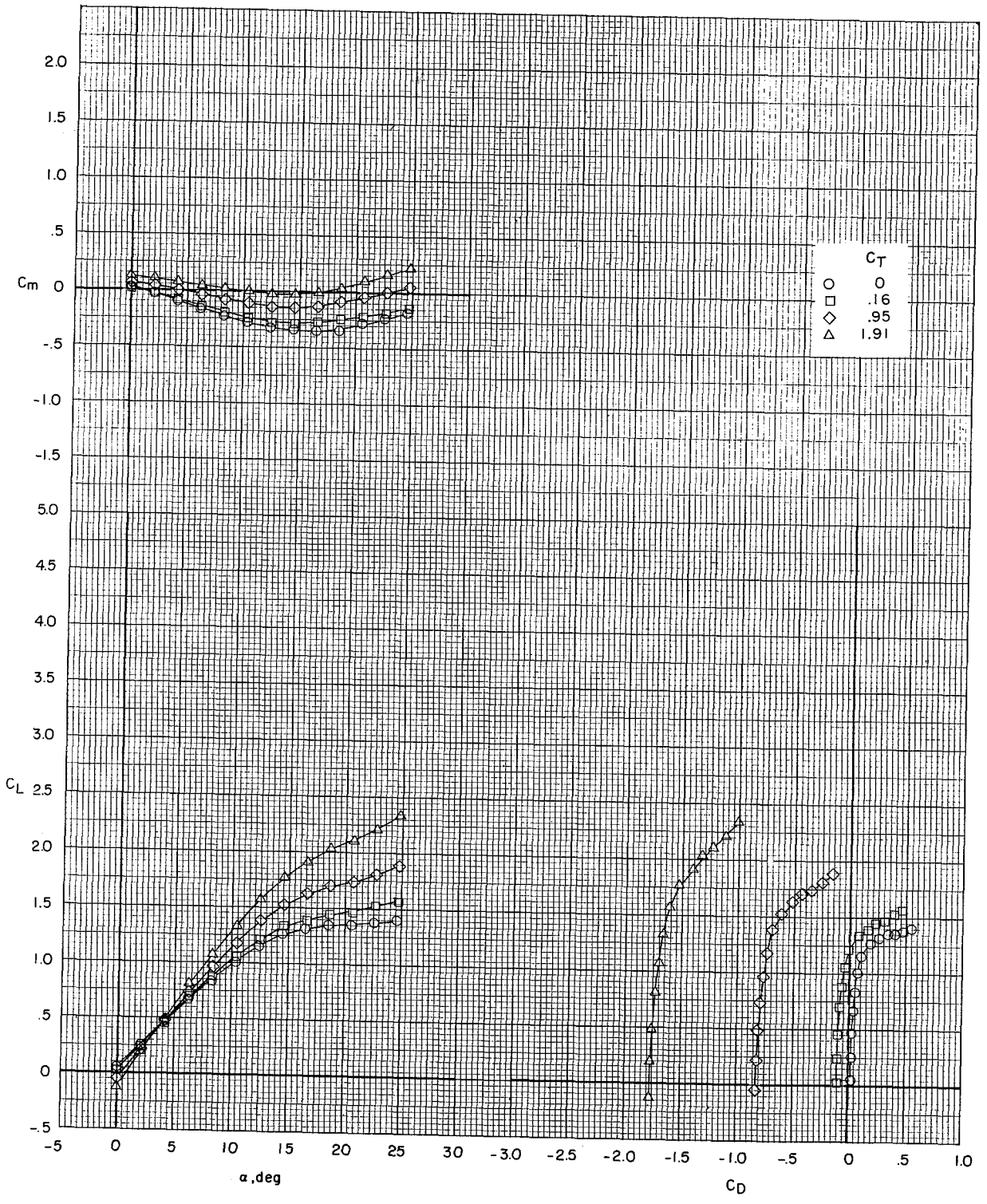

(b) $i_t = 0^o$.

Figure 26.- Continued.

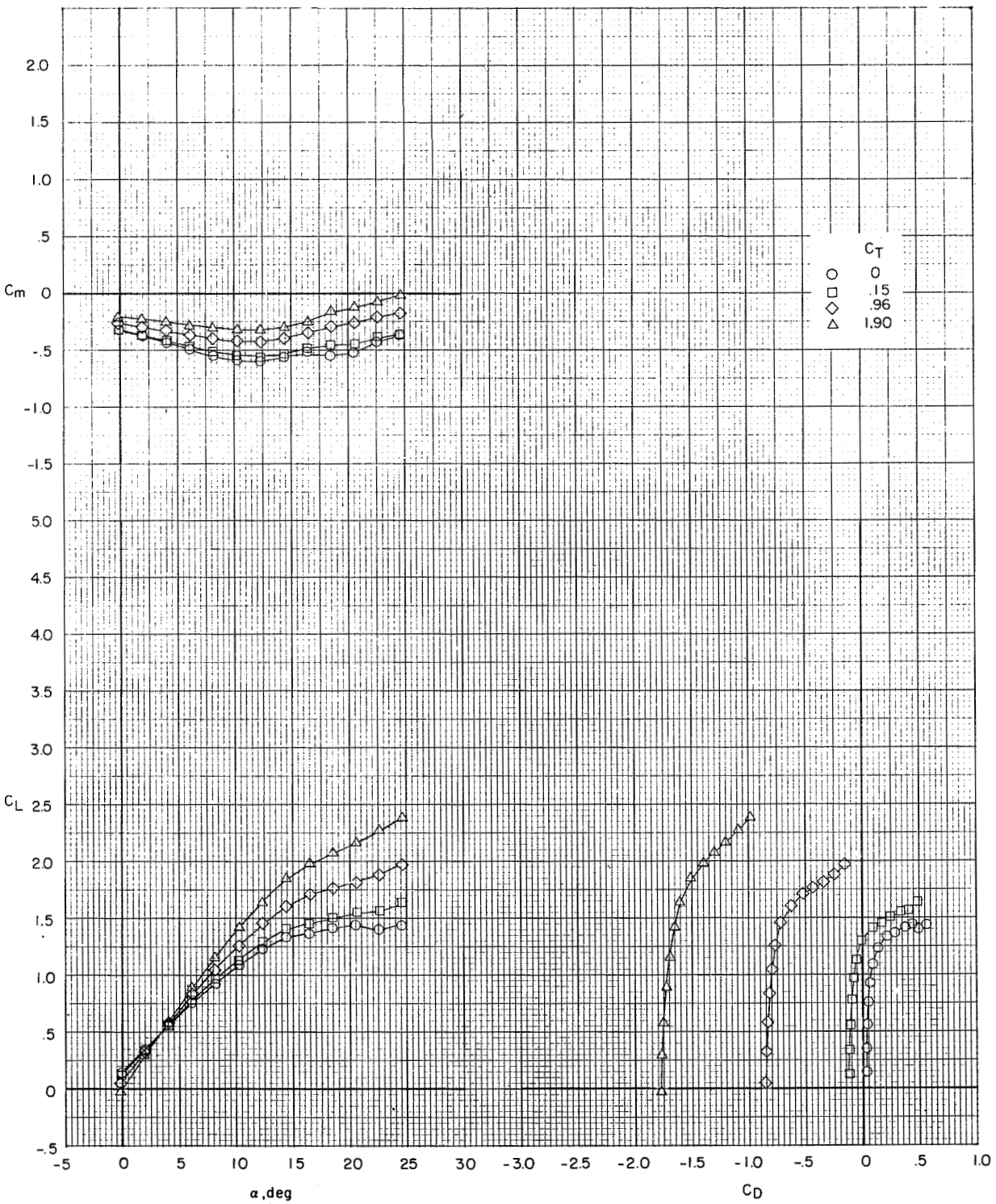

(c) $i_t = 5^o$.

Figure 26.- Concluded.

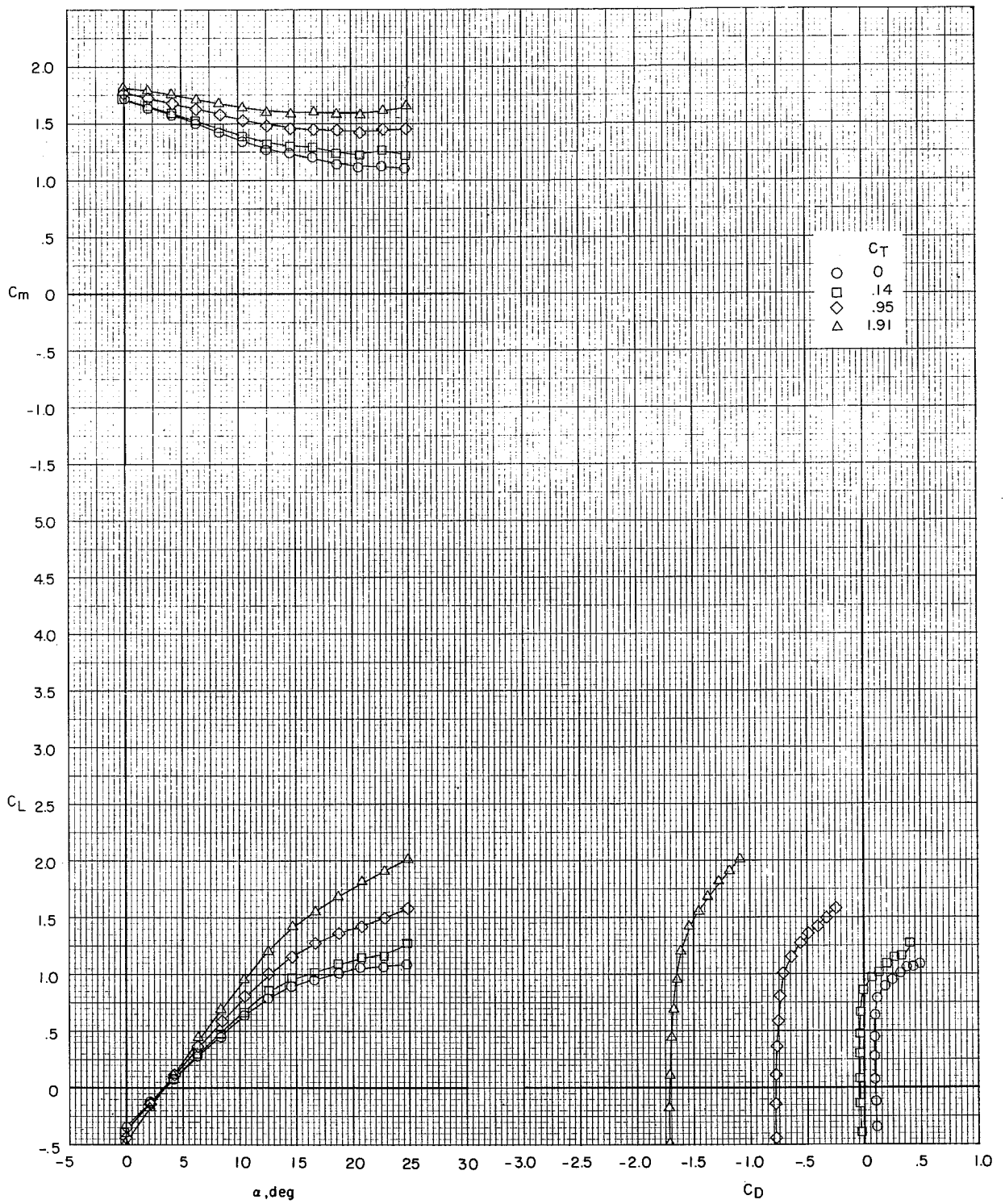

(a) $i_t = -5^o$.

Figure 27.- Effect of thrust coefficient on longitudinal aerodynamic characteristics of the cruise configuration. $\delta_e = -25^o$. Model in the V/STOL tunnel without the tunnel liner installed.

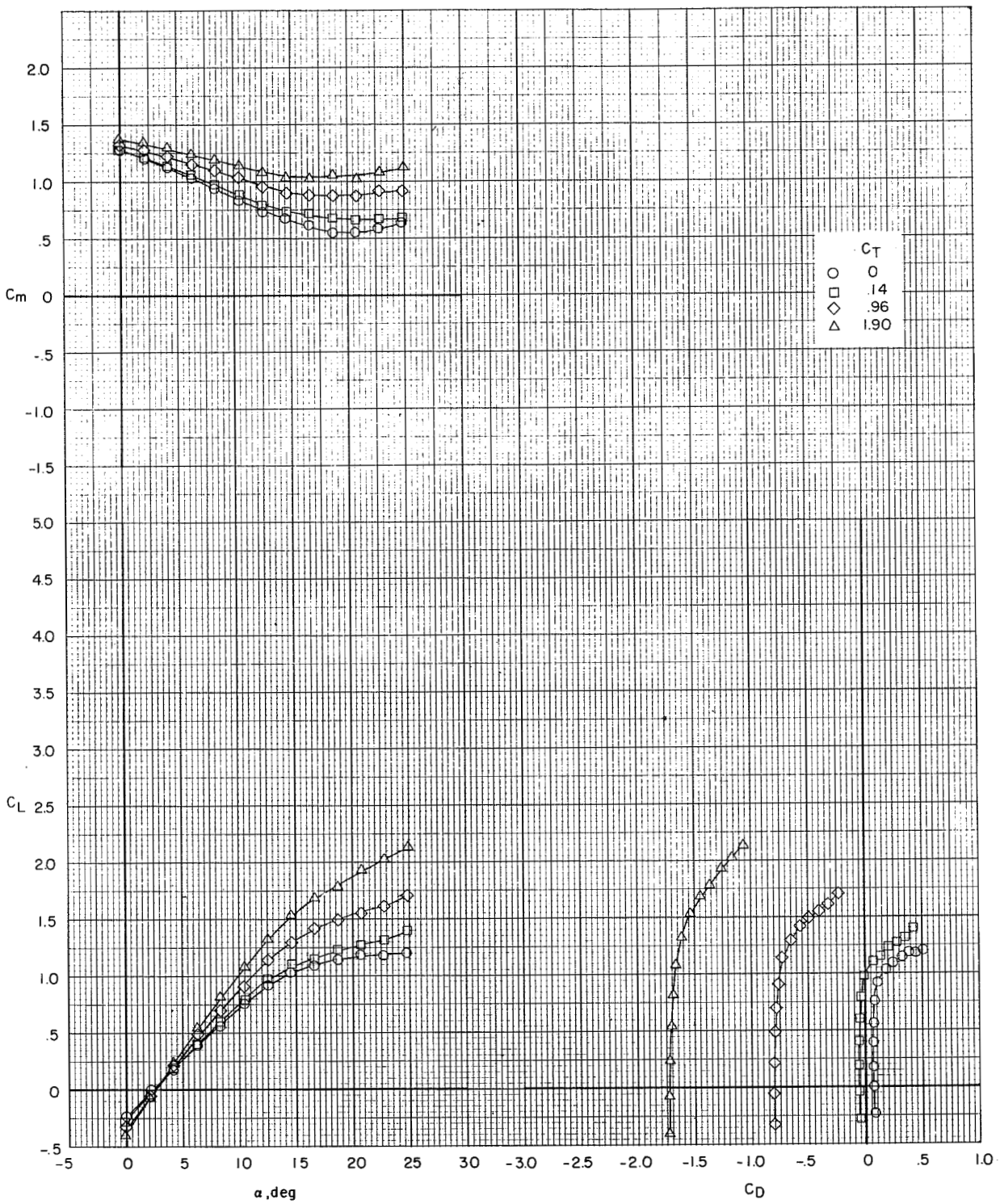

(b) $i_t = 0^o$.

Figure 27.- Continued.

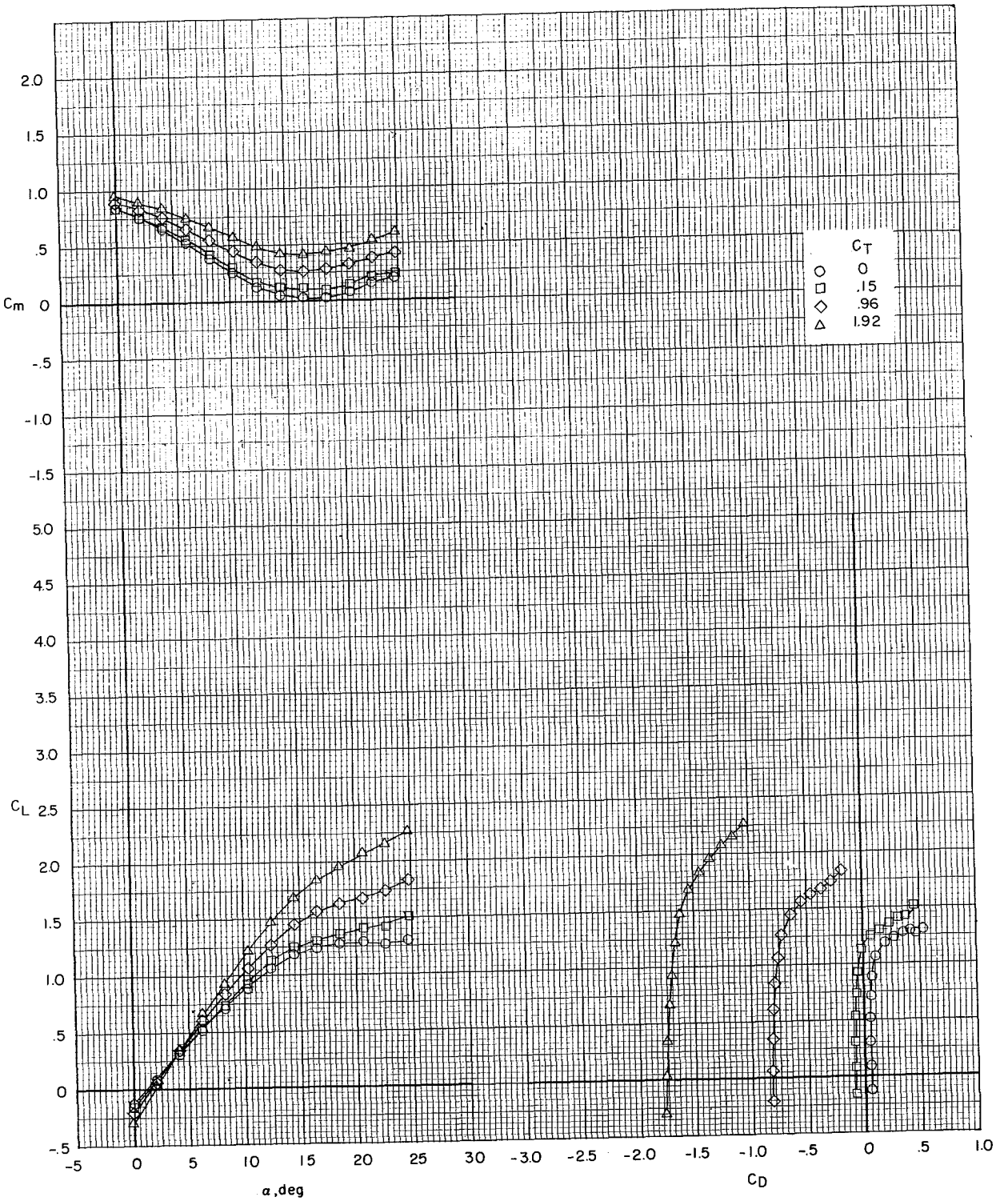

(c) $i_t = 5^o$.

Figure 27.- Concluded.

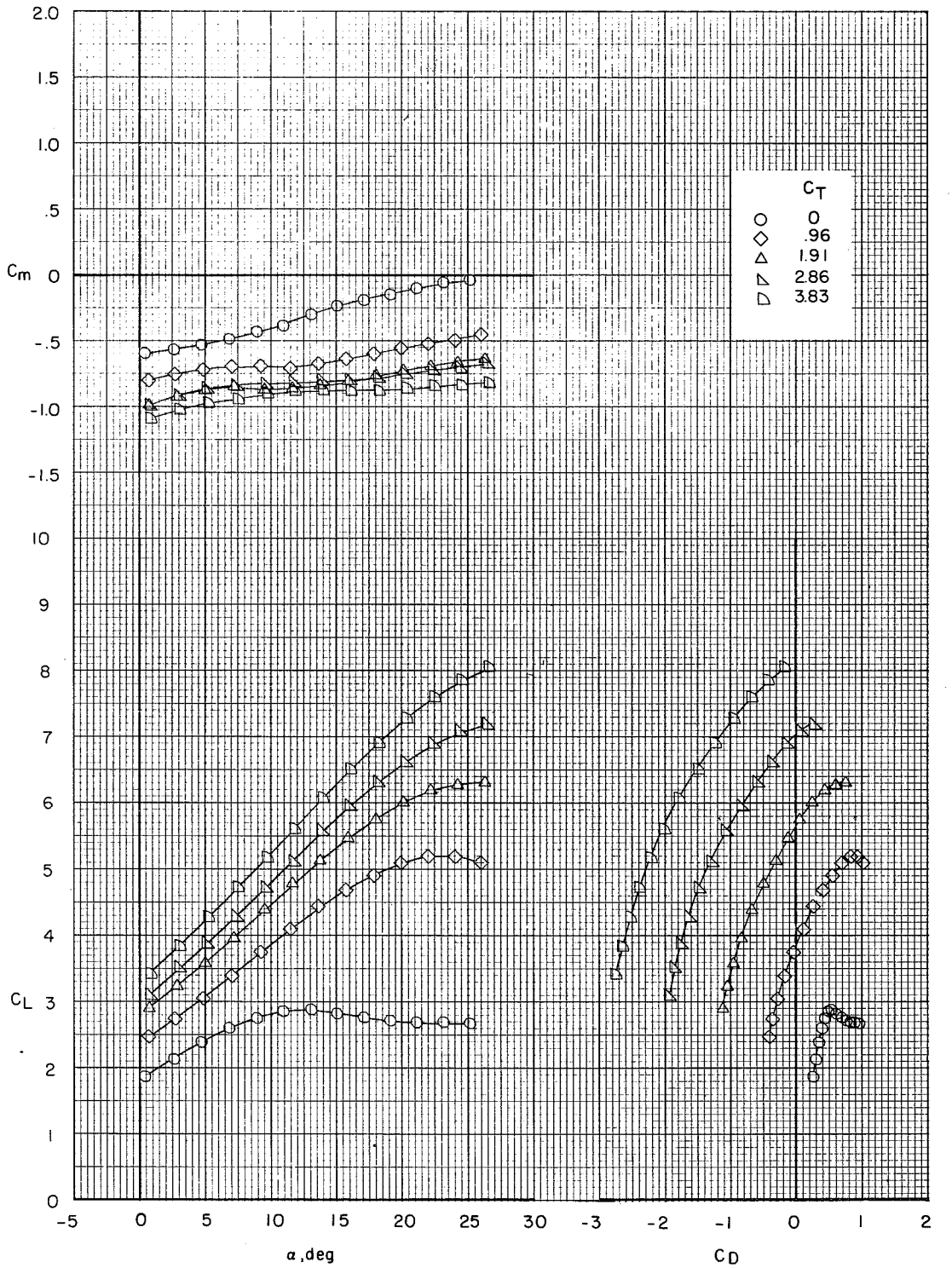

Figure 28.- Effect of thrust coefficient on longitudinal aerodynamic characteristics of the take-off configuration. Tail off. Model in the V/STOL tunnel without the tunnel liner installed.

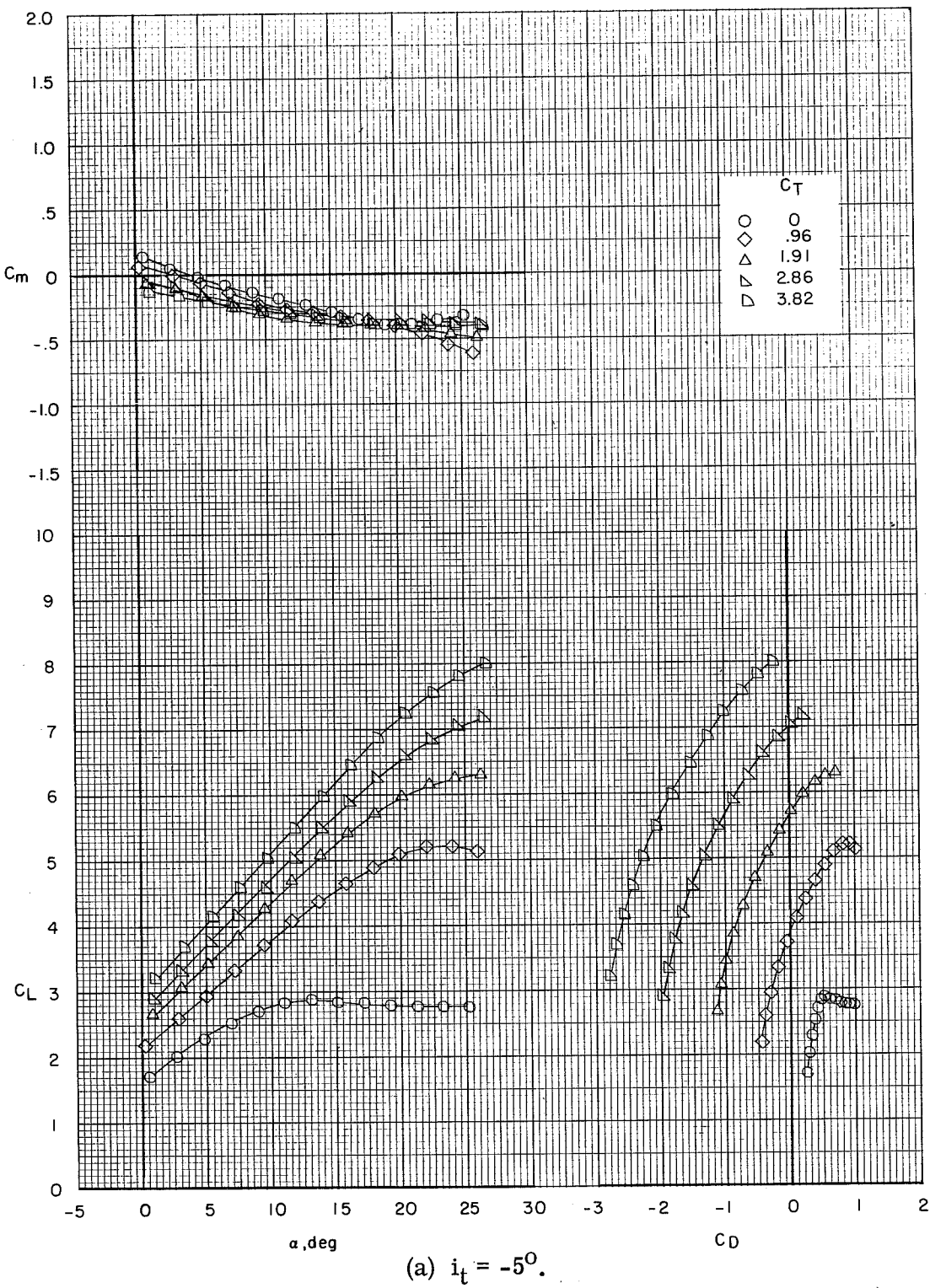

(a) $i_t = -5^o$.

Figure 29.- Effect of thrust coefficient on longitudinal aerodynamic characteristics of the take-off configuration. $\delta_e = 0^o$. Model in the V/STOL tunnel without the tunnel liner installed.

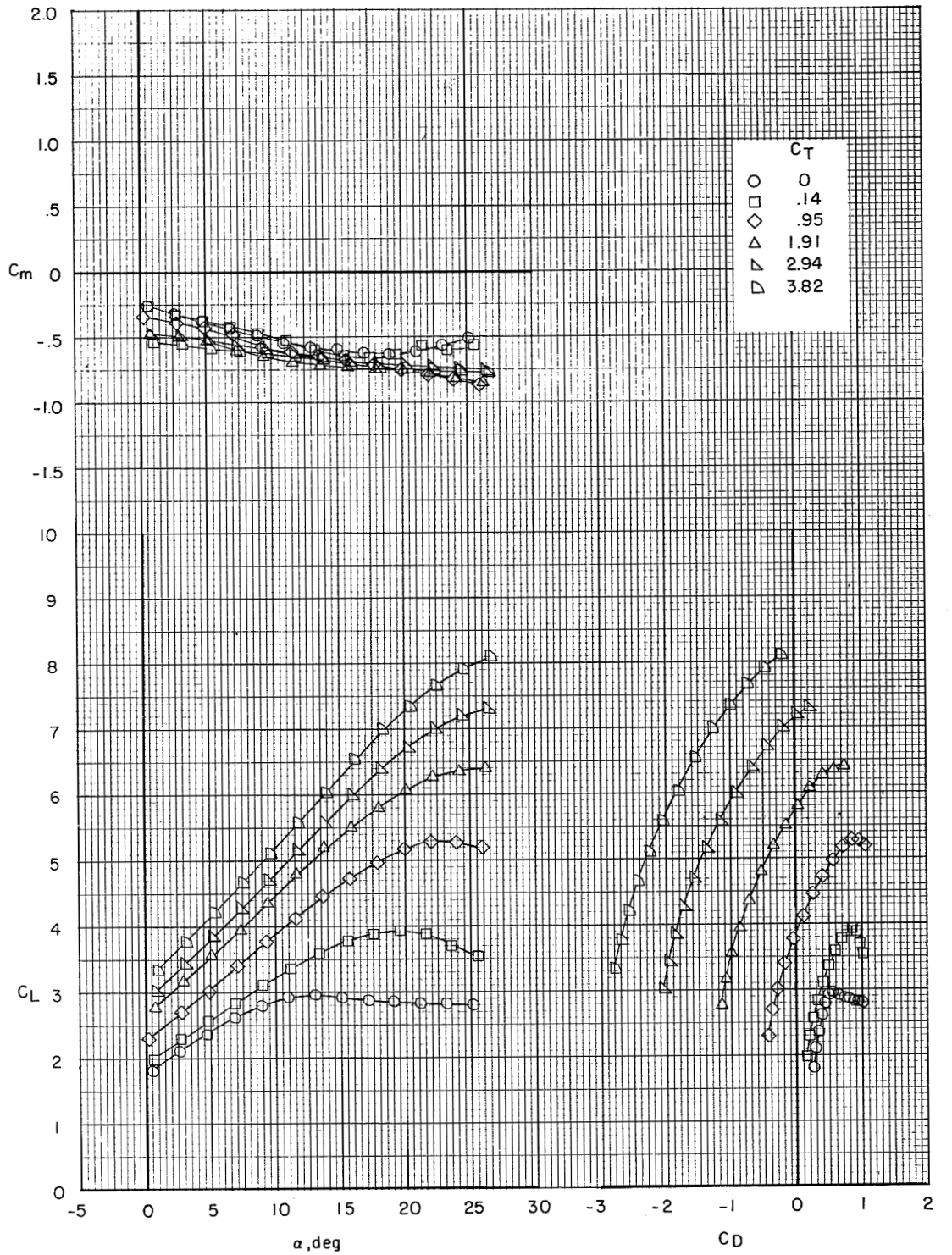

(b) $i_t = 0^o$.

Figure 29.- Continued.

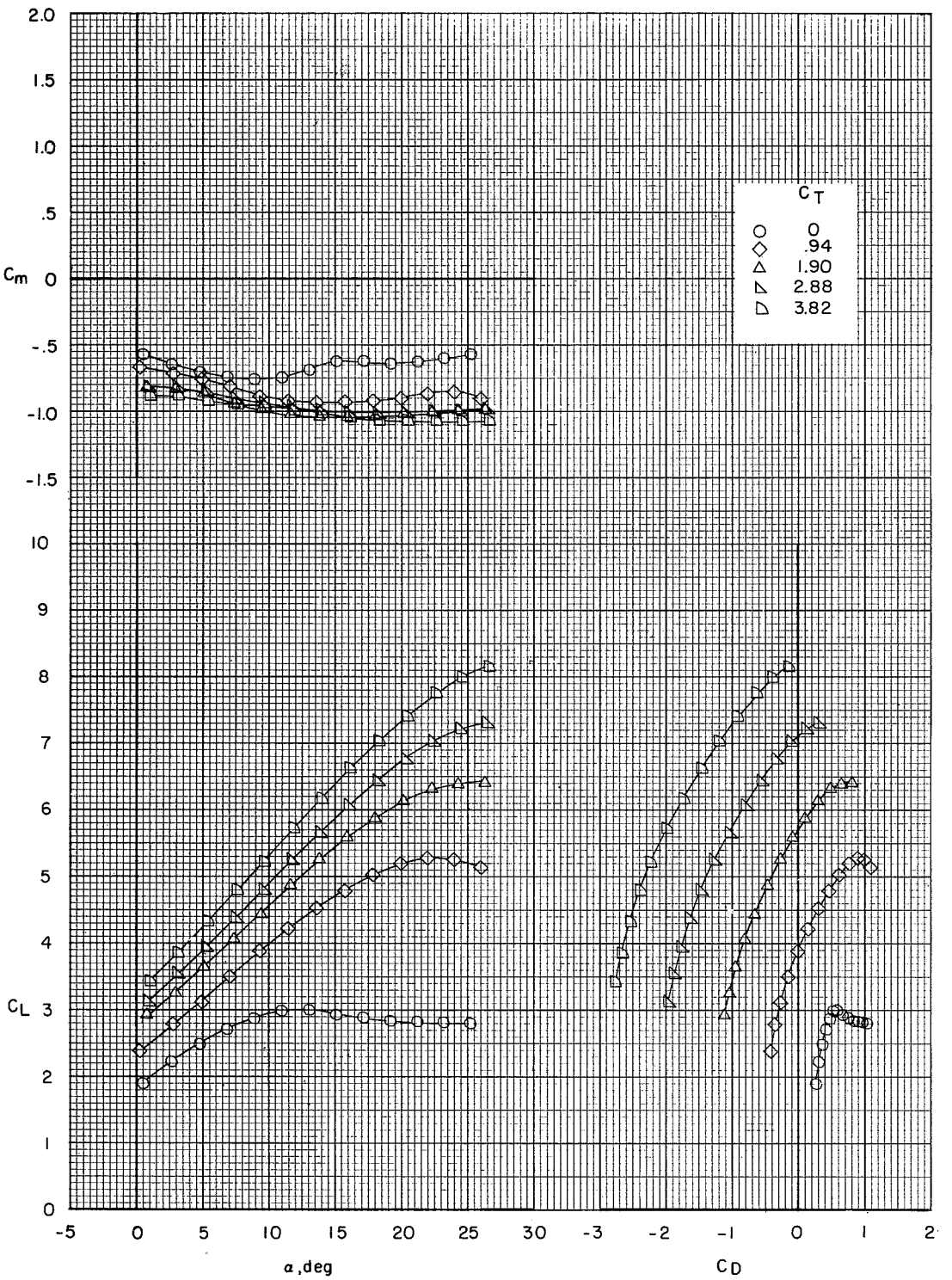

(c) $i_t = 5^o$.

Figure 29.- Concluded.

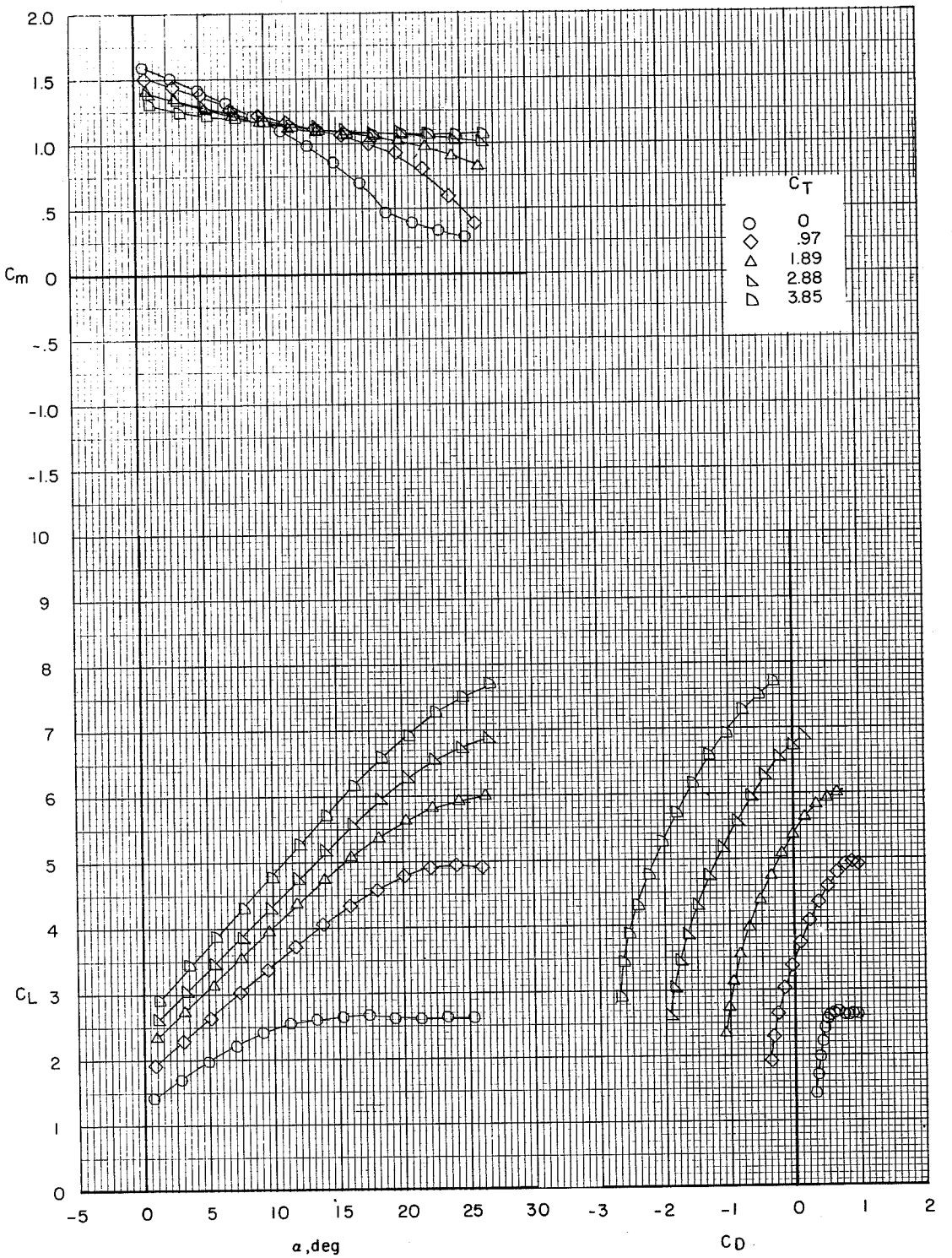

(a) $i_t = -5^o$.

Figure 30.- Effect of thrust coefficient on longitudinal aerodynamic characteristics of the take-off configuration. $\delta_e = -25^o$. Model in the V/STOL tunnel without the tunnel liner installed.

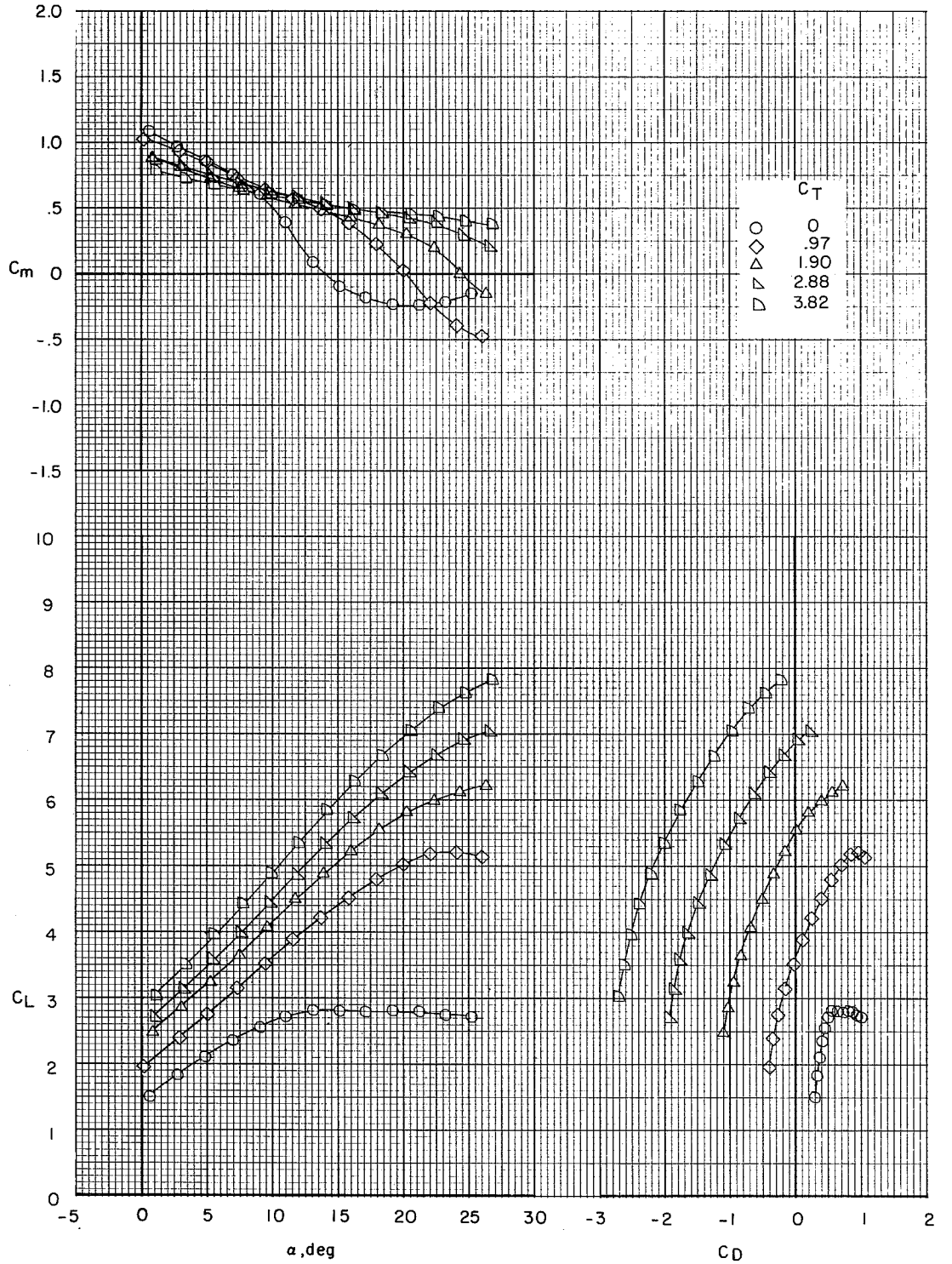

(b) $i_t = 0^o$.

Figure 30.- Continued.

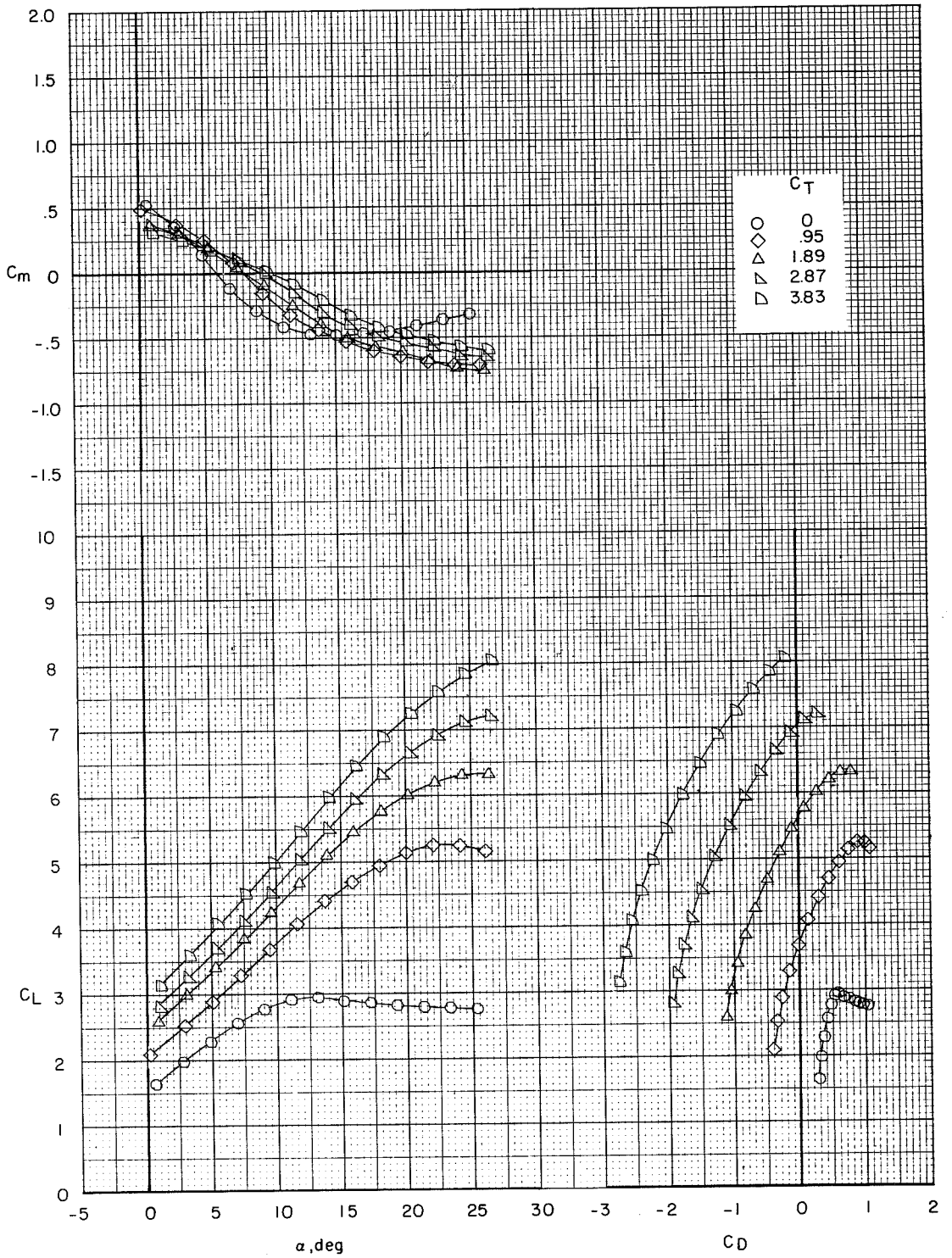

(c) $i_t = 5^o$.

Figure 30.- Concluded.

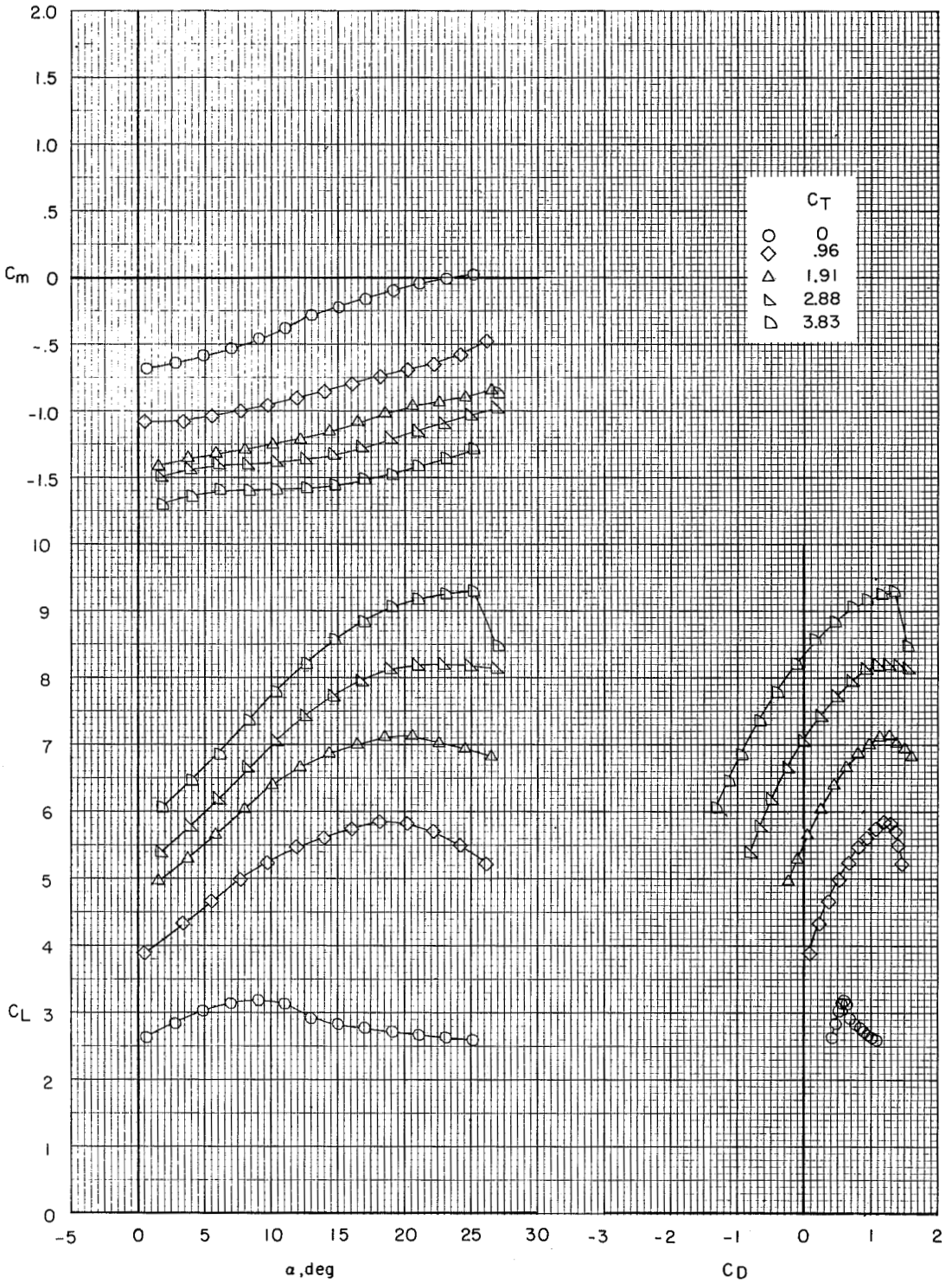

Figure 31.- Effect of thrust coefficient on longitudinal aerodynamic characteristics of the landing configuration. Tail off. Model in the V/STOL tunnel without the tunnel liner installed.

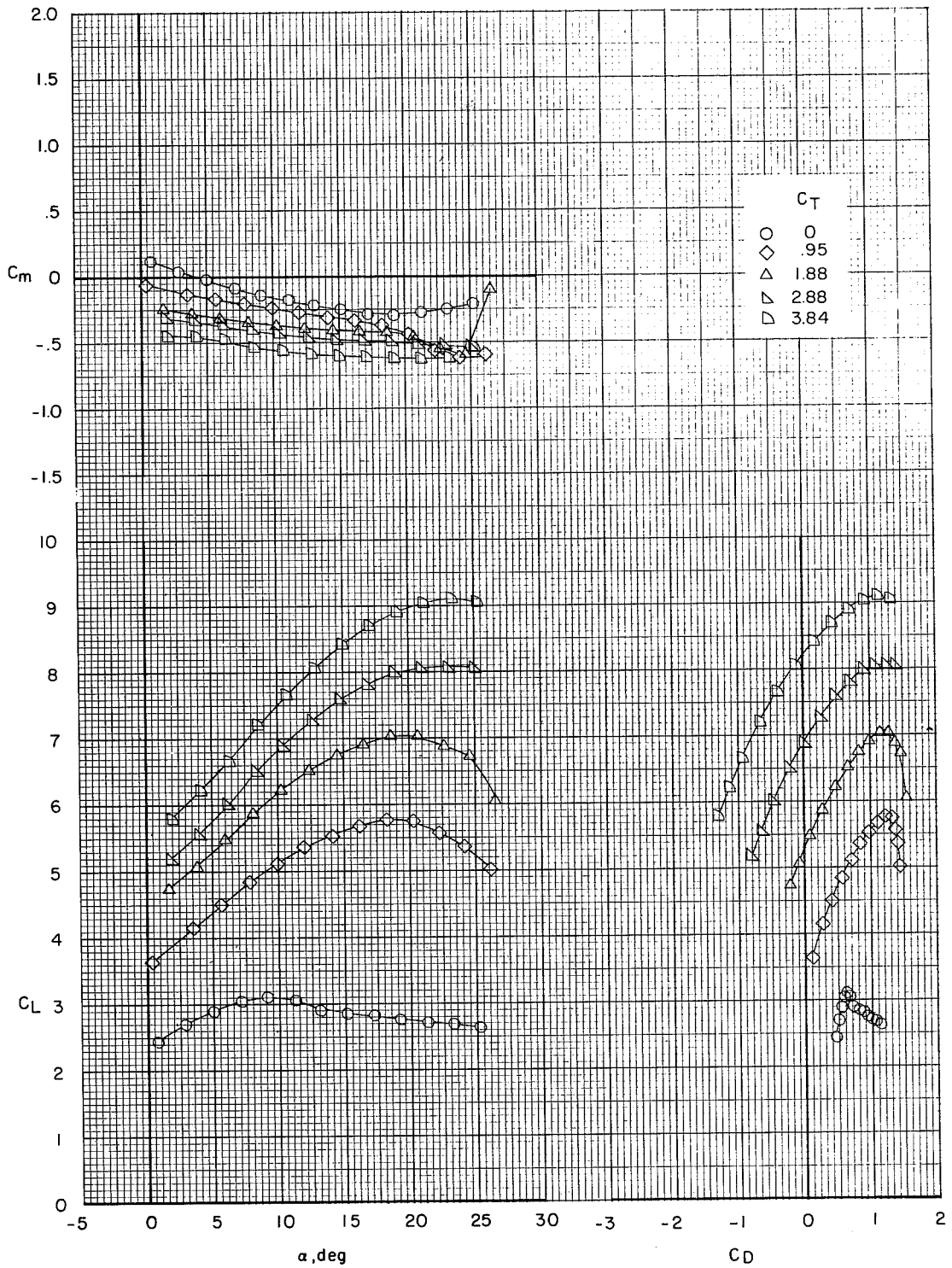

(a) $i_t = -5^o$.

Figure 32.- Effect of thrust coefficient on longitudinal aerodynamic characteristics of the landing configuration. $\delta_e = 0^o$. Model in the V/STOL tunnel without the tunnel liner installed.

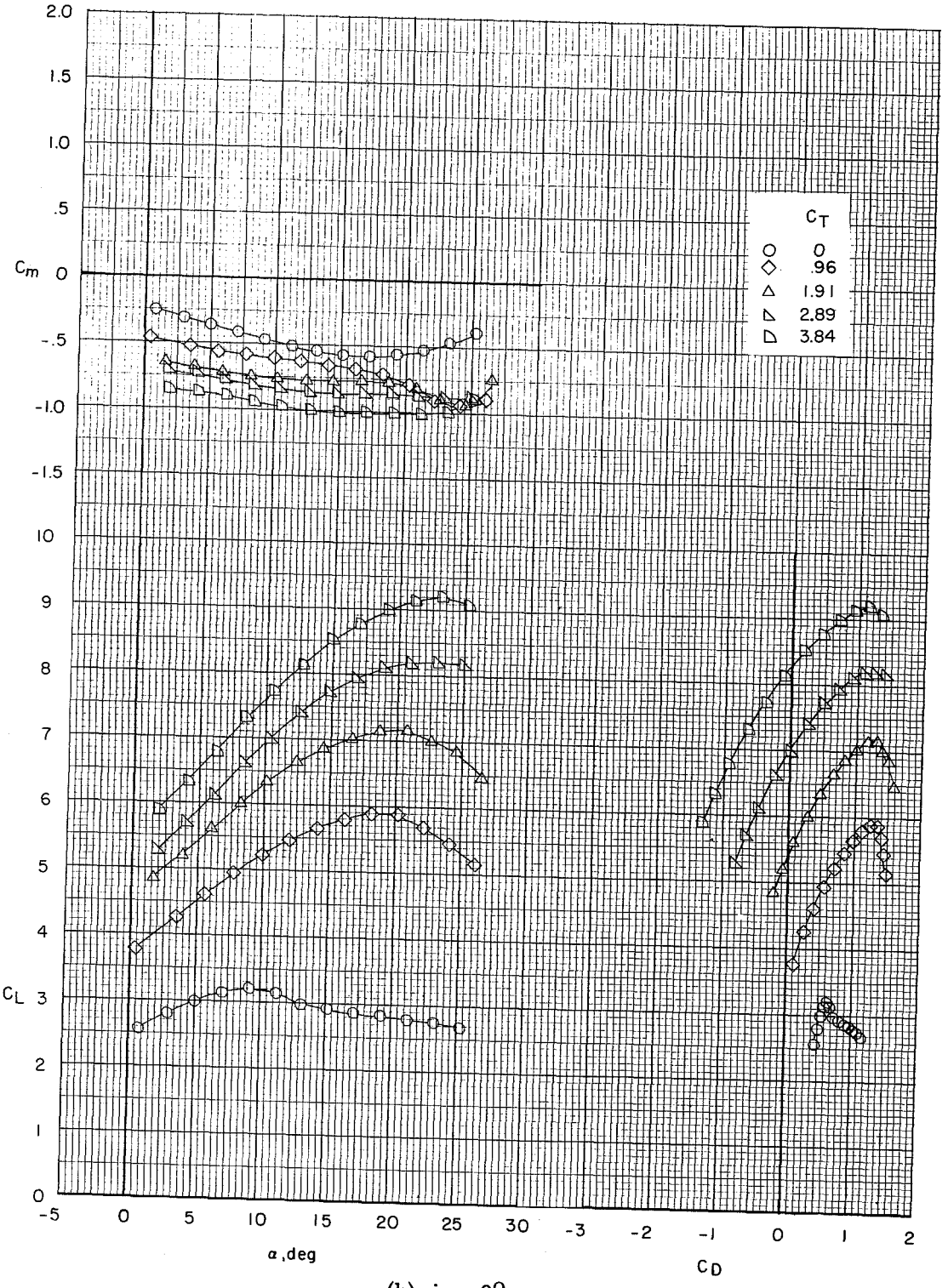

(b) $i_t = 0^o$.

Figure 32.- Continued.

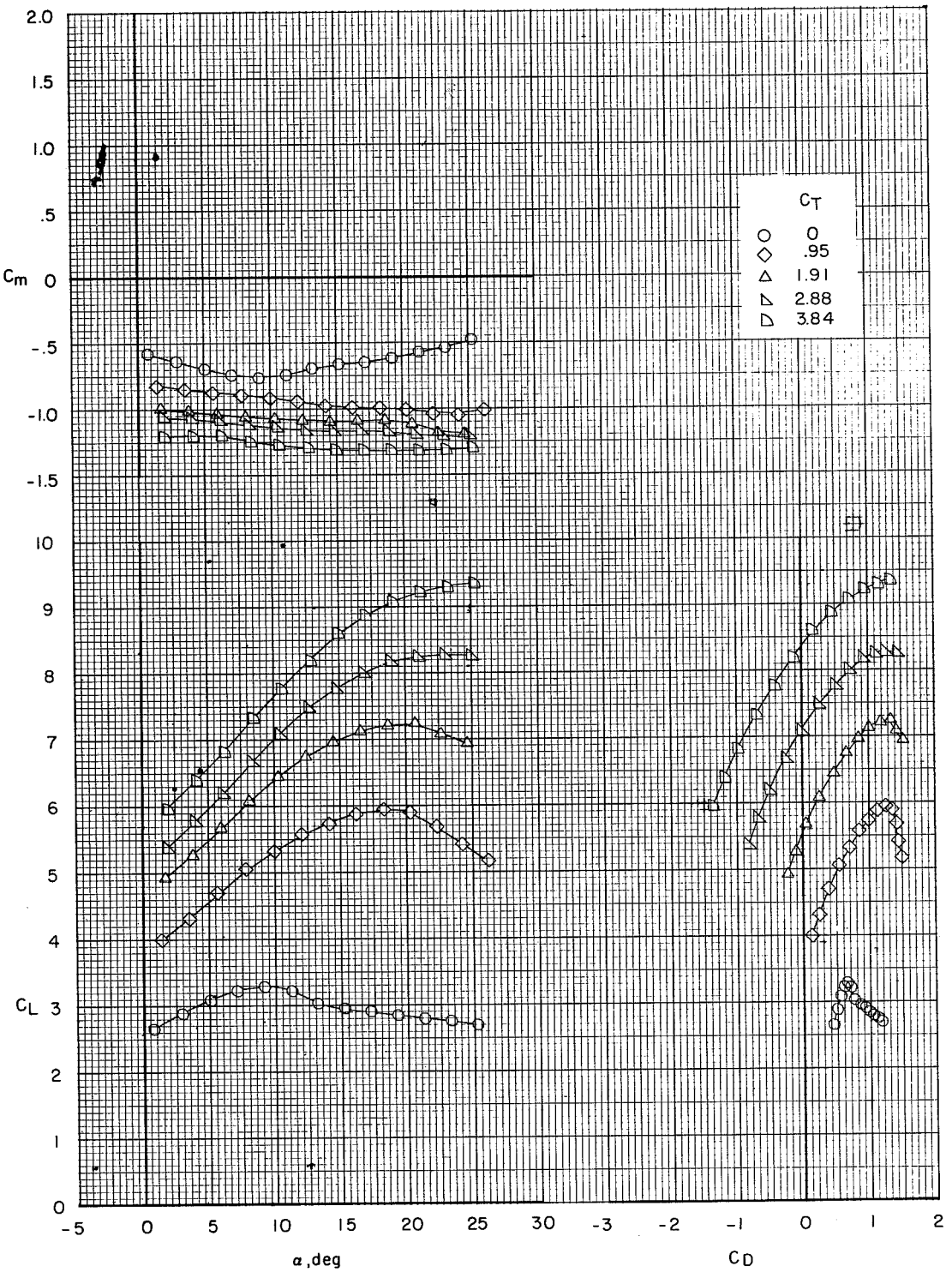

(c) $i_t = 5^o$.

Figure 32.- Concluded.

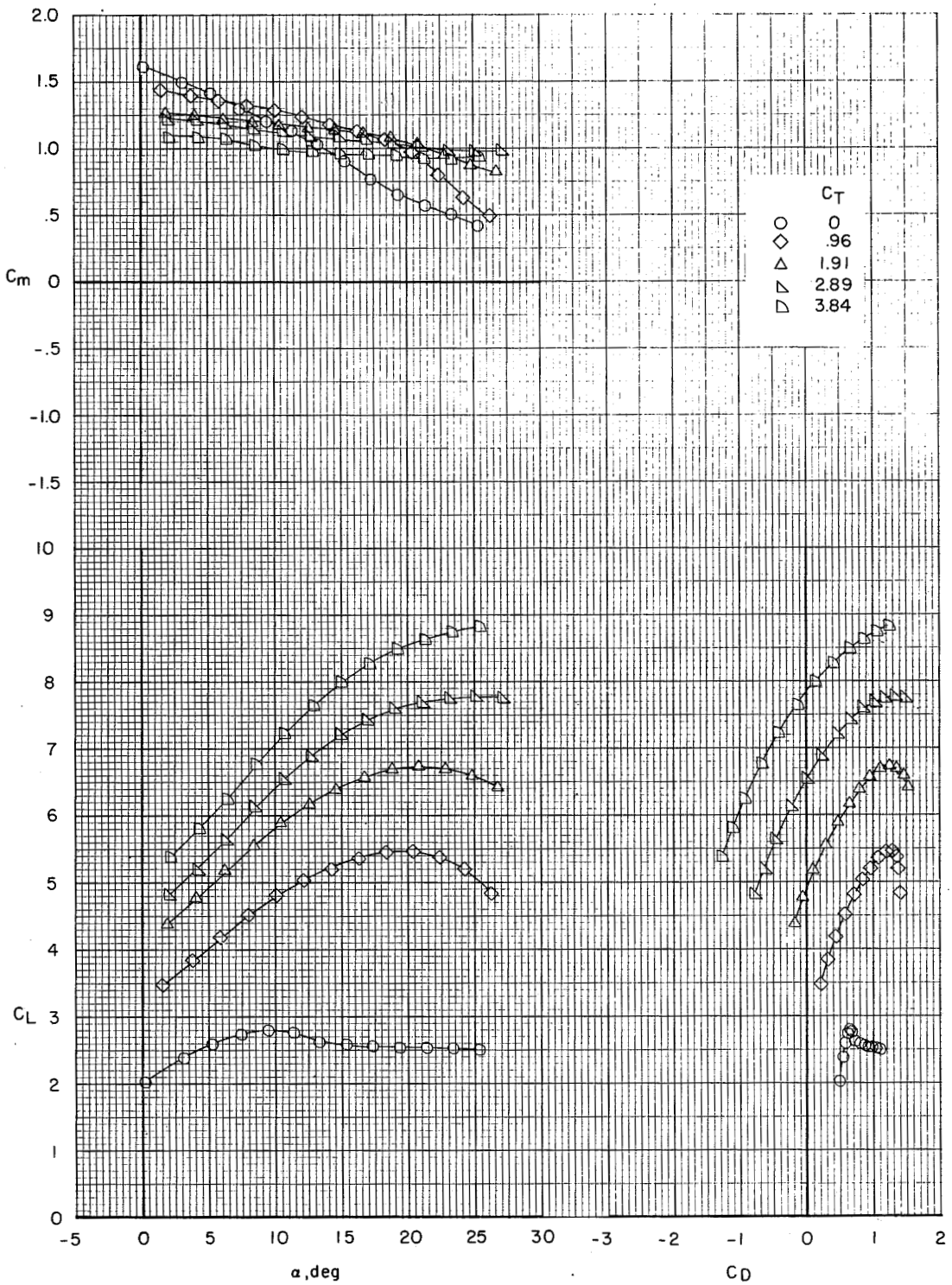

(a) $i_t = -5^o$.

Figure 33.- Effect of thrust coefficient on longitudinal aerodynamic characteristics of the landing configuration. $\delta_e = -25^o$. Model in the V/STOL tunnel without the tunnel liner installed.

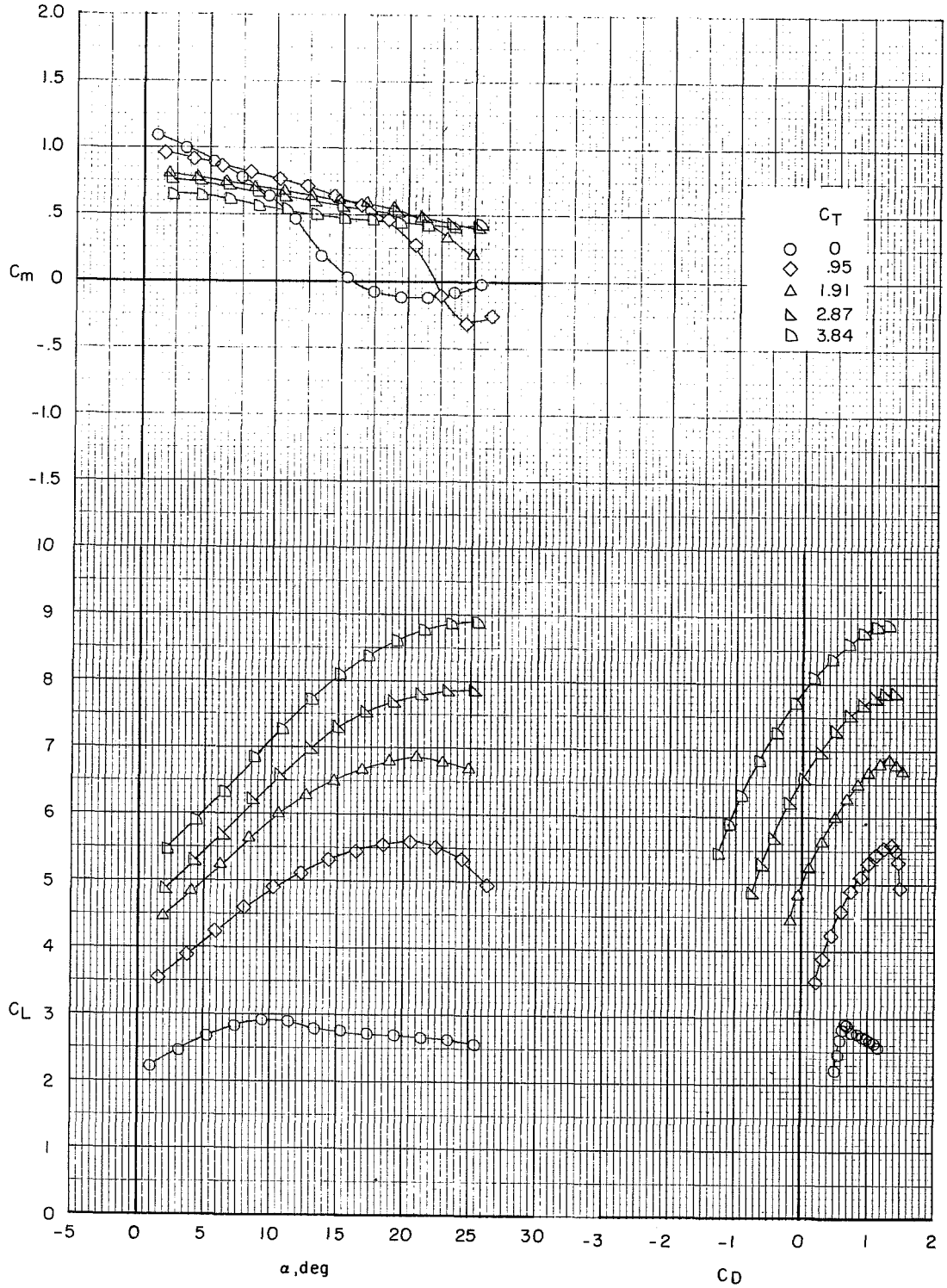

(b) $i_t = 0^o$.

Figure 33.- Continued.

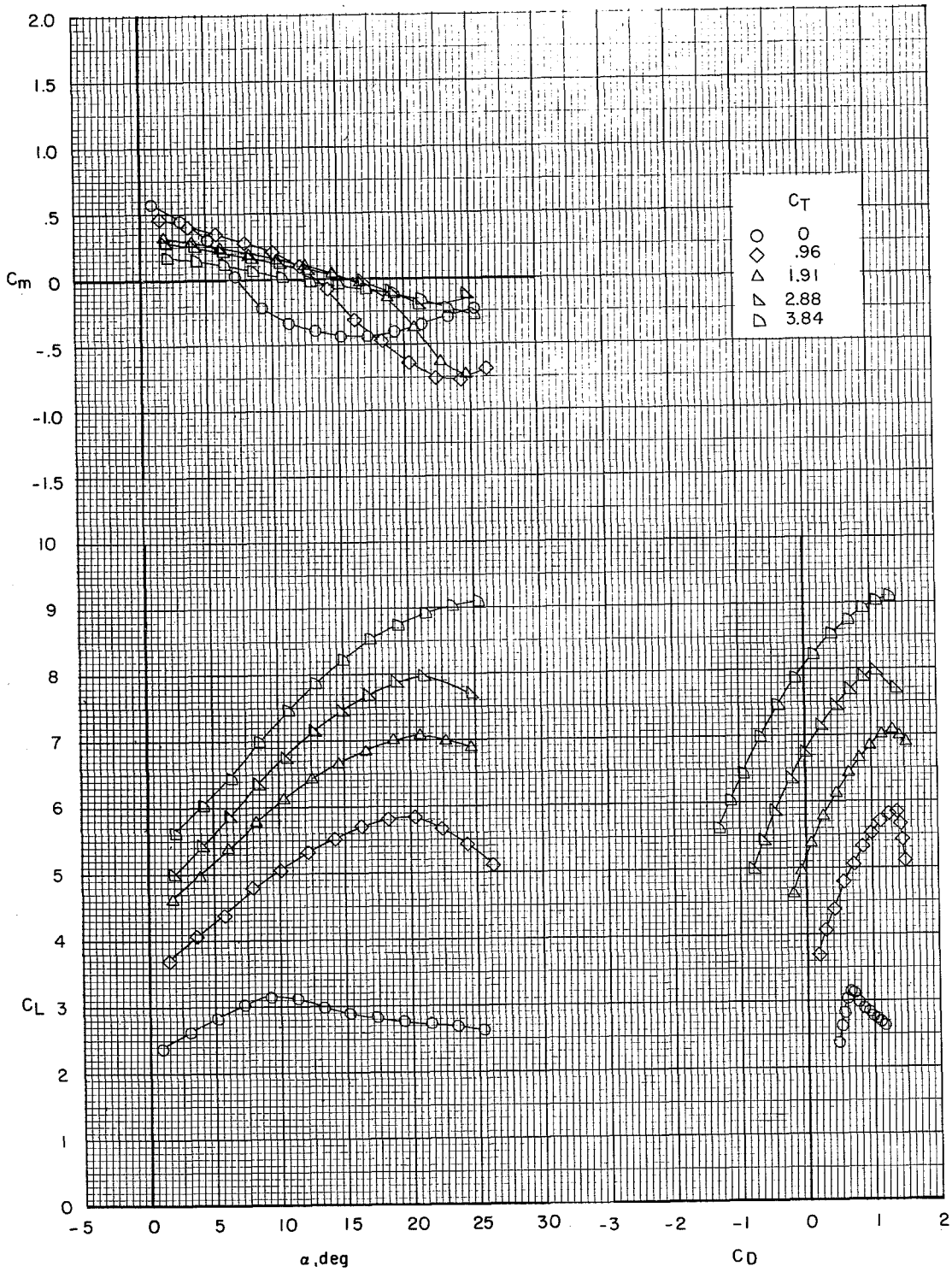

(c) $i_t = 5^o$.

Figure 33.- Concluded.

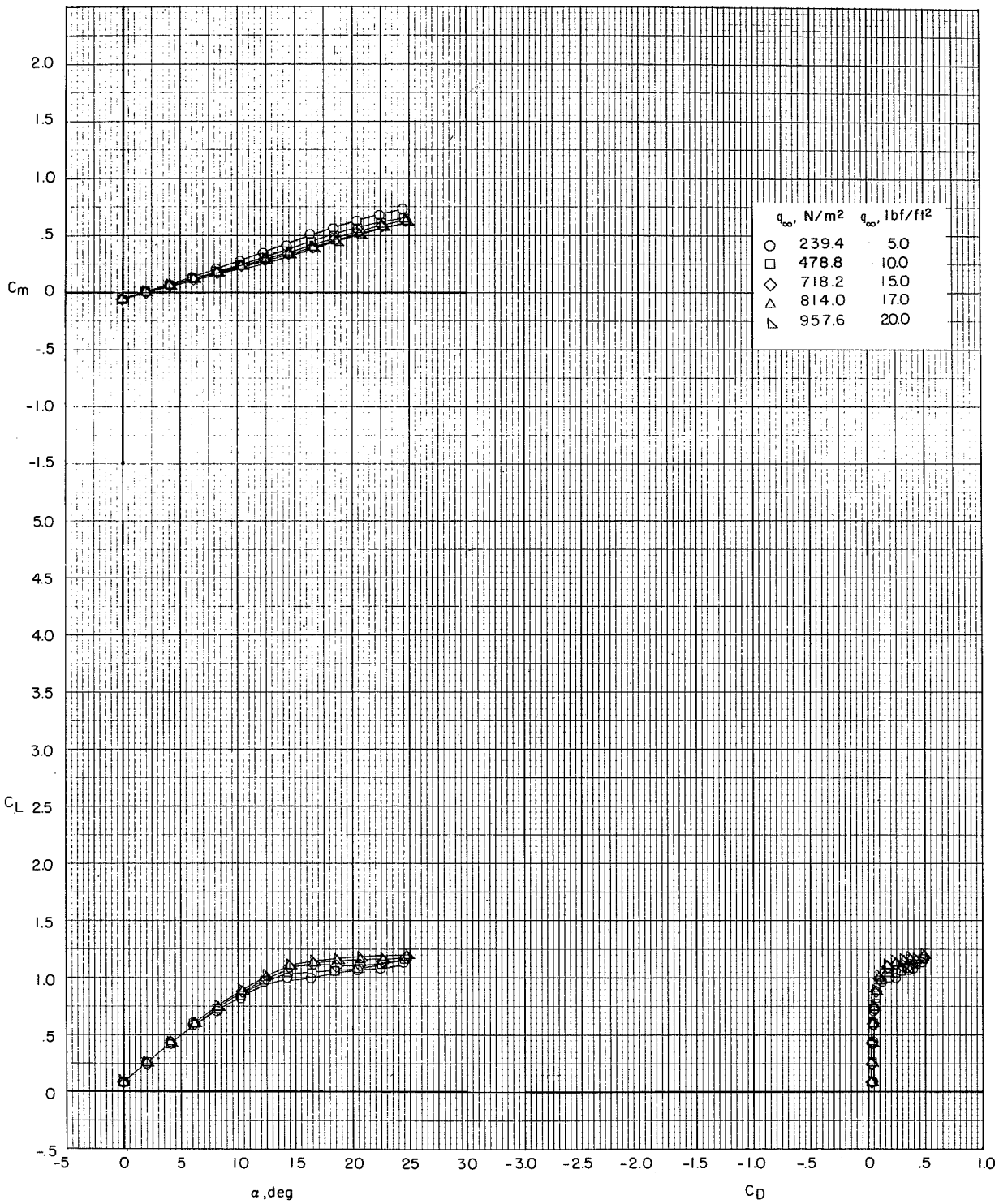

(a) $\delta_f = 0^o$.

Figure 34.- Effect of dynamic pressure on longitudinal aerodynamic characteristics. Model in the V/STOL tunnel without the tunnel liner installed. Tail off.

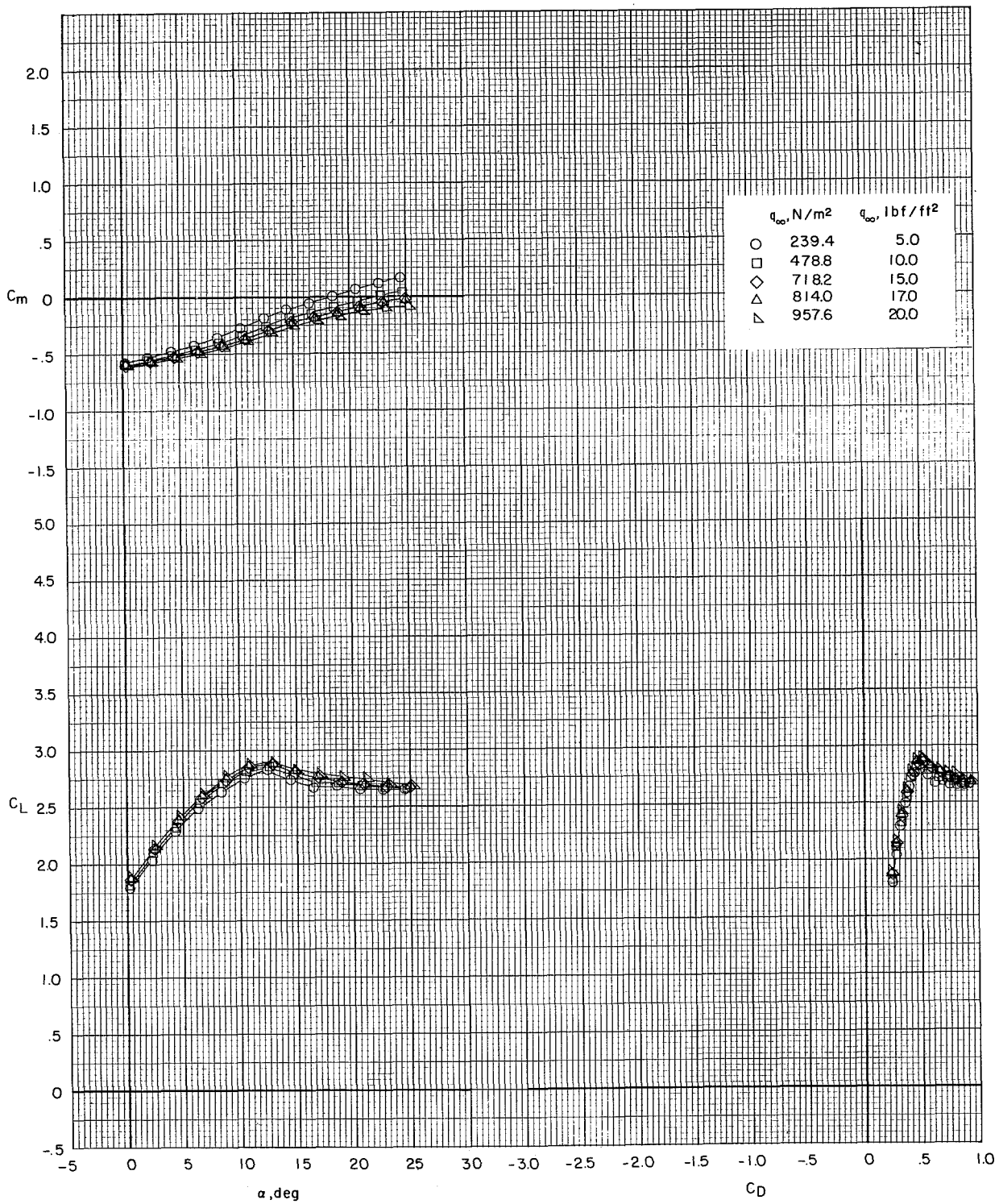

(b) $\delta_f = 40^o$.

Figure 34.- Continued.

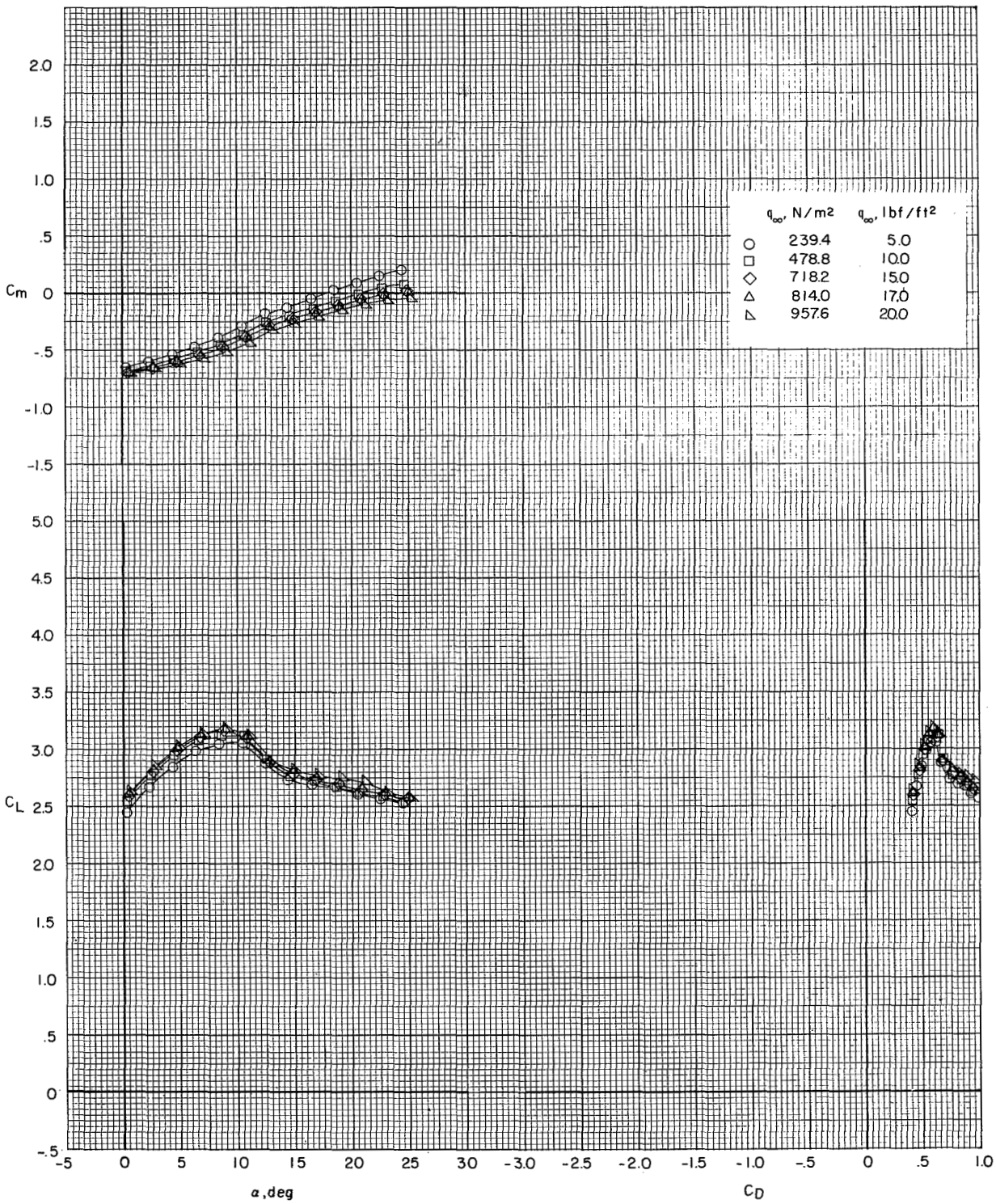

(c) $\delta_f = 55^o$.

Figure 34.- Concluded.

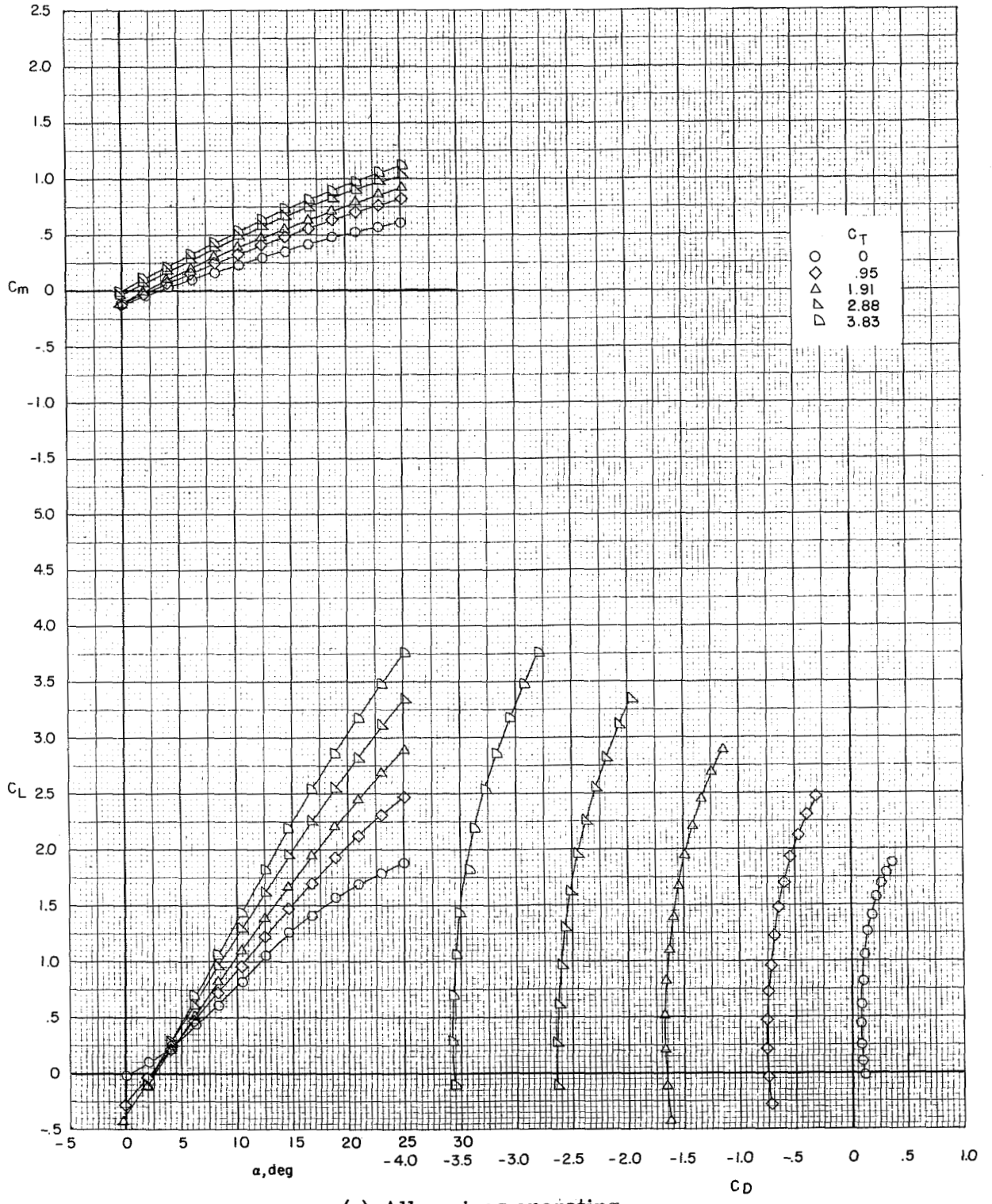

(a) All engines operating.

Figure 35.- Effect of thrust coefficient on aerodynamic characteristics of the cruise configuration. $\delta_S = 50^O$ (modified); tail off. Model in the V/STOL tunnel without the tunnel liner installed.

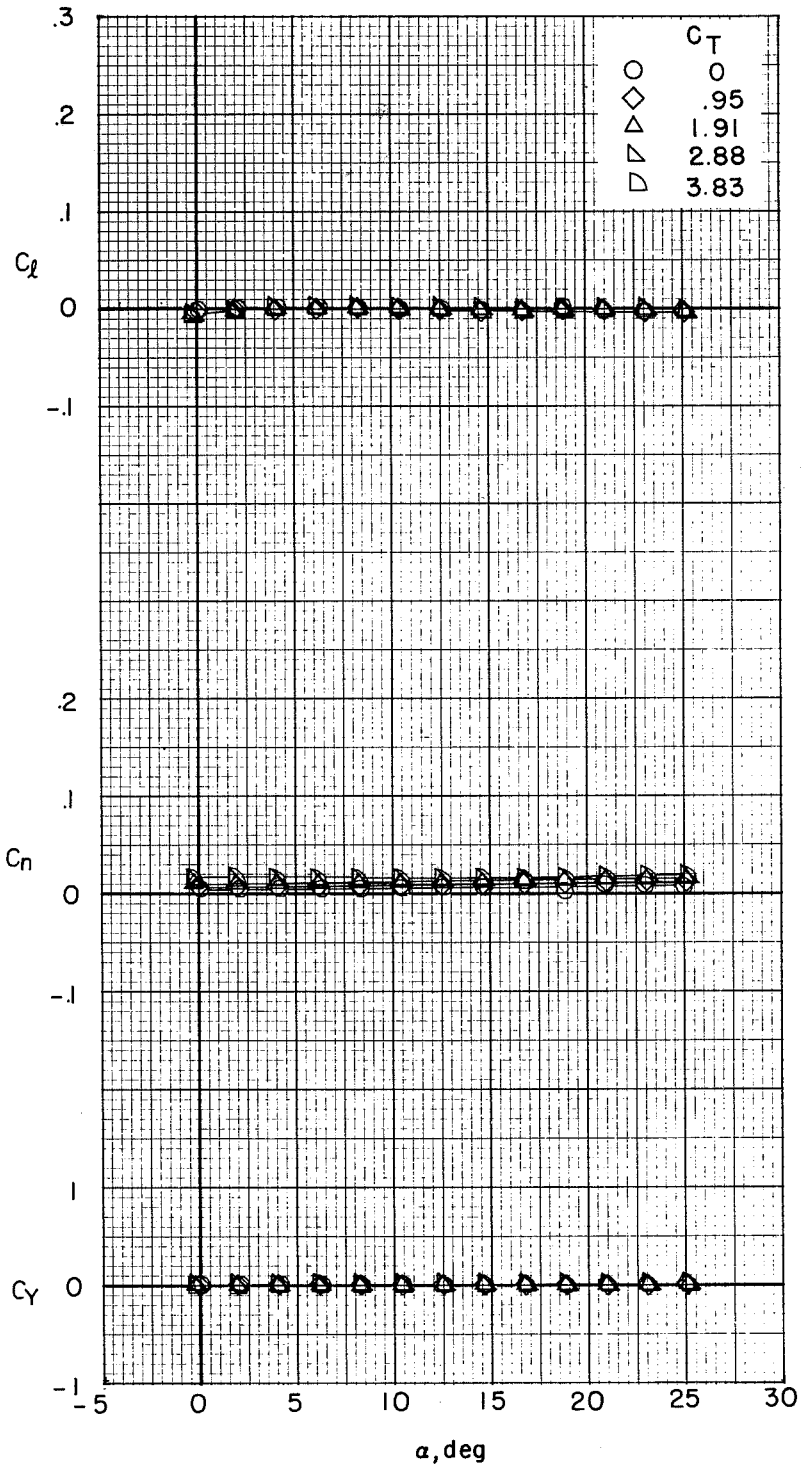

(a) Concluded.

Figure 35.- Continued.

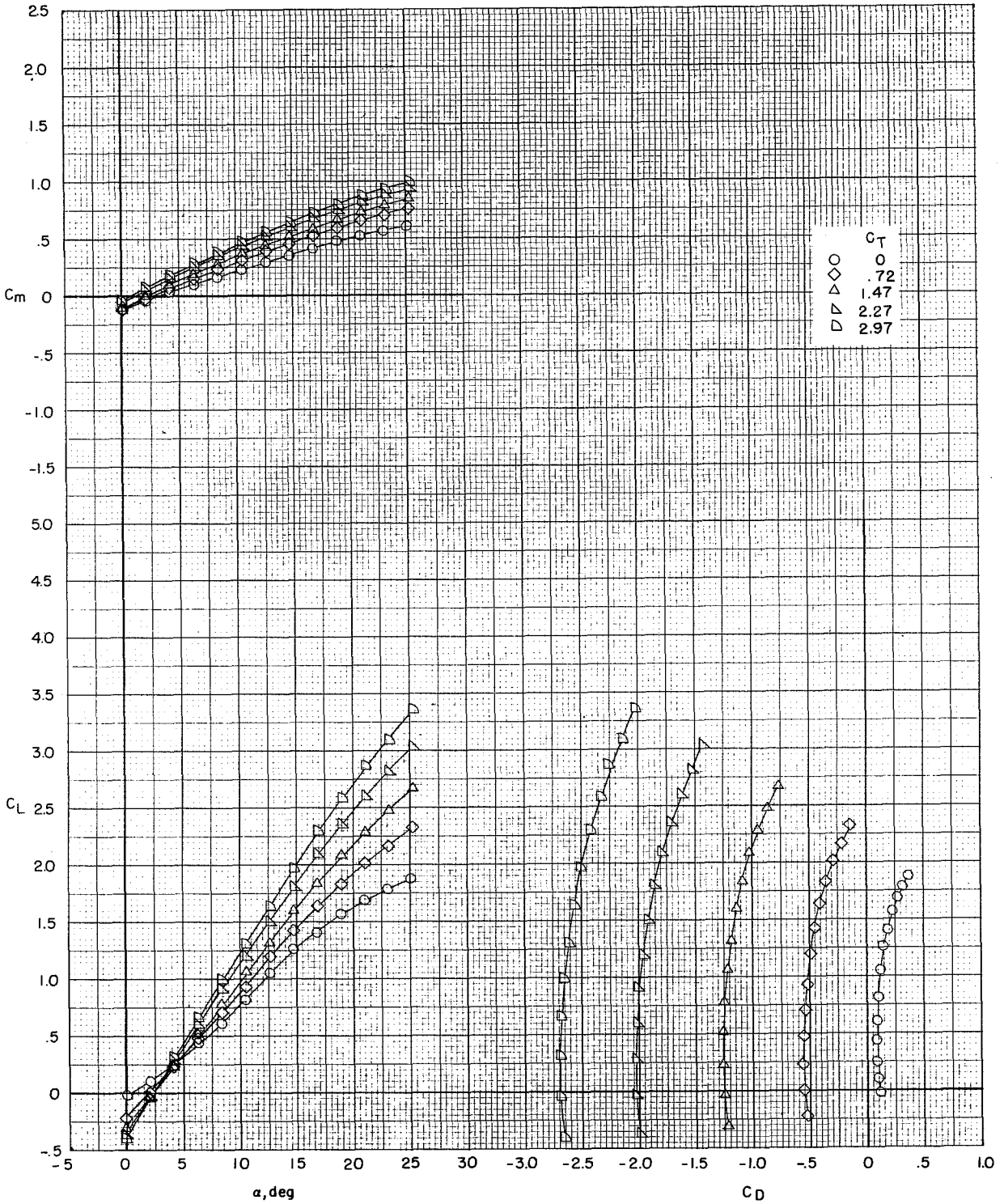

(b) Right outboard engine out.

Figure 35.- Continued.

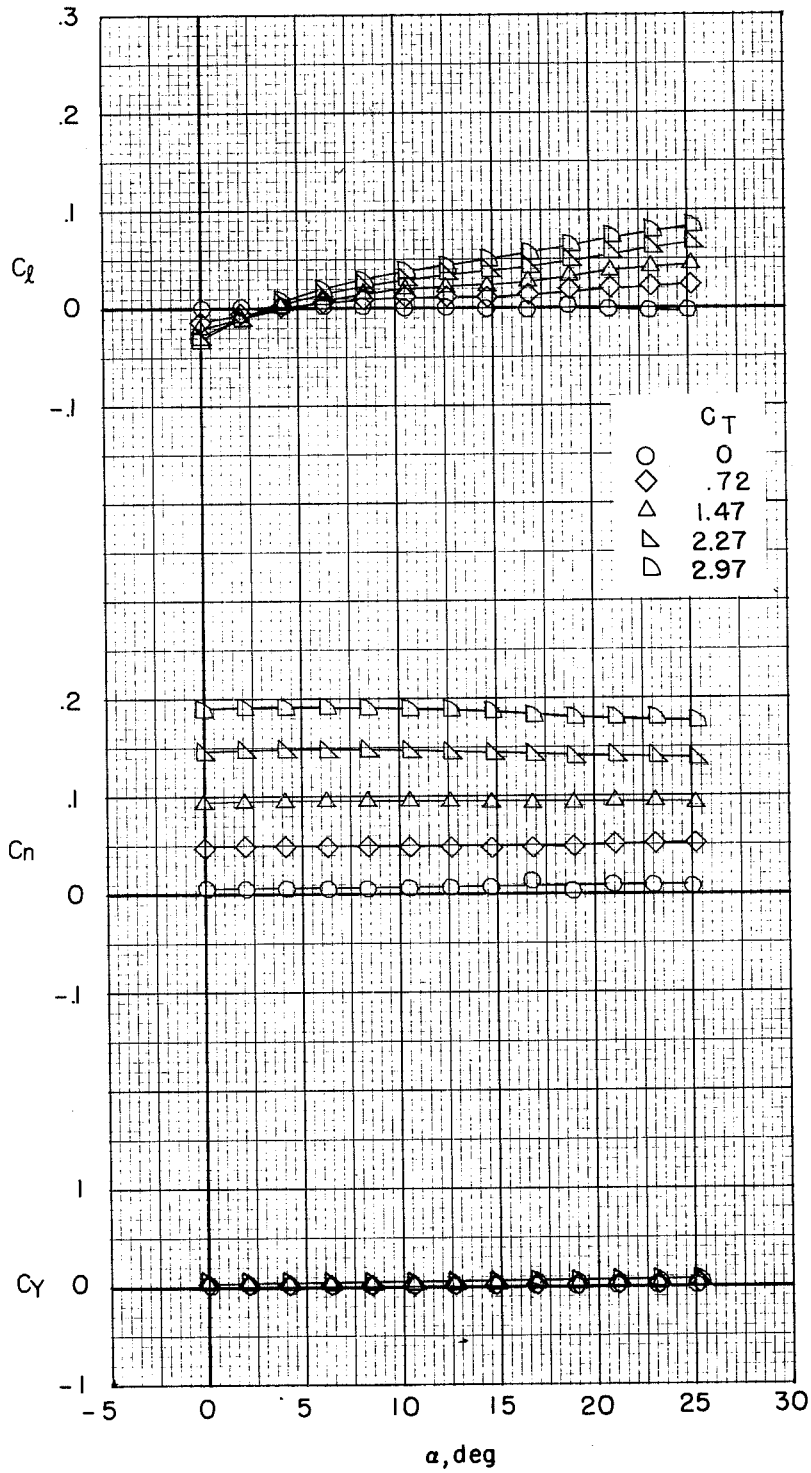

(b) Concluded.

Figure 35.- Concluded.

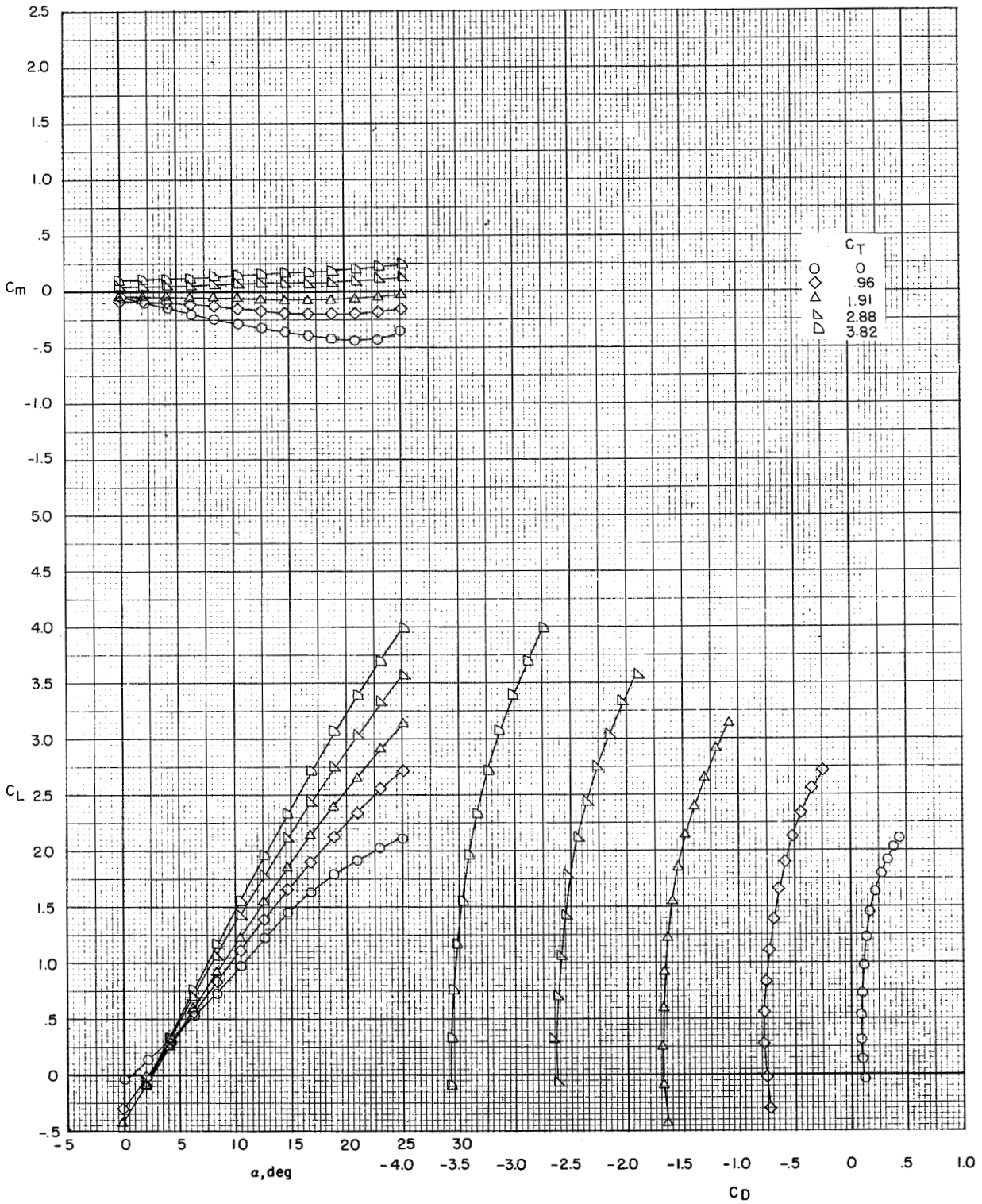

(a) All engines operating.

Figure 36.- Effect of thrust coefficient on aerodynamic characteristics of the cruise configuration. $\delta_s = 50^o$ (modified); $i_t = 0^o$. Model in the V/STOL tunnel without the tunnel liner installed.

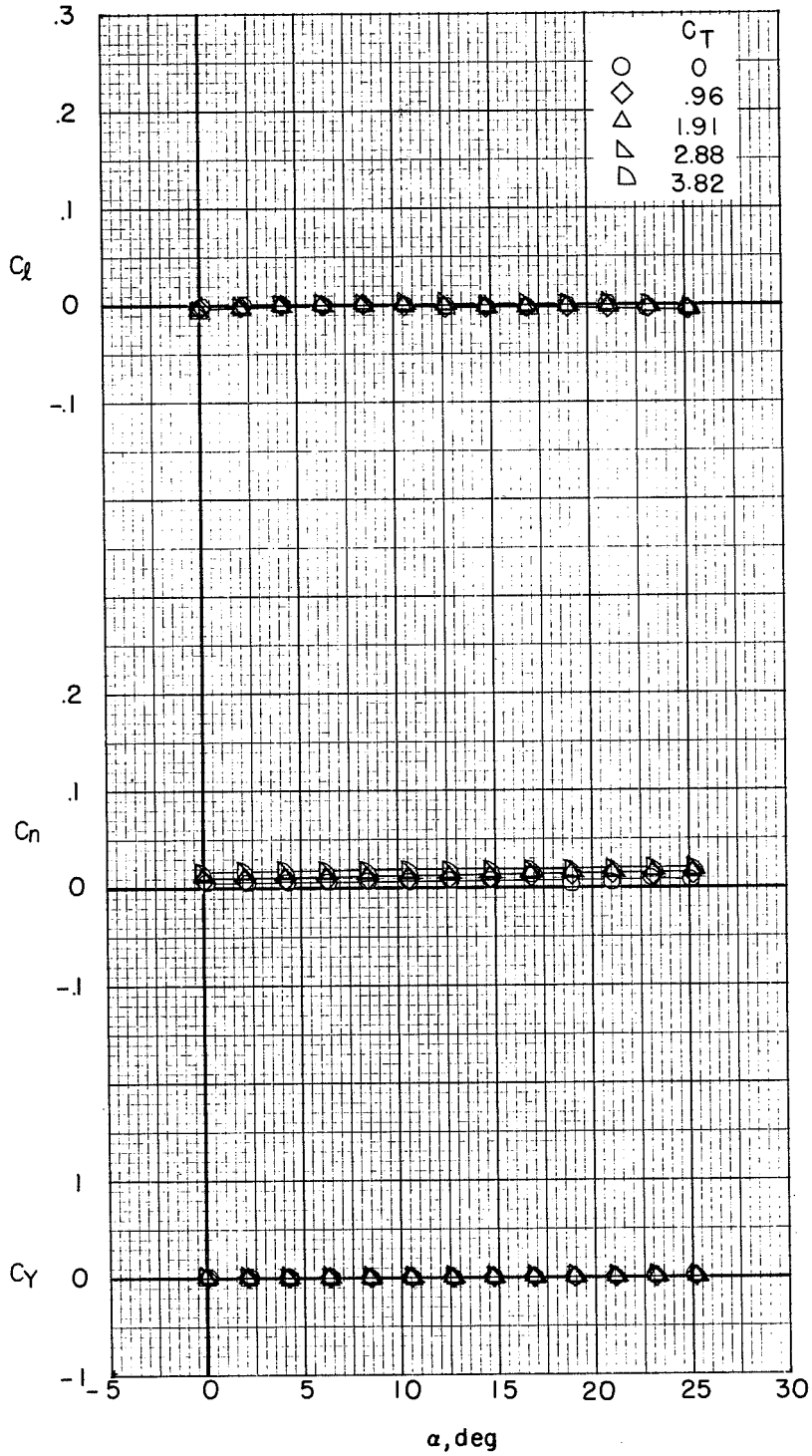

(a) Concluded.

Figure 36.- Continued.

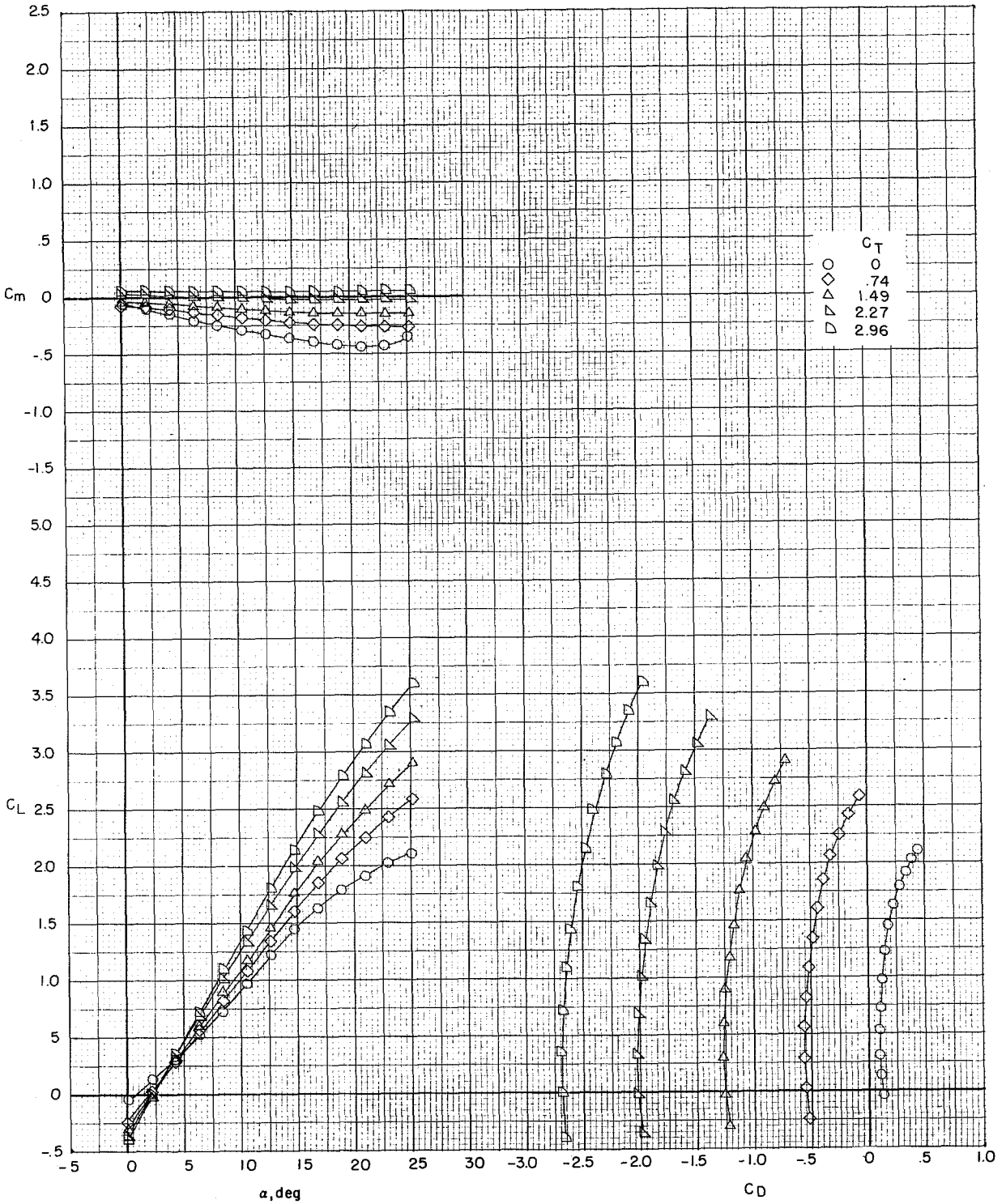

(b) Right outboard engine out.

Figure 36.- Continued.

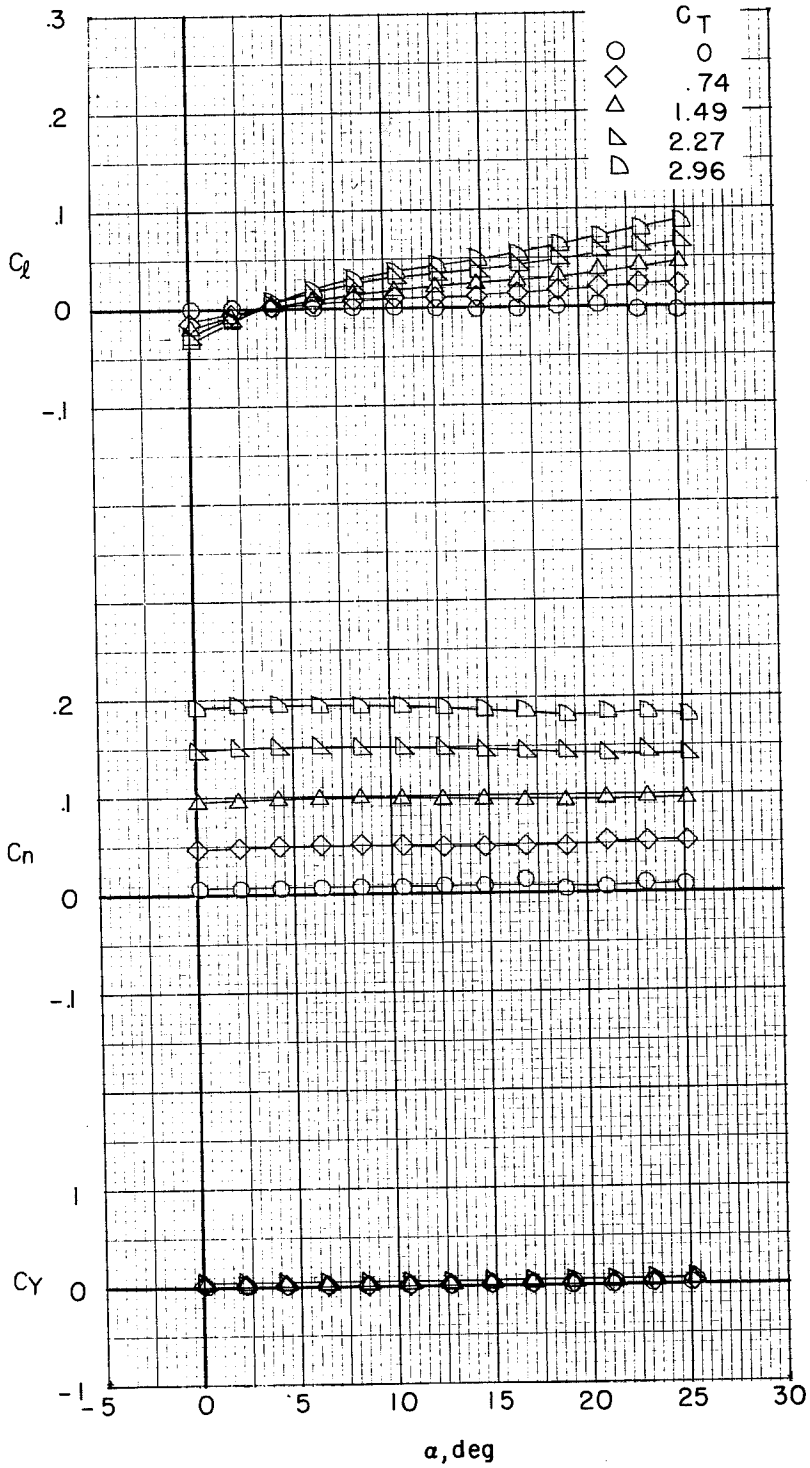

(b) Concluded.

Figure 36.- Concluded.

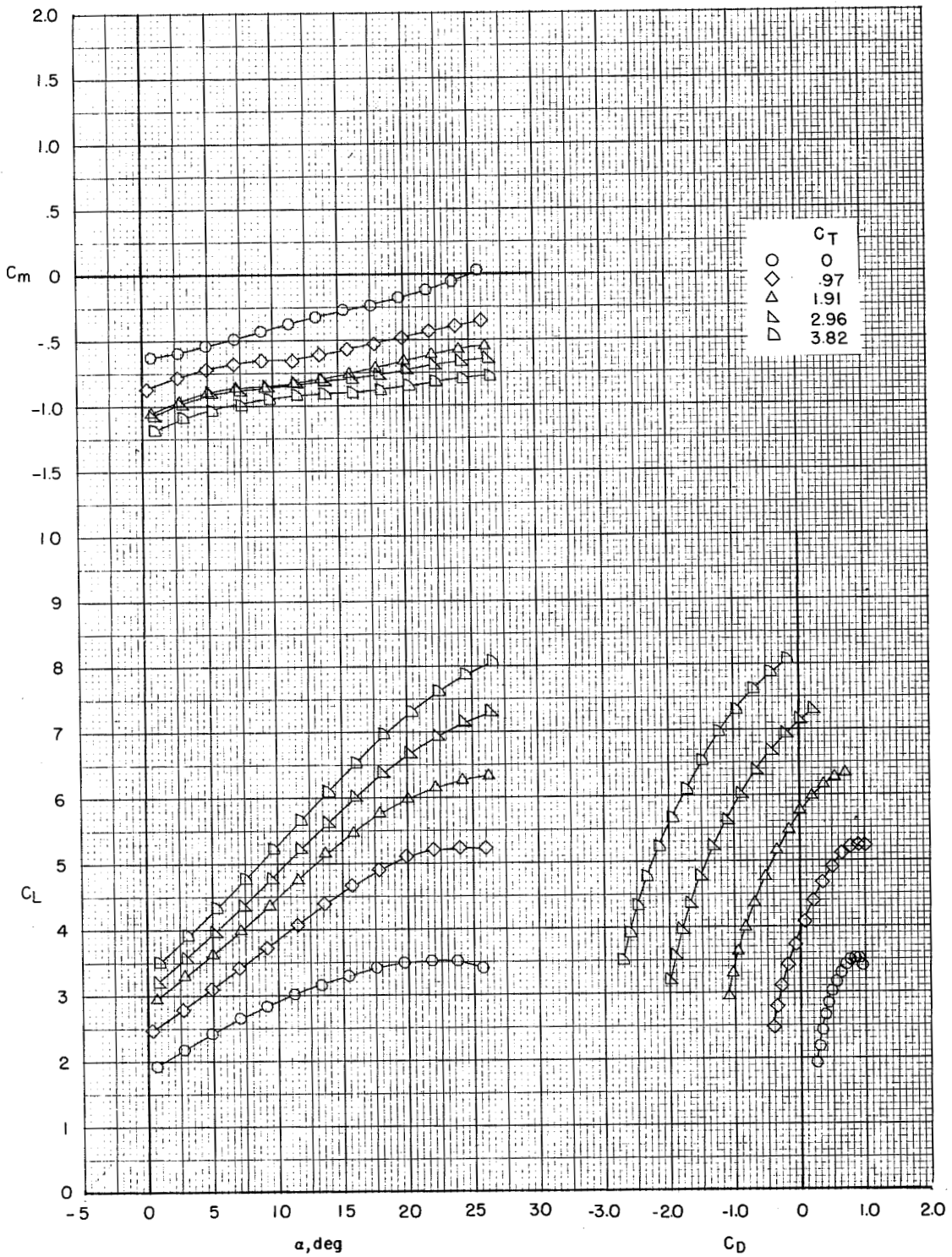

(a) All engines operating.

Figure 37.- Effect of thrust coefficient on aerodynamic characteristics of the take-off configuration. $\delta_s = 50^o$ (modified); tail off. Model in the V/STOL tunnel without the tunnel liner installed.

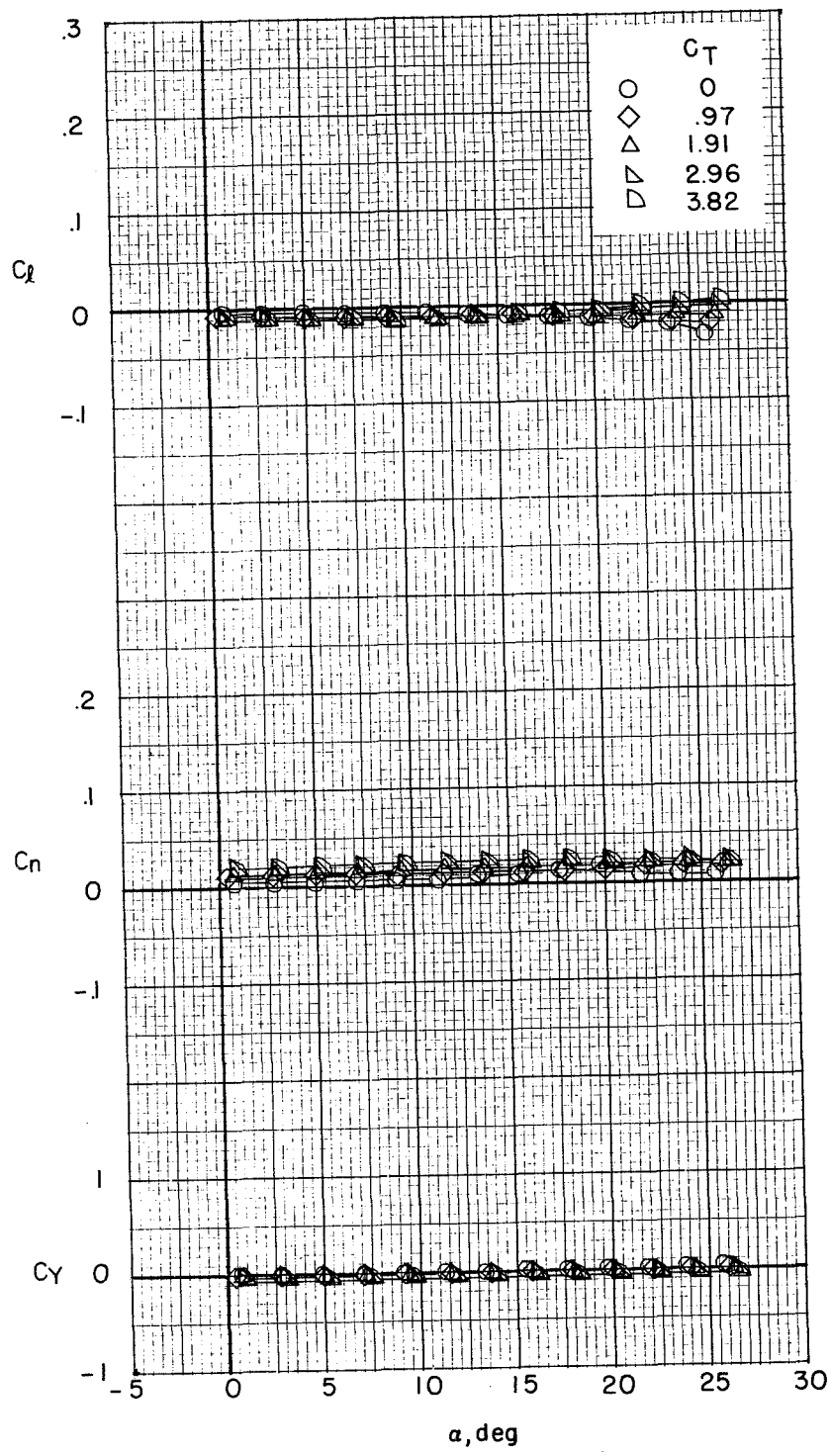

(a) Concluded.

Figure 37.- Continued.

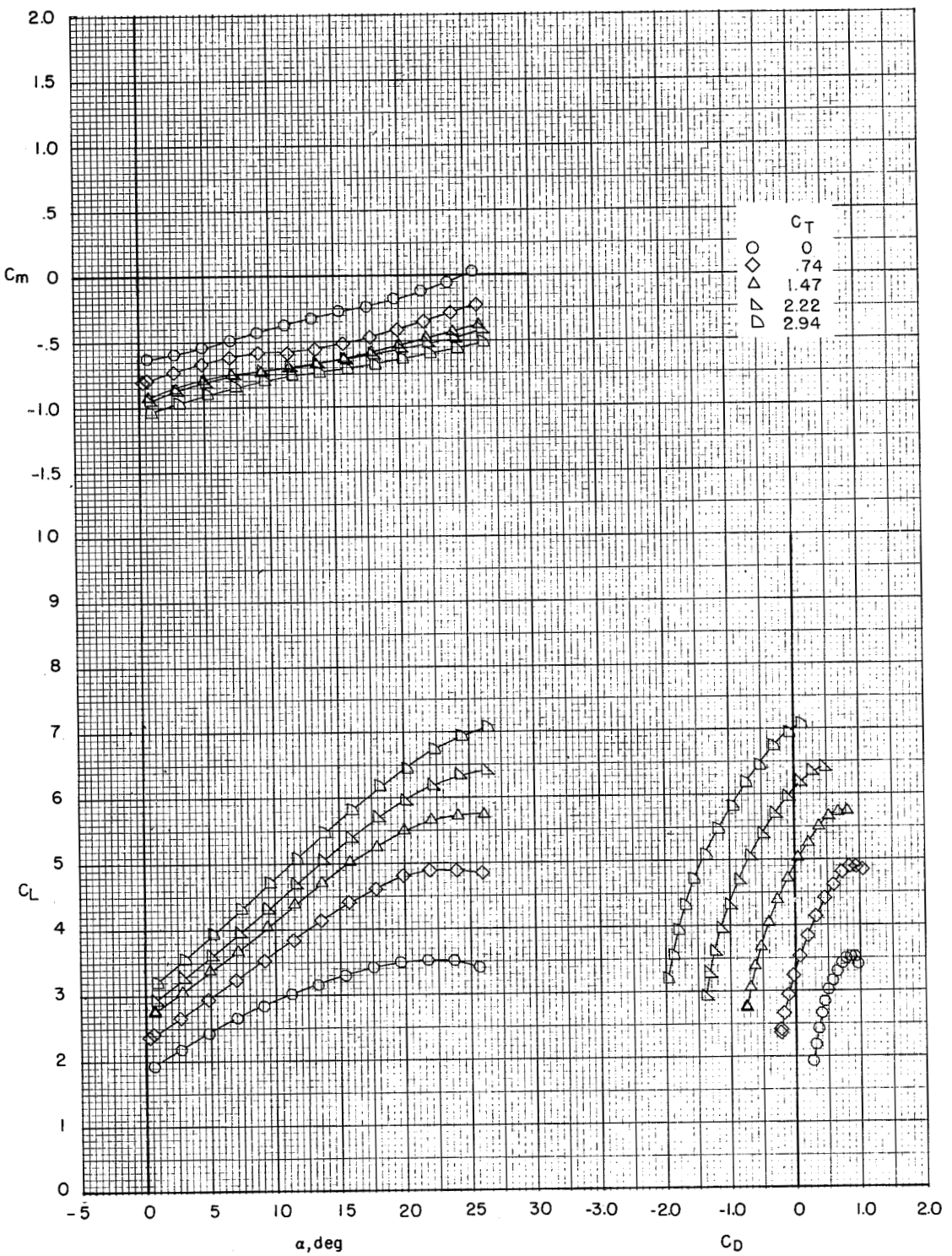

(b) Right outboard engine out.

Figure 37.- Continued.

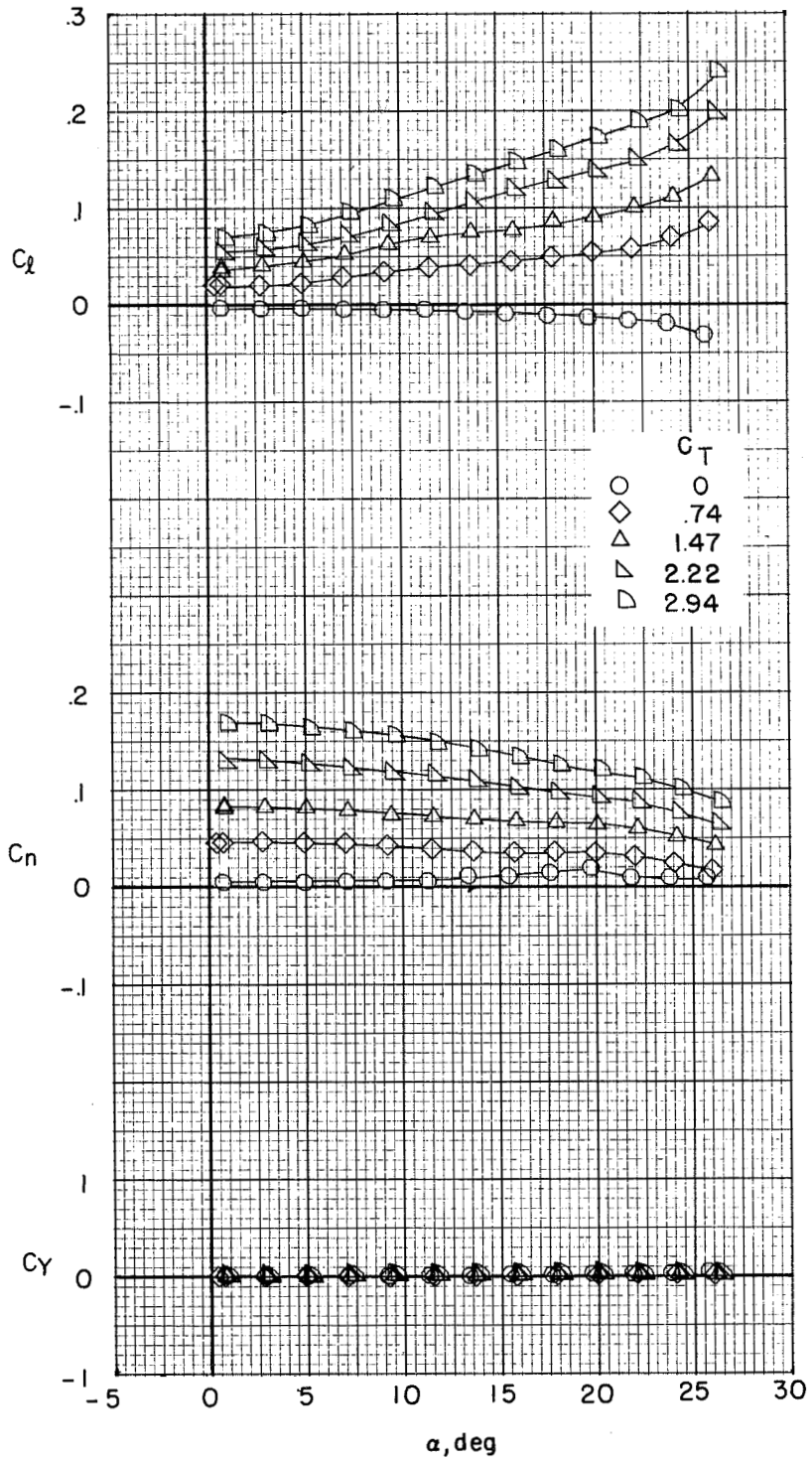

(b) Concluded.

Figure 37.- Concluded.

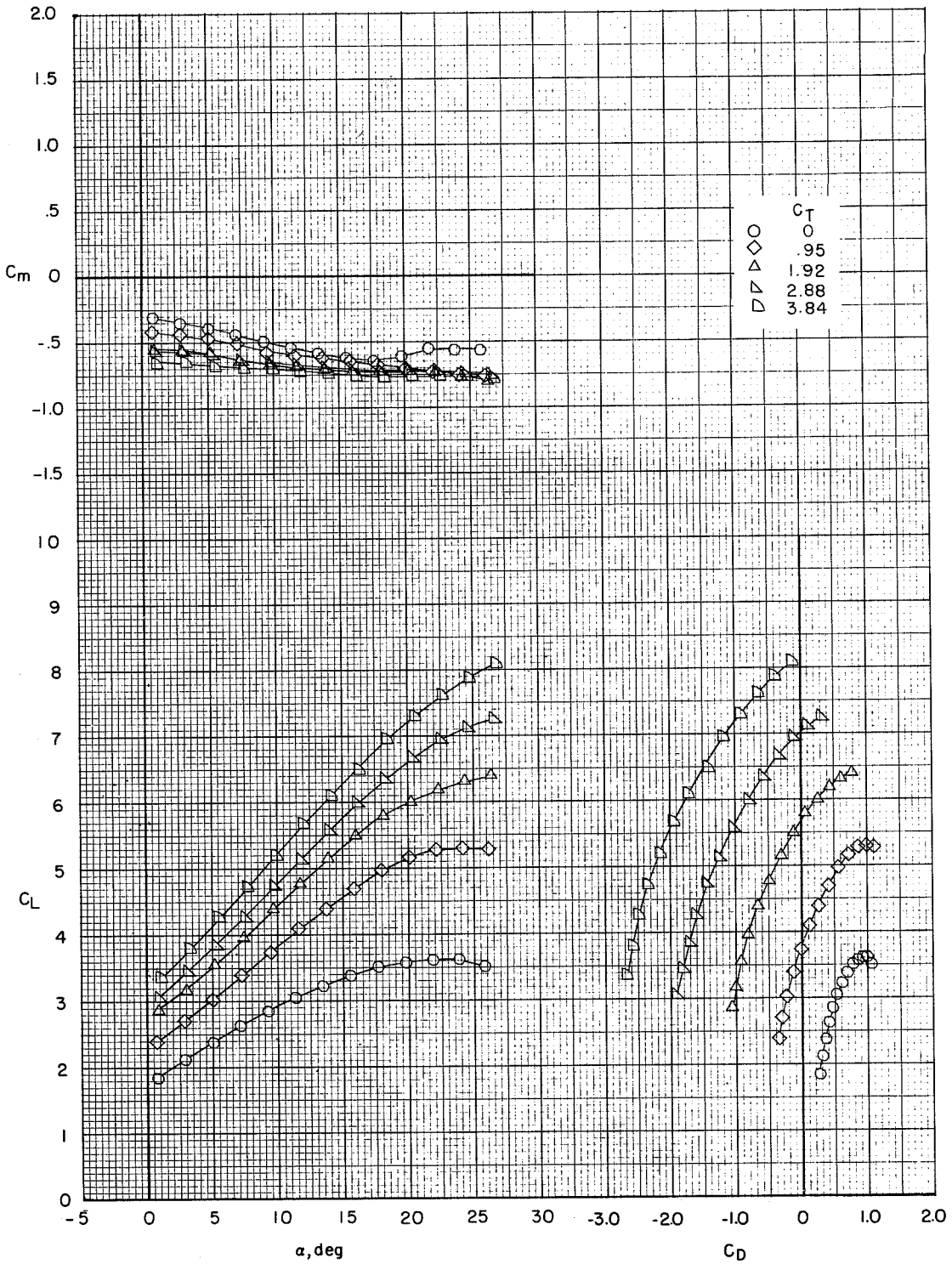

(a) All engines operating.

Figure 38.- Effect of thrust coefficient on aerodynamic characteristics of the take-off configuration. $\delta_s = 50^o$ (modified); $i_t = 0^o$. Model in the V/STOL tunnel without the tunnel liner installed.

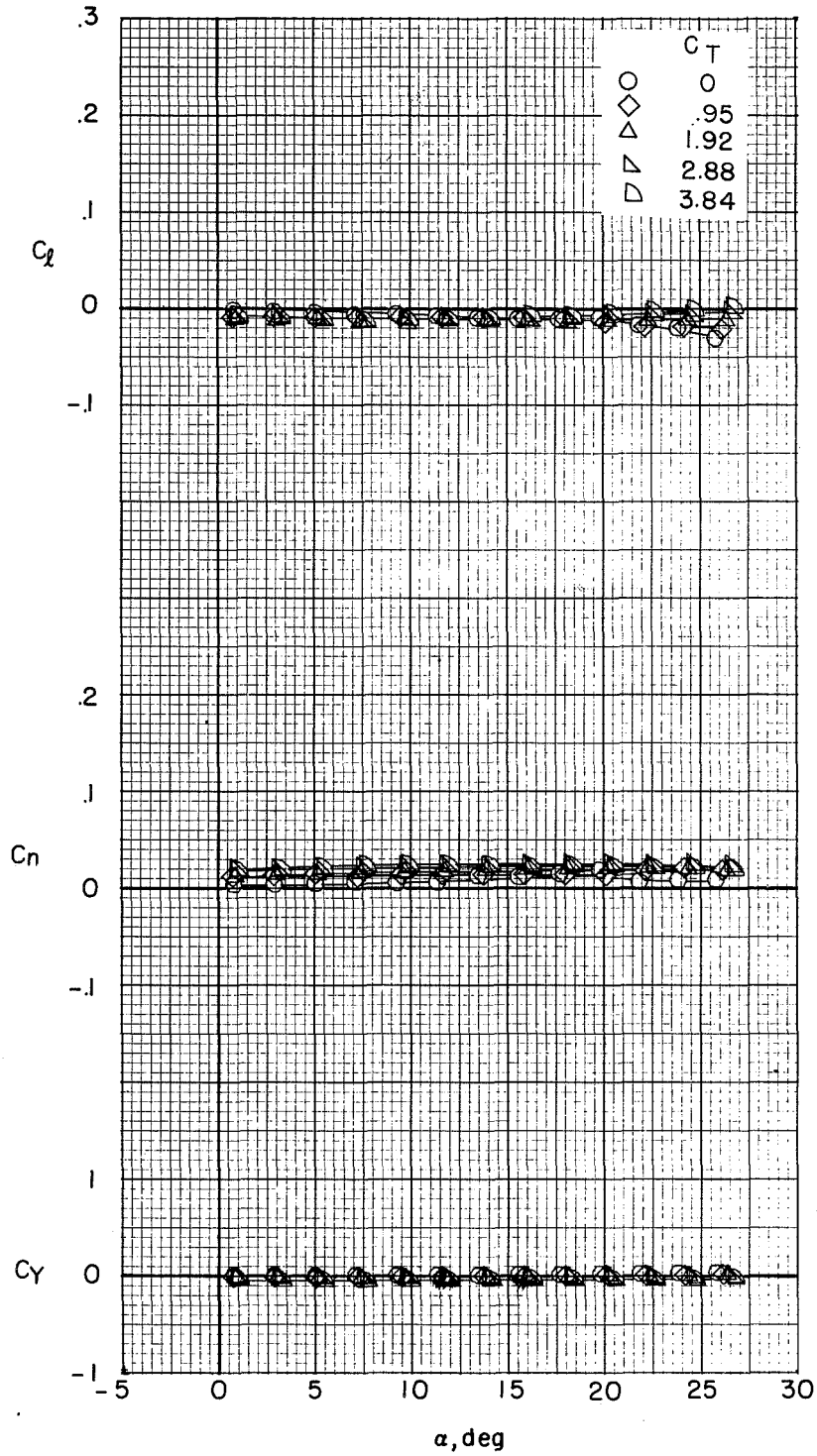

(a) Concluded.

Figure 38.- Continued.

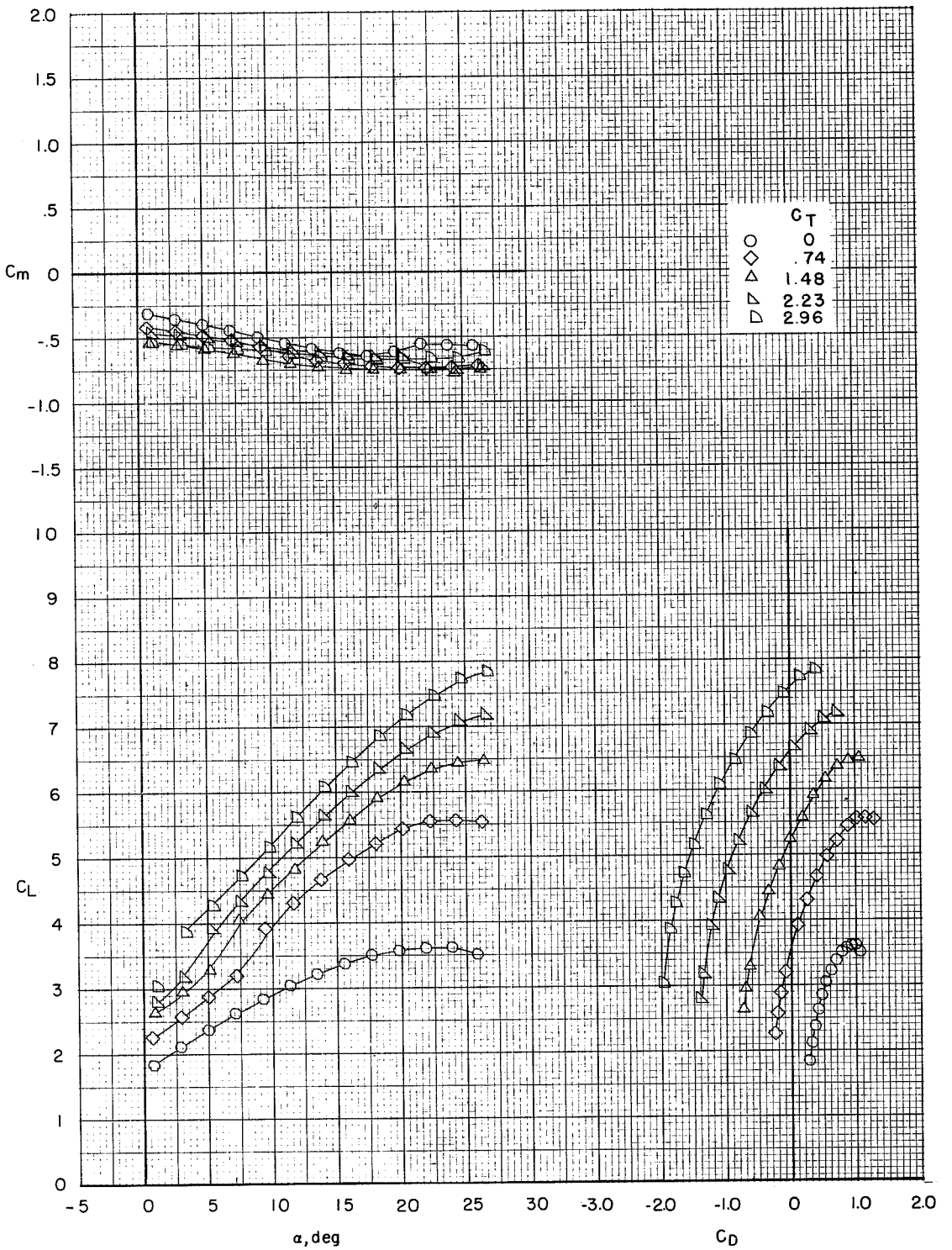

(b) Right outboard engine out.

Figure 38.- Continued.

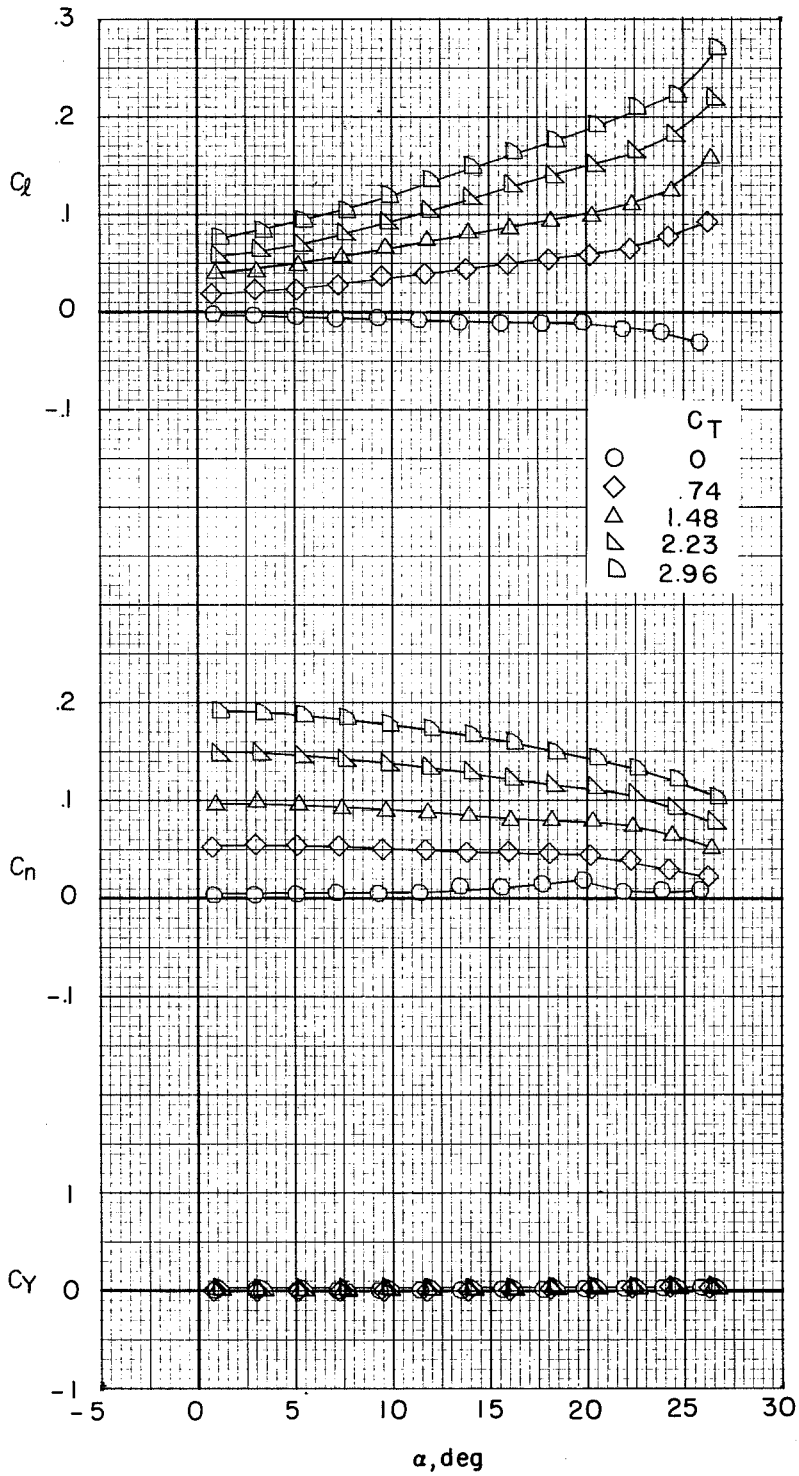

(b) Concluded.

Figure 38.- Concluded.

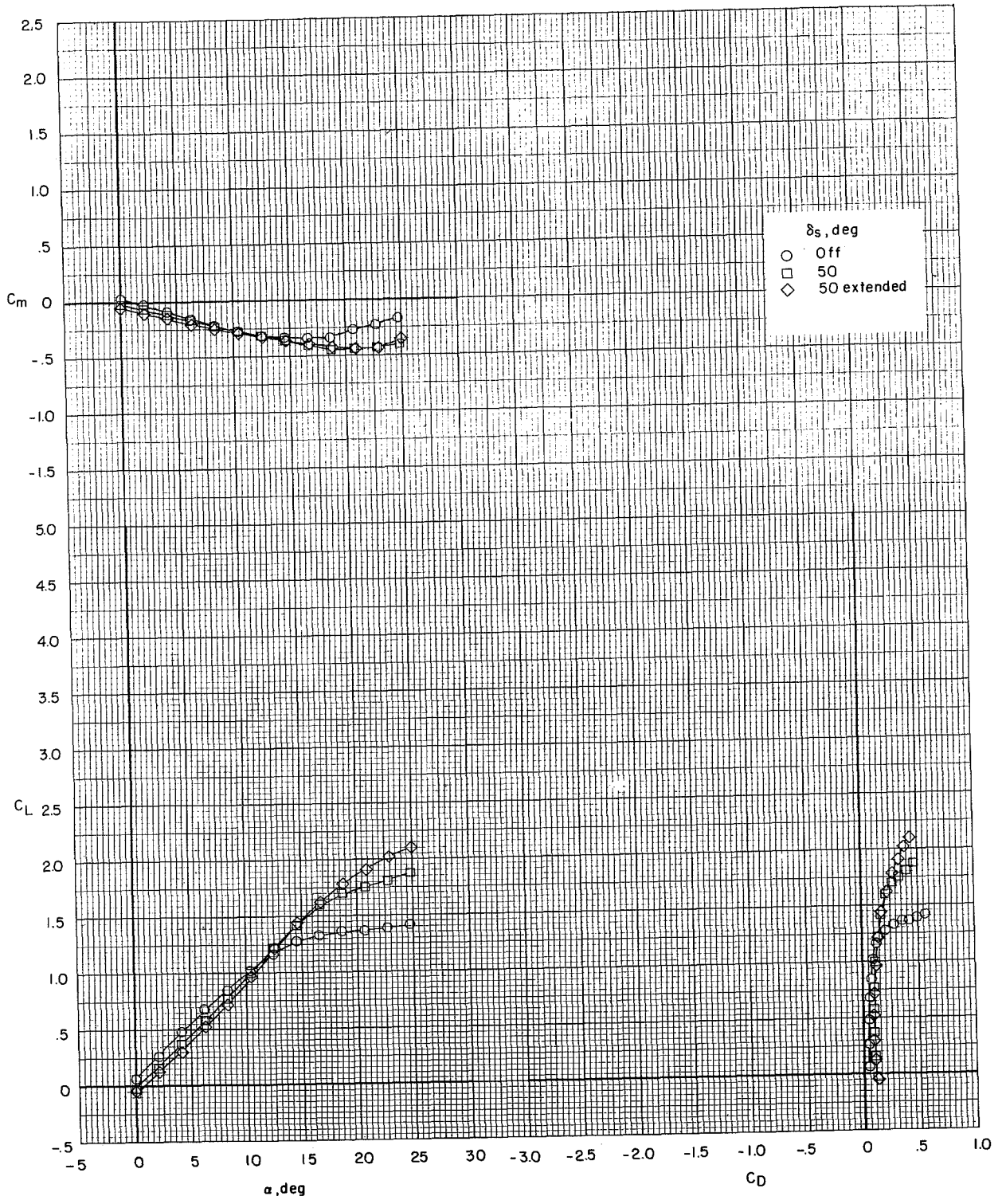

(a) $C_T = 0$.

Figure 39.- Effect of leading-edge slat on longitudinal aerodynamic characteristics in the cruise configuration. Tail off. Model in the V/STOL tunnel without the tunnel liner installed.

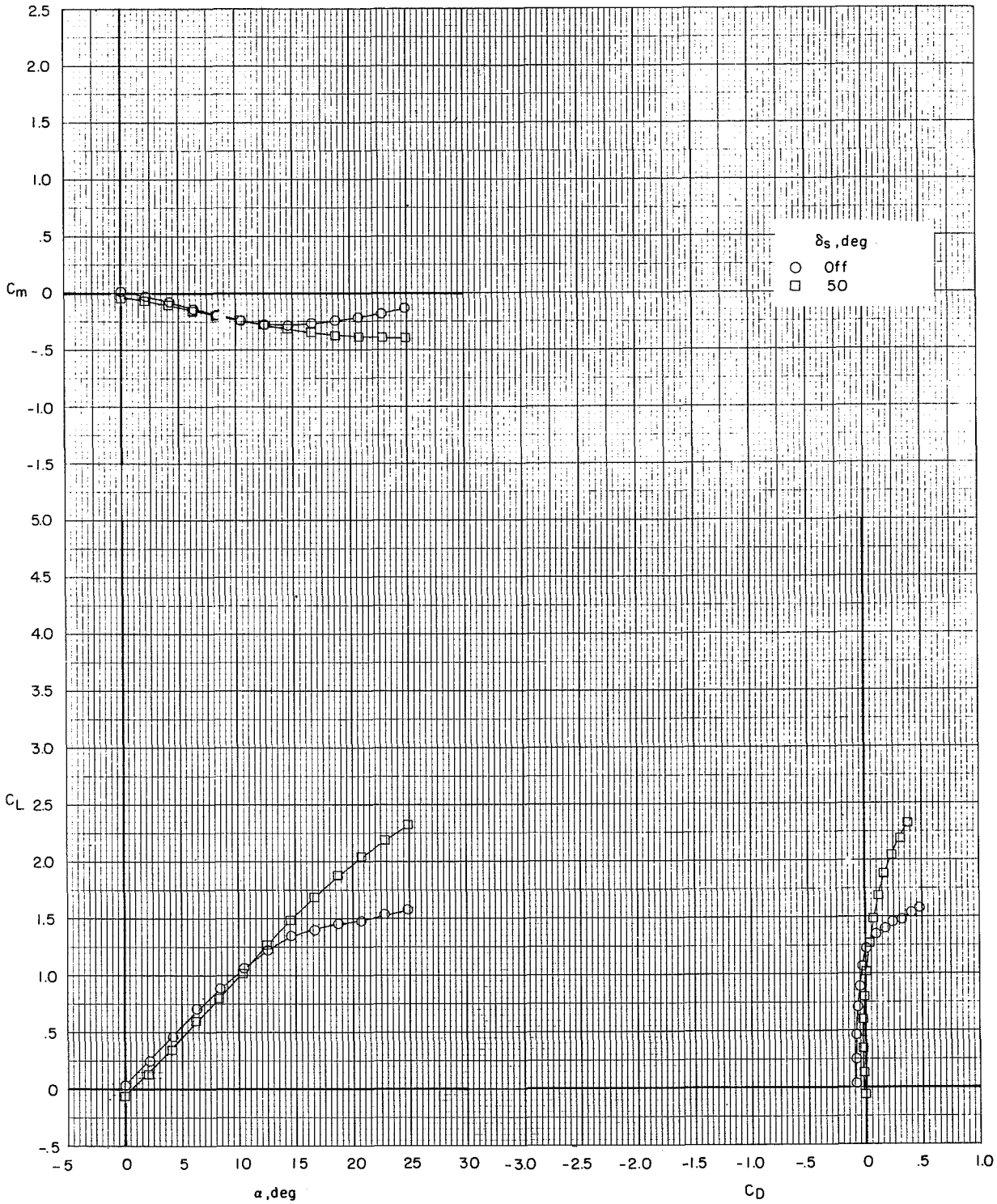

(b) $C_T = 0.15$.

Figure 39.- Continued.

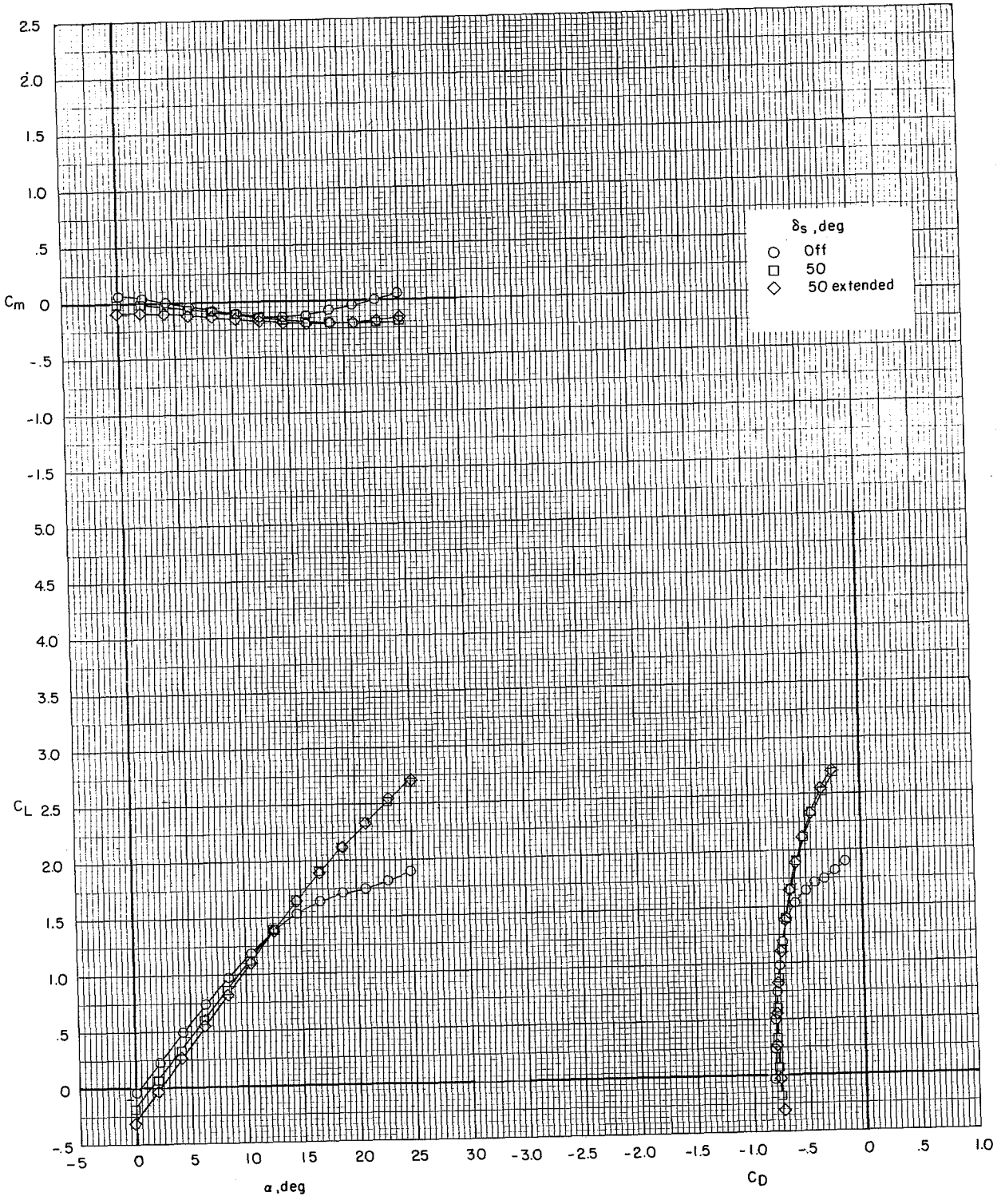

(c) $C_T = 0.96$.

Figure 39.- Continued.

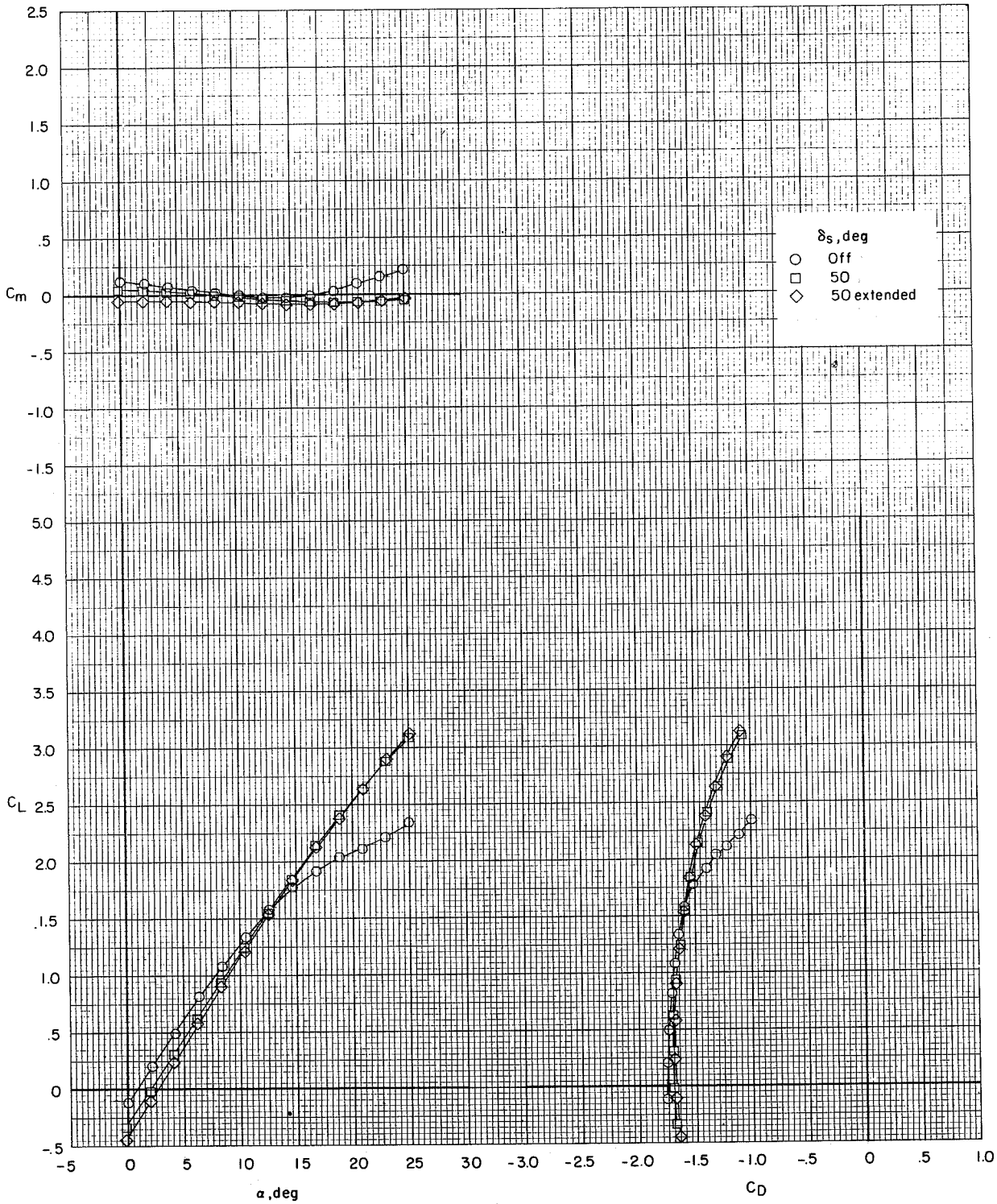

(d) $C_T = 1.91$.

Figure 39.- Concluded.

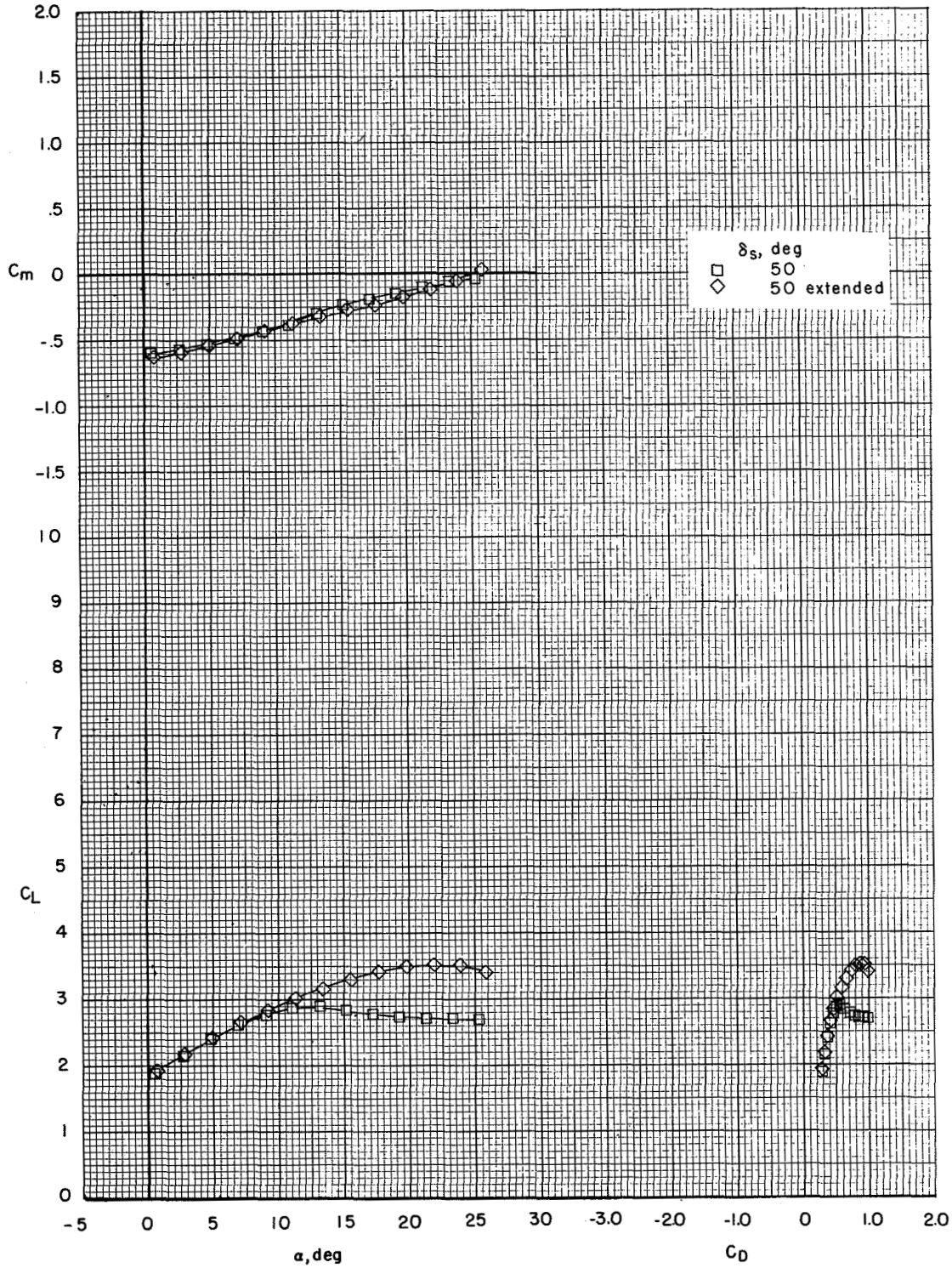

(a) $C_T = 0$.

Figure 40.- Effect of leading-edge slat on longitudinal aerodynamic characteristics in the take-off configuration. Tail off. Model in the V/STOL tunnel without the tunnel liner installed.

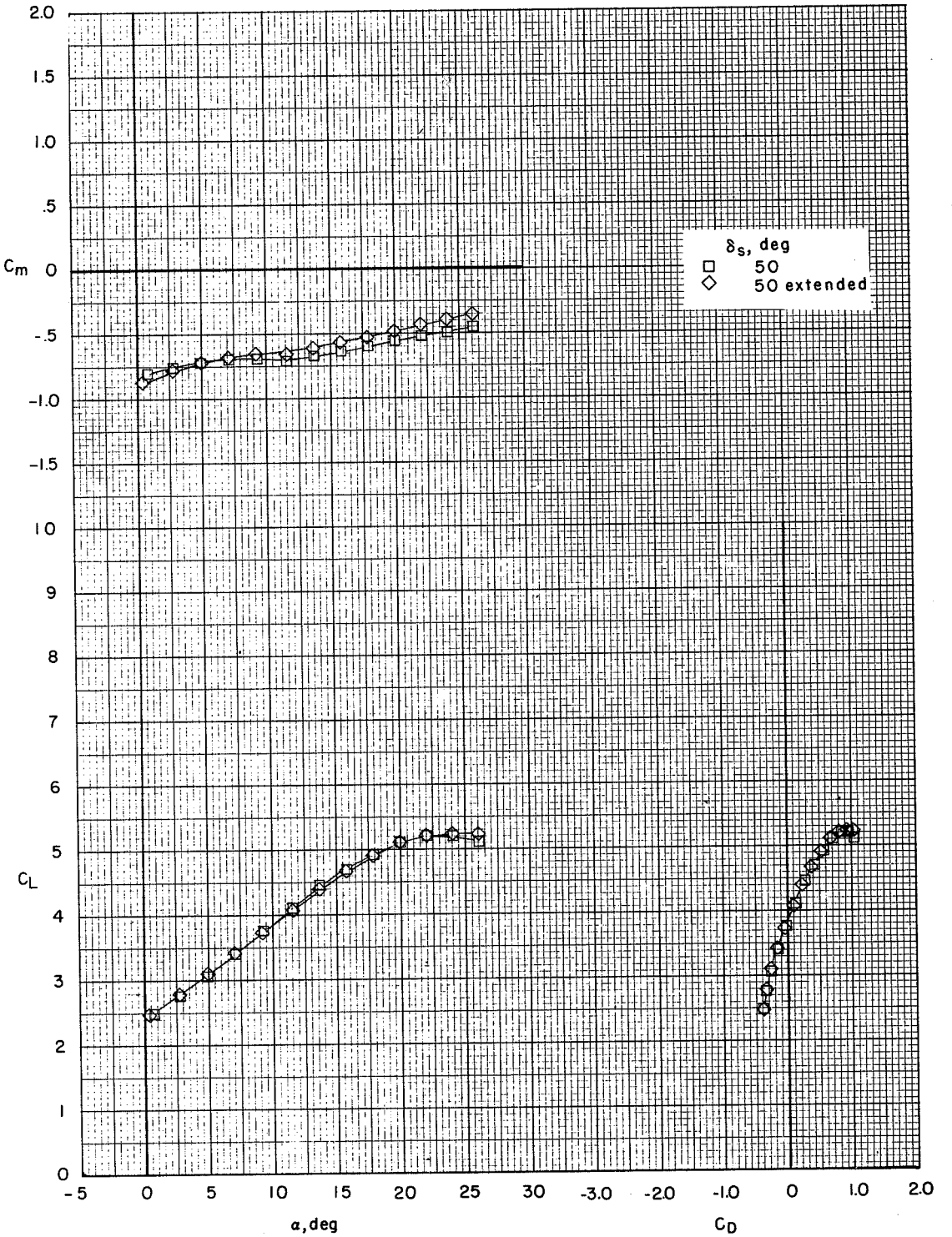

(b) $C_T = 0.96$.

Figure 40.- Continued.

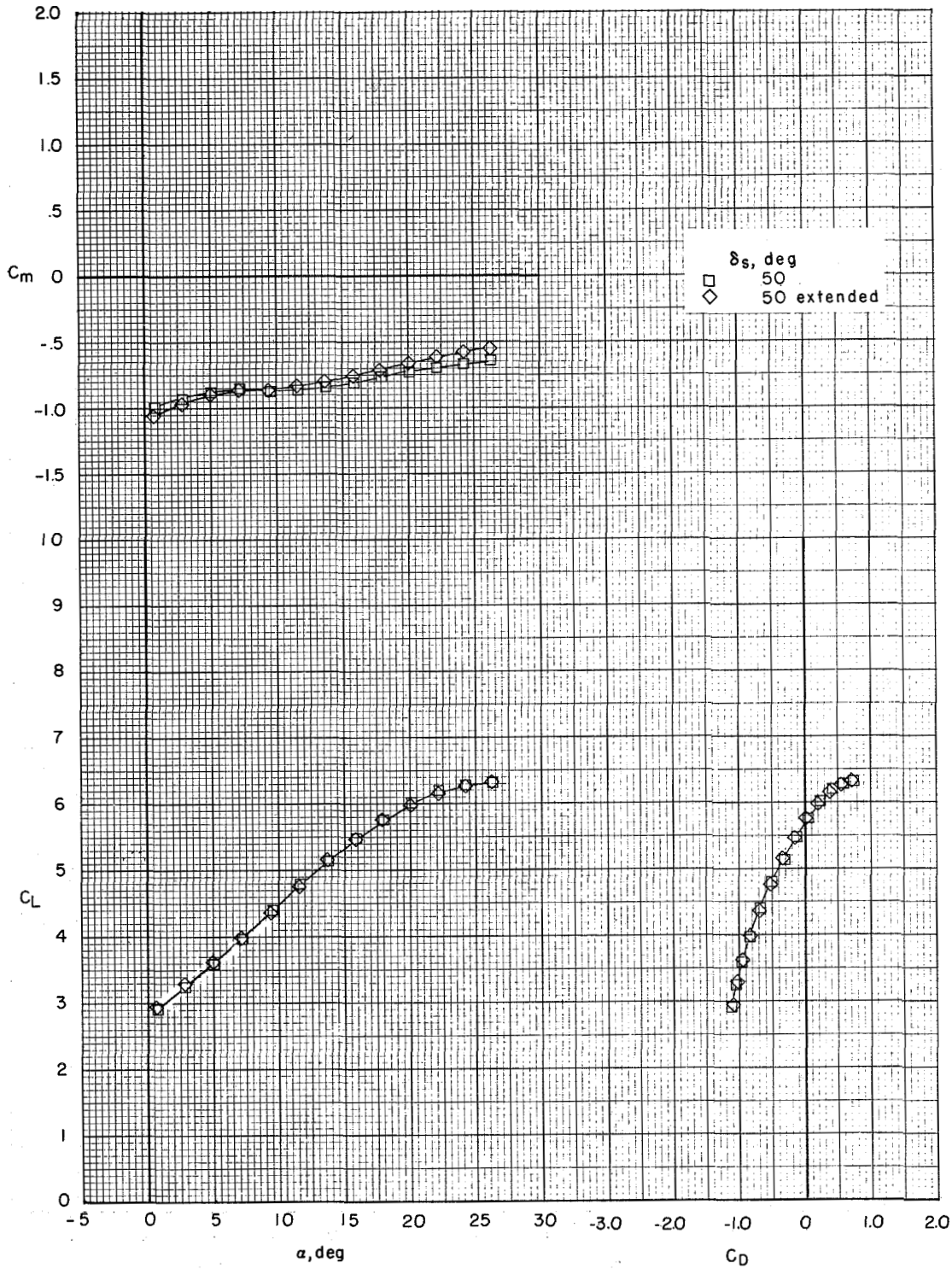

(c) $C_T = 1.91$.

Figure 40.- Continued.

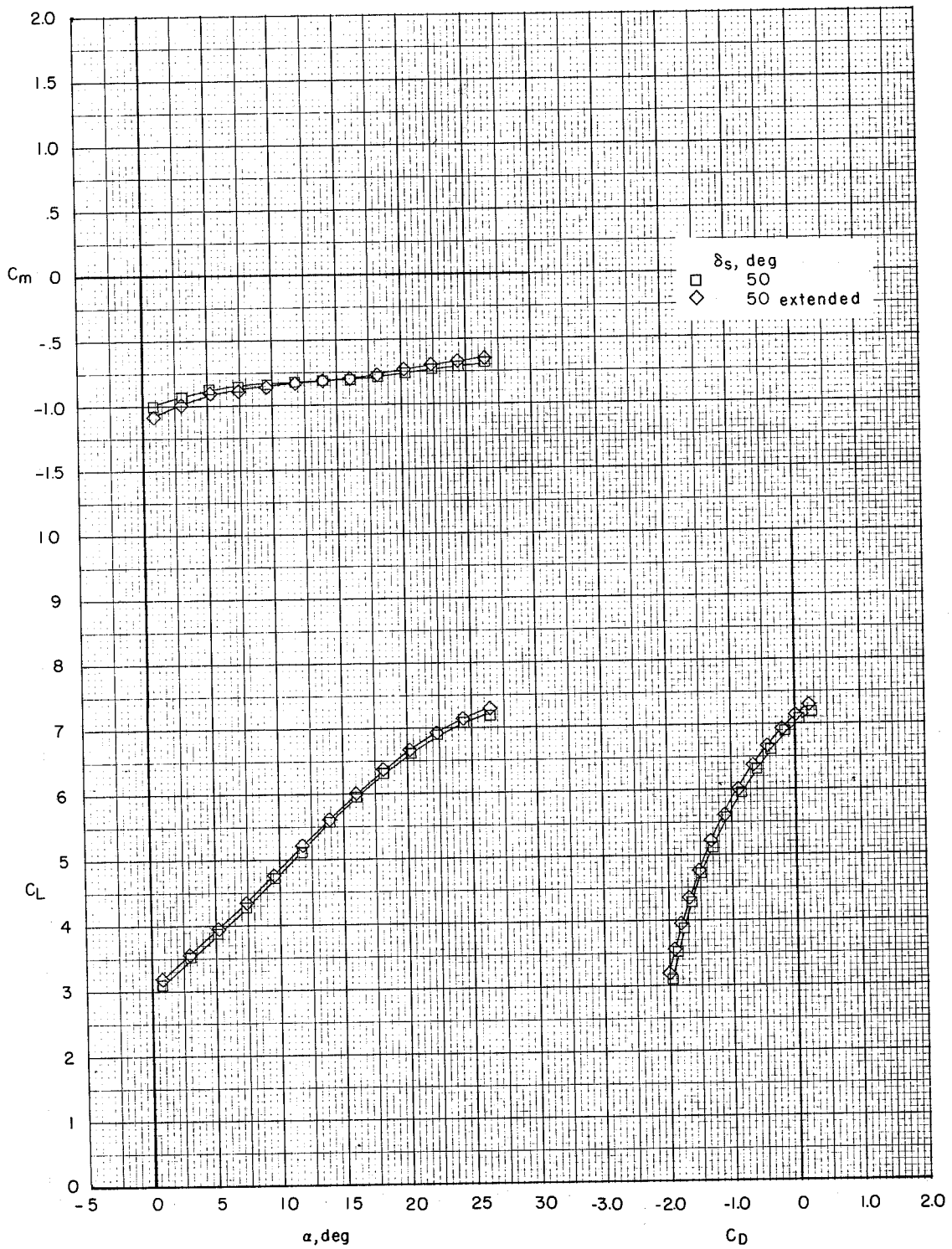

(d) $C_T = 2.91$.

Figure 40.- Continued.

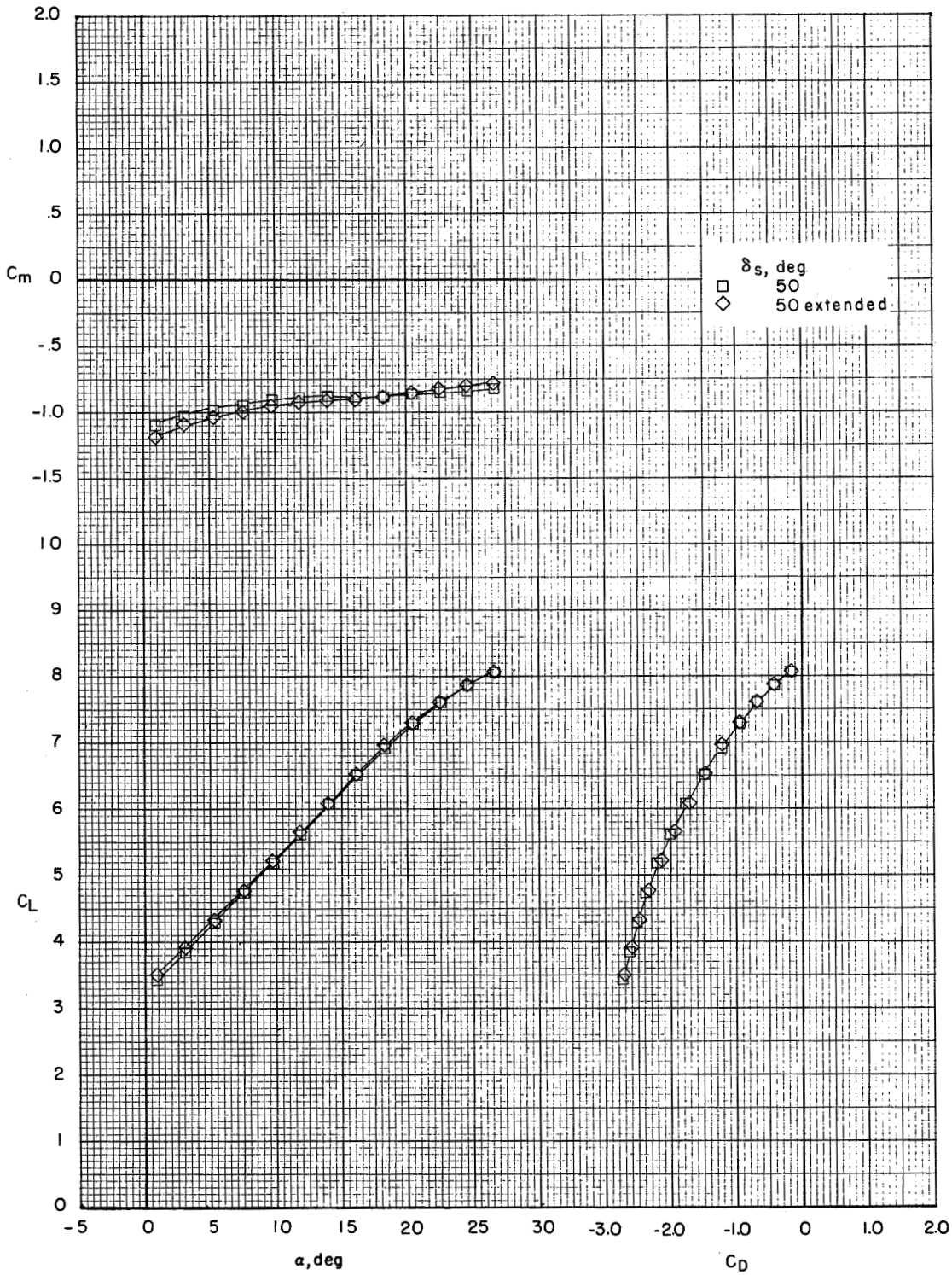

(e) $C_T = 3.83$.

Figure 40.- Concluded.

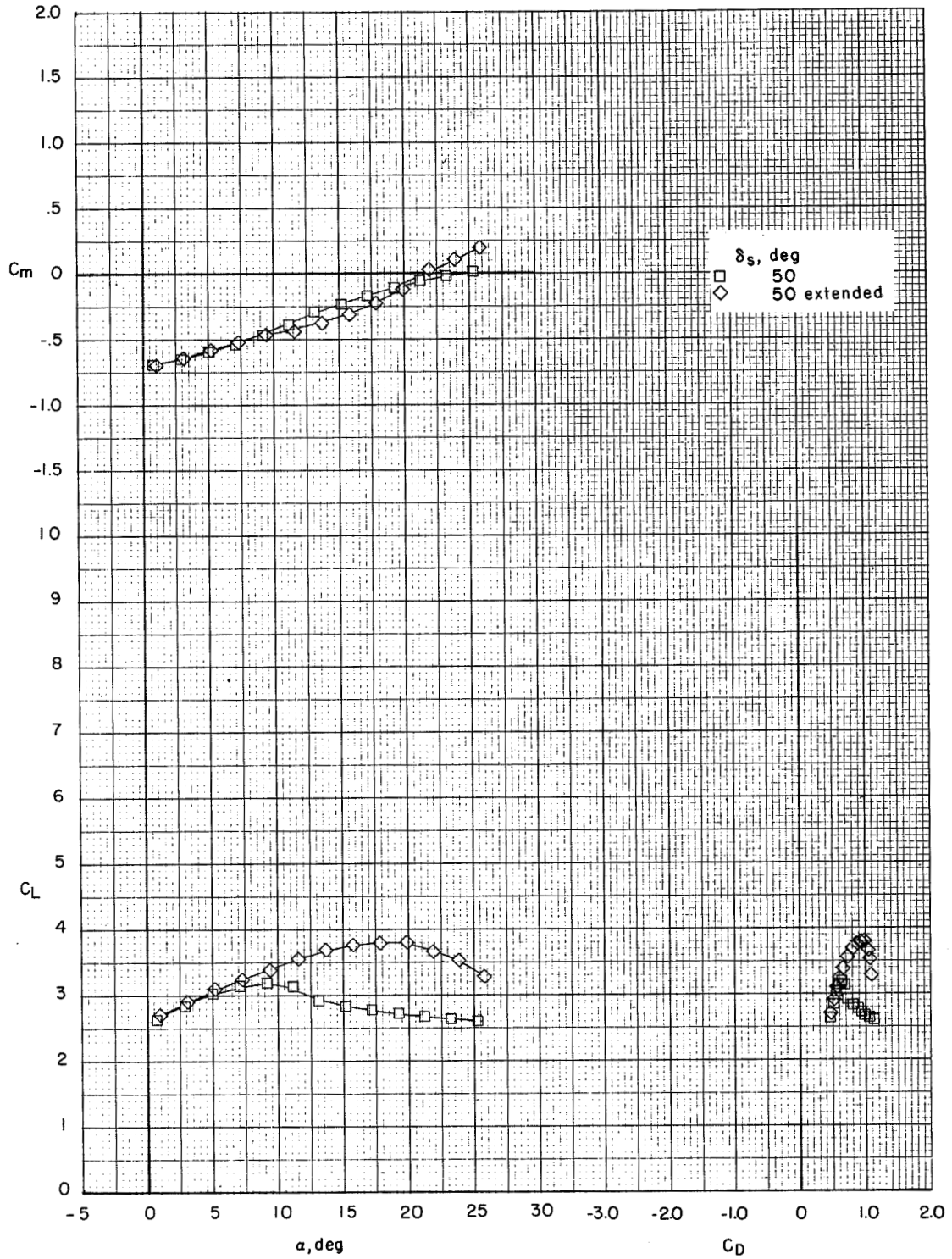

(a) $C_T = 0$.

Figure 41.- Effect of leading-edge slat on longitudinal aerodynamic characteristics in the landing configuration. Tail off. Model in the V/STOL tunnel without the tunnel liner installed.

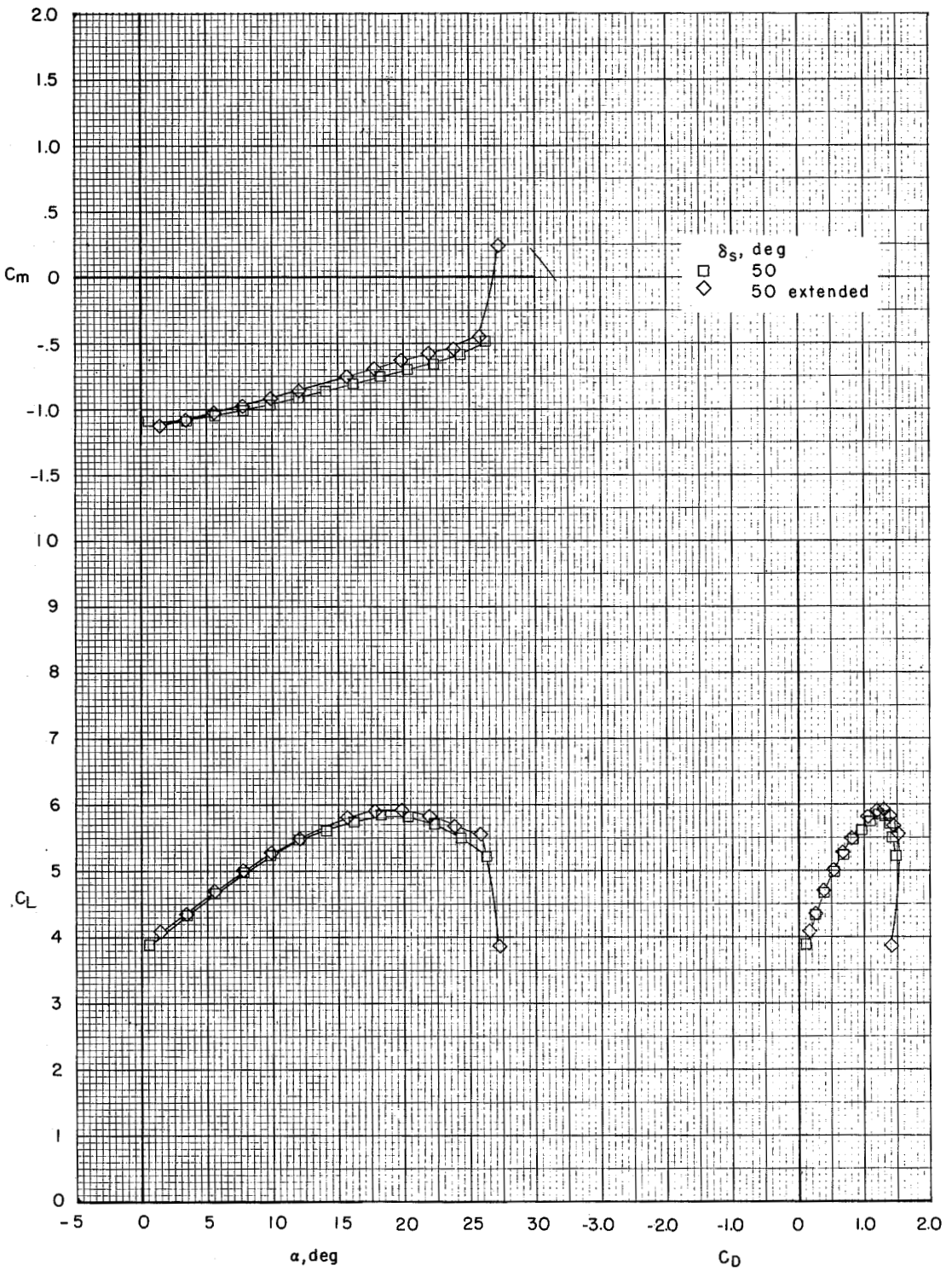

(b) $C_T = 0.96$.

Figure 41.- Continued.

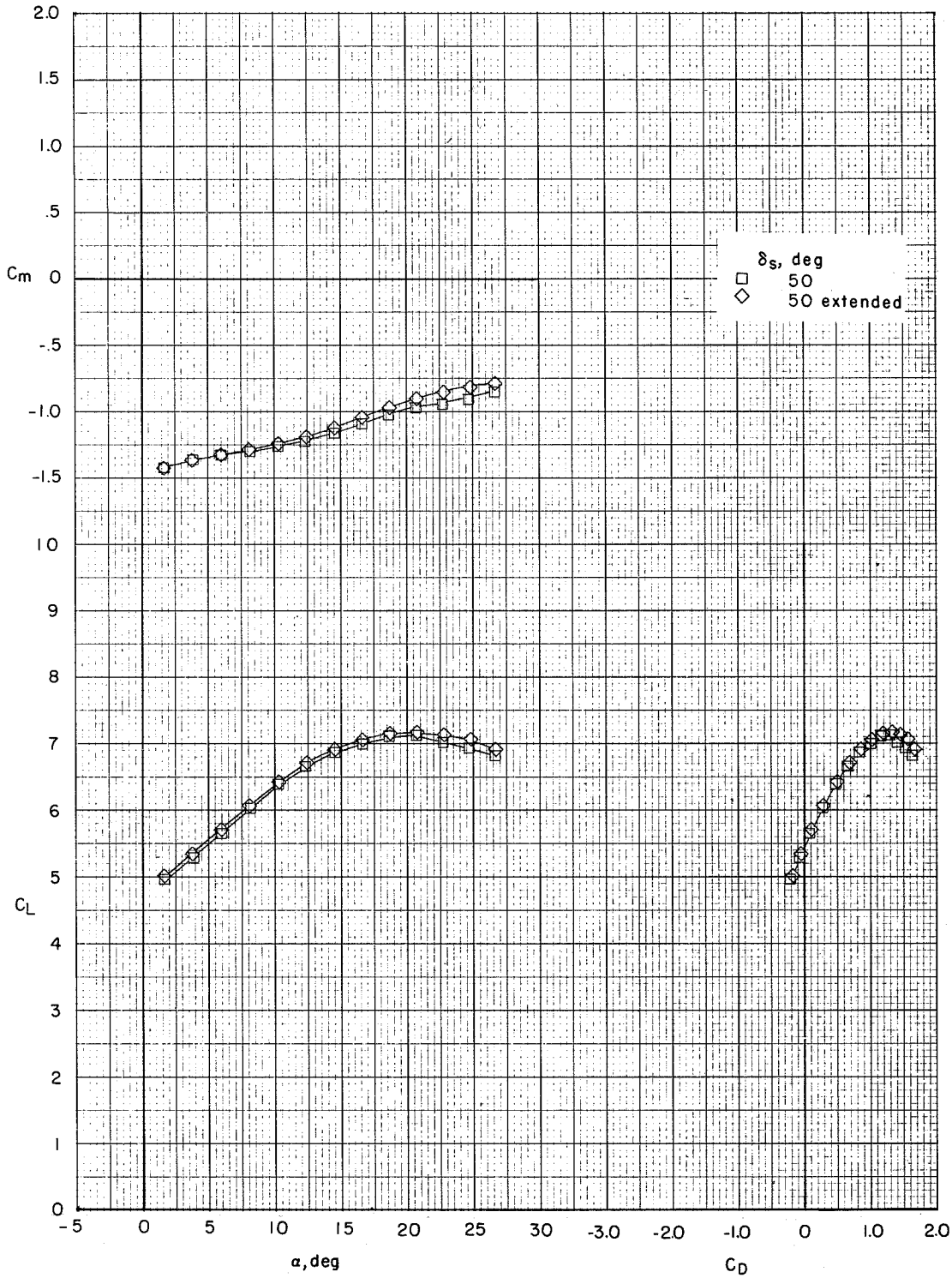

(c) $C_T = 1.91$.

Figure 41.- Continued.

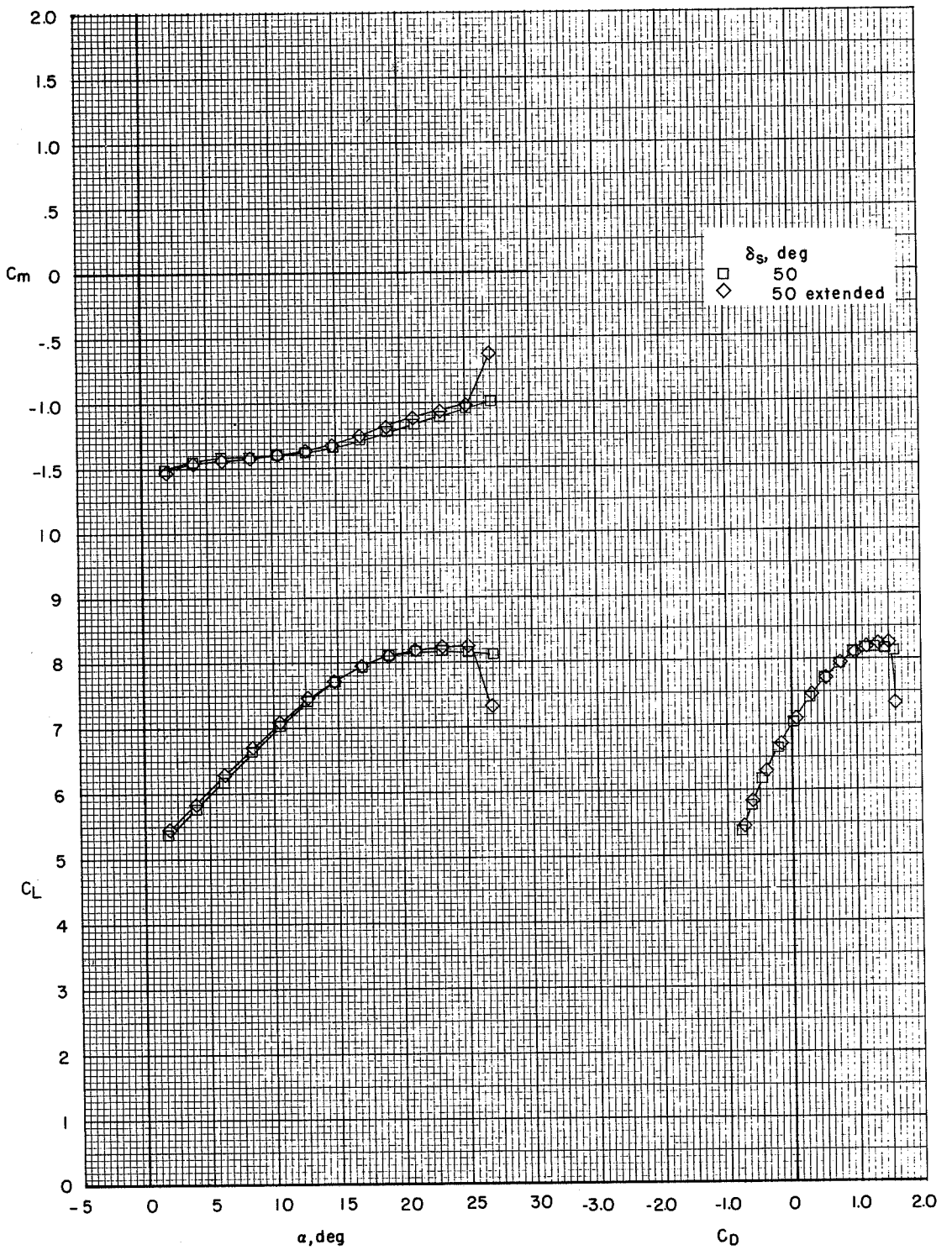

(d) $C_T = 2.87$.

Figure 41.- Continued.

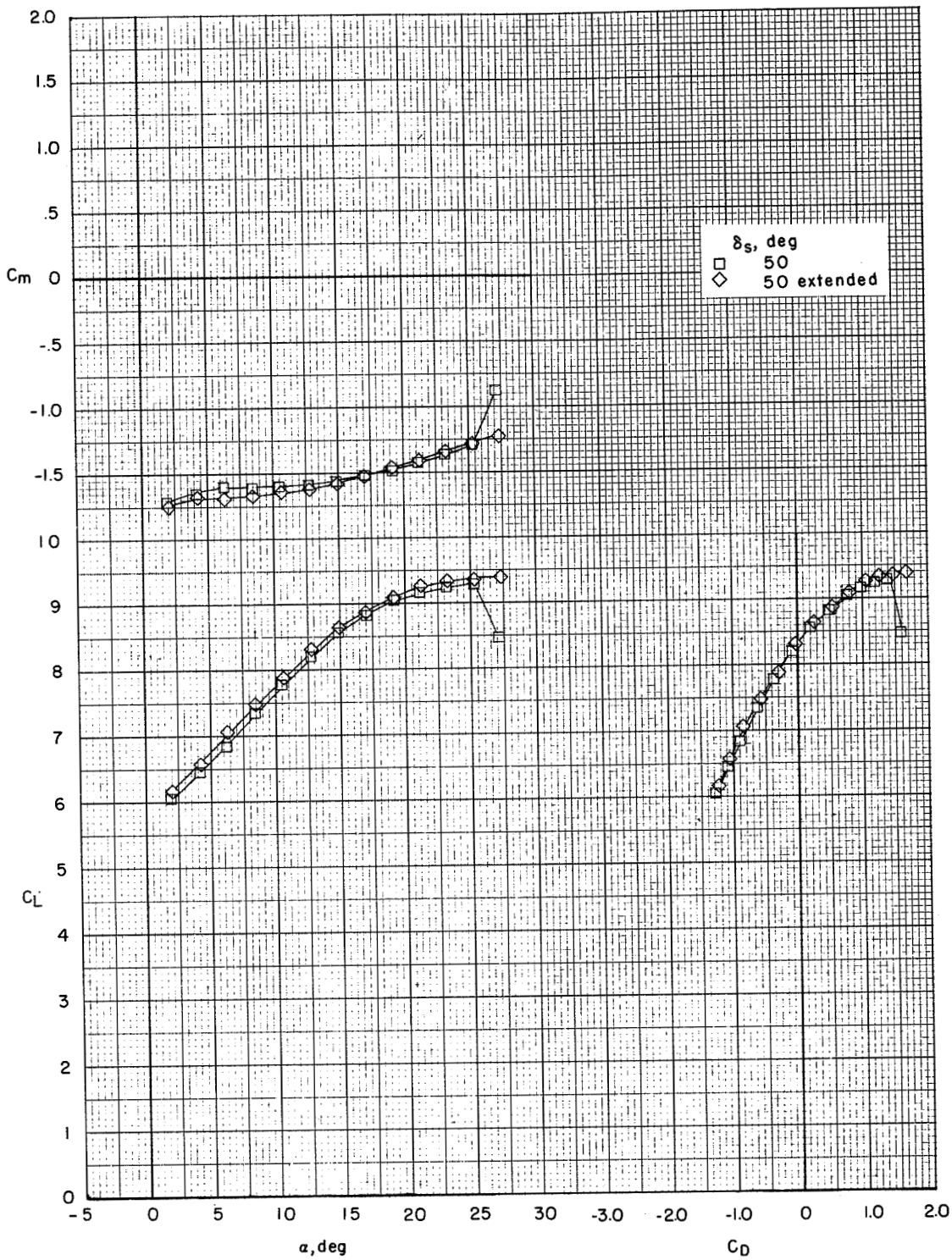

(e) $C_T = 3.83$.

Figure 41.- Concluded.

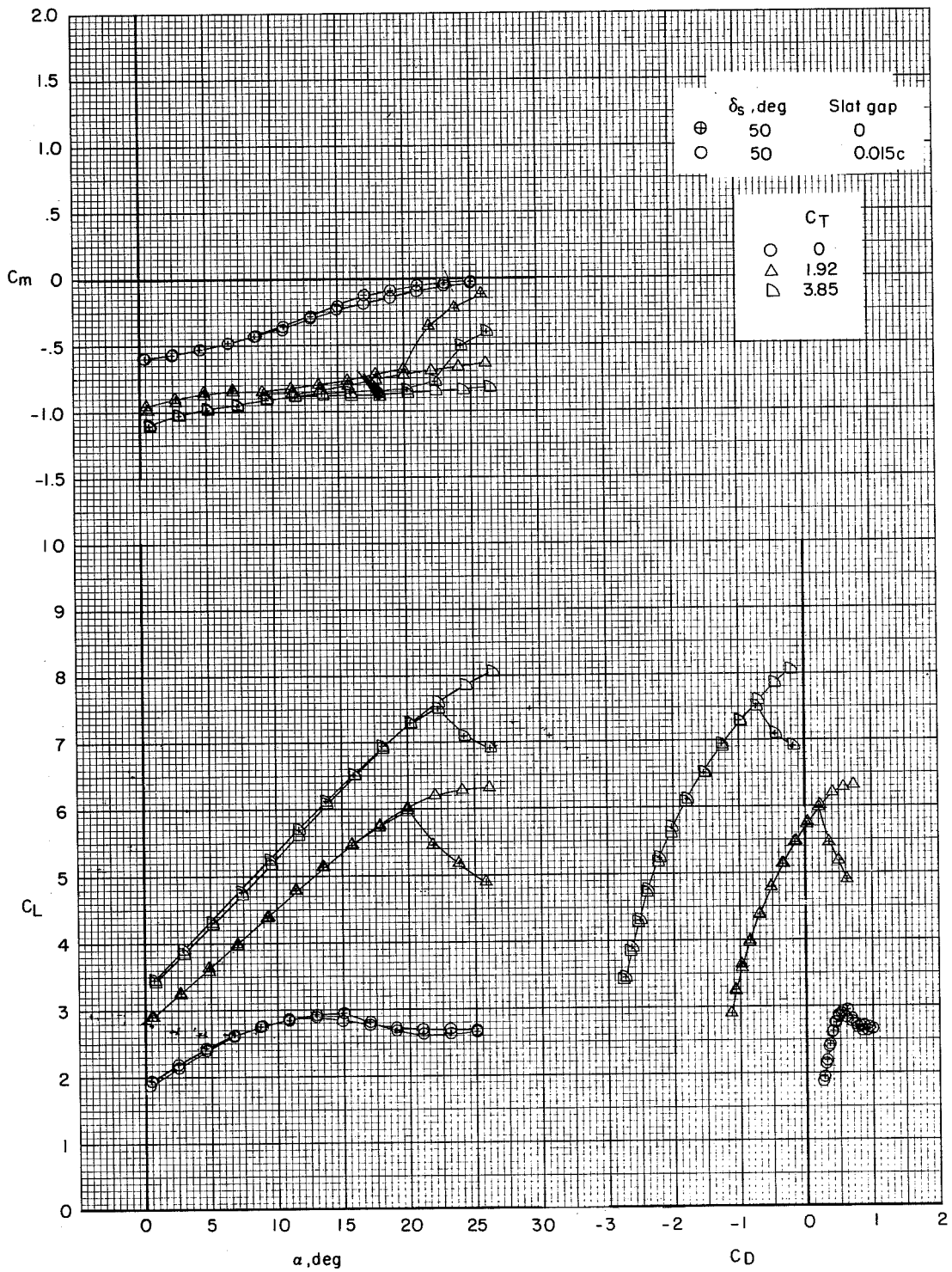

(a) $\delta_f = 40^o$.

Figure 42.- Effect of slat gap on longitudinal aerodynamic characteristics. Tail off. Model in the V/STOL tunnel without the tunnel liner installed.

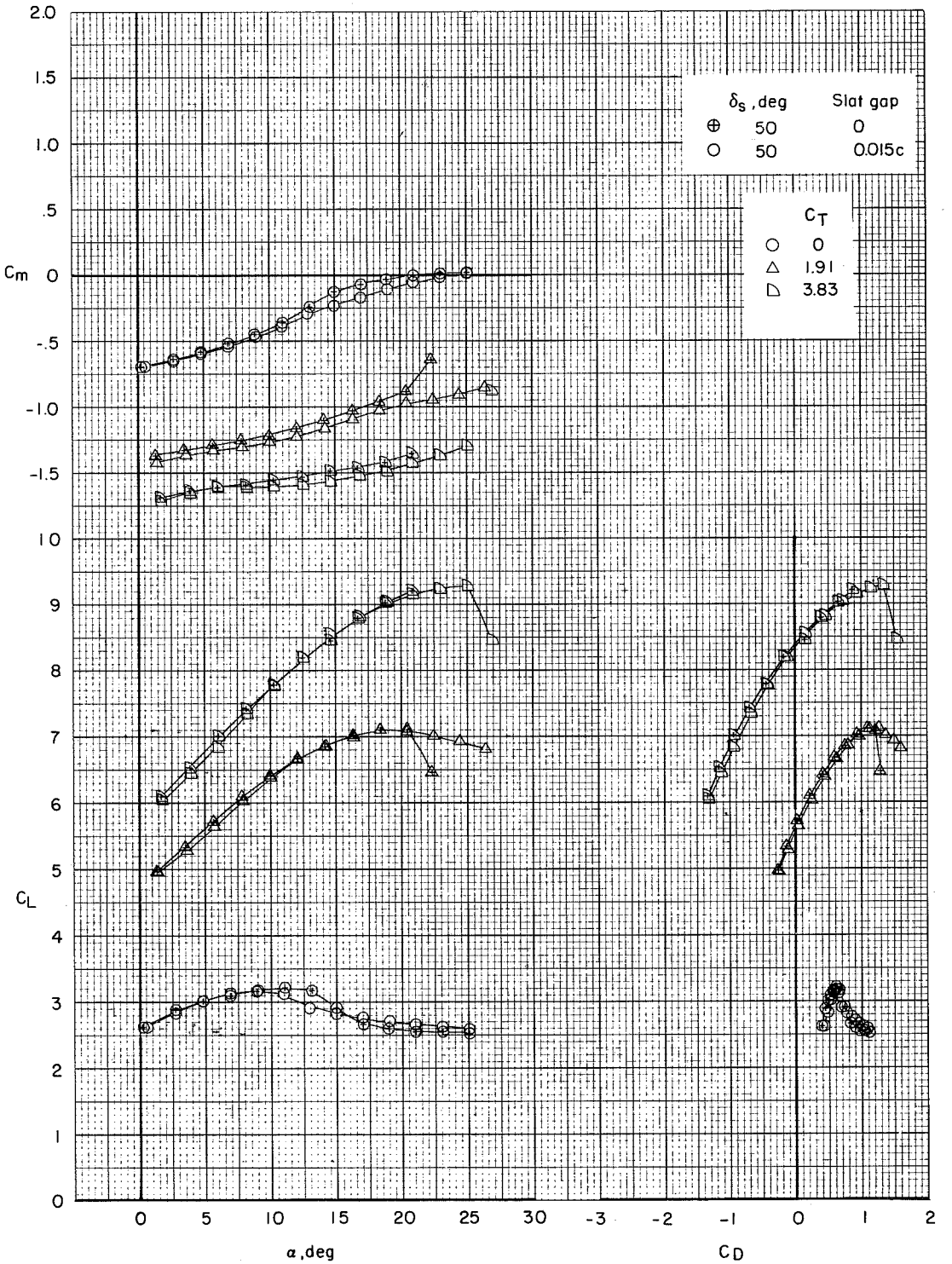

(b) $\delta_f = 55^o$.

Figure 42.- Concluded.

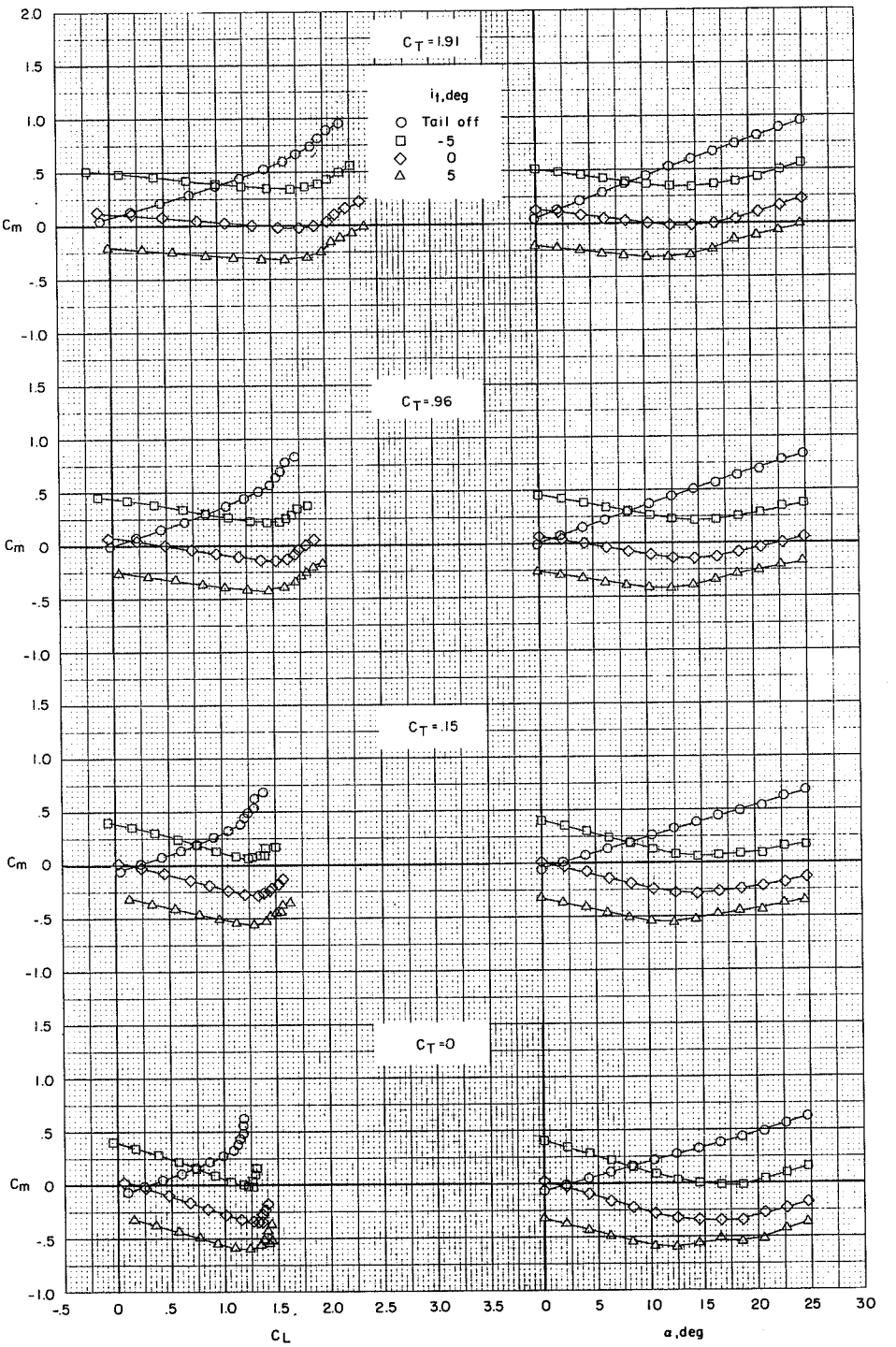

(a) $\delta_e = 0^o$.

Figure 43.- Effect of tail incidence on longitudinal aerodynamic characteristics of the cruise configuration. Model in the V/STOL tunnel without the tunnel liner installed.

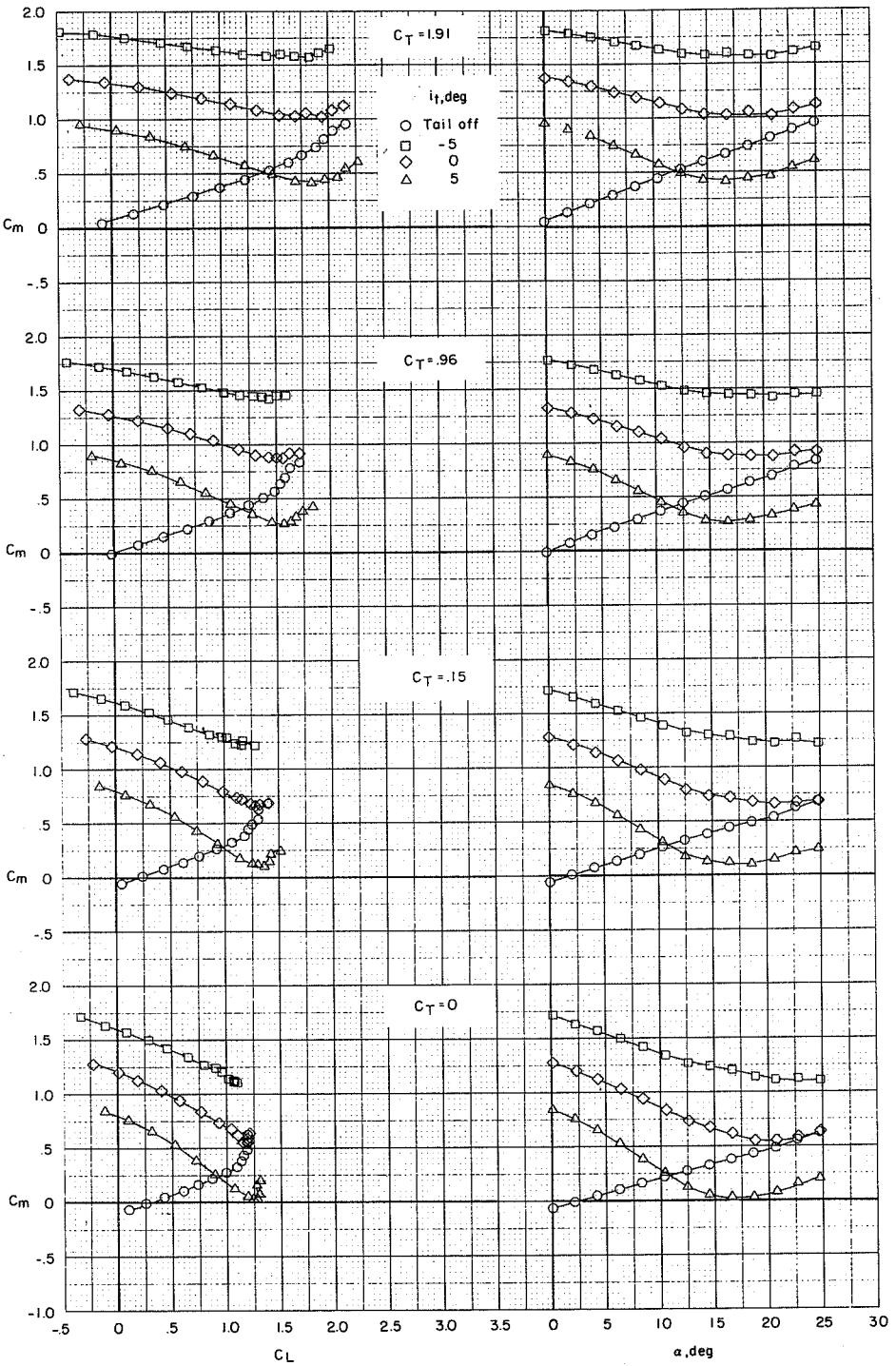

(b) $\delta_e = -25^o$.

Figure 43.- Concluded.

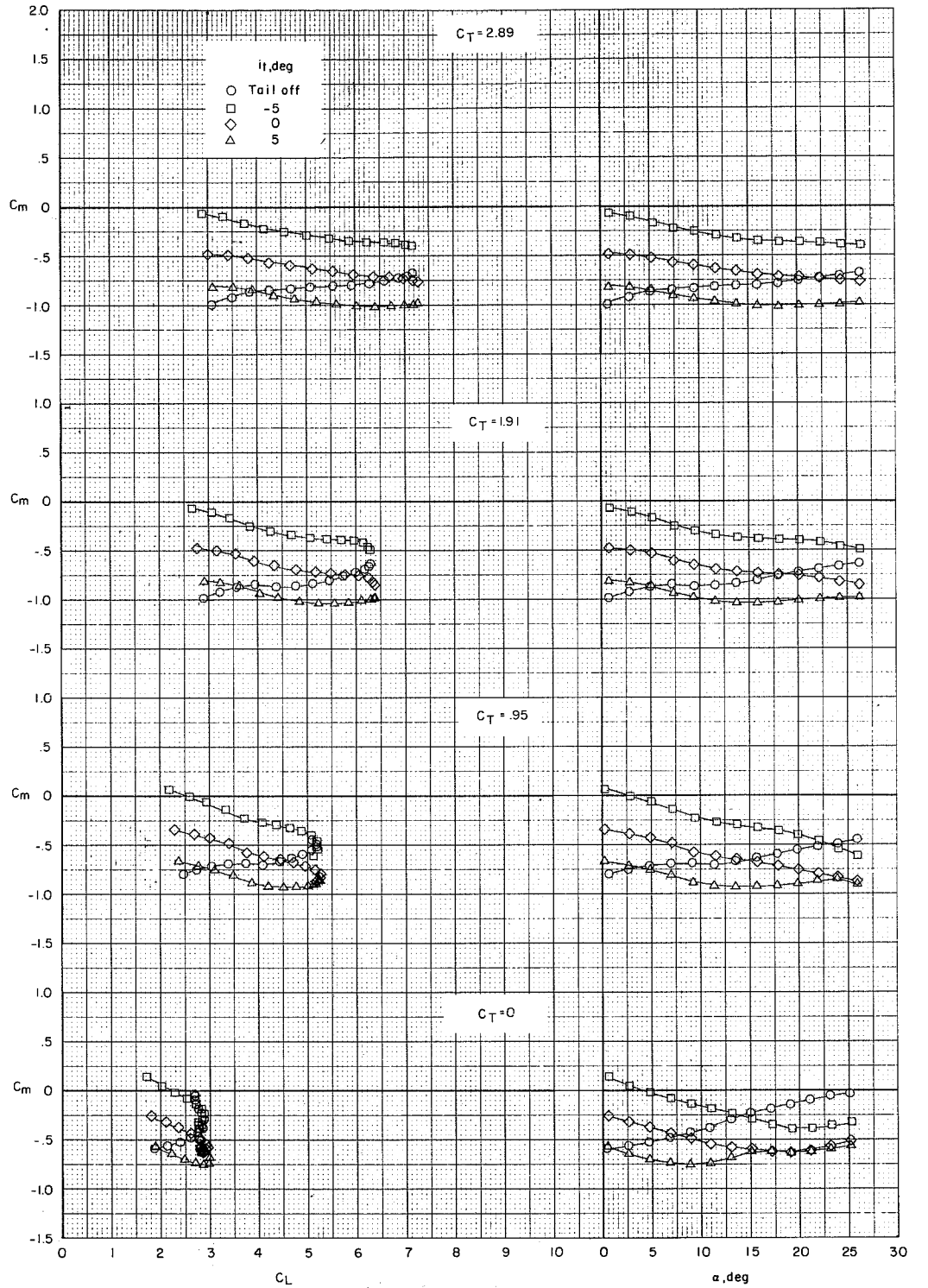

(a) $\delta_e = 0^o$.

Figure 44.- Effect of tail incidence on longitudinal aerodynamic characteristics of the take-off configuration. Model in the V/STOL tunnel without the tunnel liner installed.

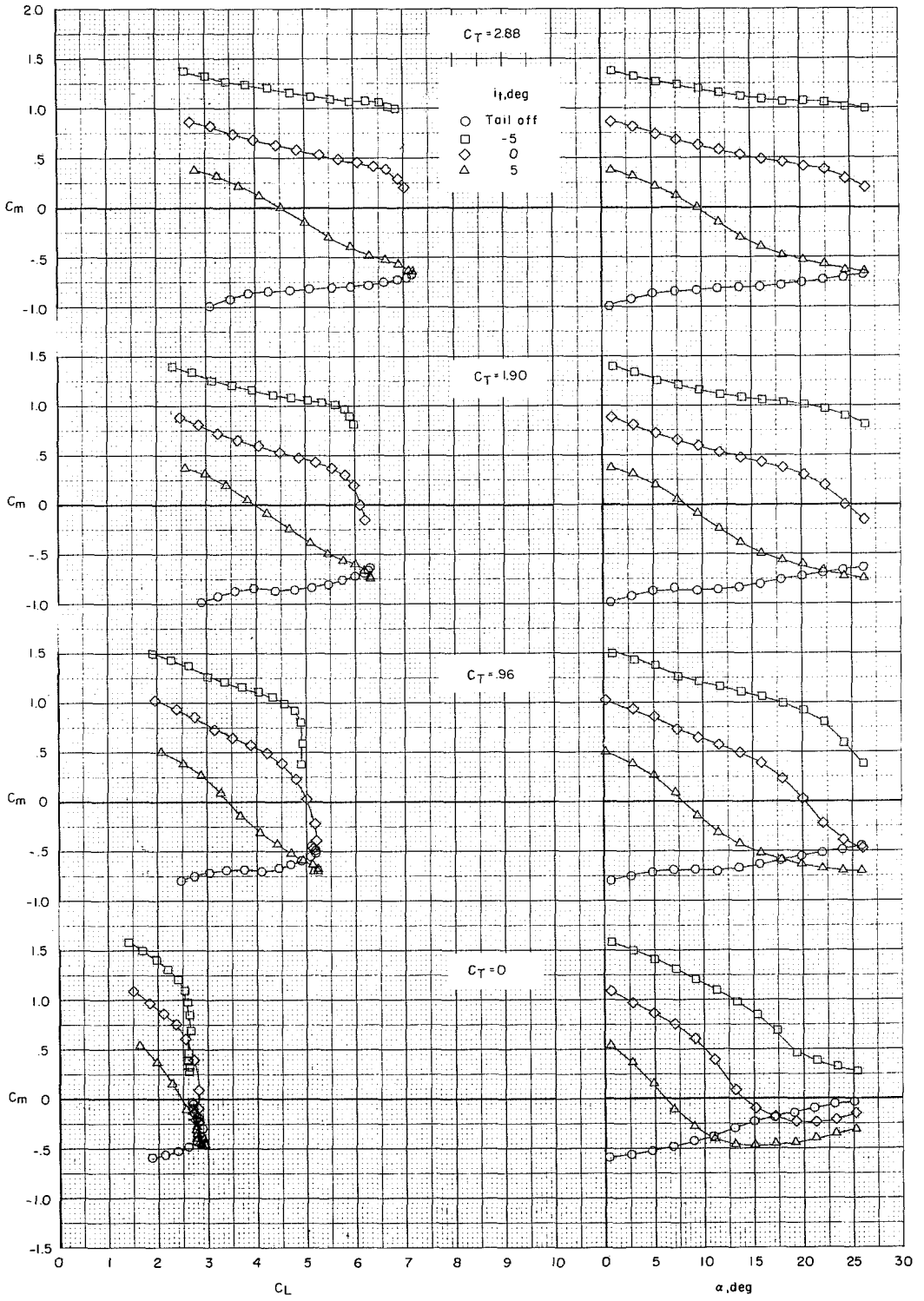

(b) $\delta_e = -25^o$.

Figure 44.- Concluded.

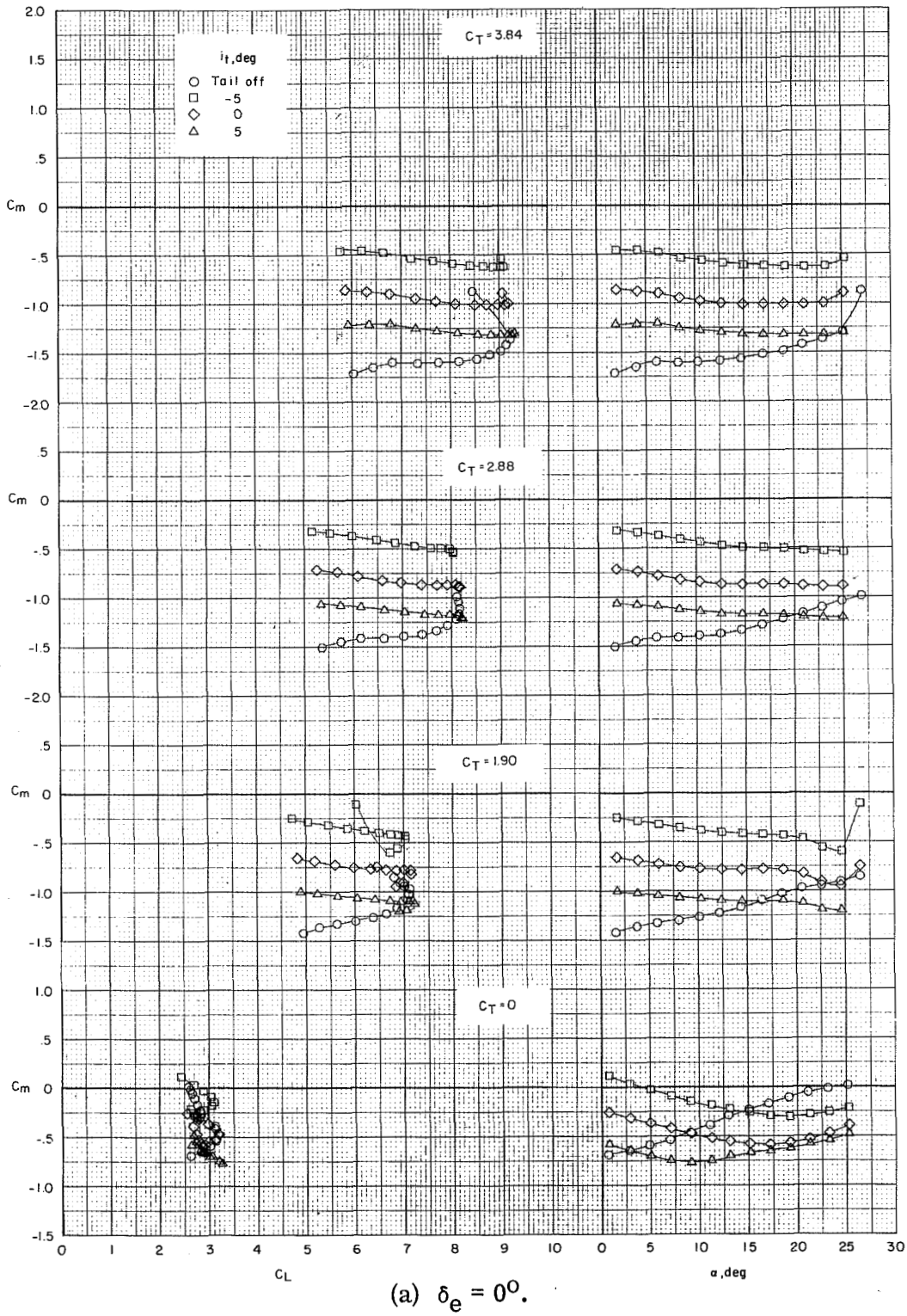

(a) $\delta_e = 0^o$.

Figure 45.- Effect of tail incidence on longitudinal aerodynamic characteristics of the landing configuration. Model in the V/STOL tunnel without the tunnel liner installed.

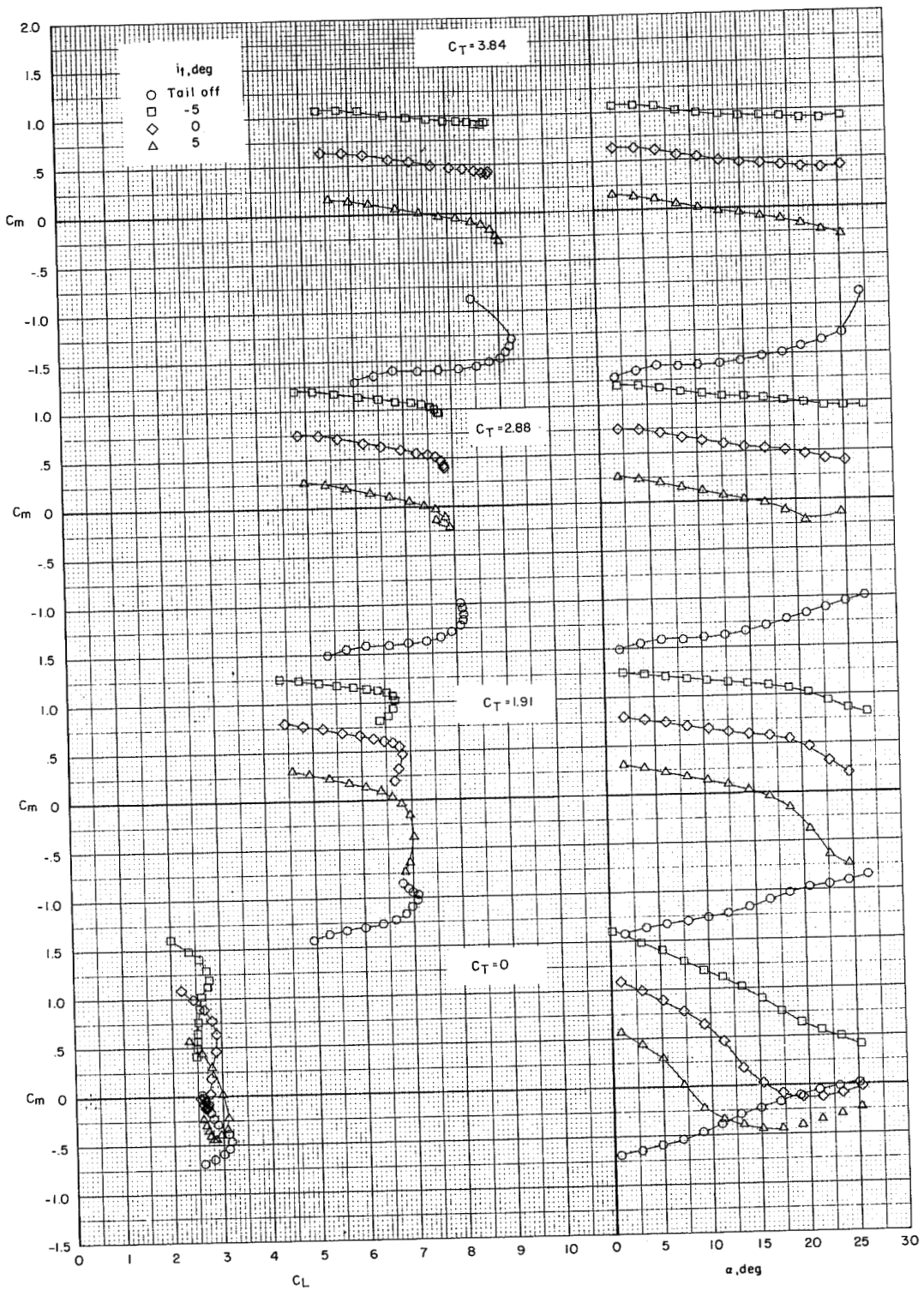

(b) $\delta_e = -25^o$.

Figure 45.- Concluded.

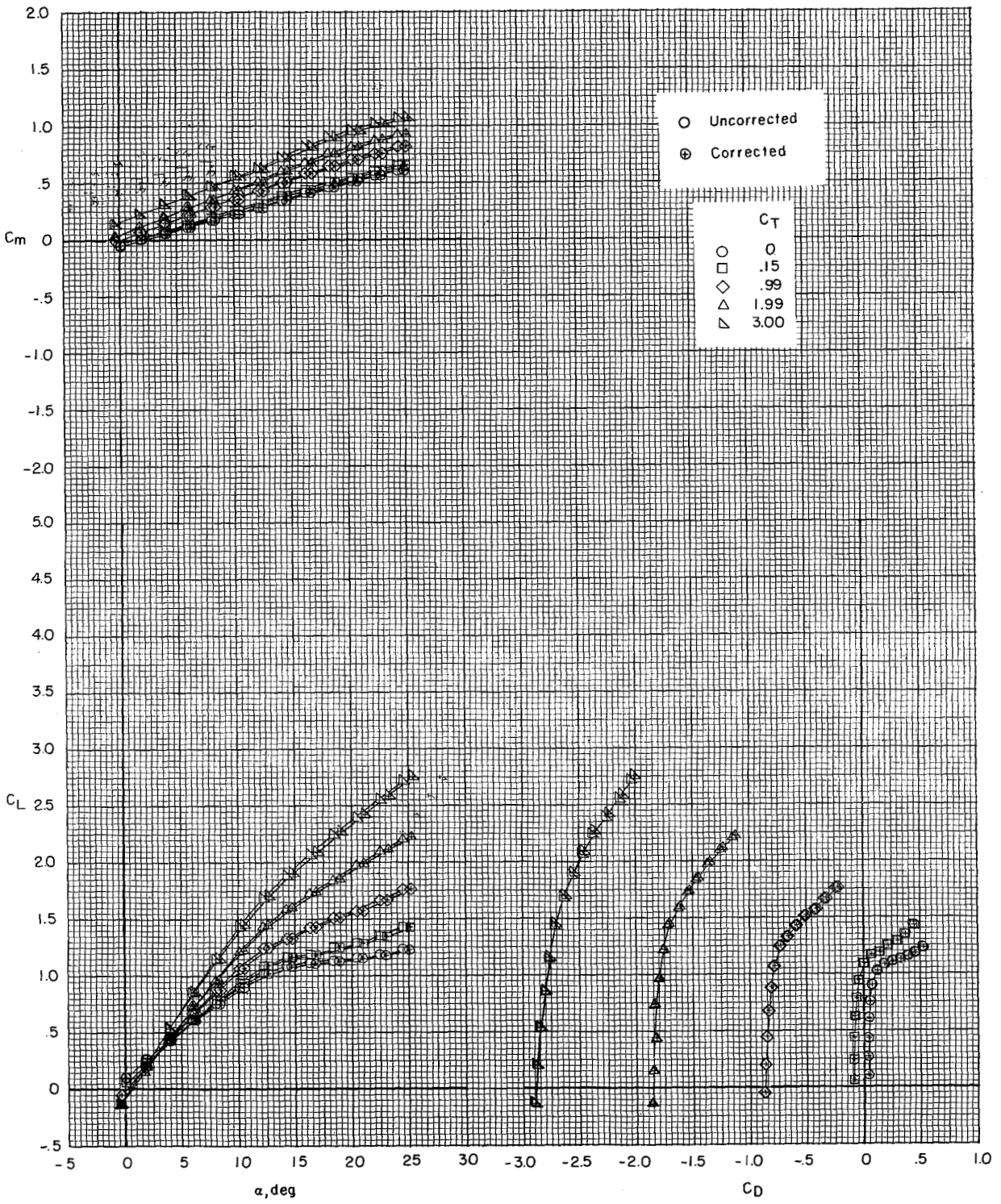

(a) Tail off.

Figure 46.- Effect of wall corrections on the data obtained in the cruise configuration with the Ames liner.

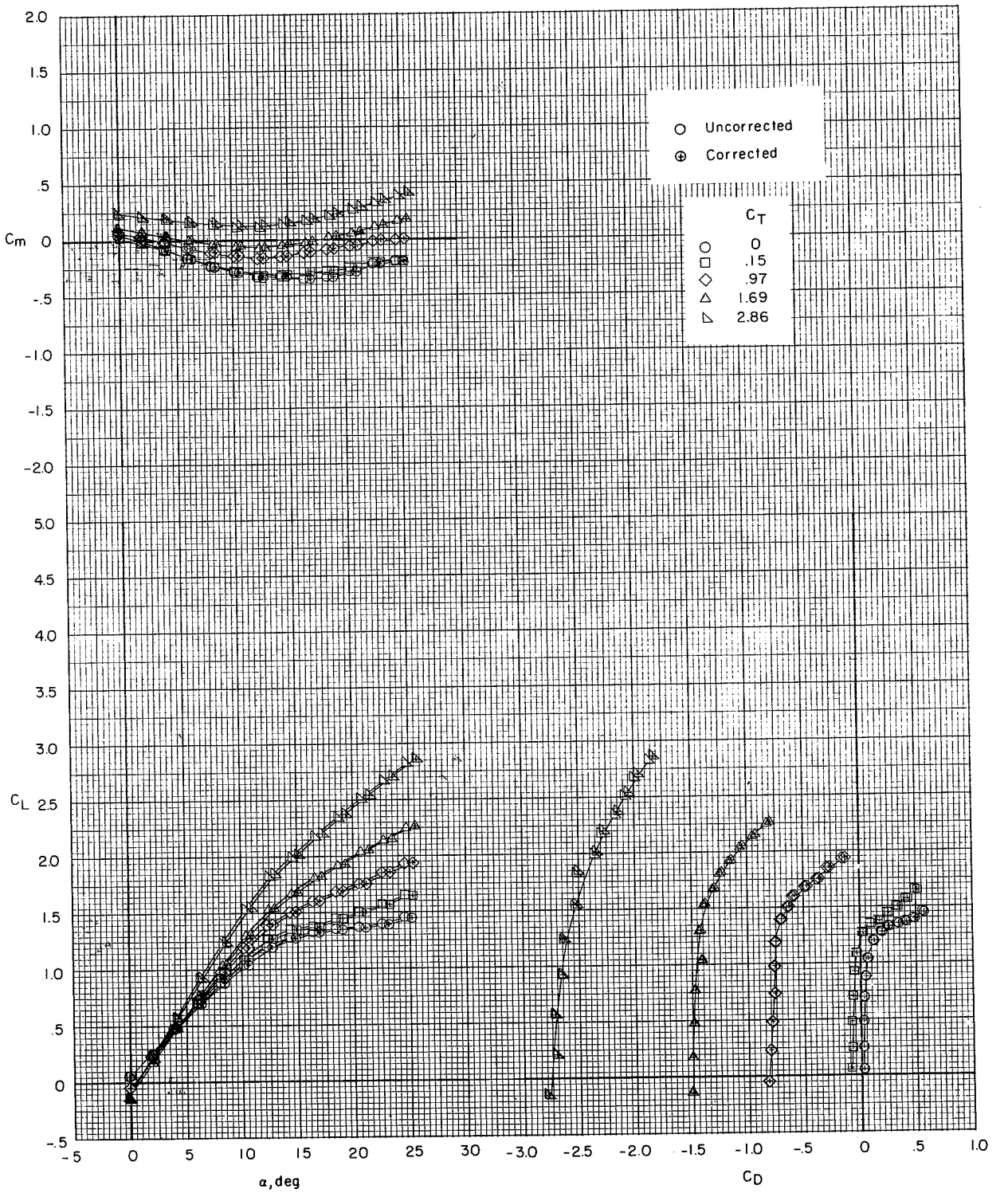

(b) $i_t = 0^o$.

Figure 46.- Concluded.

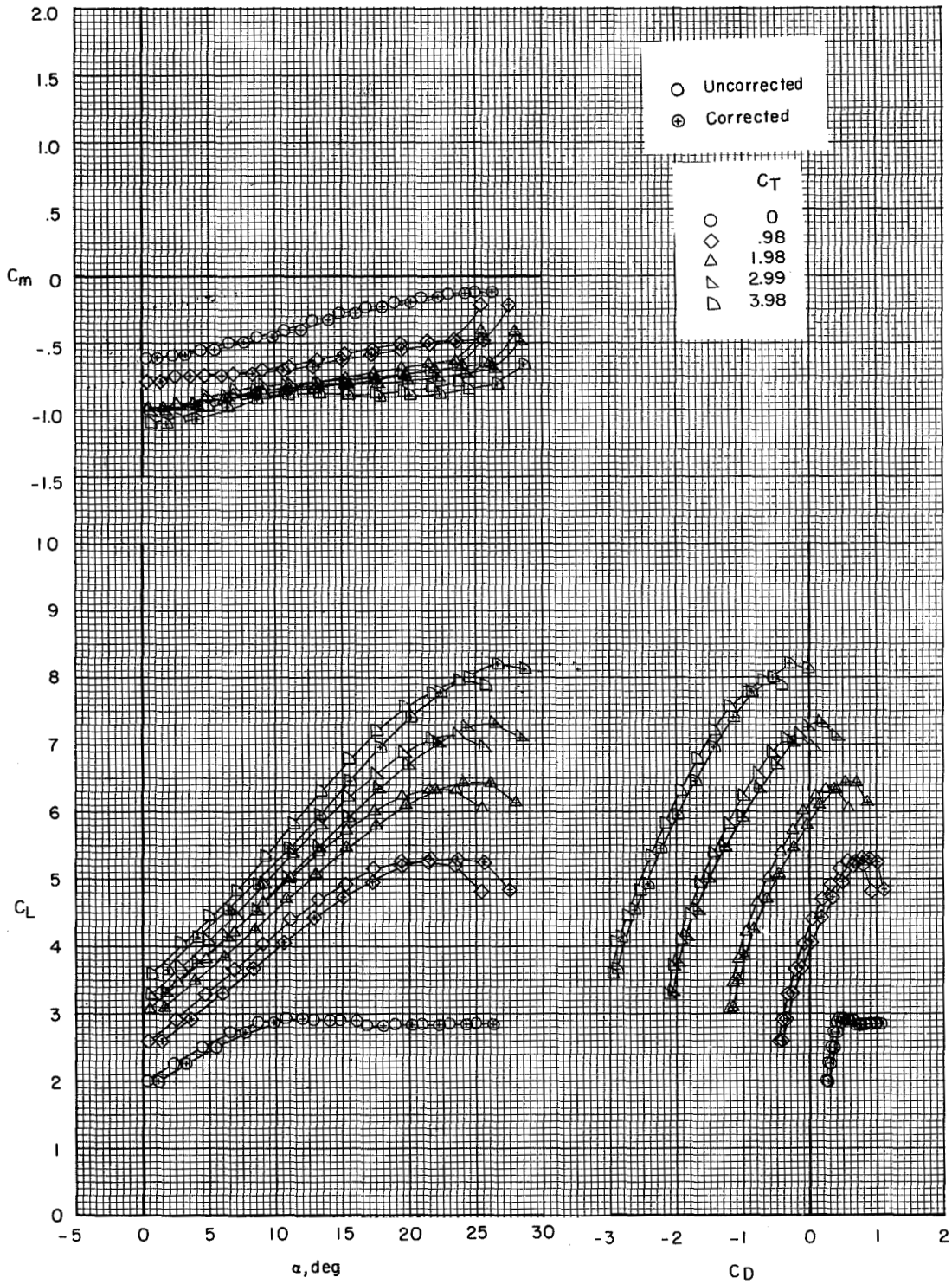

(a) Tail off.

Figure 47.- Effect of wall corrections on the data obtained in the take-off configuration with the Ames liner.

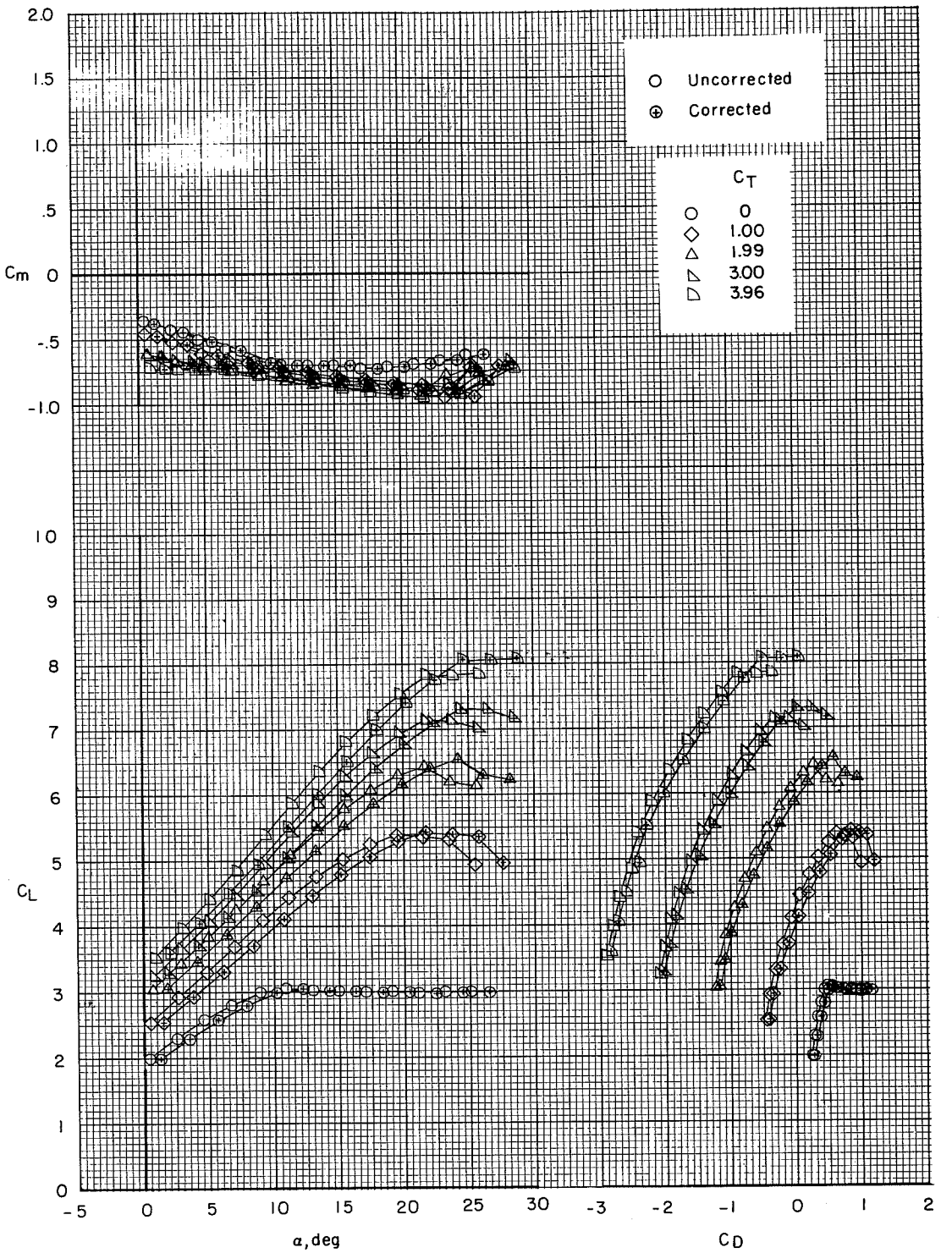

(b) $i_t = 0^o$.

Figure 47.- Concluded.

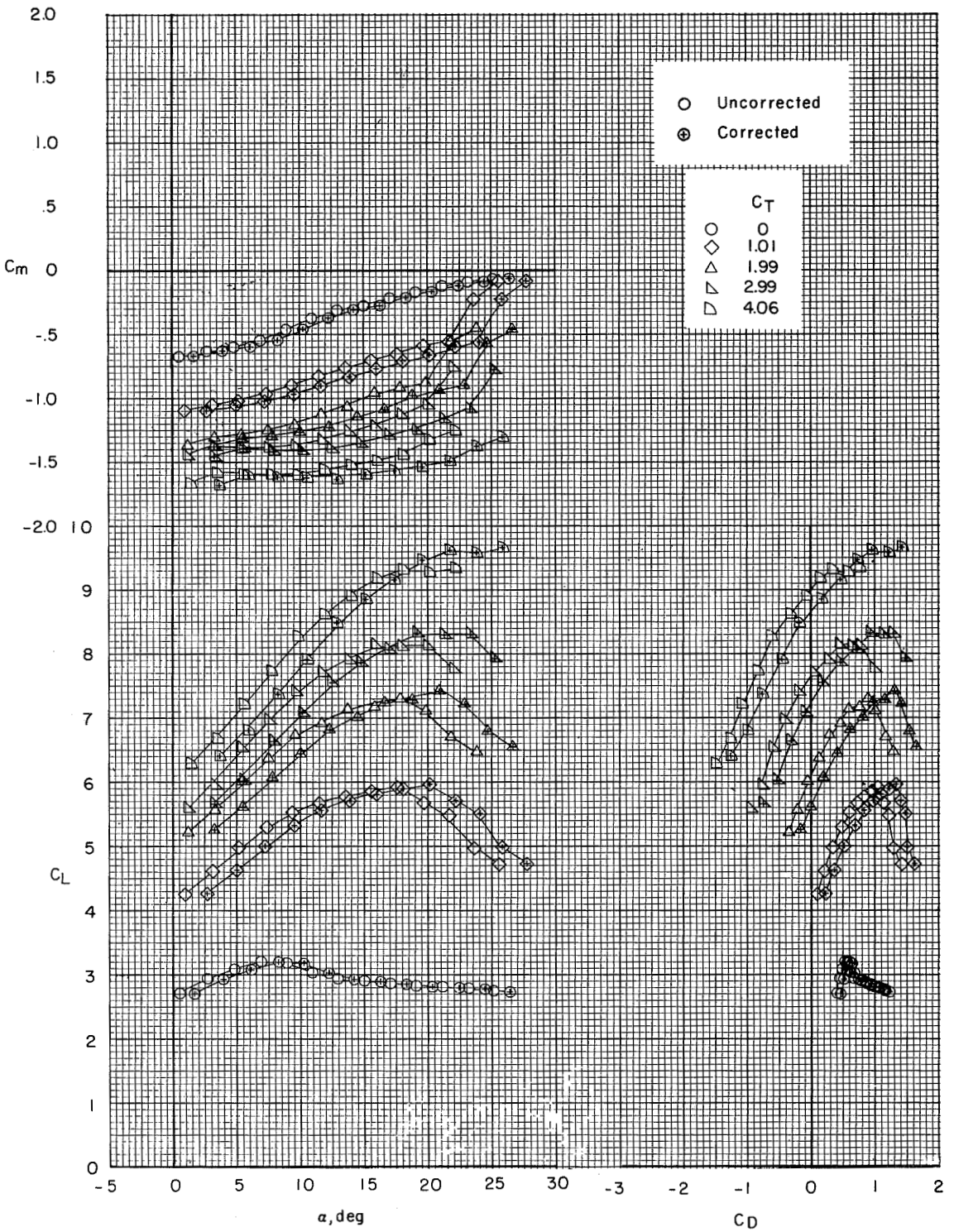

(a) Tail off.

Figure 48.- Effect of wall corrections on the data obtained in the landing configuration with the Ames liner.

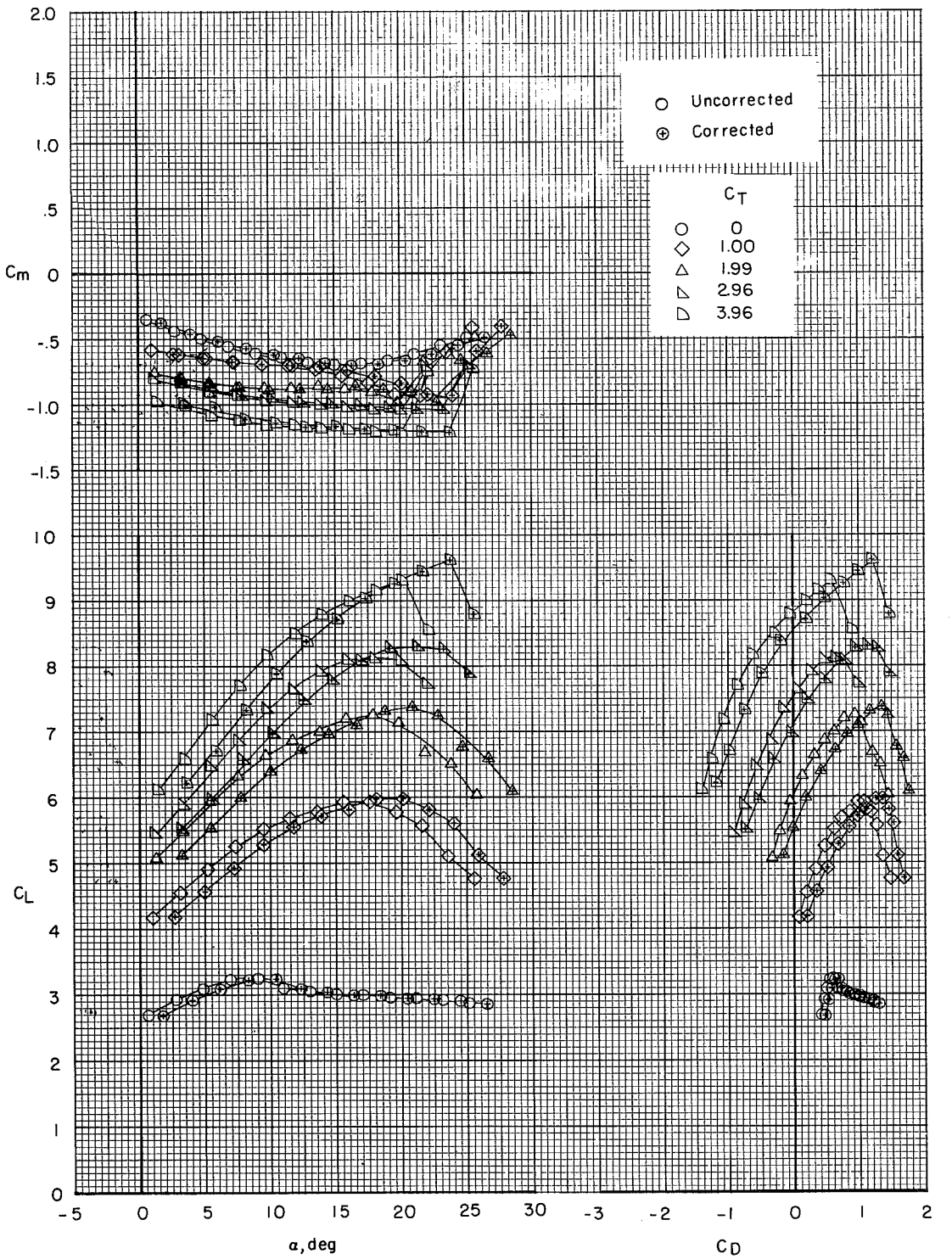

(b) $i_t = 0^o$.

Figure 48.- Concluded.

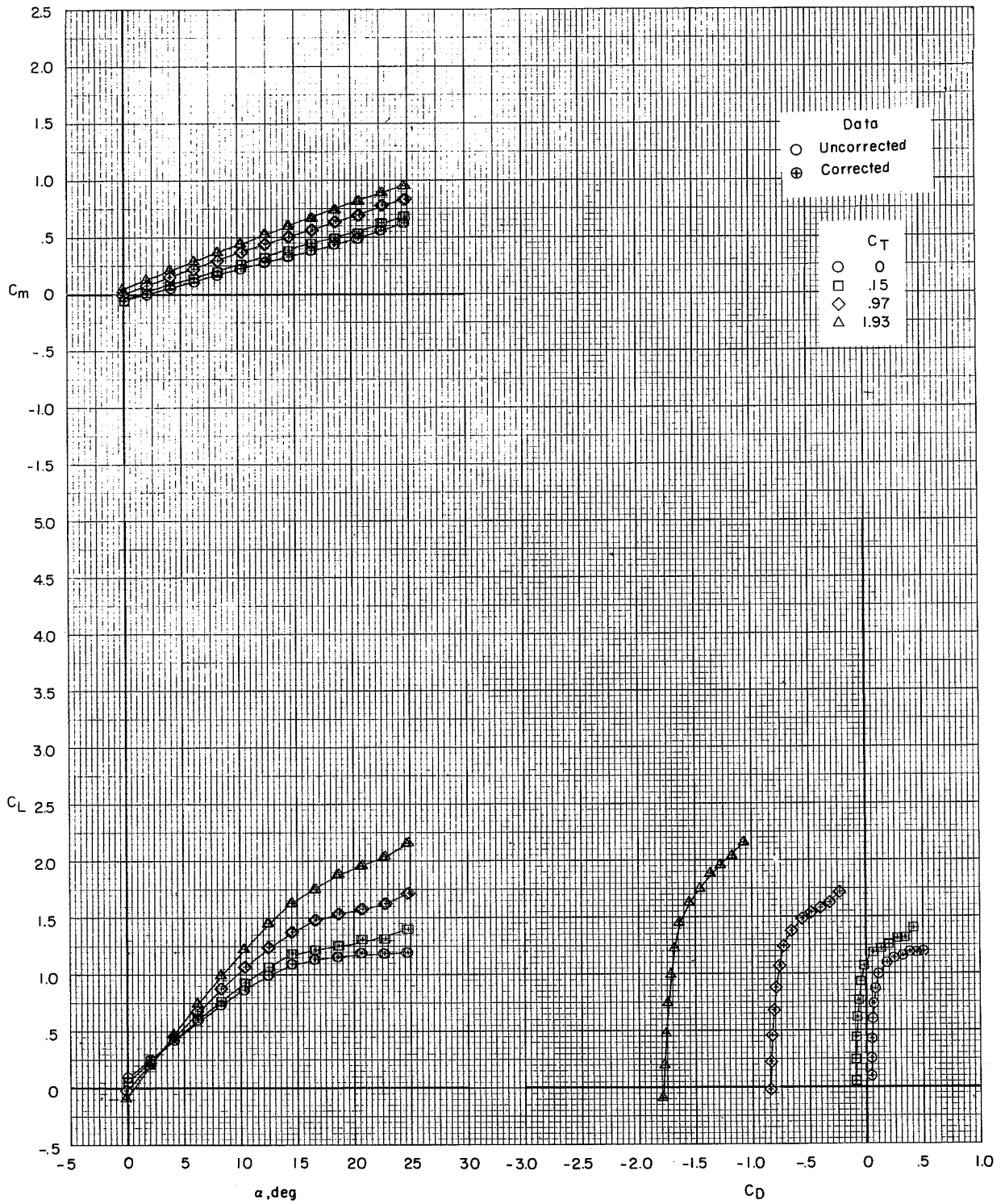

(a) Tail off.

Figure 49.- Effect of wall corrections on V/STOL tunnel data in the cruise configuration without the tunnel liner installed.

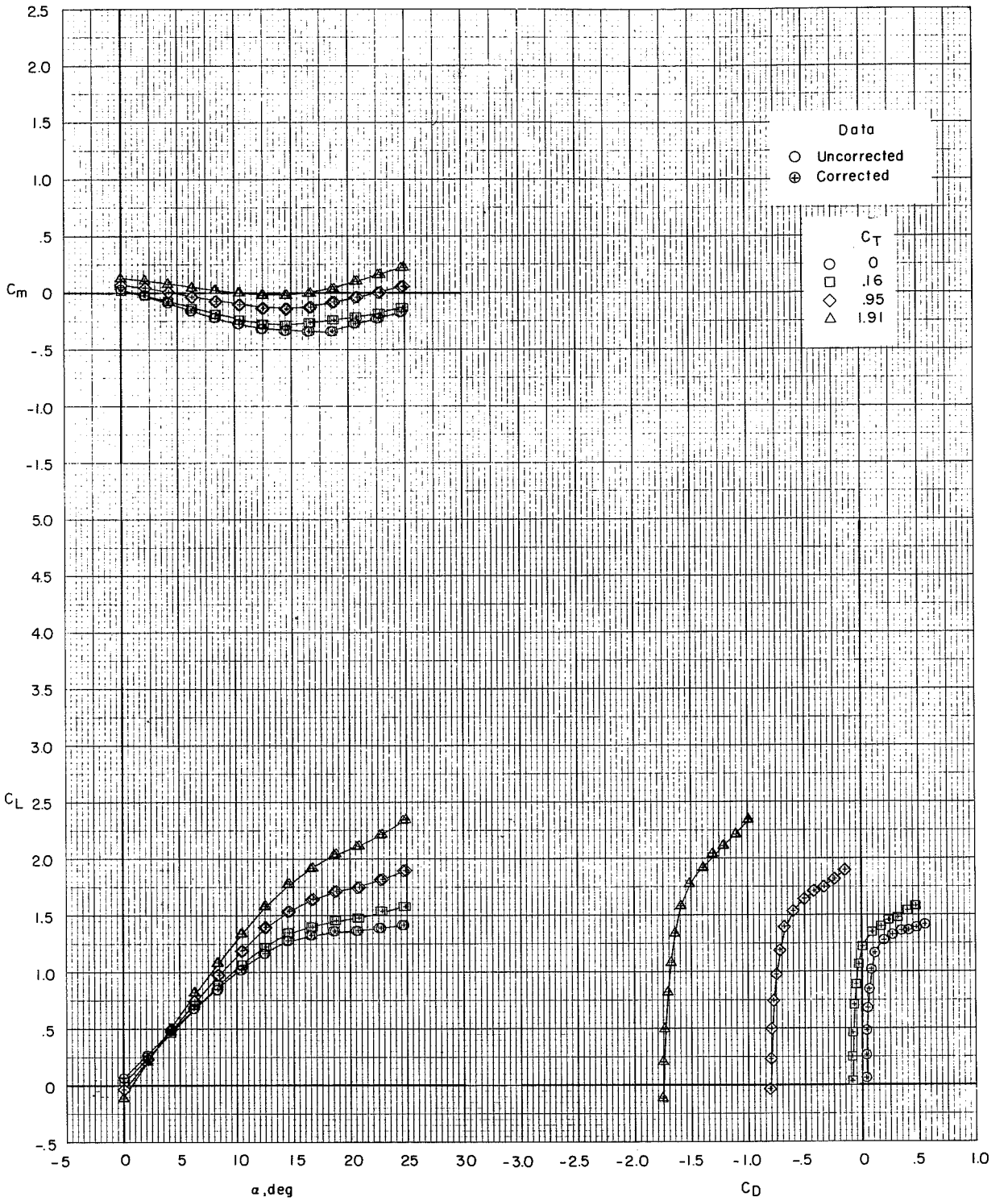

(b) $i_t = 0^o$.

Figure 49.- Concluded.

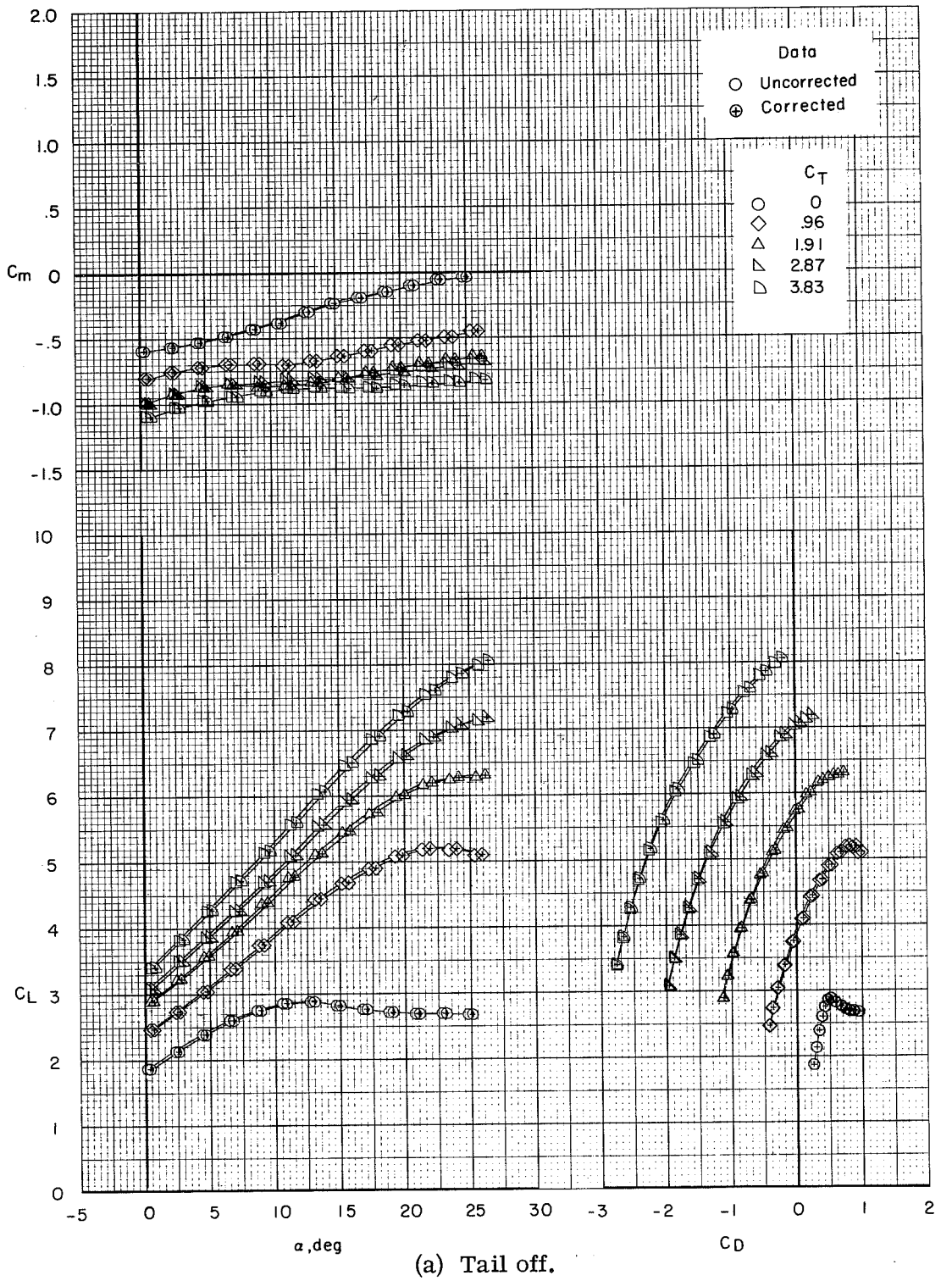

(a) Tail off.

Figure 50.- Effect of wall corrections on V/STOL tunnel data in the take-off configuration without the tunnel liner installed.

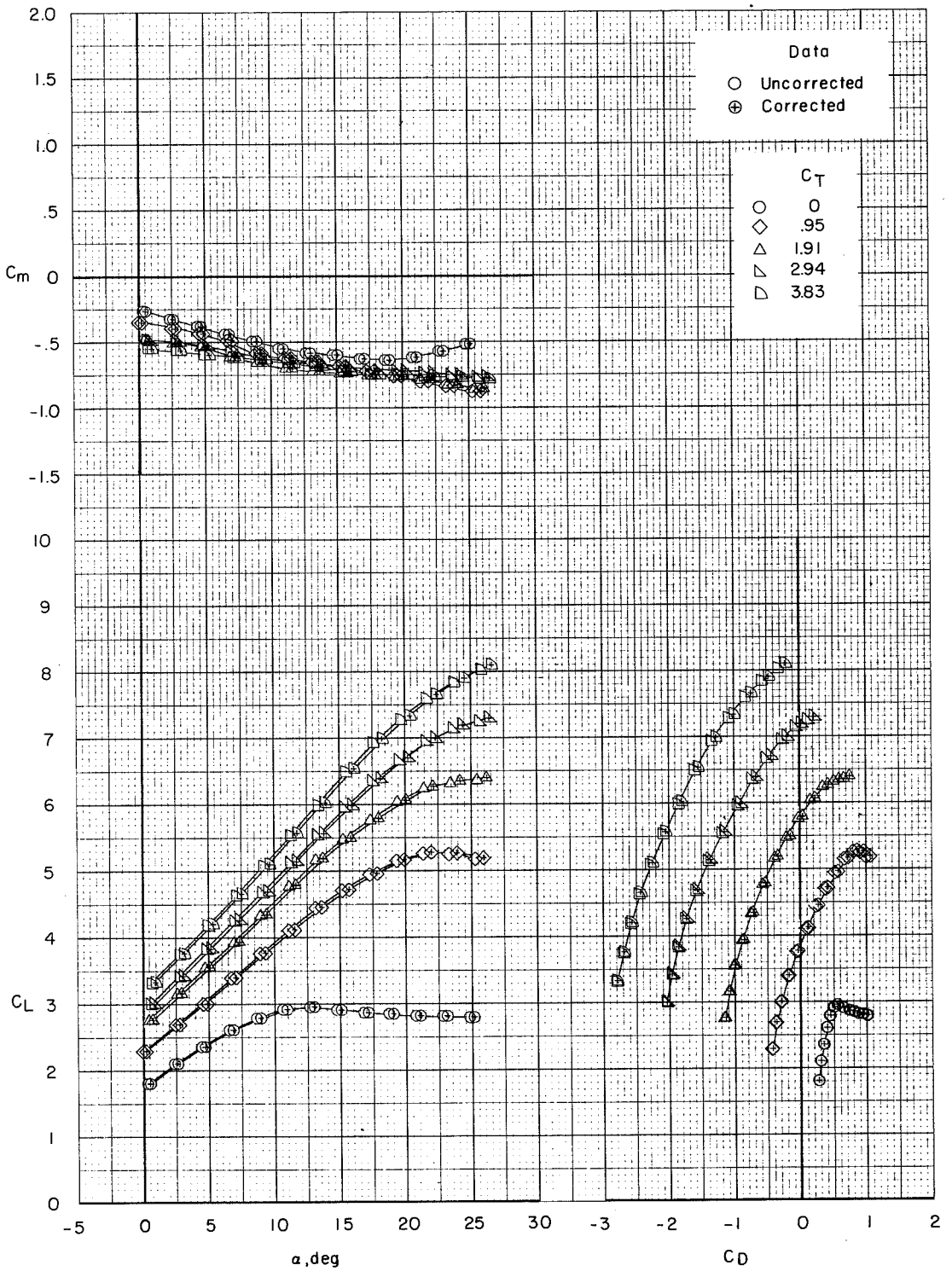

(b) $i_t = 0^o$.

Figure 50.- Concluded.

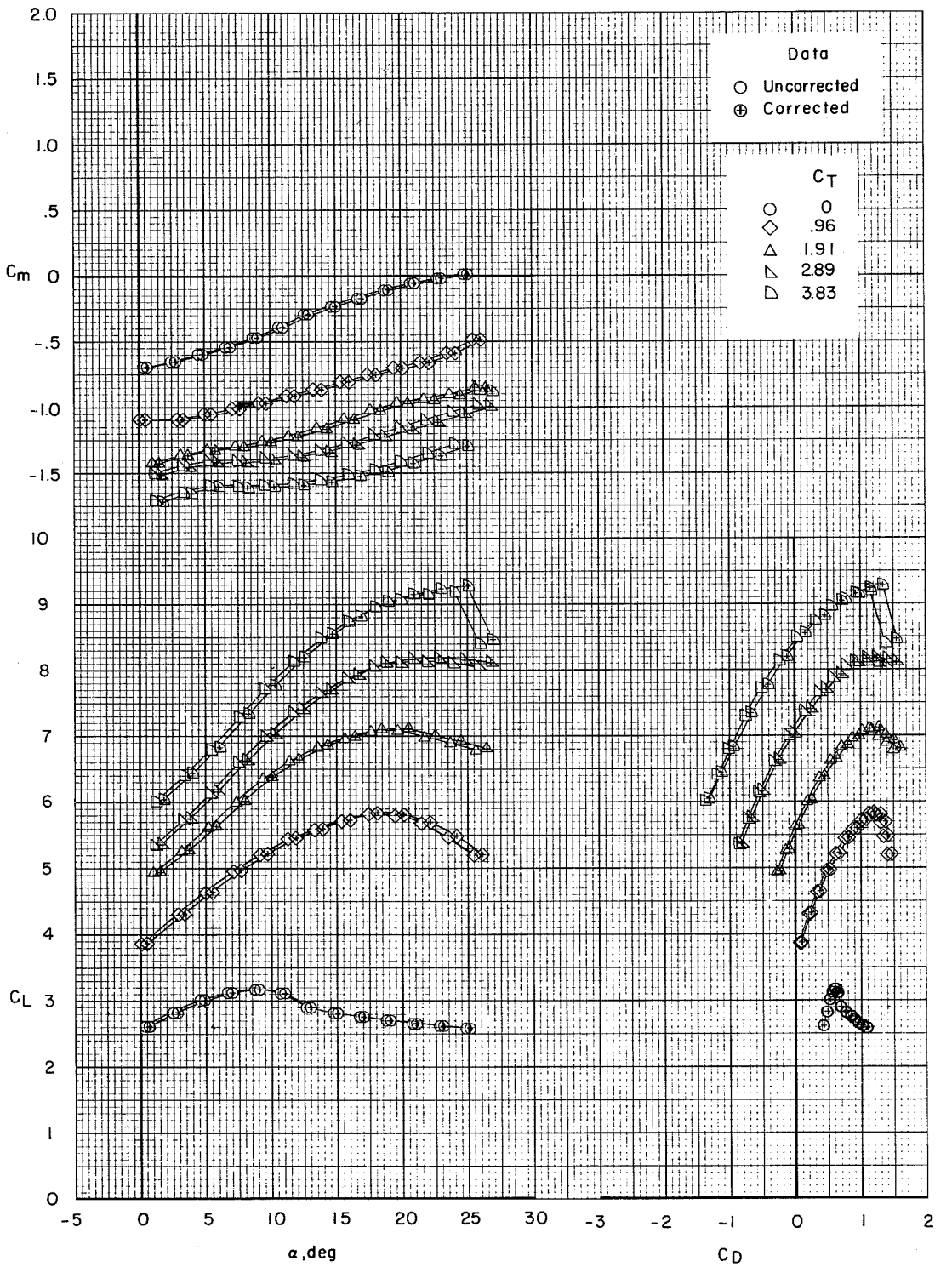

(a) Tail off.

Figure 51.- Effect of wall corrections on V/STOL tunnel data in the landing configuration without the tunnel liner installed.

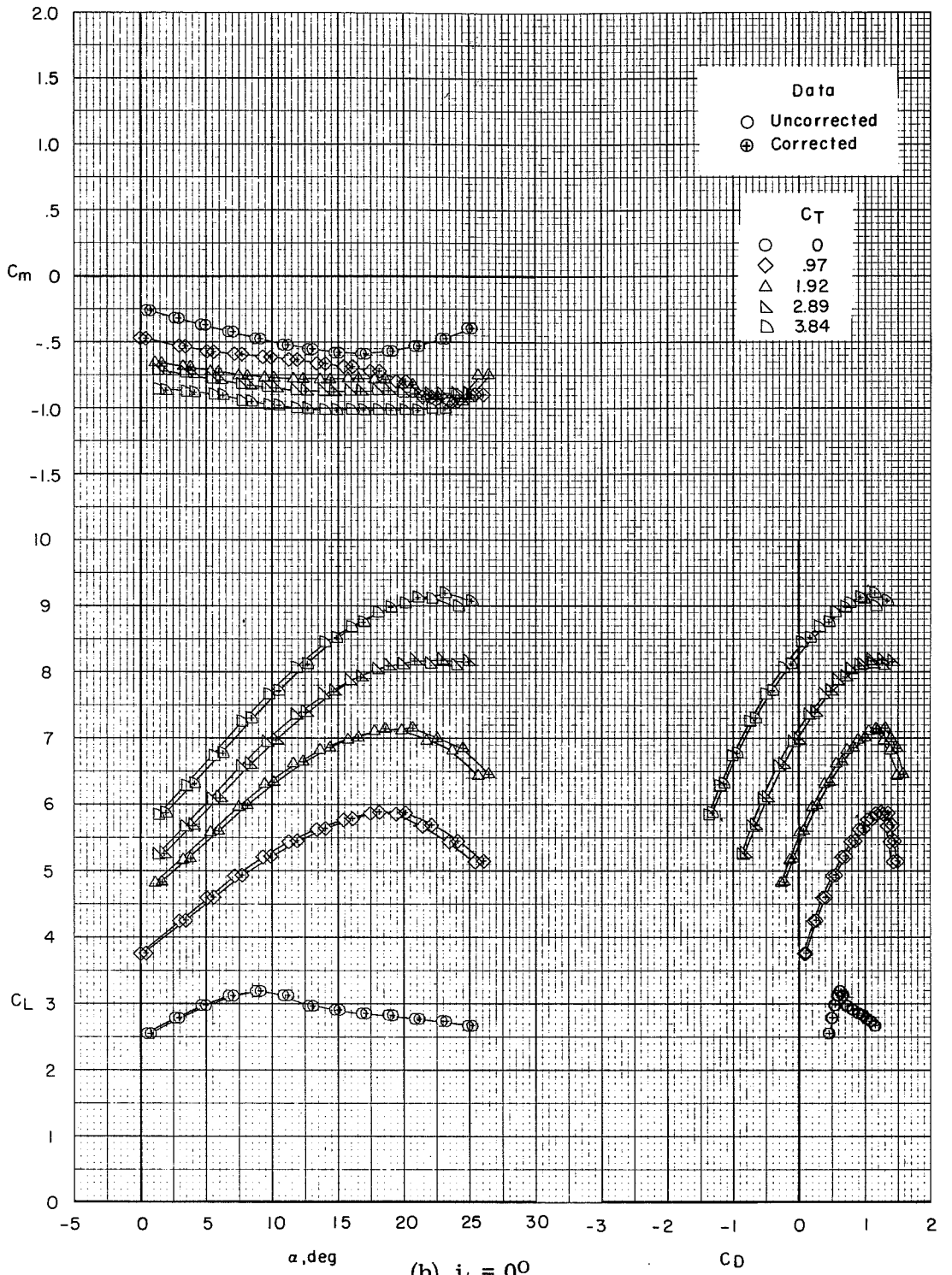

(b) $i_t = 0^o$.

Figure 51.- Concluded.

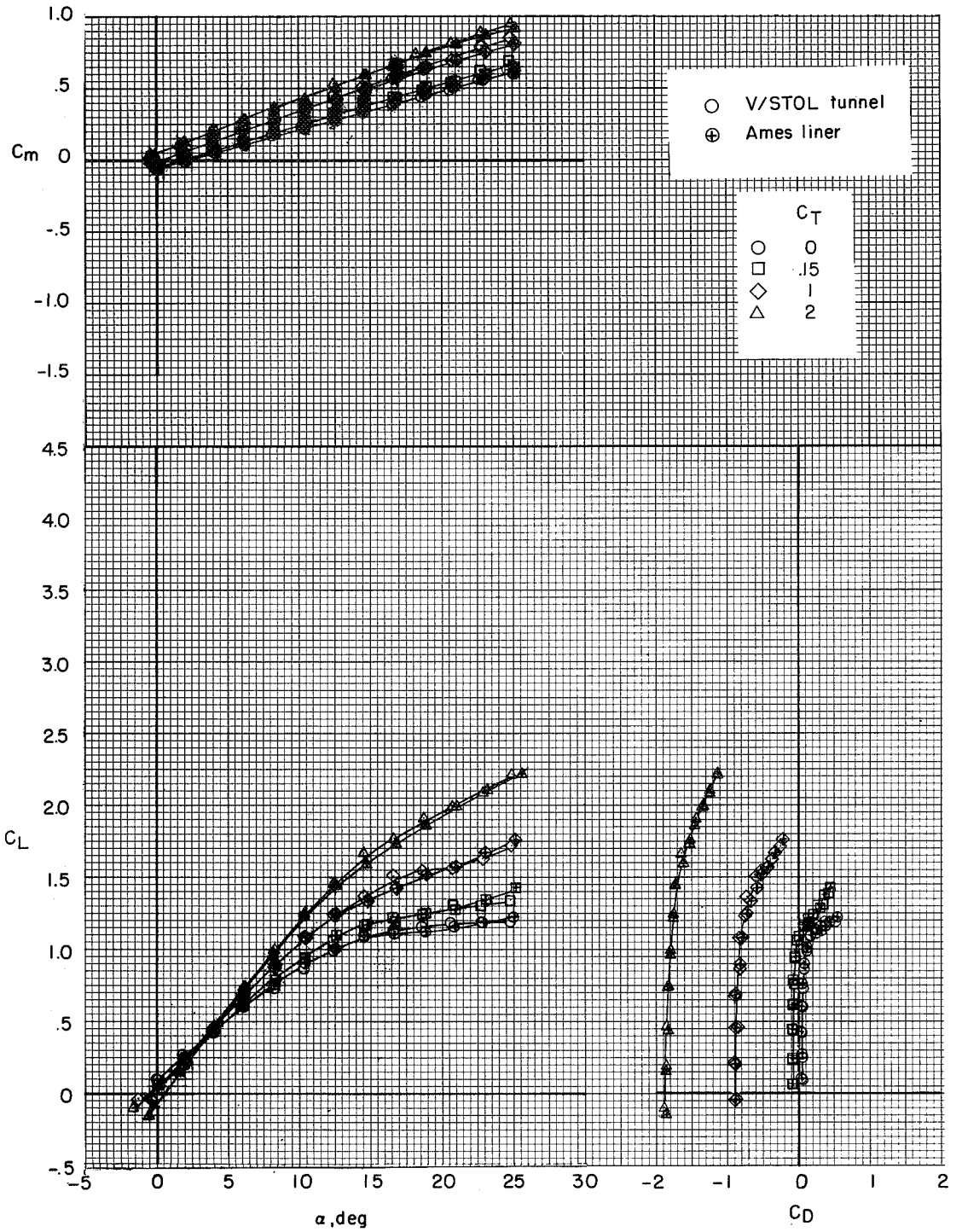

(a) Tail off.

Figure 52.- Comparison of V/STOL tunnel data with data in the cruise configuration obtained with Ames liner.

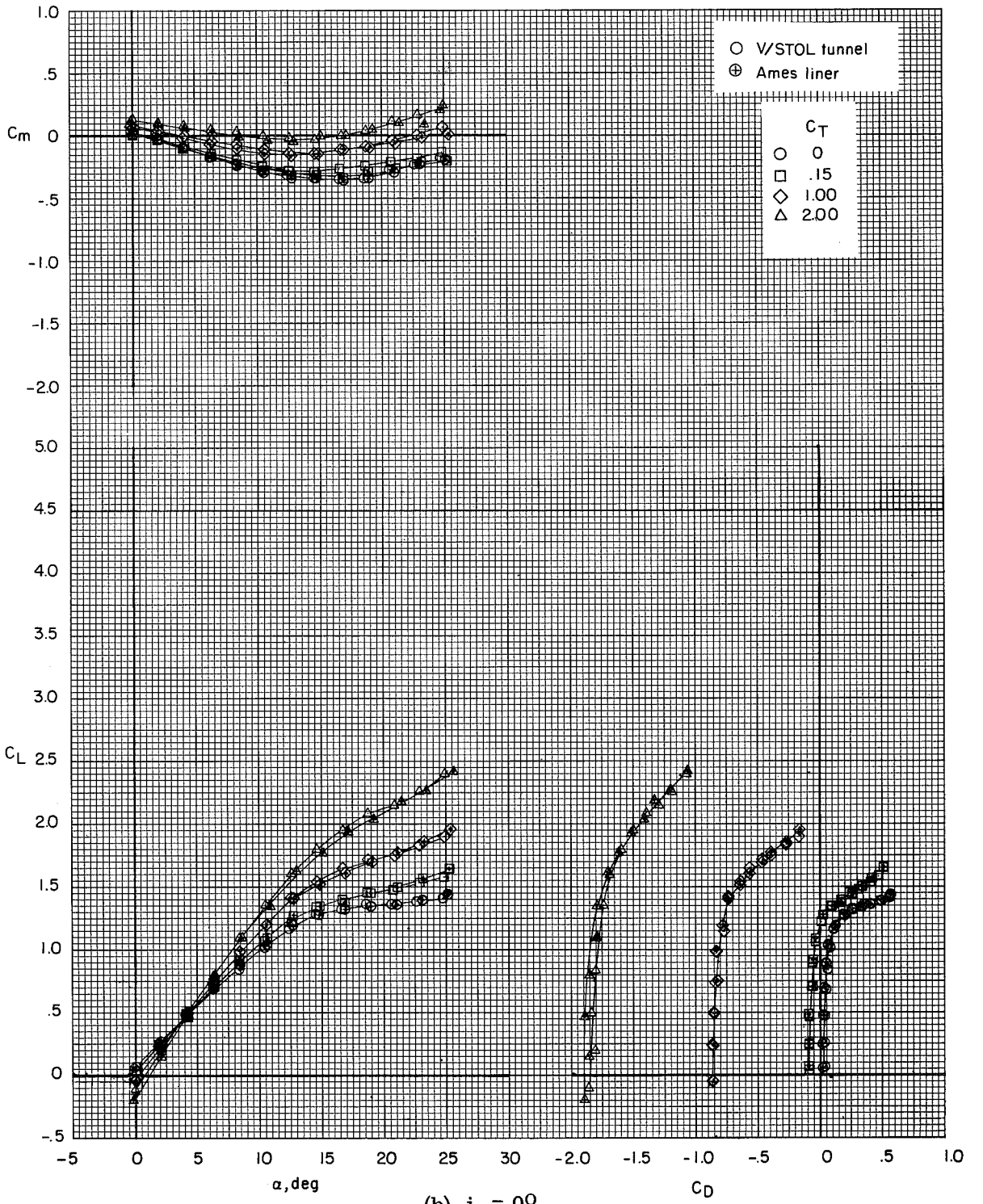

(b) $i_t = 0^o$.

Figure 52.- Concluded.

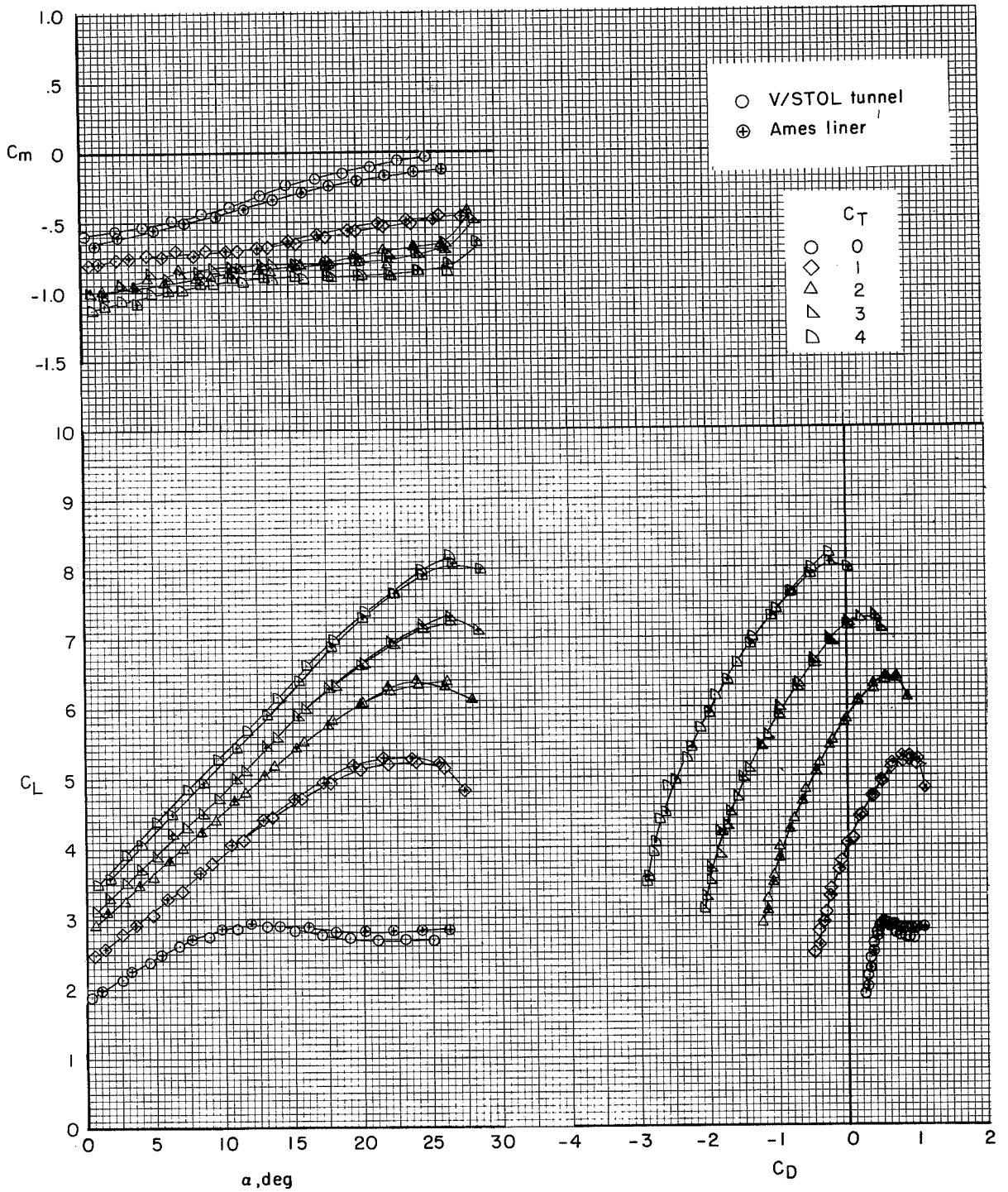

(a) Tail off.

Figure 53.- Comparison of V/STOL tunnel data with data in the take-off configuration obtained with Ames liner.

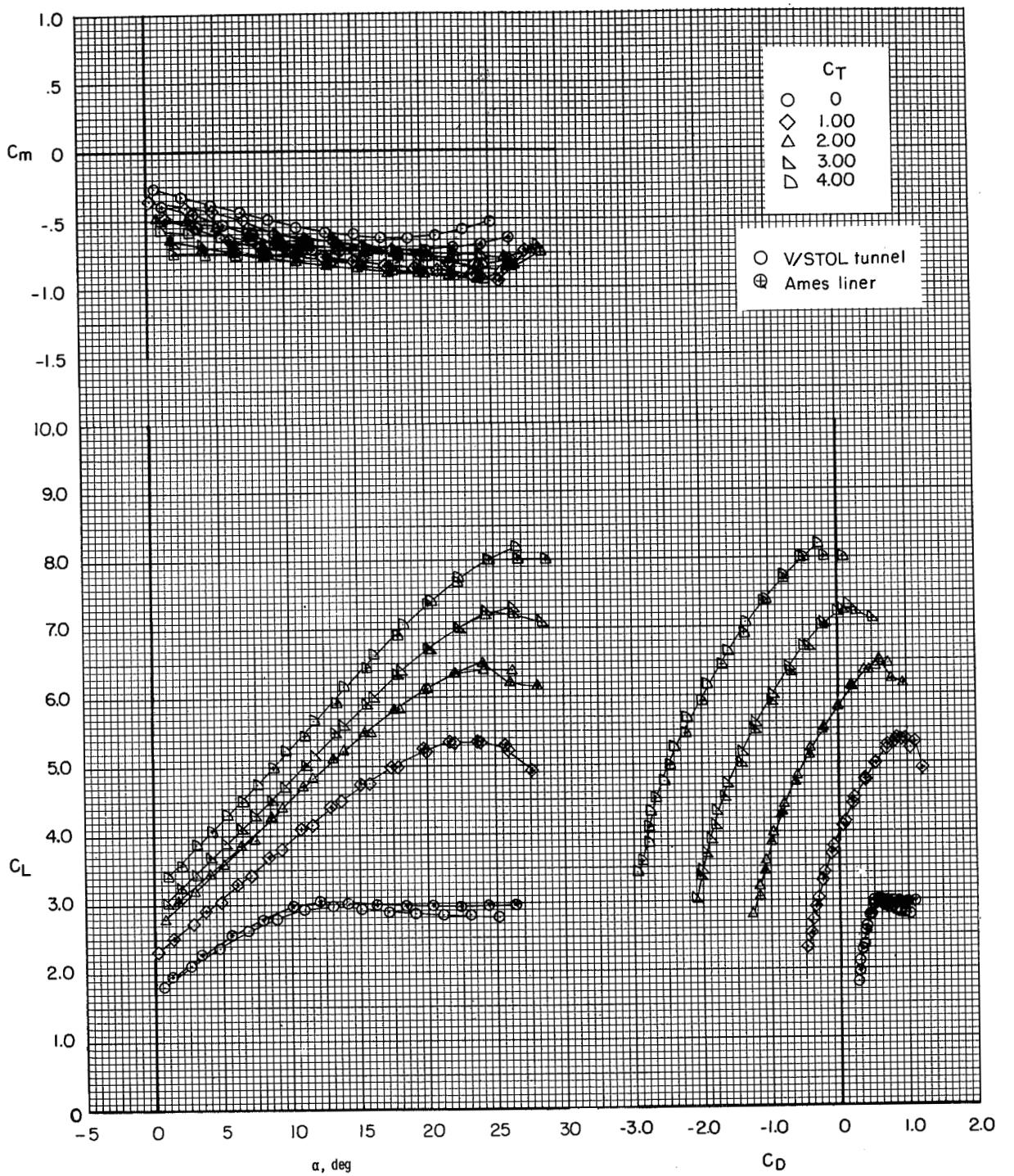

(b) $i_t = 0^o$.

Figure 53.- Concluded.

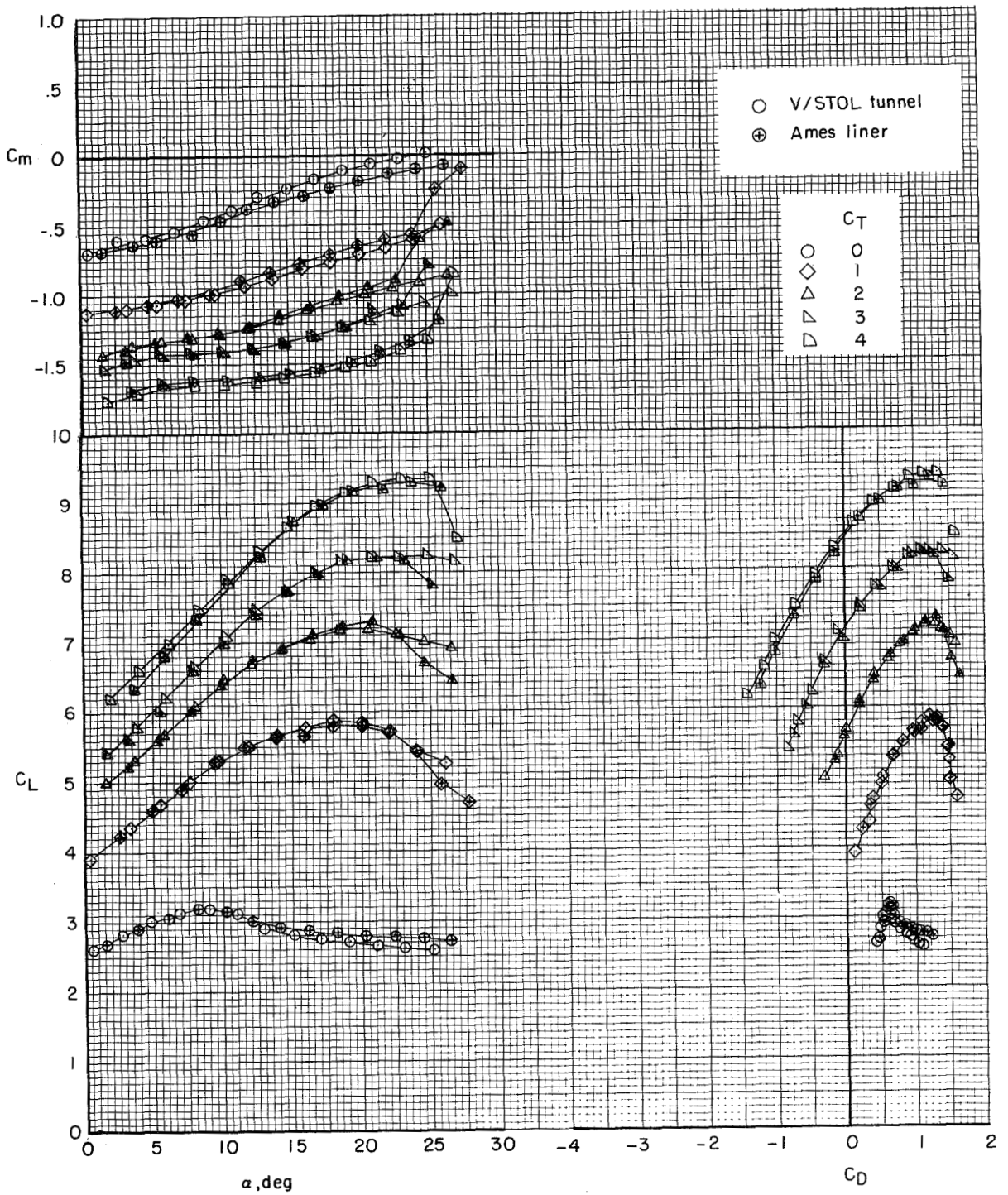

(a) Tail off.

Figure 54.- Comparison of V/STOL tunnel data with data in the landing configuration obtained with Ames liner.

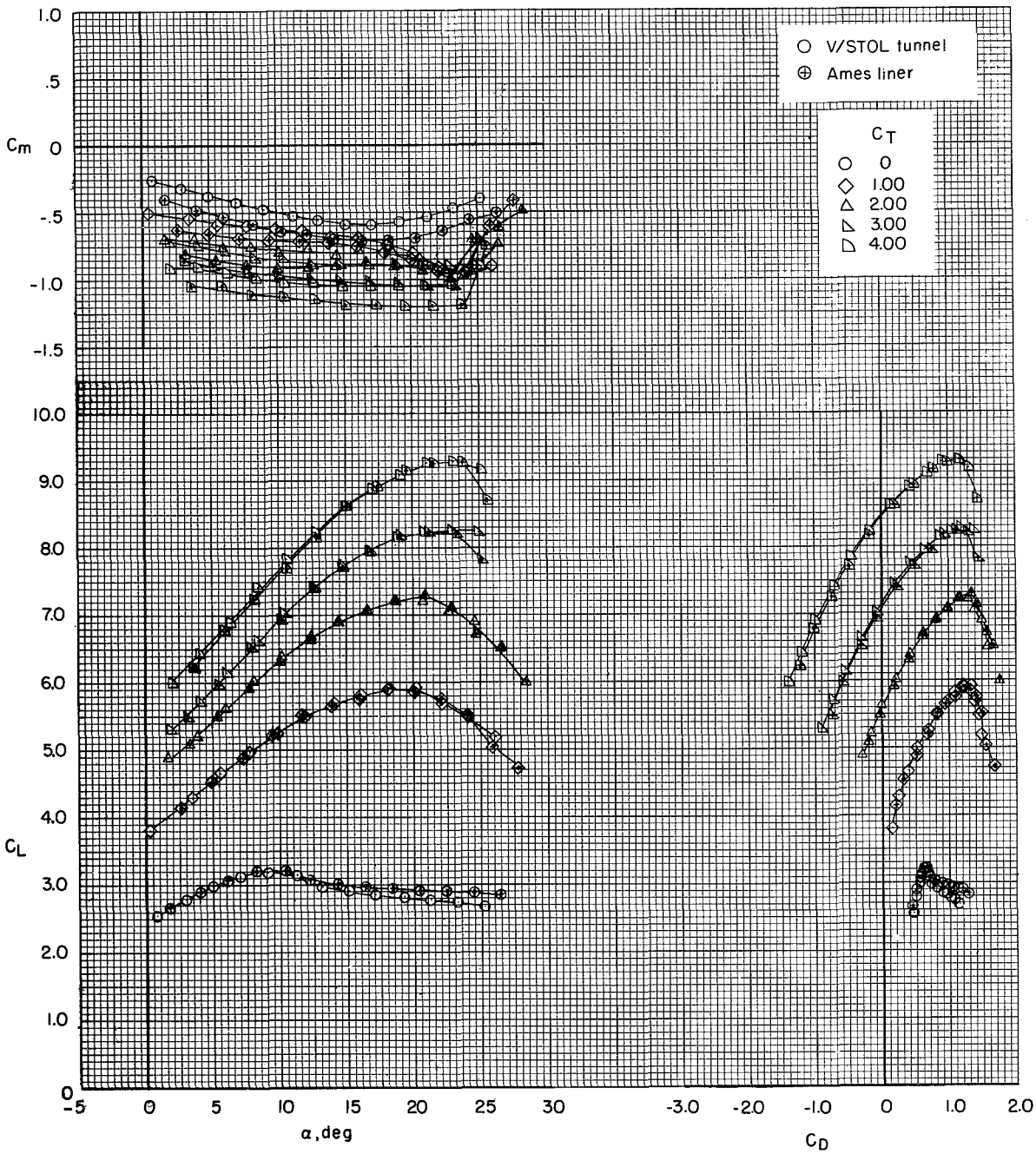

(b) $i_t = 0^o$.

Figure 54.- Concluded.

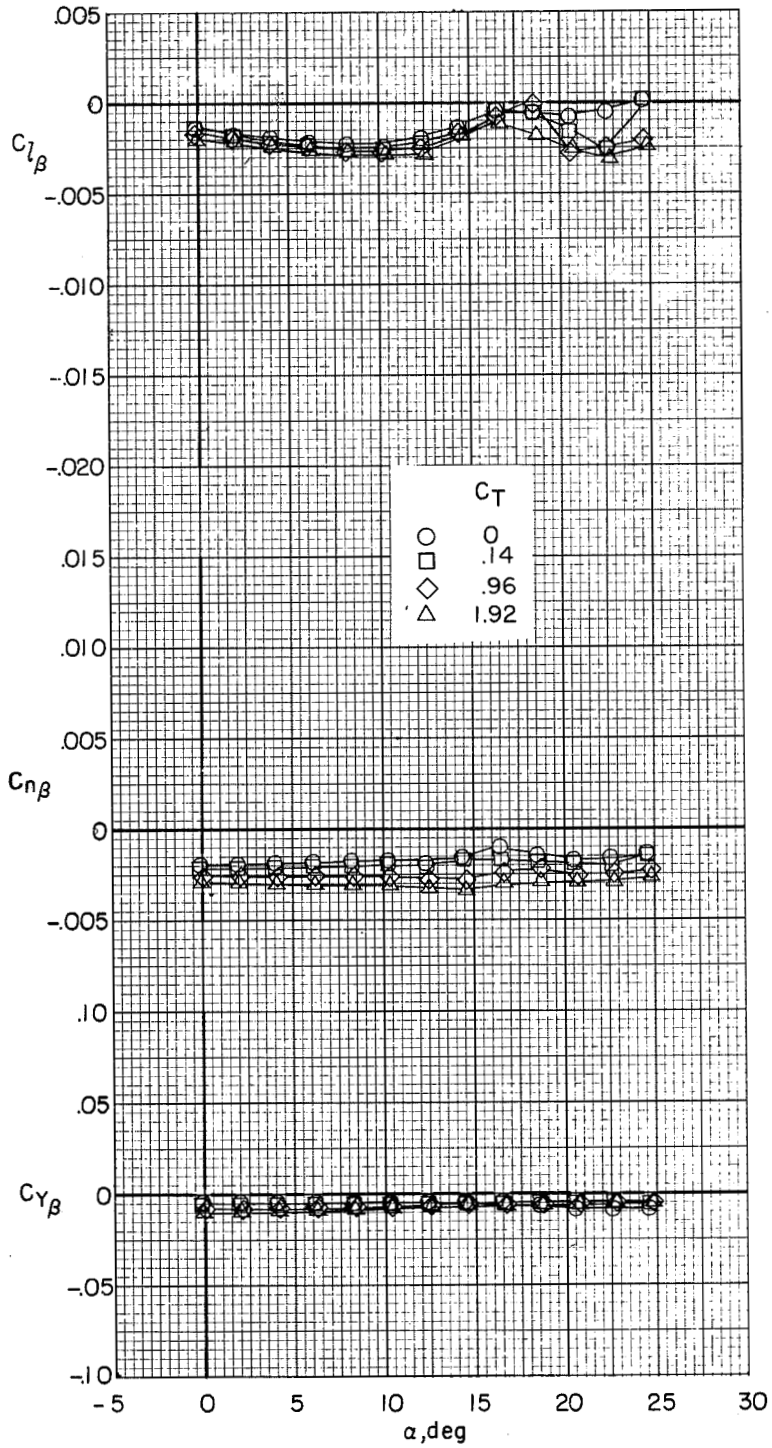

(a) Horizontal and vertical tails removed.

Figure 55.- Lateral stability characteristics of model in cruise configuration. Model in the V/STOL tunnel without the tunnel liner installed.

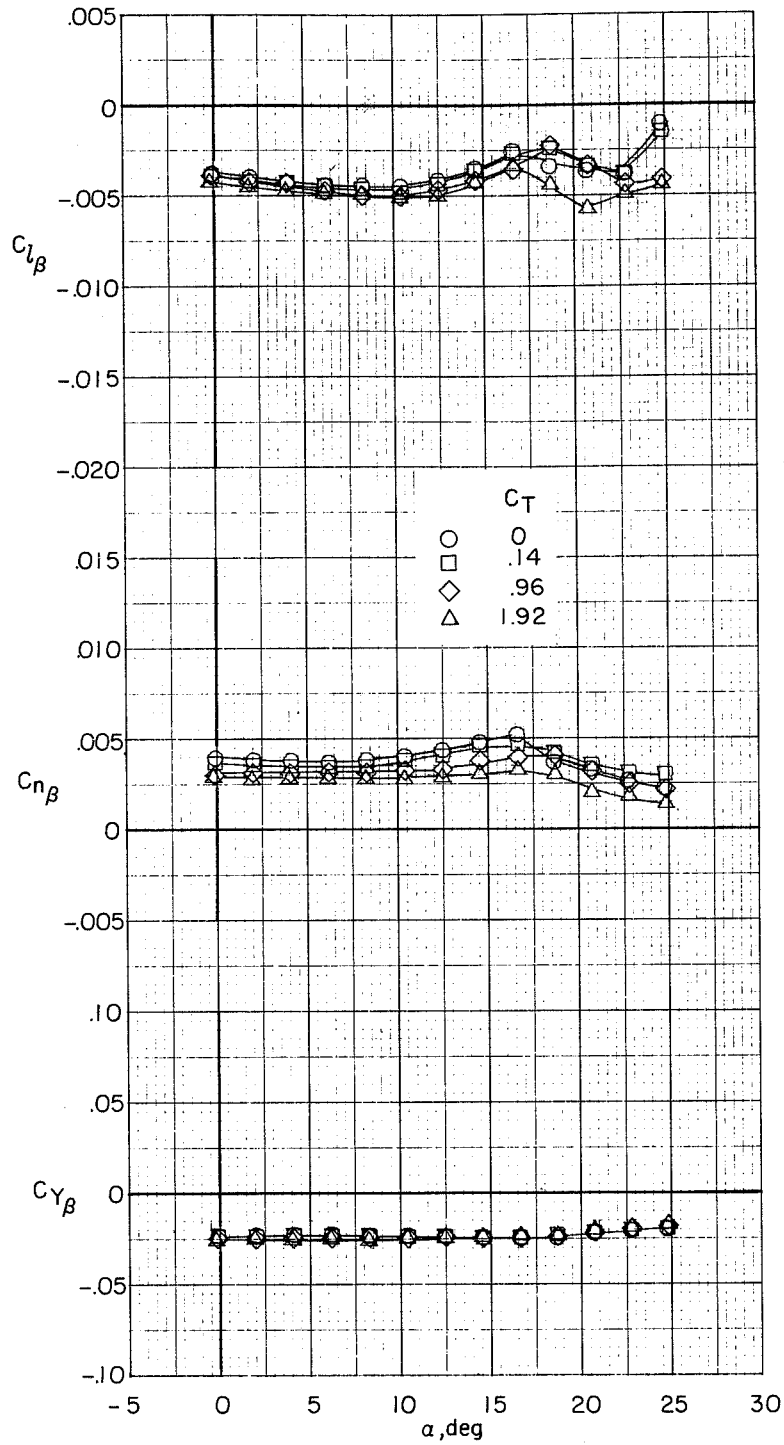

(b) Vertical tail on.

Figure 55.- Continued.

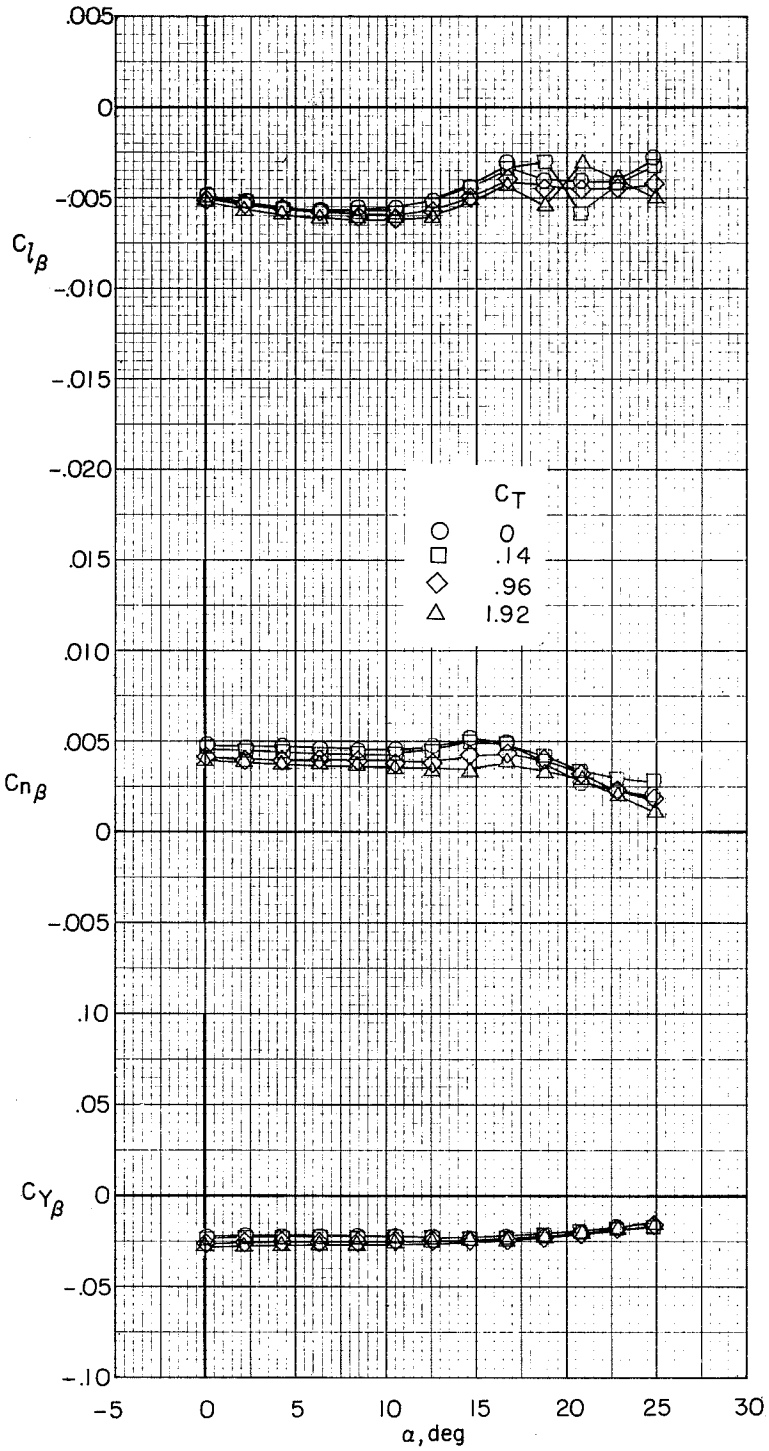

(c) Vertical and horizontal tails on; $i_t = 0^o$.

Figure 55.- Concluded.

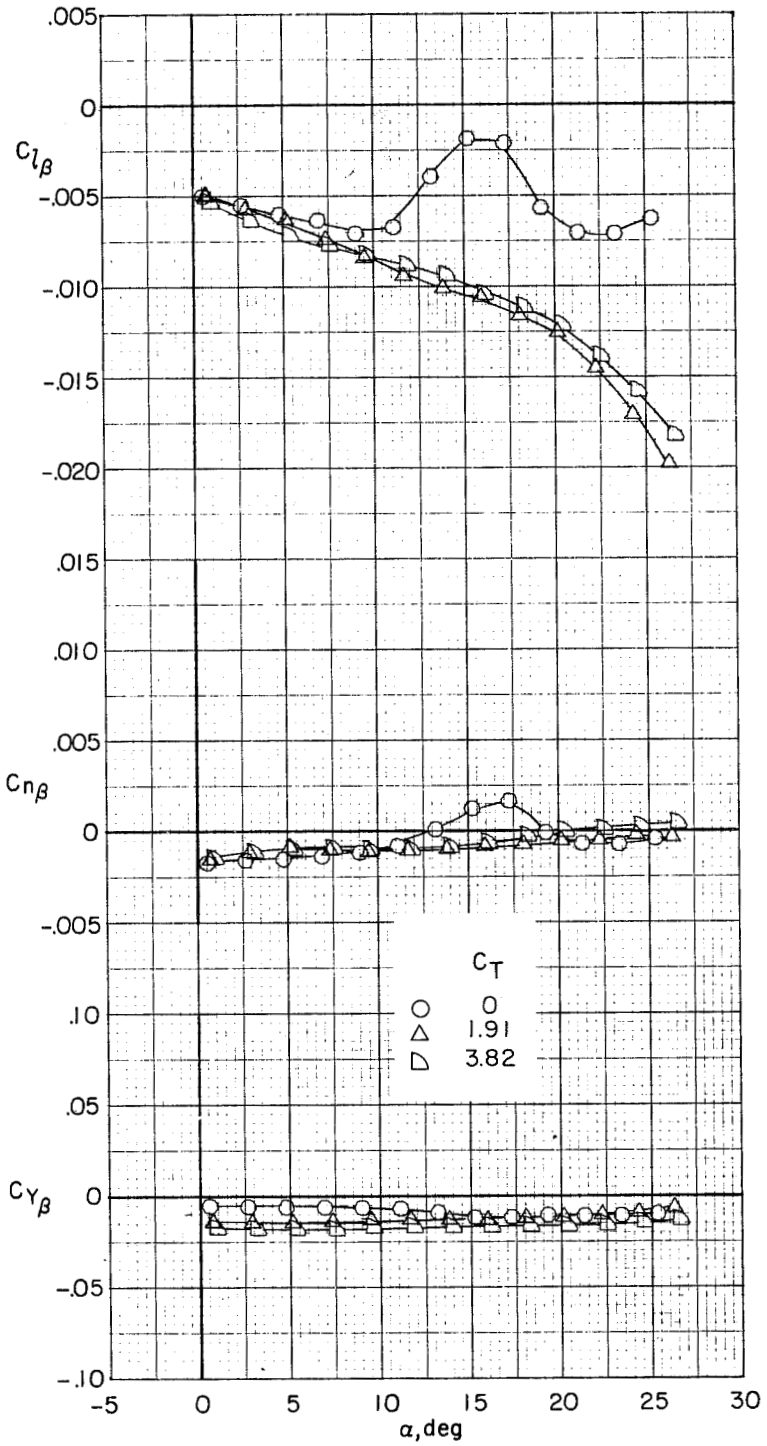

(a) Horizontal and vertical tails removed.

Figure 56.- Lateral stability characteristics of model in take-off configuration. Model in the V/STOL tunnel without the tunnel liner installed.

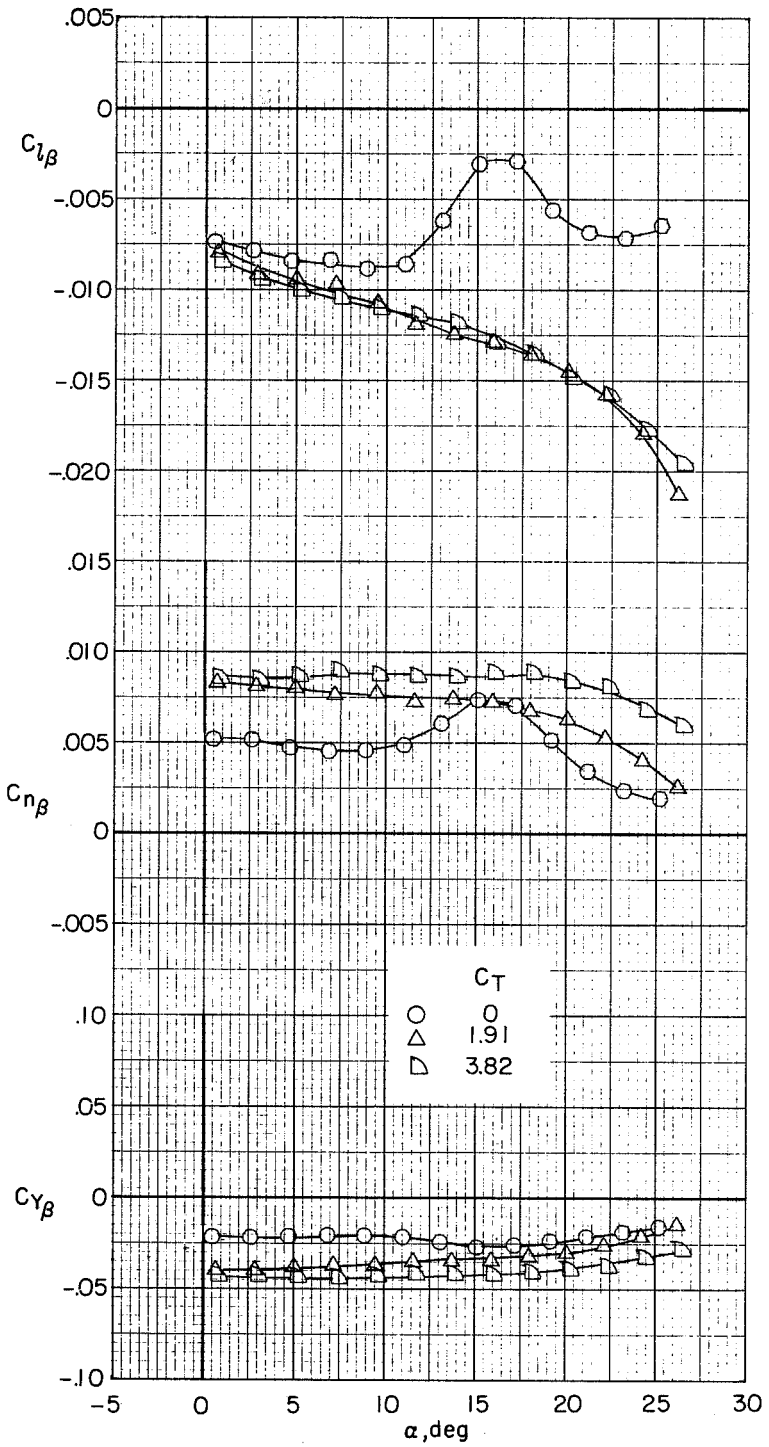

(b) Vertical tail on.

Figure 56.- Continued.

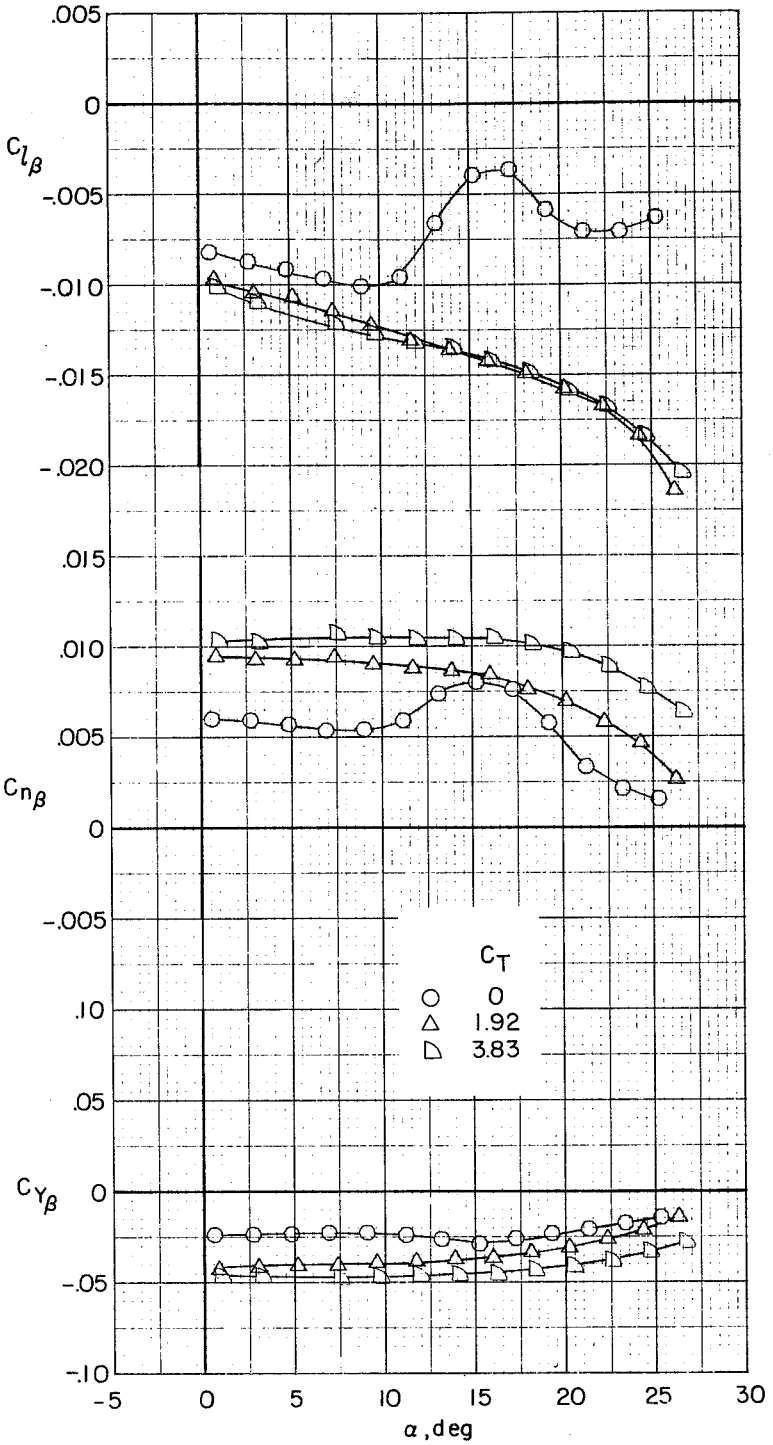

(c) Vertical and horizontal tails on; $i_t = 0^o$.

Figure 56.- Concluded.

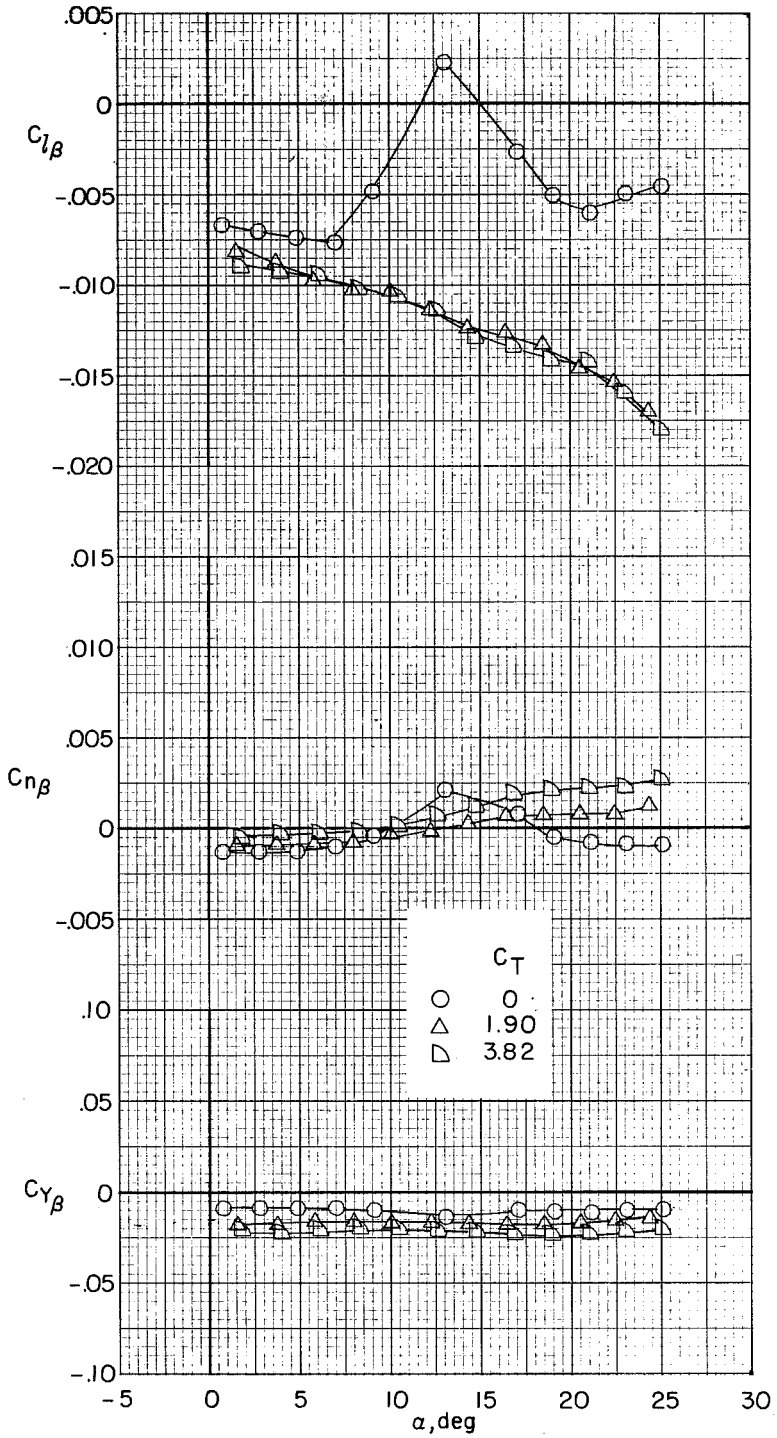

(a) Horizontal and vertical tails removed.

Figure 57.- Lateral stability characteristics of model in landing configuration. Model in the V/STOL tunnel without the tunnel liner installed.

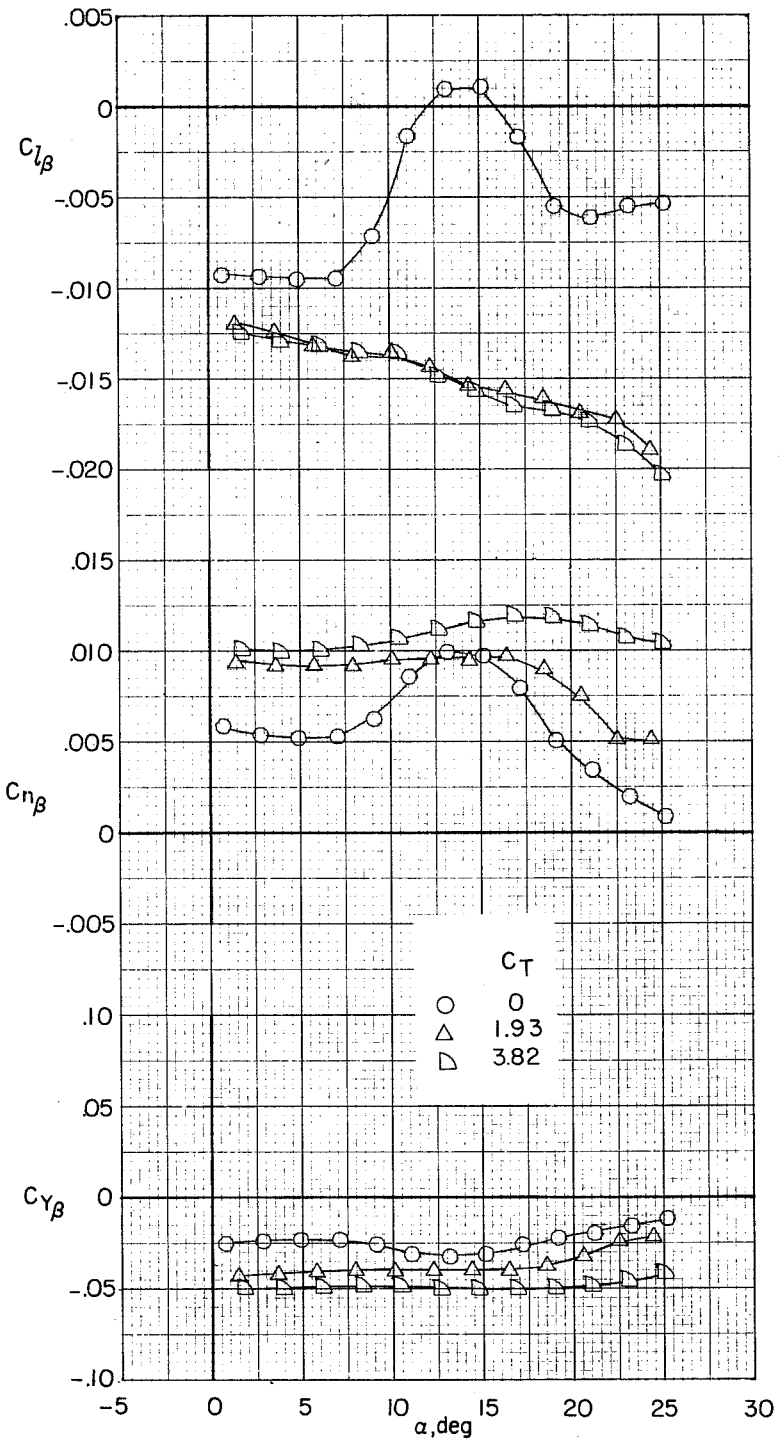

(b) Vertical tail on.

Figure 57.- Continued.

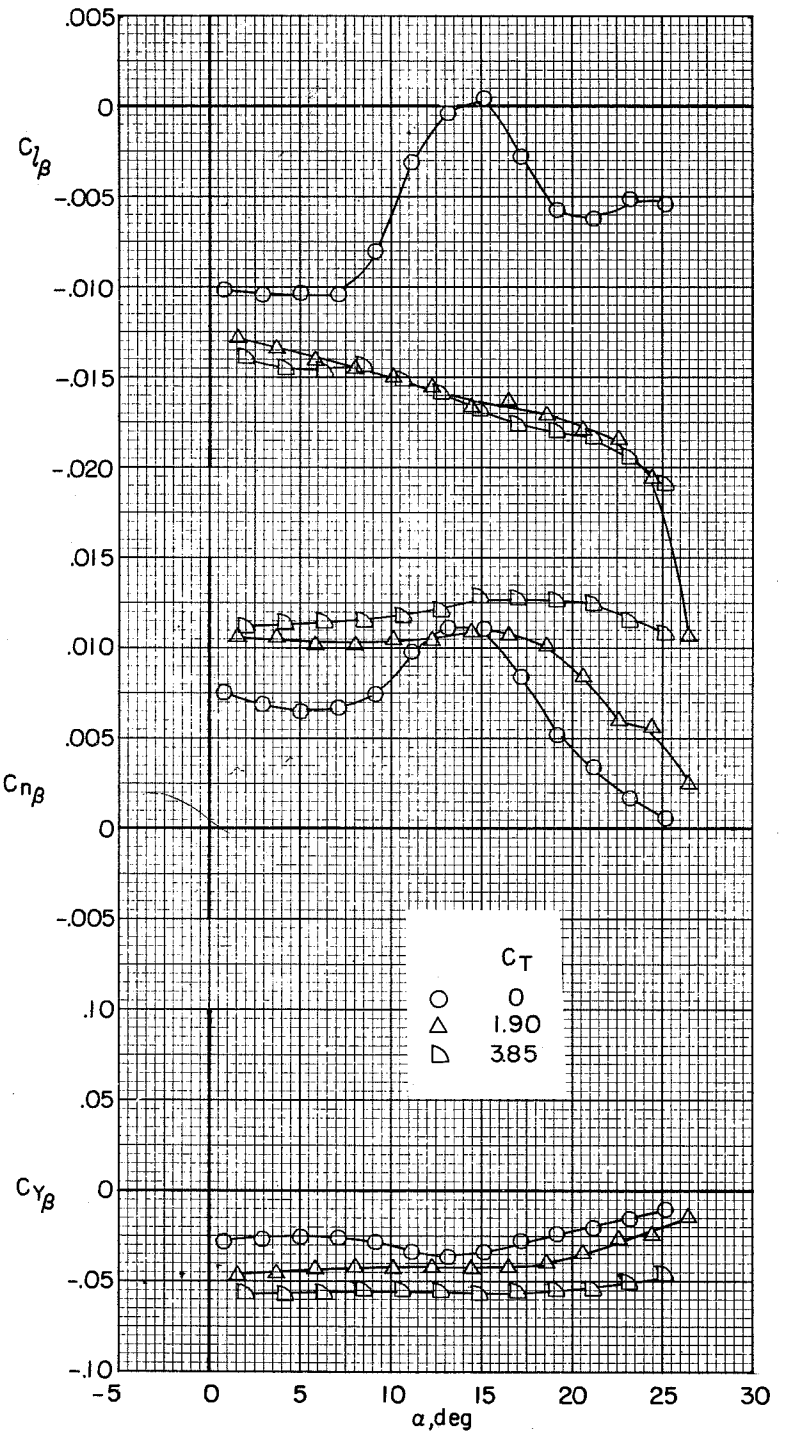

(c) Vertical and horizontal tails on; $i_t = 0^o$

Figure 57.- Concluded.

"The aeronautical and space activities of the United States shall be conducted so as to contribute . . . to the expansion of human knowledge of phenomena in the atmosphere and space. The Administration shall provide for the widest practicable and appropriate dissemination of information concerning its activities and the results thereof."

—NATIONAL AERONAUTICS AND SPACE ACT OF 1958

NASA SCIENTIFIC AND TECHNICAL PUBLICATIONS

TECHNICAL REPORTS: Scientific and technical information considered important, complete, and a lasting contribution to existing knowledge.

TECHNICAL NOTES: Information less broad in scope but nevertheless of importance as a contribution to existing knowledge.

TECHNICAL MEMORANDUMS: Information receiving limited distribution because of preliminary data, security classification, or other reasons. Also includes conference proceedings with either limited or unlimited distribution.

CONTRACTOR REPORTS: Scientific and technical information generated under a NASA contract or grant and considered an important contribution to existing knowledge.

TECHNICAL TRANSLATIONS: Information published in a foreign language considered to merit NASA distribution in English.

SPECIAL PUBLICATIONS: Information derived from or of value to NASA activities. Publications include final reports of major projects, monographs, data compilations, handbooks, sourcebooks, and special bibliographies.

TECHNOLOGY UTILIZATION PUBLICATIONS: Information on technology used by NASA that may be of particular interest in commercial and other non-aerospace applications. Publications include Tech Briefs, Technology Utilization Reports and Technology Surveys.

Details on the availability of these publications may be obtained from:

SCIENTIFIC AND TECHNICAL INFORMATION OFFICE

NATIONAL AERONAUTICS AND SPACE ADMINISTRATION

Washington, D.C. 20546